UNIVERSITÉ PARIS. DIDEROT (Paris 7)

ÉCOLE DOCTORALE D'ASTRONOMIE ET ASTROPHYSIQUE D'ÎLE-DE-FRANCE

DOCTORAT

Astronomie et Astrophysique

IVAN DEBONO

Cosmological parameter forecasts with weak gravitational lensing

Prévisions pour les paramètres cosmologiques avec le cisaillement gravitationnel

Thèse dirigée par M. Alexandre RÉFRÉGIER

Soutenue le 10 décembre 2009

JURY

M. Marcello Fulchignoni, Président
M. Filipe Abdalla
M. David Polarski
M. Carlo Schimd
Mme Sophie Maurogordato
M. Alexandre Réfrégier

Imagination knows no boundaries
and we may well find ourselves
taking the journey through the dark
but finding the melodic sounds
drawing us back to the light.

A State Of Trance Yearmix 2007

Acknowledgements

I would like to thank some of the people who have helped this thesis come to fruition: Anaïs Rassat and Tom Kitching, for their useful collaboration, and their help in clearing up the glitches in my code; Stéphane Paulin-Henriksson for his knowledge of French typographic rules; and Jean-Philippe Uzan for some interesting discussions; and a special thanks to Sacha Hony for his help in getting to grips with the intricacies of programming.

Je remercie l'Ambassade de France à Malte et le gouvernement français, qui ont financé ces trois ans de doctorat. Mes remerciements aussi à tout le personnel du Service d'Action Culturelle de l'Ambassade, en particulier Mme Anne-Louise Debeusscher et M. Ellsworth Camilleri.

Je tiens à remercier aussi le Professeur Alain Blondy, qui fut à l'origine de ce long parcours, avec sa phrase, il y a longtemps, « Pourquoi pas en France ? »

Finally, I would like to express my profound gratitude to my mentors Dr Kris Zarb Adami and Prof. Edward Mallia, for their dedication and inspiration.

Abstract

Modern concordance cosmology is faced with two tasks: Accounting for the abundance of the known constituents, and determining the nature of the unknown components — dark matter and dark energy. These make up approximately 30% and 70% of the current mass-energy budget. The nature of these components is unknown. The initial conditions which led to structure formation pose another important question. This thesis is based on a method which could, given data from future surveys, determine the nature of dark energy through its equation of state and its evolution, and advance our understanding of the distribution of the primordial density fluctuations.

The method used in this thesis is weak gravitational lensing. We use information from tomographic cosmic shear, which acts as a sensitive probe of cosmological parameters by measuring the mass distribution and the geometry of the low redshift Universe. This thesis studies the potential of an all-sky weak lensing tomographic survey to obtain joint constraints for different sets of cosmological parameters describing dark energy, massive neutrinos (hot dark matter), and the primordial power spectrum. Using the Fisher matrix formalism, we examine how the constraints vary as the parameter set is enlarged, and as the fiducial cosmology is changed. We also study the constraints when CMB priors are added to our weak lensing error forecasts.

We find that weak lensing with CMB priors provides robust constraints on dark energy parameters and can simultaneously provide strong constraints on all parameters. Thus, a future all-sky survey in conjunction with expected results from CMB anisotropy probes, could provide constraints on the dark energy equation of state parameters. Such a survey could also constrain the total neutrino mass and the number of massive neutrino species, as well as the primordial spectral index and its running.

The results presented in this thesis show that error forecasts from a future weak lensing survey are stable against the addition of parameters to the fiducial model, and that this stability is improved by adding CMB priors. This thesis also shows that the weak lensing error forecasts are robust against changes in the fiducial cosmological model.

Applying these methods to study their implications for the the planning of future surveys, we find that the design parameter which has the greatest impact on the precision is the survey area. We also show that future surveys will need to utilise a maximum multipole of 10^4 if they are to achieve their maximum potential. Our results show that the same optimisation strategy applies for dark energy, neutrino, and primordial power spectrum parameters.

Résumé

L'actuel Modèle de Concordance cosmologique doit faire face à deux défis : Établir la quantité des composantes connues, et détérminer la nature des composantes inconnues — la matière noire et l'énergie noire. Celles-ci représentent environ 30% et 70% du contenu de masse-énergie de l'Univers à l'époque actuelle. Les conditions initiales qui ont engendré la croissance des structures posent une autre question importante. Cette thèse se base sur une méthode qui pourrait, avec des données des futurs relevées, détérminer la nature de l'énergie noire à travers son équation d'état et son évolution, et faire avancer notre connaissance de la forme des perturbations primordiales de densité.

La méthode utilisée dans cette thèse est celle des lentilles gravitationnelles faibles. On utilise l'information donnée par le cisaillement cosmique tomographique, qui est une sonde très sensible aux paramètres cosmologiques par sa mesure de la distribution de masse et la géométrie de l'Univers à bas décalage spectral. Cette thèse étudie la possibilité pour un relevé de cisaillement cosmique tomographique de tout le ciel d'obtenir des contraintes conjointes pour des différents groupes de paramètres cosmologiques décrivant l'énergie noire, les neutrinos massifs (matière noire chaude), et le spectre des perturbations primordiales. En utilisant le formalisme des matrices de Fisher, on étudie comment les contraintes varient en fonction du nombre de paramètres, et en fonction des valeurs centrales des paramètres du modèle cosmologique. On étudie également les contraintes avec l'ajout des *a priori* du fond diffus cosmologique à nos prévisions des barres d'erreur du cisaillement gravitationnel.

On trouve que le cisaillement gravitationnel avec des *a priori* des mesures de l'anistropie du rayonnement du fond cosmique nous donne des contraintes robustes pour les paramètres d'énergie noire et peut simultanément donner des contraintes fortes pour tous les paramètres. Ainsi, un futur relevé de tout le ciel, en combinaison avec des prédictions des résultats des sondes d'anisotropie du fond diffus cosmologique, peut donner des contraintes sur les paramètres de l'équation d'état de l'énergie noire. Un tel relevé pourrait aussi contraindre la masse totale des neutrinos et le nombre d'espèces massives de neutrinos, ainsi que la pente du spectre primordial et sa dérivée.

Les résultats présentés dans cette thèse montrent que les prédictions pour les erreurs sur les paramètres cosmologiques d'un relevé de cisaillement gravitationnel sont stables, même avec l'ajout de paramètres dans le modèle, et que cette stabilité est améliorée avec l'addition des *a priori* du fond diffus cosmologique. Cette thèse montre aussi que les prévisions pour un relevé de cisaillement gravitationnel sont robustes à la variation des valeurs centrales du modèle cosmologique.

Passant à l'application de ces méthodes pour étudier leur implication pour la planification de futurs relevés, on trouve que le paramètre du relevé qui a l'effet majeur sur

la précision est l'étendue. On montre aussi que les futurs relevés devraient utiliser un intervalle de multipôles allant jusqu'à 10^4 pour atteindre leur potentiel maximum. Les résultats montrent que la même stratégie d'optimisation est valable pour les paramètres d'énergie noire, de neutrinos, et de spectre de puissance primordiale.

Contents

List of Tables

List of Figures

Chapter 1

Cosmology

This chapter presents an outline of Standard Cosmology, which is the theoretical paradigm on which this work is based. We explain the basic concepts in cosmology, with an emphasis on cosmological components and structure formation, which are particularly relevant to this thesis.

We start with a historical outline of gravity theories, discussing the development of General Relativity and alternative theories. We then introduce the main concepts in General Relativity, and its application to cosmological models. This is followed by a review of the components making up the mass-energy budget of the Universe, and of cosmological distance measures.

We give an overview of structure formation, highlighting its relevance to cosmological measures. We then discuss the link between cosmological observations and the theoretical framework, particularly in the context of the acceleration of the cosmic expansion. This leads to a discussion of the remarkable claim that around 70% of the mass-energy content of our Universe is made up of dark energy. Possible candidates for dark energy, and inferences upon the nature of dark energy from cosmological observations, are reviewed.

1.1 The theoretical framework

In this thesis, we work within the framework of General Relativity (GR). This theory is at the basis of the Standard Model, and here we shall discuss the development of GR. We shall also discuss why the theory has been so successful, and the criteria that must be satisfied by any alternative theory of physics, and therefore, by any alternative theory of cosmology.

Cosmology, in its broadest definition, is the study of the cosmos. It aims to provide an accurate description of the Universe. Throughout much of the history of science, the development of cosmology was hampered by the lack of a universal physical theory. Observational tools were extremely limited, and there was no mathematical formulation for physical laws. The cosmos was described in metaphysical, rather than physical terms.

The scientific revolution which brought about the development of a precise mathematical language for physical theories heralded the scientific age of cosmology. Physical laws, tested here on earth and later in the solar system, could be applied to the 'entire Universe', and could thus provide a precise physical description of the cosmos. Modern cosmology is based upon this epistemological framework. Cosmology, therefore, depends upon a fundamental premise. As a science, it must deal strictly with what can be observed, but the observable Universe forms only a fraction of the whole cosmos. One is forced, therefore, to make the fundamental assumption that the portion of the Universe which can be observed is representative of the whole, and that the laws of physics are the same throughout the whole Universe. Once we make this assumption, we can construct a model of the Universe, or cosmological model, based on a description of its observable part.

Any cosmological model which assumes the universality of physical laws must be based upon some physical theory. Since cosmology aims to describe the Universe on the largest possible scales, it must be based upon an application long-range physical interactions. Since the theory of gravitation is the physical theory at the basis of standard cosmology, and is also at the centre of the big questions facing modern cosmology, we shall give an overview of the development of theories of gravitation.

1.2 Theories of gravity

The development of physical theories of gravity was driven by the search for ever more generalised principles. Ancient Greek 'natural philosophy' provided qualitative rather than quantitative descriptions. Nonetheless, there is a certain logic to the development of physical theories from this time to the Middle Ages. Sorabji (1988, Part III, page 219) provides a very comprehensive account of the development of theories of gravitation during this period. For an overview of theories of mechanics and gravitation in the Middle Ages, see Franklin (1976). The revolution in physics came with the development of mathematical, quantitative, models to describe physical situations. Thus physicists of Newton's generation found a very different scientific environment than the one in which Galileo had started off.

For more than two centuries, Newton's theory, published in his *Principia* (Newton, 1687), was *the* standard physical description of gravity. There was no other attempt to

find a different theory for the gravitational force, although the intervening years between Newtonian gravity and Relativity produced some important physical concepts such as de Maupertuis's 'Principle of Least Action' (de Maupertuis, 1746), further developed by Euler (1750), Lagrange (1788) and Hamilton (1834, 1835). Although equivalent in classical mechanics to Newton's Laws, the action principle is better suited for generalisations.

The physical theory of gravity remained unchanged until Einstein's time. After the publication of his Theory of Special Relativity (SR) (Einstein, 1905), Einstein turned to the problem of including gravitation within four-dimensional spacetime. Newton's formulation of the gravitational laws is expressed by the equations:

$$\frac{\mathrm{d}^2 x^i}{\mathrm{d}t^2} = -\frac{\partial \Phi}{\partial x^i}, \tag{1.1}$$

$$\nabla^2 \Phi = 4\pi G\rho, \tag{1.2}$$

where Φ is the gravitational potential, G is the universal gravitational constant, and ρ is the mass density. These equations cannot be incorporated into special relativity as they stand. The equation of motion (1.1) for a particle is in three-dimensional form, so it must be modified into a four-dimensional vector equation for $\mathrm{d}^2 x^\mu/\mathrm{d}\tau^2$. Similarly, the field equation (1.2) is not Lorentz-invariant, since the three-dimensional Laplacian operator instead of the four-dimensional d'Alembertian means that the gravitational potential Φ responds instantaneously to changes in the density ρ at arbitrarily large distances. The conclusion is that Newtonian gravitational fields propagate with infinite velocity, which violates one of the postulates of SR.

Equations (1.1) and (1.2) can be generalised so that they are consistent with the postulates of Special and General Relativity. Misner et al. (1973, page 178) give the detailed calculations for three such generalisations. The simplest relativistic generalisation of Newtonian gravity is obtained by representing the gravitational field by a scalar Φ. Since matter is described in relativity by the stress-energy tensor $T_{\mu\nu}$, the only scalar with dimensions of mass density (which corresponds to ρ) is T^μ_μ. A consistent scalar relativistic theory of gravity would thus have the field equation

$$\Box^2 \Phi = 4\pi G T^\mu_\mu. \tag{1.3}$$

The equations of motion from this theory, however, when applied to a static, spherically symmetric field Φ, such as that of the sun, acting on an orbiting planet, would result in a negative precession, or *retardation* of the perihelion. Experimental evidence (observation of the orbit of Mercury) clearly shows that planets experience a precession of the perihelion. Moreover, in the limit of a zero rest-mass particle, such as a photon, the equations of motion show that the particle experiences no geodesic deviation. The existence of an energy-momentum tensor due to an electromagnetic field would also be impossible, since $(T_{\text{electromagnetic}})^\mu_\mu = 0$. The theory therefore allows neither gravitational redshift, nor deviation of light by matter, both of which are clearly observable phenomena (see Will, 2001, and references therein).

As a second generalisation, the gravitational field could be represented by a vector field Φ_μ, by analogy to electromagnetism. Following through with this analogy, the 'Coulomb' law in this theory gives a repulsion between two massive particles, which clearly

contradicts observations. The theory also predicts that gravitational waves should carry negative energy, and, like the scalar theory, predicts no deviation of light. Like the scalar theory, then, the vector theory must be discarded.

The best of the flat-space theories of gravitation is the tensor theory. The gravitational field is described by a symmetric tensor $h_{\mu\nu} = h_{\nu\mu}$. The choice of the Lagrangian in this theory is dictated by the requirement that $h_{\mu\nu}$ be a Lorentz-covariant, massless, spin-two field. Fierz & Pauli (1939) were the first to write down this Lagrangian and investigate the resulting theory. The predictions of the theory for deviation of light agree with those of general relativity, and are consistent with observations. Since the field equations and gauge properties are identical to those of Einsein's 'linearised theory', the predictions for the properties of gravitational waves, including positive energy, agree with those obtained using the linearised theory in general relativity. However, the theory differs from General Relativity (GR) in its predicted value for the perihelion precession, which is $\frac{4}{3}$ of that given by GR, and which disagrees with the value obtained from observations of Mercury's orbit. On a conceptual level, the theory has an even worse deficiency. If two gravitating bodies (that is, not test particles) are considered, and the field equations are applied to them, then the theory predicts that gravitating bodies cannot be affected by gravity, since they all move along straight lines in a global Lorentz reference frame. This holds for bodies made of arbitrary stress-energy, and since all bodies gravitate, then one must conclude that no body can be accelerated by gravity, which is a glaring self-inconsistency in the theory.

This theory is not completely without merit however. In fact it is the starting point for one version of GR, where Einstein's geometrodynamics is viewed as the standard field theory for a classical field corresponding to quantum-mechanical particles of zero rest mass and spin 2 in an unobservable flat spacetime background. This alternative route to the derivation of general relativity was developed and explored by Gupta (1954, 1957, 1962), Kraichnan (1955), Thirring (1961), Feynman (1995), and Weinberg (1965). A concise summary of the comparisons between Einstein's and the spin-2 derivation is found in Misner et al. (1973, Box 18.1, page 437). The derivation of the full Einstein equations was first carried out by Deser (1970), who followed this approach in a detailed manner. Deser summarises the analysis thus: "Consistency has therefore led us to universal coupling, which implies the equivalence principle. It is at this point that the geometric interpretation of general relativity arises, since *all matter* now moves in an effective Riemann space of metric $g^{\mu\nu} \equiv \eta^{\mu\nu} + h^{\mu\nu}$. [The] initial flat 'background' space is no longer observable."[1]. This seems to suggest that the only way in which a consistent theory of gravity can be constructed within Special Relativity is to consider the geometry of spacetime as the gravitational field itself. This is precisely General Relativity.

The existence of curved spacetime can be deduced from purely physical arguments. Einstein (1911) showed that a photon must be affected by a gravitational field, using conservation of energy applied to Newtonian gravitation theory. Schild (1960, 1962, 1967) showed by a simple thought experiment, formulated within Special Relativity, that a consistent theory of gravity cannot be constructed within this framework. His argument is based upon a gravitational redshift experiment carried out in the field of the Earth,

[1] $\eta^{\mu\nu}$ is the Minkowski metric.

using a global Lorentz frame tied to the Earth's centre. Successive pulses of light rising to the same height should experience a redshift, and therefore the pulse rate at the top should be slower than that at the bottom. But light rays are drawn at 45° in Minkowski spacetime diagrams, so that top and bottom time intervals are equal, which is impossible if redshift occurs. Hence the spacetime must be curved. The detailed argument, with some improvements, may be found in Misner et al. (1973, page 187). One therefore concludes that in the presence of gravity, Special Relativity cannot be valid over any sufficiently extended region.

1.3 Principles of General Relativity

General Relativity, as the name suggests, was Einstein's generalisation of Special Relativity. Since Special Relativity can comfortably be described using tensor calculus, it was only natural to extend the flat Minkowski spacetime of Special Relativity to the curved (in general) spacetime of General Relativity (Einstein, 1915a,b). This was simply a physical application of Riemannian geometry (Clifford, 1873; Weber, 1953), which had been developed in the second half of the 19th century. The idea of tensor calculus on curved manifolds was already mathematically well-established. Einstein's innovation lay in identifying the Einstein tensor, itself mathematically related to the Riemann curvature tensor, as the 'gravitational field' in the theory. Relativity is thus a geometrical approach to fundamental interactions. These are realised though continuous classical fields which are inseparably correlated to geometrical structures of spacetime, such as the metric, affine connection, and curvature.

Einstein's relativity has three main distinguishing characteristics: it agrees with experiment; it describes gravity entirely in terms of geometry; and it is free of any 'prior geometry'; characteristics lacking in most of the other theories. Ni (1972) and Thorne et al. (1971) contain good reviews of these theories. Apart from the issue of agreement with experiment, on which countless papers have been published in the scientific literature (one very comprehensive review is the article by Will 2001), Einstein's theory is unique in its conceptual simplicity. Every other theory introduces auxiliary gravitational fields, or involves prior geometry.

Prior geometry is any aspect of the geometry of spacetime which is fixed immutably, that is, it cannot be changed by changing the distribution of gravitating sources. One such theory involving prior geometry was formulated by Nordstrøm (1913). In this theory, the physical metric of spacetime $\boldsymbol{g}$ is generated by a background flat spacetime metric $\boldsymbol{\eta}$, and by a scalar gravitational field ϕ. Stress-energy generates ϕ:

$$\eta^{\alpha\beta}\phi_{,\alpha\beta} = -4\pi\phi\eta^{\alpha\beta}T_{\alpha\beta} \tag{1.4}$$

and $\boldsymbol{g}$ is constructed from ϕ and $\boldsymbol{\eta}$:

$$g_{\alpha\beta} = \phi^2\eta_{\alpha\beta}. \tag{1.5}$$

Prior geometry cannot be removed by rewriting Nordstrøm's equations in a form devoid of $\boldsymbol{\eta}$ and ϕ (Einstein & Fokker, 1914). Mass only influences one degree of freedom in

the spacetime geometry, while the other degrees of freedom are fixed *a priori*. This prior geometry, if it existed, could be detected by physical experiments. Whitehead (1922), formulated a two-tensor theory of gravity in which the prior geometry is quite different from Ni's (Ni, 1972). Whitehead's theory is remarkable in that it agrees with Einstein's in its predictions for the 'four standard tests' (bending of light, gravitational redshift, perihelion shift, and time delay). It was accepted as a viable alternative for Einstein's theory until Will (1971) showed that it predicts velocity-independent anisotropies in the Cavendish constant (the gravitational constant G in Newtonian theory). This would produce time-dependent Earth tides which are clearly contradicted by everyday observations. Any valid theory of gravity must not only agree with relativistic experiments, but also with 'past experiments' in the Newtonian regime.

One theory which disagrees violently with non-relativistic experiments is due to Birkhoff (1943). It predicts the same redshift, perihelion shift, deflection and time-delay as General Relativity, but it requires that the pressure inside gravitating bodies should be equal to the total density of mass-energy ($p = \rho$), so that sound waves travel with the speed of light. This clearly contradicts everyday experiments.

Einstein described both the demand for 'no prior geometry' and for a 'geometric, coordinate-independent formulation of physics' by the single phrase 'general covariance', but the two concepts are not quite the same. While many physical theories can be formulated in a generally covariant way, General Relativity is actually based on the 'no prior geometry' demand. This distinction was not always made, especially in the first decades after Einstein's publications (Kretschmann, 1917). Norton (2003), and references therein, contains a discussion of the controversy surrounding Kretschmann's objection to Einstein's interpretation. Anderson (1967) treats the distinction between prior geometry and dynamic fields in a very systematic manner in his textbook on relativity.

One notable theory which introduces auxiliary gravitational fields is Dicke-Brans-Jordan theory, sometimes called Brans-Dicke, or Jordan-Fierz-Brans-Dicke theory (Jordan, 1959; Brans & Dicke, 1961). The different names arise from the fact that the theory is a special case of Jordan's, with $\eta = -1$. An alternative mathematical representation of the theory is given by Dicke (1962). Brans and Dicke took the equivalence principle as the starting point of their theory, and thus they describe gravity in terms of spacetime curvature, but their gravitational field, unlike Einstein's, is a scalar-tensor combination. In this way it overcomes the difficulties associated with tensor or scalar-only theories mentioned earlier. The trace of the energy-momentum tensor $(T_{\mathrm{M}})_{\mu\nu}$ (representing matter) and a coupling constant λ generate the long-range scalar field ϕ via the equation

$$\Box^2\phi = 4\pi\lambda(T_{\mathrm{M}})^{\mu}_{\mu}. \tag{1.6}$$

The scalar field ϕ fixes the value of G, which is therefore not a constant, but simply the coupling strength of matter to gravity. The gravitational field equations relate the curvature to the energy-momentum tensors of the scalar field and matter:

$$R_{\mu\nu} - \tfrac{1}{2}g_{\mu\nu}R = -\frac{8\pi}{c^4\phi}\left[(T_{\mathrm{M}})_{\mu\nu} + (T_{\Phi})_{\mu\nu}\right], \tag{1.7}$$

where $(T_{\mathrm{M}})_{\mu\nu}$ is the energy-momentum tensor of matter and $(T_{\Phi})_{\mu\nu}$ is the energy-momentum

tensor of the scalar field ϕ. For historical reasons, it is usual to write the coupling constant as

$$\lambda = \frac{2}{3 + 2\omega}, \tag{1.8}$$

where ω is the dimensionless 'Dicke coupling constant'. In the limit $\omega \to \infty$, we have $\lambda \to 0$, so ϕ is not affected by the matter distribution, and can be set to a constant $\phi = 1/G$. Hence Dicke-Brans-Jordan theory reduces to Einstein's theory in the limit $\omega \to \infty$.

The equivalence principle is satisfied in this theory since the special-relativistic laws are valid in the local Lorentz frames of the metric g of spacetime. The scalar field does not exert any direct influence on matter. It only enters the field equations that determine the geometry of spacetime. On a conceptual level, Brans-Dicke theory can be seen as more fully Machian than Einstein's theory. Einstein himself attempted to incorporate Mach's Principle into his theory, but in Einstein's General Relativity, the inertial mass of an object will always be independent of the mass distribution in the Universe. In Brans-Dicke theory, the long-range scalar field is an indirectly coupling field, so it does not directly influence matter, but the Einstein tensor is determined partly by the energy-momentum tensor, and partly by the long-range scalar field.

Dicke-Brans-Jordan theory is self-consistent and complete, but experimental evidence, based on Solar-system tests, shows that, as a conservative estimate, $\omega \geq 600$ (Will, 1993). Some recent calculations raise this limit even higher, with $\omega \gtrsim 10^4$ (Psaltis, 2005), so Einstein's theory seems to be valid after all. Brans-Dicke theory is a special case of general tensor-scalar theories with $\omega(\phi) =$ constant, where ϕ is a value depending on the cosmological epoch. In these theories, the function $\omega(\phi)$ could be such that the theory is very different from GR in the early Universe or in future epochs, but very close to GR in the present. Indeed, Damour & Nordtvedt (1993a,b) have shown that GR is a natural 'attractor' for such scalar-tensor theories, since cosmological evolution naturally drives the fields towards large values of ω.

The experimental tests to which Brans-Dicke theory was subjected constitute just one of three fundamental criteria which any viable theory must satisfy: *self-consistency, completeness, and agreement with past experiment*. It is self-evident that any alternative theory to General Relativity must satisfy experimental tests which have already been carried out ('past experiment'). The other two criteria can be investigated on a theoretical level.

To be self-consistent, a theory must not contain any internal contradictions. The spin-two field theory of gravity (Fierz & Pauli, 1939) described earlier is equivalent to linearised General Relativity but it is internally inconsistent since it predicts that gravitating bodies should have their motion unaffected by gravity. When one tries to remedy this inconsistency, the resulting theory is nothing but General Relativity. Another self-inconsistent theory is due to Kustaanheimo (1966). It predicts zero gravitational redshift when the wave version of light (Maxwell theory) is used, and nonzero redshift when the particle version (photon) is used.

To be complete, a theory must be able to analyse the outcome of any experiment. This means that it must be compatible with other physical theories which describe any other forces that are present in experiments. This can only be achieved if the theory is derived from first principles, since the theoretical postulates must be as general as possible

if the theory is to cover the widest range of phenomena.

A viable theory must agree with past experiment, which includes experiments in the Newtonian regime, and the standard tests of General Relativity. This means that its results must agree with those obtained from Newtonian theory in the weak field limit, and with GR in relativistic situations. It also means that the theory must agree with cosmological observations.

The experimental criterion also works the other way. Any alternative to General Relativity that claims to have a smaller set of limiting cases must be experimentally distinguishable, perhaps by future experiment. At some point, the divergence between GR and other theories must manifest itself physically, in the form of predictions which can be verified by experiment.

Most theories of gravity incorporate two principles: *spacetime possesses a metric; and that metric satisfies the equivalence principle*. Such theories are called metric theories. One notable exception is Cartan's theory. It is generally easier to incorporate the non-gravitational laws of physics within metric theories, since other theories would result in greater complexity, rendering calculations difficult. The only way in which metric theories significantly differ from each other is in their laws for the generation of the metric. In General Relativity and Brans-Dicke theory, for example, the metric is generated by different fields.

1.4 Formalism of General Relativity

The two central notions in GR, sometimes referred to collectively as the Equivalence Principle, are:

- **The Strong Equivalence Principle:** The laws of physics take the same form in a freely-falling reference frame as in Special Relativity (SR), and
- **The Weak Equivalence Principle:** An observer in freefall should experience no gravitational field.

In GR, the distance between two points in 4-dimensional spacetime is described by the metric tensor. The separation $\mathrm{d}s$ is given by

$$\mathrm{d}s^2 = c^2\,\mathrm{d}\tau^2 = g_{\mu\nu}\,\mathrm{d}x^\mu\,\mathrm{d}x^\nu. \tag{1.9}$$

The Equivalence Principle allows us to construct the metric and the equation of motion by transforming from a freely-falling to an accelerating frame. The General Relativistic equation of motion is therefore given by

$$\frac{\mathrm{d}^2x^\mu}{\mathrm{d}\tau^2} + \Gamma^\mu_{\alpha\beta}\frac{\mathrm{d}x^\alpha}{\mathrm{d}\tau}\frac{\mathrm{d}x^\beta}{\mathrm{d}\tau} = 0 \tag{1.10}$$

where x^μ is some set of coordinates for a point in spacetime. $\Gamma^\mu_{\alpha\beta}$ are the components of the affine connection (or metric connection). The fundamental theorem of Riemannian

geometry states that the affine connection can be expressed entirely in terms of the metric:

$$\Gamma^{\alpha}_{\lambda\nu} = \frac{1}{2} g^{\alpha\nu}(g_{\mu\nu,\lambda} + g_{\lambda\nu,\mu} - g_{\mu\lambda,\nu}), \tag{1.11}$$

where the comma denotes a derivative, i.e. $g_{\mu\nu,\lambda} = \frac{\partial g_{\mu\nu}}{\partial x^{\lambda}}$.

We need to construct invariant quantities in GR (quantities that are the same for all observers). To achieve this, we need to contract the the covariant A_{μ} and contravariant A^{μ} components of a vector or tensor A by using the metric to raise or lower indices: $A_{\mu} = g_{\mu\nu}A^{\mu}$. Thus the equation of motion (1.10) can be made covariant by recasting it as the covariant derivative of the 4-velocity $U^{\mu} = \gamma(c, \mathbf{v})$:

$$\frac{D_{\mu}U^{\mu}}{\mathrm{d}\tau} = 0 \tag{1.12}$$

where the covariant derivative is defined as

$$D_{\mu}A^{\mu} = \mathrm{d}A^{\mu} + \Gamma^{\mu}_{\alpha\beta}A^{\alpha}\,\mathrm{d}x^{\beta} \tag{1.13}$$

The transformation from SR to GR is then carried out by mapping the Minkowski metric to a general metric: $\eta \to g$ and by mapping $\partial \to D$.

In GR, freely-falling bodies travel along a geodesic. Geometrically, this is the shortest distance between two points in spacetime. The path length along a geodesic is given by

$$S = \int (g_{\mu\nu}\,\mathrm{d}x^{\mu}\,\mathrm{d}x^{\nu})^{1/2}. \tag{1.14}$$

In cosmology it is essential for us to be able to describe spacetime which is not 'empty'. In the presence of a perfect fluid (an inviscid fluid with density ρ and isotropic pressure p), the energy and momentum of spacetime is described by the energy-momentum tensor (or stress-energy tensor)

$$T^{\mu\nu} = \left(\rho + \frac{p}{c^2}\right) U^{\mu}U^{\nu} - pg^{\mu\nu}. \tag{1.15}$$

Classical energy and momentum conservation are generalised in GR as the four conservation laws

$$D_{\mu}T^{\mu\nu} = 0. \tag{1.16}$$

In other words, the stress-energy tensor has a vanishing covariant divergence. In the absence of a component possessing pressure or density, or both, the energy-momentum tensor is zero.

The central notion in General Relativity is that gravitation can be described by a metric. The Einstein equations give us the relation between the metric and the matter and energy in the Universe:

$$G^{\mu\nu} = -\frac{8\pi G}{c^4}T^{\mu\nu}. \tag{1.17}$$

The left-hand side of this equation is a function of the metric: $G^{\mu\nu}$ is the Einstein tensor, defined as:

$$G^{\mu\nu} = R^{\mu\nu} - \frac{1}{2}g^{\mu\nu}R, \tag{1.18}$$

where $R^{\mu\nu}$ is the Ricci tensor, which depends on the metric and its derivatives, and the Ricci scalar R is the contraction of the Ricci tensor ($R = g_{\mu\nu}R^{\mu\nu}$). The right-hand side of Equation 1.17 is a function of the energy: G is Newton's constant, and $T^{\mu\nu}$ is the energy-momentum tensor.

1.5 Standard Cosmology

When Einstein published his seminal GR papers it became almost immediately apparent that the theory could be applied to the whole Universe, under certain assumptions, to obtain a relativistic cosmological description. If the content of the Universe is known, then the energy-momentum tensor can be constructed, and the metric derived using Einstein's equations. The first expanding-universe solutions to the relativistic field equations, describing a universe with positive, zero and negative curvature, were discovered by Friedmann (1922, 1924), even before Hubble's observations of galactic redshifts empirically proved that the Universe is not static. The problem was independently followed up during the 1930s by Lemaître (1927), and by Robertson (1935, 1936a,b) and Walker (1937).

These exact solutions define what came to be known as the Friedmann-Lemaître-Robertson-Walker (FLRW) metric[2]. This metric starts with the assumption of spatial homogeneity and isotropy, allowing for time-dependence of the spatial component of the metric. Indeed, it is the only metric which can exist on homogenous and isotropic spacetime. The assumption of homogeneity and isotropy, known as the Cosmological Principle, follows from the Copernican Principle, which states that we are not privileged observers in the Universe. This is of course not true below a certain scale, but it does simplify the description of the distribution of mass in the Universe.

The FLRW metric, therefore, describes a homogeneous, isotropic universe, with matter uniformly distributed as a perfect fluid, and is written as:

$$-\mathrm{d}s^2 = c\mathrm{d}\tau^2 - R^2(t)[\mathrm{d}r^2 + S_k^0(r)(\mathrm{d}\theta^2 + \sin^2\theta\mathrm{d}\phi^2)], \tag{1.19}$$

where r is a time independent comoving distance, θ and ϕ are the transverse polar coordinates, and t is the cosmic time. $R(t)$ is the scale factor of the Universe, which shall be discussed further in the following section. The function $S_k^0(r)$ is defined as:

$$S_k^0(r) = \begin{cases} \sin(r) & (k = +1) \\ r & (k = 0) \\ \sinh(r) & (k = -1) \end{cases} \tag{1.20}$$

where k is the geometric curvature of spacetime, the values 0, 1, and -1 indicating flat,

[2]It is also referred to as the FRW, RW, or FL metric.

positively curved, and negatively curved spacetime respectively. Another common form of the metric defines the comoving distance as $S_k^0(r) \to r$, so that

$$-\,\mathrm{d}s^2 = c\,\mathrm{d}t^2 - R^2(t)\left[\frac{\mathrm{d}r^2}{1-kr^2} + r^2(\,\mathrm{d}\theta^2 + \sin^2\theta\,\mathrm{d}\phi^2)\right]. \tag{1.21}$$

The dimensionless scale factor $a(t)$ is defined as

$$a(t) \equiv \frac{R(t)}{R_0} \tag{1.22}$$

where R_0 is the present scale factor (i.e. $a = 1$). The scale factor is therefore a function of time, so it can be abbreviated to a. The metric can then be written in a dimensionless form

$$-\,\mathrm{d}s^2 = c^2\,\mathrm{d}\tau^2 = c^2\,\mathrm{d}t^2 - a^2\left[\,\mathrm{d}r^2 + S_k^2(r)(\,\mathrm{d}\theta^2 + \sin^2\theta\,\mathrm{d}\phi^2)\right], \tag{1.23}$$

where $S_k(r)$ can be redefined as

$$S_k(r) = \begin{cases} R_0\sin(r/R_0) & (k=+1) \\ r & (k=0) \\ R_0\sinh(r/R_0) & (k=-1). \end{cases} \tag{1.24}$$

Equivalently, using the definition in Equation 1.21,

$$-\,\mathrm{d}s^2 = c^2\,\mathrm{d}t^2 - a^2\,\mathrm{d}t^2 - a^2\left[\frac{\mathrm{d}r^2}{1-k(r/R_0)^2} + r^2(\,\mathrm{d}\theta^2 + \sin^2\theta\,\mathrm{d}\phi^2)\right]. \tag{1.25}$$

1.5.1 Cosmological redshift and expansion

The FLRW metric relates the spacetime interval $\mathrm{d}s$ to the cosmic time t and the comoving coordinates through the scale factor $R(t)$. The scale factor is the key quantity of any cosmological model, since it describes the evolution of the Universe. We therefore need to measure distances (in an expanding universe) if we are to find $R(t)$. We can measure two kinds of distances: the comoving distance or the physical distance, which will be discussed in the next section. The comoving distance between a source and an observer is defined to be a constant:

$$r = \int_0^e \mathrm{d}s = \int_{t_\epsilon}^{t_0} \frac{c\,\mathrm{d}t}{a(t)} = \text{constant} \tag{1.26}$$

Differentiating with respect to t_e we obtain the inverse time interval

$$\frac{\mathrm{d}t_0}{\mathrm{d}t_e} = \frac{a(t_0)}{a(t_e)}, \tag{1.27}$$

which can be interpreted in terms of the frequency of emitted and received light:

$$\frac{\mathrm{d}t_0}{\mathrm{d}t_e} = \frac{\nu_e}{\nu_o} = \frac{\lambda_0}{\lambda_e}. \tag{1.28}$$

The redshift is then defined as the relative change in wavelength between emission and observation:

$$z = \frac{\lambda_0 - \lambda_e}{\lambda_e}, \tag{1.29}$$

so that the redshift is related to the scale factor by:

$$\frac{a(t_0)}{a(t_e)} = 1 + z \tag{1.30}$$

and $a = (z+1)^{-1}$ since we have defined $a(t_0) = 1$. The redshift is related, via the Doppler effect, to the apparent recessional velocity of a source by:

$$1 + z \approx 1 + \frac{v}{c}. \tag{1.31}$$

Hubble (1929) observed that the redshift of a galaxy is proportional to its distance and (via Equation 1.31) formulated Hubble's law: $v = H_0 r$, where H_0 is the constant of proportionality. The Hubble constant H_0 is the value of the Hubble parameter at the present epoch. In general, the time-varying Hubble parameter is related to the scale factor by:

$$H(t) = \frac{\dot{a}(t)}{a(t)}. \tag{1.32}$$

The Hubble constant is usually expressed as:

$$H_0 = 100h\,\mathrm{kms}^{-1}\mathrm{Mpc}^{-1}. \tag{1.33}$$

The Megaparsec is the standard distance measure used in cosmology for convenience, and $1\,\mathrm{Mpc} = 3.08568025 \times 10^{22}\,\mathrm{m}$.

1.5.2 Dynamics of the expansion

By combining the GR field equations (1.17) and the definition of the metric (Equation 1.25), we obtain two independent Einstein equations:

$$\left(\frac{\dot{a}}{a}\right)^2 + \frac{kc^2}{a^2} = \frac{8\pi G}{3}\rho \tag{1.34}$$

and

$$2\left(\frac{\ddot{a}}{a}\right) + \left(\frac{\dot{a}}{a}\right) + \frac{kc^2}{a^2} = -\frac{8\pi G}{c^2}p. \tag{1.35}$$

Equation 1.34 is known as the Friedmann equation. It relates the total density ρ of the Universe, including all contributions, to its global geometry. There exists a critical density ρ_c for which $k = 0$. By rearranging the Friedmann equation and using the definition of the Hubble parameter (Equation 1.32) we then obtain

$$\rho_c(t) = \frac{3H^2(t)}{8\pi G}. \tag{1.36}$$

A universe whose density is above this value will have a positive curvature, that is, it will be spatially closed (k=+1); one whose density is less than or equal to this value will be spatially open ($k = 0$ or $k = -1$).

A dimensionless density parameter for any fluid component of the Universe can be defined by

$$\Omega(t) = \frac{\rho(t)}{\rho_c(t)} = \frac{8\pi G\rho(t)}{3H^2(t)}. \tag{1.37}$$

The current value of the density parameter is denoted Ω_0.

Subtracting Equation 1.34 from 1.35 yields the acceleration equation:

$$\frac{\ddot{a}}{a} = -4\pi G\left(\frac{\rho}{3} + \frac{p}{c^2}\right). \tag{1.38}$$

We can also use the same equations to construct the fluid equation, or continuity equation, which describes the relation between the density and pressure, and their evolution:

$$\dot{\rho} + 3\frac{\dot{a}}{a}\left(\rho + \frac{p}{c^2}\right) = 0. \tag{1.39}$$

This is valid for any fluid component of the Universe: baryonic and nonbaryonic matter, radiation, etc.

1.6 Cosmological components

It is a convenient approximation to divide the components of the Universe into distinct parts, which are assumed to evolve independently. This is physically valid at late cosmological times, when the components are decoupled, so the density evolutions are distinct. We shall now review the properties of the different mass-energy components.

1.6.1 Dust

Matter which is pressureless is referred to as 'dust'. This is a useful approximation for cosmological structures which do not interact, such as individual galaxies. Substituting $p_m = 0$ in the equation of state for dust shows that the density of this component scales as:

$$\rho_m(a) = \frac{\rho_{m,0}}{a^3} \tag{1.40}$$

where $\rho_{m,0}$ is the current density. Assuming spatial flatness, the time evolution of the scale factor is then

$$a(t) = \left(\frac{t}{t_0}\right)^{2/3}, \tag{1.41}$$

which gives us

$$H(t) = \frac{2}{3t}. \tag{1.42}$$

This is known as the Einstein-de Sitter (EdS) solution, and it describes the evolution of H in a constant-curvature homogeneneous universe with a pressureless fluid as the only

component.

1.6.2 Radiation

In the early Universe, the energy content was dominated by photons and relativistic particles (especially neutrinos). The expansion of the Universe dilutes the radiation fluid, and the wavelength is increased by the expansion so that the energy decreases. From thermodynamics,

$$E_{\rm rad} = \rho_{\rm rad} c^2 = \alpha T^4, \tag{1.43}$$

where T is the radiation temperature and α is the Stefan-Boltzmann constant. The equation of state for radiation can then be derived from the fluid equation (1.39):

$$\rho_{\rm rad}(a) = \frac{\rho_{\rm rad,0}}{a^4} \quad ; \quad p_{\rm rad} = \frac{\rho_{\rm rad} c^2}{3}. \tag{1.44}$$

Combining this with the Friedmann equations, and assuming flatness ($k = 0$), we obtain the time dependence of the scale factor and the Hubble parameter:

$$a(t) = \left(\frac{t}{t_0}\right)^{1/2} \quad ; \quad H(t) = \frac{1}{2t}. \tag{1.45}$$

1.6.3 Dark energy

In this section we shall briefly introduce dark energy as a fluid component with a distinct equation of state, without going into the historical background, and without justifying the equations on physical grounds. These details will be discussed in Section 1.13.

Dark energy is a fluid component whose equation of state is:

$$p_{\rm DE} = w c^2 \rho_{\rm DE}. \tag{1.46}$$

This is the equation of state in its most general form, since w can be any function of redshift, scale factor or cosmic time, with the constraint that $w \leq 0$ (i.e. the fluid has a negative pressure). Assuming that $w = w(a)$, and using the fluid Equation 1.39, we have the following density-scale relation:

$$\rho_{\rm DE}(a) = \rho_{\rm DE,0} \mathrm{e}^{-3\int_a^1 [1+w(a')]\,\mathrm{d}(\ln a')}. \tag{1.47}$$

It can be seen that in the special case of a constant $w = -1$, the fluid equation implies that the density is constant. Using the Friedmann equation (1.34), we can show that in this case, as the scale factor increases, kc^2/a^2 becomes negligible compared to the other terms. The scale factor then has the functional form:

$$a(t) = a(t_0) \mathrm{e}^{\left(\frac{8\pi G \rho_{\rm DE}}{3}\right)^{1/2} t} = a(t_0) \mathrm{e}^{\left(\frac{\Lambda c^2}{3}\right)^{1/2} t}, \tag{1.48}$$

where $\Lambda = 8\pi G \rho_{\rm DE}/c^2$. This is the same as the de Sitter solution.

1.7 The Hubble parameter

In the previous section we have described the various cosmological components in the Standard Model. The total density of the Universe in terms of its constituent components can be written as the sum of the densities of these components at any given time or scale factor:

$$\rho = \rho_m + \rho_{\rm rad} + \rho_{\rm DE} \tag{1.49}$$

The total dimensionless density can then be written:

$$\Omega = \Omega_m + \Omega_{\rm rad} + \Omega_{\rm DE}, \tag{1.50}$$

where we have dropped the subscript for clarity, i.e. $\Omega_{m,0} = \Omega_m$, etc. This notation will be used throughout this thesis, unless otherwise specified. The Friedmann equation (1.34) can now be rewritten using the equations of state for the different components:

$$H^2(a) = \frac{8\pi G}{3}\left(\rho_m a^{-3} + \rho_{\rm rad} a^{-4} + \rho_{\rm DE} \mathrm{e}^{-3\int_a^1 [1+w(a')]\,\mathrm{d}(\ln a')}\right) - \frac{kc^2}{a^2}. \tag{1.51}$$

This can be rearranged to give:

$$H^2(a) = H_0^2\left[\Omega_m a^{-3} + \Omega_{\rm rad} a^{-4} + \Omega_{\rm DE} \mathrm{e}^{-3\int_a^1 [1+w(a')]\,\mathrm{d}(\ln a')} + (1-\Omega)a^{-2}\right], \tag{1.52}$$

or, in terms of redshift:

$$\begin{aligned} H^2(z) = H_0^2\Big[&\Omega_m(1+z)^3 + \Omega_{\rm rad}(1+z)a^4 \\ &+ \Omega_{\rm DE}\mathrm{e}^{-3\int_0^z [1+w(z')]/(1+z')\,\mathrm{d}(\ln z')} + (1-\Omega)(1+z)^2\Big]. \end{aligned} \tag{1.53}$$

The term $1-\Omega$ is sometimes replaced by Ω_k, the density due to the intrinsic geometry of spacetime. Equation 1.53 is of central importance since it relates the redshift of an object to the global density components and geometry of the Universe.

One parameter which has become defunct since the discovery of dark energy and the acceleration of the Universe's current expansion is the deceleration parameter, defined as:

$$q = -\frac{a\ddot{a}}{\dot{a}^2}. \tag{1.54}$$

1.8 Cosmological distance measures

The notion of distance is fairly straightforward in Euclidean geometry. In General Relativity, however, where we work with generally curved spacetime, the meaning of 'distance' is no longer unique. The separation between events in spacetime depends on the definition of the distance being used.

1.8.1 Proper distance

In cosmology, the proper distance between two events at redshifts z_1 and z_2 is defined as the light travel time between them: $\mathrm{d}D_{\mathrm{proper}} = c\,\mathrm{d}t$, which after rearranging becomes:

$$\mathrm{d}D_{\mathrm{proper}} = c\frac{\mathrm{d}a}{a}. \tag{1.55}$$

This gives us:

$$D_{\mathrm{proper}}(z_1, z_2) = \int_{a_2(z_2)}^{a_2(z_1)} \frac{c\,\mathrm{d}a}{aH(a)} \tag{1.56}$$

$$= \int_{z_2}^{z_1} \frac{c\,\mathrm{d}z}{H(z)(1+z)}. \tag{1.57}$$

Hence, for an observer at $z_1 = 0$, the proper distance to an object at redshift z is:

$$D_{\mathrm{proper}}(z) = \int_0^z \frac{c\,\mathrm{d}z'}{H(z')(1+z')}. \tag{1.58}$$

1.8.2 Comoving distance

The comoving distance is defined as the distance on the spatial hypersurface at $t = t_0$ between the worldline of two events. Rearranging $\mathrm{d}r = \mathrm{d}D_{\mathrm{com}} = a^{-1}c\,\mathrm{d}t$ gives us $\mathrm{d}r = \mathrm{d}D_{\mathrm{com}} = c\frac{\mathrm{d}a}{a\dot{s}}$ so that:

$$D_{\mathrm{com}}(z_1, z_2) = \int_{a_2(z_2)}^{a_2(z_1)} \frac{c\,\mathrm{d}a}{a^2H(a)} \tag{1.59}$$

$$= \int_{z_2}^{z_1} \frac{c\,\mathrm{d}z}{H(z)} \tag{1.60}$$

For an observer $z_1 = 0$ the comoving distance distance to an object at redshift s is:

$$D_{\mathrm{com}}(z) = \int_0^z \frac{c\,\mathrm{d}z'}{H(z')}. \tag{1.61}$$

Note that the comoving distance r, defined in Equation 1.26, is equal to D_{com}.

1.8.3 Angular diameter distance

The angular diameter distance relates the redshift of an object to the angle it subtends. In Euclidean geometry, the angular diameter distance relates the cross-sectional area of an object $\mathrm{d}A$ to the solid angle subtended by the object, as measured by an observer $\mathrm{d}\Omega$:

$$\mathrm{d}A = D^2_{\mathrm{ang}}(z_1, z_2)\,\mathrm{d}\Omega. \tag{1.62}$$

For an object at redshift z_2, the surface area of a sphere of radius $\mathcal{R} = a(z_2)S_k[D_{\mathrm{com}}(z_1, z_2)]$ centred on the object will be $A = 4\pi\mathcal{R}^2 = 4\pi a^2(z_2)S_k^2[D_{\mathrm{com}}(z_1, z_2)]$, and the angle sub-

tended would be 4π, so that

$$\frac{\mathrm{d}A}{4\pi a^2(z_2)S_k^2[D_{\mathrm{com}}(z_1,z_2)]} = \frac{\mathrm{d}\Omega}{4\pi}. \tag{1.63}$$

The angular diameter distance between objects at z_1 and z_2 is then defined as:

$$D_{\mathrm{ang}}(z_1,z_2) = a(z_2)S_k[D_{\mathrm{com}}(z_1,z_2)]. \tag{1.64}$$

Thus, for an observer at $z_1 = 0$, an object at redshift z will have an angular diameter distance

$$D_{\mathrm{ang}}(z) = (1+z)^{-1}S_k[D_{\mathrm{com}}(z)]. \tag{1.65}$$

1.8.4 Luminosity distance

Like the angular diameter distance, the luminosity distance can be defined by analogy to Euclidean geometry. The luminosity distance can be visualised as the distance at which a source would be if the inverse-square law were to apply. It is related to the observed flux S and the luminosity L of a source by:

$$D_{\mathrm{lum}} = \left(\frac{L}{4\pi S}\right)^{1/2}. \tag{1.66}$$

The luminosity distance is given in terms of the comoving and angular diameter distance by:

$$D_{\mathrm{lum}}(z_1,z_2) = \left[\frac{a(z_1)}{a(z_2)}\right]^2 D_{\mathrm{ang}}(z_1,z_2) = \frac{a(z_1)^2}{a(z_2)}S_k[D_{\mathrm{com}}(z_1,z_2)]. \tag{1.67}$$

Therefore, for an observer at $z_1 = 0$, an object at redshift z will have:

$$D_{\mathrm{lum}}(z) = (1+z)S_k[D_{\mathrm{com}}(z)]. \tag{1.68}$$

Equation 1.67 involves three factors which are related to the frequency and flux of incoming photons. Firstly, the photons are cosmologically redshifted by a factor $a(z_1)/a(z_2)$. Secondly, time dilation adds a further frequency shift of $a(z_1)/a(z_2)$. Finally, the size of the sphere centred on an observer, upon which photons arrive, will increase in surface area between z_1 and z_2 by a factor of $[a(z_1)/a(z_2)]^2$. These effects combine to give a total factor of $[a(z_1)/a(z_2)]^4$ in Equation 1.67.

1.9 The early Universe

In order to explain the Standard Model, and the current Universe and its components, it is necessary for us to review the early Universe. In the Standard Model, it is generally accepted that the Universe arose from an initial singularity, often termed the 'Big Bang', which occurred some 13.7 billion years ago (as measured by WMAP-5, Dunkley et al., 2009). This is not discussed here, but it should be noted that there are several proposals for the mechanism of this singularity. During this epoch, we are dealing with Planck

scale physics, so most of these mechanisms involve quantum gravity. Other proposals (such as some superstring and braneworld theories) do away with the need for an initial singularity altogether. The aspects of the early Universe are approximately, though not precisely, presented in cosmological chronological order.

1.9.1 The Cosmic Microwave Background

We have seen that $\rho_{\rm rad} \propto a^{-4}$, so the temperature evolution of the Universe, from an initial T_0, is:

$$T = \frac{T_0}{a}. \tag{1.69}$$

In other words, the Universe cools as it expands. Conversely, this means at early times, when the scale factor was close to zero, the temperature was very high (hence the 'Hot Big Bang'). The radiation left from the early hot Universe, cooled by expansion, is known as the Cosmic Microwave Background, or CMB.

The first direct observational evidence for the Hot Big Bang was the discovery of the CMB by Penzias & Wilson (1965). The CMB is an extremely isotropic source of microwave radiation, with a spectrum corresponding to a perfect blackbody at a temperature $T_0 = 2.728 \pm 0.004/, \mathrm{K}$. Using the current temperature and $E_{\rm rad} = \rho_{\rm rad} c^2 = \alpha T^4$, the radiation density is given by:

$$\Omega_{\rm rad} = 2.47 \times 10^{-5} h^{-2}. \tag{1.70}$$

At some time in the early Universe, the ambient radiation temperature corresponded to the ionisation potential of hydrogen, which is 13.6 eV. During this epoch, the Universe was filled with a sea of highly energetic particles and photons — a hot ionised plasma. The particles were mainly electrons and protons. Other fundamental particles (quarks) existed earlier when the ambient energy corresponded to their rest mass. At some point, as the Universe expanded and cooled, the energy of the photons was no longer sufficient to ionise the hydrogen, and within a relatively short time, all of the electrons and protons combined to form neutral hydrogen. The photons were then free to move through the Universe. This process is known as decoupling and it occurred at a temperature of $\sim 2500\,\mathrm{K}$, when the Universe was approximately 375938^{+3148}_{-3115} years old (Dunkley et al., 2009). It is these decoupled photons which make up the CMB. The surface on the sky from which these photons originate is known as the surface of last scattering.

1.9.2 Matter-radiation equality

At the present epoch, neglecting dark energy, the Universe is dominated by matter. This component is characterised by the fact that the particles can be treated in a non-relativistic régime, whereas photons and relativistic neutrinos both behave like radiation. The total contribution to the energy density from non-relativistic components and relativistic components can be written as $\rho_{\rm NR}$ and $\rho_{\rm R}$, respectively. The ratio of the contributions of the components is (see Dodelson, 2003):

$$\frac{\rho_{\rm R}}{\rho_{\rm cr}} = \frac{4.15 \times 10^{-5}}{h^2 a^4} \equiv \frac{\Omega_{\rm rad}}{a^4}. \tag{1.71}$$

Then there must exist a scale factor for which the ratio is unity. This is given by:

$$a_{\rm eq} = \frac{4.15 \times 10^{-5}}{\Omega_m h^2}, \tag{1.72}$$

or, in terms of redshift,

$$1 + z_{\rm eq} = 2.4 \times 10^4 \Omega_m h^2. \tag{1.73}$$

The epoch at which the matter energy density equals the radiation energy density is called matter-radiation equality, and it has a special role in large-scale structure formation.

1.9.3 Nucleosynthesis and baryogenesis

The temperature during the early Universe was high enough for nuclear reactions to occur. This is termed the epoch of primordial nucleosynthesis. Similarly to decoupling, before ~ 400 seconds the energy of the ambient photons (~ 0.1 MeV) was such that any nuclei formed would be dissociated, since the photon energy was greater than the binding energy of the nuclei. When the temperature fell, nucleosynthesis became possible. This occurred at a temperature when the nucleons were non-relativistic.

Before this point, protons and neutrons were in thermal equilibrium, and the respective population numbers were nearly equal. The decay of a proton to a neutron occurs via β^- decay:

$$n \rightleftharpoons p + e^- + \overline{\nu}_e + 0.8\,{\rm MeV}. \tag{1.74}$$

The nucleon plasma remains in equilibrium while the temperature remains 0.8 MeV or higher. Once the temperature drops below this, the leftward reaction becomes harder, and neutrinos freeze out of the plasma. At this point, nucleosynthesis can proceed, with the creation of the lightest elements (deuterium, helium-3, lithium-7, beryllium-7).

It is beyond the scope of this thesis to go into the details of primordial nucleosynthesis. We simply note that the present epoch baryon and photon densities determine the primordial abundance of light elements. This abundance can be measured from absorption lines in the line-pf-sight to high-redshift objects and from CMB observations, and therefore provides a constraint for the present-epoch baryon density Ω_b. WMAP-5 has constrained this value to $\Omega_b = 0.0462 \pm 0.0015$ (Dunkley et al., 2009). The term 'baryonic matter' is taken to mean any form of non-relativistic, gravitating matter which interacts with photons. Thus we include all nuclei and electrons under the heading 'baryonic matter', even though electrons are leptons.

1.9.4 Neutrinos

Unlike photons and baryons, cosmic neutrinos have not been observed. However, particle physics allows us to chart the history of this particle during nucleosynthesis, and to relate the neutrino temperature to the photon temperature today. The details of the calculations can be found in Dodelson (2003), and in the review by Quigg (2008).

Neutrinos are fermions, with a Fermi-Dirac distribution with zero chemical potential. When they decoupled from the plasma, their distribution remained Fermi-Dirac, with their temperature falling as a^{-1}. This decoupling occurred slightly before the annihilation

of electrons and positrons, which occurred when the cosmic temperature was of the order of the electron mass ($T \approx m_e$). Neutrinos decoupled when the cosmic plasma had a temperature of around 1 MeV. The energy associated with this annihilation was therefore not inherited by the neutrinos, and the entropy was completely transferred to the entropy of the photon background. Thus:

$$(S_\mathrm{e} + S_\gamma)_\mathrm{before} = (S_\gamma)_\mathrm{after}, \tag{1.75}$$

where S_e and S_γ are respectively the entropy of the electron-positron pairs and the photon background, and 'before' and 'after' refer to the annihilation time.

The entropy per particle species, ignoring constant factors, is $S \propto gT^3$, where g is the statistical weight of the species. For bosons, $g = 1$ and for fermions, $g = 7/8$ per spin state. From particle physics, we know that the neutrino has one spin degree of freedom, that each neutrino has an antiparticle, and that there are three generations, also called 'families' or 'species' (μ, τ and electron neutrinos). This means that the degeneracy factor of neutrinos is equal to six. Before annihilation, the fermions are electrons (2 spin states), positrons (2), neutrinos and antineutrinos (6 spin states). The bosons are photons (2 spin states). We therefore have $g_\mathrm{before} = 4(7/8) + 2 = 11/2$, while after annihilation $g = 2$ because only photons remain. Applying entropy conservation and counting relativistic degrees of freedom, the ratio of neutrino and photon temperatures below m_e is therefore:

$$\frac{T_\nu}{T} = \left(\frac{4}{11}\right)^{1/3}, \tag{1.76}$$

so that the present neutrino temperature is

$$T_{\nu,0} = \left(\frac{4}{11}\right)^{1/3} T_\mathrm{CMB} = 1.945\,\mathrm{K}. \tag{1.77}$$

The number density of neutrinos is then (see Elgarøy & Lahav, 2005)

$$n_\nu = \frac{6\zeta(3)}{11\pi^2} T_\mathrm{CMB}^3, \tag{1.78}$$

where $\zeta(3) \approx 1.202$, which gives $n_\nu \approx 112\,\mathrm{cm}^{-}3$ at the present epoch. At late times, when massive neutrinos have become non-relativistic, their contribution to the mass density $m_\nu n_\nu$, giving

$$\Omega_\nu h^2 = \frac{m_\nu}{94\mathrm{eV}} \tag{1.79}$$

for $T_\mathrm{CMB} = 2.726\,\mathrm{K}$. This is the expression used in our calculations to relate the total neutrino mass to the neutrino fraction. It should be noted that this equation can be modified by many factors: a non-zero initial chemical potential, or a sizeable neutrino-antineutrino asymmetry, or even a fourth, 'sterile' neutrino, for instance (see the references in Elgarøy & Lahav 2005). However, Equation 1.78 should be accurate in the Standard Model, and therefore any constraint on the neutrino fraction can be translated on a constraint on the total neutrino mass via Equation 1.79. In Chapter 4 we shall discuss the effect of neutrino physics on the matter power spectrum.

1.10 Inflation and the primordial power spectrum

The Hot Big Bang model was successful in explaining many interlinked phenomena which were subsequently confirmed by observation: The Hubble Law and the expansion of the Universe, the thermal history of the Universe, primordial nucleosynthesis, the existence of the cosmic microwave background, the relation between the temperature and scale factor, and finally the blackbody nature of the CMB. The remarkable fact is that these phenomena occur on extremely different scales, and are observed via different physical processes, and yet they all fit neatly within one model. However, the Hot Big Bang model fails to provide a solution to a number of outstanding cosmological problems. This gave rise to the idea of a model in which the early Universe undergoes a period of exponential accelerated expansion. This theory, called 'inflation', was first formulated by Guth (see Guth, 1997).

It was realised that inflation solves a number of these cosmological problems linked to the primordial Universe, the most commonly cited being the following (for details see Guth, 1997; Peacock, 1999; Liddle & Lyth, 2000, and references therein):

- The Horizon Problem: How did causally-disconnected regions of the CMB come to be in thermal equilibrium?
- The Flatness Problems: Why is the global geometry of the Universe so flat?
- The Monopoles Problem: Grand Unified Theories predict the production of a large number of monopoles. Why are none observed?

In the context of this thesis, our interest in inflation lies in its link with structure formation: it provides a mechanism for the power spectrum of primordial perturbations. In the Standard ΛCDM Model, the initial perturbations from which structure evolved are assumed to have a scale-invariant spectrum (this will be explained in Section 1.12.4). Reconstructing the primordial power spectrum is no easy task, and poses two main problems. Observationally, we want to extract the amplitude and scale variation from the data. Theoretically, we seek to explain the origin of the perturbations. At present, the leading theoretical paradigm for the primordial fluctuations is inflation, which provides initial conditions for both large-scale structure and the cosmic microwave background radiation. The theory of inflation offers a plethora of models, each of which predicts a certain power spectrum of primordial fluctuations $\mathcal{P}(k)$. Since the inflationary paradigm is linked to the theoretical description of the primordial power spectrum, it is necessary to briefly explain some of the main concepts here. We shall not go into the details of the theory, nor the motivation for inflation (see Liddle & Lyth, 2000, for the full details).

The precise definition of inflation is any period during which the scale factor of the Universe is accelerating, that is, $\ddot{a} > 0$. Equivalently, we can use the expression

$$\frac{\mathrm{d}}{\mathrm{d}t}\frac{H^{-1}}{a} < 0, \tag{1.80}$$

which physically means that the observable Universe becomes smaller during inflation.

The basic theory of inflation states that from the initial big bang singularity to approximately 10^{-37} seconds, there existed a set of highly energetic scalar fields. By

definition, Ω is driven towards 1 during inflation. Inflationary theories assume that gravity is described by GR, which means that the component driving inflation must satisfy $\rho + 3P < 0$. The Universe was dominated during the inflationary phase by a scalar field (or set of fields) ϕ with a self-interaction potential $V(\phi)$. It is the form of this potential which differentiates the various inflationary theories. Most theories assume a 'Mexican hat' potential, with a single field, while chaotic inflation assumes a simple power law potential with a slowly varying field (see e.g. Linde 1989). The action for this potential is then (Lidsey et al., 1997)

$$S = -\int \mathrm{d}^4x\sqrt{-g}\left[\frac{m_{\mathrm{Pl}}^2 R}{16\pi} - \frac{1}{2}(\nabla\phi)^2 + V(\phi)\right], \tag{1.81}$$

where m_{Pl} is the Planck mass. As the Universe cooled, the scalar field became trapped in a false vacuum, so its energy density became constant. The potential energy, however, is nonzero, so the pressure is negative. The scale factor during inflation has the de Sitter form:

$$a(t) = \mathrm{e}^{(\Lambda_{\mathrm{I}}/3)^{1/2}t}, \tag{1.82}$$

where Λ_{I} represents the energy density of the inflationary field (sometimes called the inflaton).

Since the energy density of the inflaton field was very high, the associated magnitude of the negative pressure would have been very large as well. The scale factor is thought to have increased during inflation by $\sim \mathrm{e}^{65}$, and any point in the Universe which found itself in a false vacuum state would have undergone inflation. The accelerated expansion lasted until the field rolled down to a minimum, when it decays into the familiar particles of the Standard Model, and the Universe can then be described by an FRW model.

There are two points of interest in connection with inflation where dark energy and large-scale structure are concerned. Firstly, inflation solves the flatness problem. Using Equation 1.82, the evolution of Ω during inflation can be written as:

$$|\Omega(t) - 1| \propto \mathrm{e}^{-(4\Lambda_{\mathrm{I}}/3)^{1/2}t}, \tag{1.83}$$

so that $|\Omega - 1|$ is driven very close to 0 as t increases. This explains why the Universe is flat. It also means that this value has not deviated significantly from its initial value right after expansion. We can therefore safely assume spatial flatness throughout the history of the Universe. Given the observational difficulties, this provides a theoretical motivation for taking the idea of a large Ω_{DE} seriously.

Secondly, the inflationary scenario provides a natural explanation for the origin of structure. An initially smooth background needs seed fluctuations around which gravitational collapse can occur. The inflationary scenario attributes their origin to quantum fluctuations in the inflaton field potential. Different points in the Universe inflate from slightly different points on the potential, separated by $\delta\phi$. Inflation for these two points ends at different times, separated by $\delta t = \delta\phi/\dot{\phi}$. This induces a density fluctuation $\delta = H\delta t$ (see Peacock, 1999). Since all the points undergoing inflation are part of the same potential field, the initial fluctuations are nearly scale invariant. This means that

the density amplitude on the horizon scale will also be constant:

$$\delta_{\rm H} = H\delta t = \frac{H^2}{2\pi\dot{\phi}} = \text{constant}. \tag{1.84}$$

Most models of inflation are slow-roll models, in which the Hubble rate varies slowly (see Liddle & Lyth, 2000, 1992; Liddle & Lyth, 1993). It is beyond the scope of this thesis to go into the detail of the theory, but it is necessary for us to briefly refer to the link between this theory and the spectral index of primordial fluctuations.

To quantify slow roll, cosmologists typically use two parameters ϵ and η which vanish in the limit that ϕ becomes constant. The first parameter is defined as:

$$\epsilon \equiv \frac{\mathrm{d}}{\mathrm{d}t}\left(\frac{1}{H}\right) = \frac{-\dot{H}}{aH^2}, \tag{1.85}$$

which is always positive, since H is always decreasing. The second complementary variable which defines how slowly the field is rolling is:

$$\eta \equiv \frac{1}{aH\dot{\phi}^{(0)}}\left[3aH\dot{\phi}^{(0)} + a^2V'\right], \tag{1.86}$$

where $\phi^{(0)}$ is the zero-order field, and V is the potential (see Dodelson 2003 for details).

The scalar spectral index can be defined in terms of some function, usually a polynomial, involving the two slow-roll parameters ϵ and η. As an example we shall give two such parameterisations: $n = 1 - 4\epsilon - 2\eta$ (Dodelson, 2003) and $n = 1 - 6\epsilon + 2\eta$ (Liddle & Lyth, 1992). The rate of change of n can also be expressed in terms of inflationary parameters: $\mathrm{d}n/\,\mathrm{d}\ln k = 16\epsilon\eta + 24\epsilon^2 + 2\xi^2$ (Kosowsky & Turner, 1995), where

$$\xi^2 \equiv M_{\rm Pl}^4 \frac{V'(\mathrm{d}^3/\mathrm{d}\phi^3)}{V^2}, \tag{1.87}$$

$M_{\rm Pl}$ being the reduced Planck mass ($4.342 \times 10^{-6}\,\mathrm{g}$).

Therefore, by extracting the values of ϵ and η from the data, using methods such as weak lensing, we can directly probe the the potential of of the inflaton field.

1.11 Dark matter

The observed value of the matter density in the Universe is $\Omega_m = 0.2792 \pm 0.0145$. But we have seen that density of baryonic matter is $\Omega_b = 0.0462 \pm 0.0015$. What constitutes the missing mass? This fluid component that accounts for the majority of matter in the Universe is called dark matter. The name is an indication of its nonbaryonic nature: it cannot be observed by emission of photons. The evidence for the existence of dark matter comes from a variety of sources, which be reviewed here (see Freese 2009 for a recent review, including a review of current attempts to detect dark matter) .

Anisotropies in the CMB are related to anisotropies in the baryonic density field by the Sachs-Wolfe effect (see Dodelson, 2003). This means that the baryon density field

variation at the time of decoupling can be linked to CMB anisotropies. If all matter were made of baryons, the amplitude of the density fluctuations should have reached $\delta \sim 10^{-2}$ at the present epoch. But we observe structures with $\delta \ll 1$ at the present epoch (e.g. galaxies and galaxy clusters). The discrepancy can only be explained by the presence of additional matter, which created potential wells for the baryons to fall into after decoupling. These potential wells would have had to be formed by a weakly interacting fluid that decoupled well before baryons and began to cluster much earlier. Such a fluid would only interact via the gravitational and possibly the weak nuclear force. As the baryons accumulated in the potential wells, their pressure would have built up, leading to oscillations in the baryon fluid, termed 'baryon acoustic oscillations' (BAO). These oscillations leaves an imprint on the CMB power spectrum, which has been confirmed observationally, and which constrains the mass density, leading to a further confirmation of the existence of this missing mass.

Another piece of evidence for dark matter comes from galaxy rotation curves. These curves relate the tangential velocity of the constituent stars (or gas) about the centre of the galaxy to their radius from the centre. Observations of the velocities of globular clusters about galaxies show that at large radii the velocities are approximately constant, implying that the amount of mass in the galaxies is much higher than the visible mass (see Freese 2009 for a review of the literature on the subject). The difference must come from some non-emitting component: dark matter.

Gravitational lensing (see Chapter 2) shows that the amount of lensing of galaxies around galaxy clusters is too high to be caused by the visible matter. Apart from the stars themselves, a galaxy cluster also has a gas component, but X-ray observations show that this is still not enough to account for the extra mass. The cluster must therefore have a non-emitting halo of dark matter around it.

We shall not go into the details of the various dark matter candidates that have been proposed in the literature (see Salati 2009 for a recent review). However, all these candidates have one common characteristic: a very small reaction cross-section, making them extremely difficult to detect directly. Experiments have, however, placed limits on the mass of Weakly Interacting Massive Particles (WIMPs), which are the current (2009) best candidate for dark matter (together with axions). These results show that even the lightest dark matter particle should have a mass which is not below ~ 10 MeV. We also know that $\Omega_{\mathrm{CDM}} = 0.233 \pm 0.013$ (Dunkley et al., 2009). The conclusion is that $\Omega_\nu \ll \Omega_m$, implying that hot dark matter (i.e. neutrinos) cannot account for the dark matter density Ω_{CDM}.

1.12 The matter-dominated Universe

After the epoch of matter-radiation equality, and before the onset of dark energy domination, the mass-energy content of the Universe became dominated by matter. The assumption of a homogeneous Universe evidently breaks down below a certain scale, and we therefore need a model to describe the evolution of mass structures, i.e. a model of the behaviour of the matter component of the Universe. From an initially smooth background (as evidenced by CMB observations), structures have evolved to a scale of more

than 100 Mpc, with the term 'large scale structure' being used to refer to objects modelled on this scale. Below this scale we observe galaxy clusters, individual galaxies, and stars. The model of structure formation must be accurate enough to provide an accurate description of the Universe on a wide range of scales.

1.12.1 Structure formation

The standard model for the formation of structure assumes that at some early time there existed small fluctuations, which grew by gravitational instability. The origins of these fluctuations are unclear, but they are thought to arise from quantum fluctuations of the primordial Universe, uncorrelated and with Gaussian amplitudes, which were then amplified during a later inflationary phase. The subject is presented in more detail in Liddle & Lyth (2000). The assumption that the amplitudes of the relative density contrasts is much smaller than unity means that we can think of the primordial fluctuations as small perturbations on a homogeneous and isotropic background density. This ensures that we can describe them using linear theory.

Heuristically, the mechanism of structure formation can be understood in terms of gravitational self-collapse. Matter collapses gravitationally around initial mass overdensities. This increases the relative density of that region, causing further collapse of more matter, and amplifying the effect. The linear theory of structure formation needs to be relativistic, because the perturbations on any length scale are comparable or larger than the horizon size[3] at sufficiently early times. Dissipative effects and pressure also affect structure formation, as explained below. For details of the theory, see Bardeen (1980) and Lifshitz (1946).

The relative density is the density ρ at a particular point in space $\mathbf{x}$ relative to the mean $\overline{\rho}$ at some time parameterised by the scale factor a, and can be expressed as a dimensionless density contrast:

$$\delta(\mathbf{x}, a) = \frac{\rho(\mathbf{x}, a) - \overline{\rho}(a)}{\overline{\rho}(a)}. \tag{1.88}$$

This quantity can be understood as the dimensionless density perturbation of some background matter distribution.

There are two types of density perturbations that can occur within a matter-radiation fluid. If the fluid could be compressed adiabatically in space, the perturbations have a constant matter-to-radiation ratio everywhere. Since the energy density of radiation is proportional to T^4, and the number density is proportional to T^3, the energy densities of radiation and matter are related by:

$$\delta_{\mathrm{rad}} = \frac{4}{3}\delta_m. \tag{1.89}$$

Isocurvature perturbations occur when the entropy density is perturbed, but not the energy density. Since the total energy density remains constant, there is no change in the

[3]The horizon size is defined as the distance ct which light can travel in time t since the big bang.

spatial curvature and

$$\rho_{\rm rad}\delta_{\rm rad} = \rho_m\delta_m. \tag{1.90}$$

Perturbations can occur at different scales, or 'modes'. The latter term is used when the amount of perturbation on a particular scale is expressed using Fourier analysis. The Fourier transform pair of $\delta\mathbf{x}$ is:

$$\begin{aligned}\hat{\delta}(\mathbf{k}) &= \int \mathrm{d}^3x\delta(\mathbf{x})\mathrm{e}^{i\mathbf{k}.\mathbf{x}} \quad ; \\ \delta(\mathbf{x}) &= \int \frac{\mathrm{d}^3k}{(2\pi)^3}\hat{\delta}(\mathbf{k})\mathrm{e}^{-i\mathbf{k}.\mathbf{x}},\end{aligned} \tag{1.91}$$

with each mode assumed to evolve independently. In the Einstein-de Sitter régime, linear adiabatic perturbations scale with time as follows:

$$\delta \propto \begin{cases} a(t)^2 & \text{(radiation domination)} \\ a(t) & \text{(matter domination)} \end{cases} \tag{1.92}$$

while isocurvature perturbation are initially constant and then decline:

$$\delta \propto \begin{cases} \text{constant} & \text{(radiation domination)} \\ a(t)^{-1} & \text{(matter domination).} \end{cases} \tag{1.93}$$

In both cases, the overall shape of the spectrum of the perturbations over all modes is preserved, while the amplitude changes with time. The evolution described above is affected on small scales by a number of processes, which are described below.

1.12.2 Evolution on small scales

During the radiation-dominated epoch the growth of certain modes is suppressed. This behaviour can be modelled in terms of the horizon scale $\lambda_H(a)$, which is the distance ct that light could have travelled since the initial singularity (a comoving horizon size). A mode k is said to enter the horizon when $\lambda = \lambda_H(a)$, where $\lambda = (2\pi)/k$. If $\lambda < \lambda_H(a_{\rm eq})$ then a mode enters the horizon during the radiation-dominated epoch. The time scale for collapse of matter during this epoch is larger than the typical expansion time scale ($t \sim 1/H(a)$) due to the relatively rapid expansion $\rho_{\rm rad} \propto a^{-4}$. The growth of these modes is therefore suppressed. After the epoch of matter-radiation equality ($a = a_{\rm eq}$), these perturbations can then start to collapse gravitationally. We can define the suppression factor for a particular mode as the factor by which the amplitude is reduced had it not entered the horizon:

$$f_{\rm sup} = \left(\frac{a_{\rm enter}}{a_{\rm eq}}\right)^2 = \left(\frac{k_0}{k}\right)^2 \tag{1.94}$$

where the mode evolves as $\propto a^2$ until it enters the horizon at $a_{\rm enter}$ and is suppressed until $a_{\rm eq}$, when its evolution resumes as $\propto a$. The second equality in the above equation comes from applying an Einstein-de Sitter approximation where $k_0 = 1/\lambda_H(a_{\rm eq})$ (see Bartelmann & Schneider, 2001).

Pressure opposes gravitational collapse for modes with a wavelength less than the Jeans length (sometimes called the free-streaming scale), defined as

$$\lambda_J = c_s \sqrt{\frac{\pi}{G\rho}}. \tag{1.95}$$

During the radiation-dominated epoch, the sound speed $c_s = c/\sqrt{3}$ and the Jeans length is always close to the horizon size. The Jeans length then reaches a maximum at $a = a_{\rm eq}$ and then begins to decrease as the sound speed declines. This means that on scales larger than the comoving horizon size, perturbations are only affected by gravity, and the spectrum starts to turn over at this point (where the effects of pressure begin to dominate). The comoving horizon size at $z_{\rm eq}$ is given by:

$$R_0 r_H(z_{\rm eq}) \approx \frac{16.0}{\Omega_m h^2}{\rm Mpc}. \tag{1.96}$$

Another important scale occurs where photon diffusion erases perturbations in the matter-radiation fluid. This process is termed Silk damping. The scale at which it occurs is characterised by the distance travelled by the photon in a random walk by the time of last scattering:

$$\lambda_S \approx 16.3(1+z)^{-5/4}(\Omega_b^2 \Omega_m h^6)^{-1/4}{\rm Gpc}. \tag{1.97}$$

All of the effects mentioned above are particularly important where the behaviour of massive neutrinos is concerned. The details will be discussed later on, but heuristically we can understand the complexity of their behaviour by considering them as a component whose equation of state changes as the Universe evolves. From a component which behaves like photons (since the particles have a very small mass and relativistic speeds), massive neutrinos lose energy and start behaving like baryonic matter[4].

1.12.3 Growth of perturbations in the presence of dark energy

All of the above effects were described in an Einstein-de Sitter universe. In a universe with a smooth non-clustering dark energy component below the horizon scale, the matter perturbation fields evolves according to:

$$\begin{aligned} \ddot{\delta} + 2H\dot{\delta} - (3/2)H^2\Omega_m\delta = 0 \\ \delta'' + (2-q)a^{-1}\delta' - (3/2)\Omega_m a^{-2}\delta = 0, \end{aligned} \tag{1.98}$$

where a dot denotes a time derivative and a dash denotes a derivative with respect to a. The term q is the deceleration parameter. This can be interpreted in the following way: the perturbations grow according to a source term which involves the amount of matter (Ω_m) but the growth is suppressed by the friction term due to the expansion of the universe. The latter is also known as the Hubble drag, which avoids the use of the term 'friction' (which implies a force).

If we define the growth as the ratio of the amplitude of a perturbation at a time a

[4]One of the earliest discussions of this mechanism is found in Silk (1982).

to some initial amplitude, i.e.

$$D(a) = \frac{\delta(a)}{\delta(a_{\rm initial})}, \tag{1.99}$$

the equation becomes, for a general dark energy scenario where $w = w(a)$ (see Linder & Jenkins, 2003)

$$D'' + \frac{3}{2}\left(1 - \frac{w(a)}{1+X(a)}\right)\frac{D'(a)}{a} - \frac{3}{2}\left(\frac{X(a)}{1+X(a)}\right)\frac{D}{a^2} = 0, \tag{1.100}$$

where

$$X(a) = \frac{\Omega_m}{\Omega_{\rm DE}} \mathrm{e}^{-3\int_a^1 \mathrm{d}\ln a' w(a')} \tag{1.101}$$

is the ratio of the matter density to the dark energy density. For large X (i.e. $\Omega_m \sim 1$ where $\Omega_{\rm DE} \sim 1 - \Omega_m$) we recover the matter-dominated behaviour ($D \sim a$). To parameterise deviations from this behaviour we define the 'normalised growth' as $G = D/a$. The evolution equation is then:

$$G'' + \left[\frac{7}{2} - \frac{3}{2}\left(\frac{w(a)}{1+X(a)}\right)\right]\frac{G''}{a} + \frac{3}{2}\left(\frac{1-w(a)}{1+X(a)}\right)\frac{G}{a^2} = 0. \tag{1.102}$$

This equation allows us to physically interpret the effects of dark energy. In the presence of dark energy, the Hubble drag term is increased, so that growth is suppressed in a universe with an accelerating expansion. This is similar to the suppression due to radiation dominance.

1.12.4 The matter power spectrum

In an FRW universe, the homogeneity and isotropy assumption means that any statistical properties must also be homogeneous and isotropic. The implication for the matter perturbation field is that its Fourier modes must be uncorrelated (due to homogeneity). Usually, we assume that the mode amplitudes are Gaussian. This assumption is well motivated since the theory for the seed fluctuations assumes that they have a quantum origin. Due to the central limit theorem, the sum of a sufficiently large number of mode amplitudes will tend towards a Gaussian distribution.

Such a field, with uncorrelated modes, and a Gaussian distribution of mode amplitudes is called a Gaussian random field, and can be entirely described by its two-point correlation function:

$$\langle \delta(\mathbf{x})\delta^*(\mathbf{y})\rangle = C_{\delta\delta}(|\mathbf{x}-\mathbf{y}|). \tag{1.103}$$

The angled brackets denote an ensemble average (an average over a multitude of realisations). The value of δ at a given point in the Universe will have a different value in each realisation, with a variance $\langle\delta^2\rangle$. Since we can only observe one realisation of our Universe (in other words, at most only a finite region in this one Universe), we apply the ergodic principle: The average over a sufficiently large volume is equal to the ensemble average.

In Fourier space, the correlation function can be written as:

$$\langle\hat{\delta}(\mathbf{k})\hat{\delta}^*(\mathbf{k}')\rangle = \int \mathrm{d}^3x \mathrm{e}^{i\mathbf{k}.\mathbf{x}} \int \mathrm{d}^3x' \mathrm{e}^{-i\mathbf{k}'.\mathbf{x}'}\langle\delta(\mathbf{x})\delta^*(\mathbf{x}')\rangle. \tag{1.104}$$

Replacing $\mathbf{x}' = \mathbf{x} + \mathbf{y}$, and substituting Equation 1.103, this can be written as:

$$\langle\hat{\delta}(\mathbf{k})\hat{\delta}^*(\mathbf{k}')\rangle = \int \mathrm{d}^3x \mathrm{e}^{i\mathbf{k}.\mathbf{x}} \int \mathrm{d}^3y \mathrm{e}^{-i\mathbf{k}'.(\mathbf{x}+\mathbf{y})} C_{\delta\delta}(|\mathbf{y}|) \tag{1.105}$$

$$= (2\pi)^3\delta_D(\mathbf{k}-\mathbf{k}') \int \mathrm{d}^3y \mathrm{e}^{-i\mathbf{k}.(\mathbf{y})C_{\delta\delta}(|\mathbf{y}|)} \tag{1.106}$$

$$= (2\pi)^3\delta_D(\mathbf{k}-\mathbf{k}')P_\delta(|\mathbf{k}|). \tag{1.107}$$

The power spectrum has been defined as the Fourier transform of the correlation function:

$$P_\delta(|\mathbf{k}|) = \int \mathrm{d}^3y \mathrm{e}^{i\mathbf{k}.(\mathbf{y})} C_{\delta\delta}(|\mathbf{y}|). \tag{1.108}$$

Hereafter, $P_\delta(|\mathbf{k}|)$ will be abbreviated to $P(k)$, where $k = |\mathbf{k}|$, following the standard convention in cosmology. The power spectrum can be expressed in dimensionless form as the variance per $\ln k$, so that:

$$\Delta^2(k) = \frac{k^3P(k)}{2\pi^2}. \tag{1.109}$$

One very important type of power spectrum in cosmology is the scale-invariant power spectrum, also known as the Harrison-Peebles-Zel'dovich spectrum. This is the form assumed in most cases within the Standard Model, as it corresponds very closely to the observed power spectrum in the Universe. This type of spectrum was first proposed in the 1970s by Harrison (1970), Zel'dovich (1972) and Peebles & Yu (1970), who were working independently, as the spectrum for initial density fluctuations. This hypothesis was subsequently closely borne out by observations. The defining characteristic of this spectrum is that it describes a fractal metric, where the degree of perturbation is the same on all scales (hence the term 'scale-invariant'), so that $P(k) \propto k$. If we assume scale invariance for the power spectrum on large scales, and combine this with Equation 1.94, this implies the following general shape for the matter power spectrum in the Einstein-de Sitter scenario:

$$P(k) \propto \begin{cases} k & \text{for} \quad k \ll k_0 \\ k^{-3} & \text{for} \quad k \gg k_0. \end{cases} \tag{1.110}$$

The actual form of the spectrum depends in non-trivial ways on the parameters in the cosmological model, including the 'slope' of the initial power spectrum n_s, where $P(k) \propto k^{n_s}$. In a scale-invariant spectrum in the linear régime, the fiducial value of n_s is taken to be 1.

1.12.4.1 The nonlinear power spectrum

The power spectrum gives us the evolution of the initial matter density fluctuations. The linear evolution breaks down at small scales, when complex structures begin to form,

and perturbations grow nonlinearly (that is, they cannot be treated as perturbations on an unperturbed background). The scale above which nonlinearities cannot be ignored is approximately set by $\Delta(k_{\rm NL}) \simeq 1$, which corresponds to $k_{\rm NL} \simeq 0.2\,h{\rm Mpc}^{-1}$ in most cosmological models. The standard model for nonlinear evolution is the spherical collapse model by Hamilton et al. (1991), known as the HKLM model. In their stable clustering hypothesis, they assume that these nonlinear collapsed objects form isolated, virialised systems that are decoupled from the expansion of the Universe. The HKLM model was extended by Jain et al. (1995) and by Peacock & Dodds (1996). Their approach uses a scaling ansatz, in which the nonlinear spectrum is some function f of the linear spectrum:

$$\Delta_{\rm NL}(k_{\rm NL}) = f_{\rm NL}[\Delta_{\rm L}(k_{\rm NL})], \tag{1.111}$$

where L and NL denote linear and nonlinear, respectively, and $k_{\rm NL} = [1+\Delta_{\rm NL}(k_{\rm NL})]^{1/3}k_{\rm L}$. The functional scaling relations are calibrated using N-body simulations.

Smith et al. (2003) took a different approach known as the halo model (see Seljak 2000 and Peacock & Smith 2000 for details). In the halo model, the density field is decomposed into individual clumps of matter with some density profile and varying mass. By using this model to calculate the number of clumps within a given volume, the halo profile can be calculated. This is the equivalent of the power spectrum for these matter halos. A functional relation between the linear power spectrum and this halo profile is then derived and calibrated using large N-body simulations. This relation is then used to calculate the nonlinear power spectrum. This approach produced `halofit` (Smith et al., 2003), which is a fitting formula to numerical simulations, where the halo model is combined with HKLM scaling. The `halofit` formula produces accurate power spectra within the nonlinear régime.

It must be noted, however, that the `halofit` code may not be accurate enough to to compute the *derivatives* of the nonlinear power spectrum over all scales. These derivatives are needed to calculate the Fisher matrix (see Chapter 3).

1.12.4.2 Normalisation

The power spectrum needs to be normalised to a chosen value. There exist several normalisation schemes, depending on which probe is used, which determines the scale at which quantities are best constrained. Following most of the literature on weak lensing, we choose to normalise our power spectra by using σ_8. The quantity σ_8 is defined as the root mean square variation of the density field when smoothed by a top-hat filter of radius $R = 8\,h{\rm Mpc}^{-1}$. This is written as

$$\sigma^2(R,z) = \int_0^\infty \frac{{\rm d}k}{k}\Delta_2(k,z)W^2(kR), \tag{1.112}$$

where the weighting function is defined as the Fourier transform of a sphere of uniform weight

$$W(k,R) = \frac{3j_1(kR)}{kR}, \tag{1.113}$$

so that $W_\sigma(R) = 3R^{-3}(\sin R - R\cos R)$. The spherical Bessel function $j_1(x)$ is of order 1, so that $\sigma_8 \equiv \sigma(8\,h\mathrm{Mpc}^{-1})$. It should be noted that the value of σ_8 is calculated using a linear extrapolation of the clustering of matter, so the calculated value will not match the observed value perfectly.

Normalisation using the CMB and σ_8 proceed in different ways. CMB normalisation usually involves normalising the primordial power spectrum, with the most commonly used parameter being the WMAP parameter A, which depends on δ_ζ, the amplitude of fluctuations from WMAP (Bunn & White, 1997):

$$A = (1.84\delta_\zeta \times 10^4)^2, \tag{1.114}$$

where $\delta_\zeta \approx 5.07e^{-(0.17-\tau)} \times 10^{-5}$. This normalisation, therefore, depends on the fiducial value of the reionisation optical depth τ, unlike σ_8, which does not.

The WMAP normalisation is related to σ_8 via the definition of the matter power spectrum:

$$P(k,z) = \frac{2\pi^2}{k^3} A k^{n_s(k)+3} T^2(k,z) \left(\frac{D(z)}{D(0)}\right)^2. \tag{1.115}$$

Integrating this using Equation 1.112 above gives us σ_8.

The COBE normalisation parameter δ_H is related to the WMAP parameter A_s by:

$$\delta_\mathrm{H} \equiv A_s(a_0 H_0). \tag{1.116}$$

1.13 Dark energy

In a previous section (1.6.3), we have alluded to the existence of a fluid component with a negative pressure. Here we discuss the justification for the dark energy paradigm within the inflationary ΛCDM model, and the process which led to its acceptance by the scientific community. We also discuss different theories about the nature of dark energy, and possible alternatives. For a comprehensive review, see Peebles & Ratra (2003).

Einstein (1917) revised his field equations of GR to read:

$$G_{\mu\nu} - 8\pi G\rho_\Lambda g_{\mu\nu} = 8\pi G T_{\mu\nu} \tag{1.117}$$

where ρ_Λ is proportional to the cosmological constant Λ. It can be seen from this equation that Einstein did not consider the cosmological constant to be part of the stress-energy term. One could, of course, put $\rho_\Lambda g_{\mu\nu}$ on the right-hand side of the equation and count it as part of the source term of the stress-energy tensor. This is not just a semantic distinction. When ρ_Λ takes part in the dynamics of the Universe, then the field equation is properly written with ρ_Λ, or its generalisation, as part of the stress-energy tensor:

$$G_{\mu\nu} = 8\pi G(T_{\mu\nu} + \rho_\Lambda g_{\mu\nu}). \tag{1.118}$$

The equation describing gravity is then unchanged from its original form — there is no new physical theory. Instead, there is a new component in the content of the Universe.

This component must satisfy Special Relativity (that is, an observer can choose

coordinates so that the metric tensor has Minkowskian form). An observer moving in spacetime in such a way that the Universe is observed to be homogeneous and isotropic would measure the stress-energy tensor to be

$$T_{\mu\nu} = \begin{pmatrix} \rho & 0 & 0 & 0 \\ 0 & p & 0 & 0 \\ 0 & 0 & p & 0 \\ 0 & 0 & 0 & p \end{pmatrix}. \tag{1.119}$$

This means that the new component in the stress-energy tensor looks like an ideal fluid with negative pressure:

$$p_\Lambda = -\rho_\Lambda. \tag{1.120}$$

In modern concordance cosmology, this component is usually termed 'dark energy'. We shall retain this term since it best describes the unknown nature of this component, without assuming anything about its properties (unlike the terms 'vacuum energy', 'quintessence', or 'cosmological constant'). If the equation of state parameter of dark energy is constant ($w(z) = -1$), then its energy density will be constant regardless of the expansion of the Universe.

Einstein inserted the cosmological constant because he felt that the non-static universe predicted by the formalism of GR was incorrect, given the data available at that time (particularly the observed low velocities of stars). Meanwhile, Slipher (1917) published his measurements of the spectra of spiral nebulae, which showed that most were shifted towards the red. The breakthrough came when the linear redshift-distance relation was formulated by Hubble (1929), which showed that the Universe was expanding. Einstein then dropped his support for the cosmological constant.

In the FLRW cosmological model, the expansion history of the Universe is determined by the mass density of the different components, whose sum is normalised to unity:

$$\Omega_{m,0} + \Omega_{\mathrm{rad},0} + \Omega_{X,0} + \Omega_{k,0} = 1, \tag{1.121}$$

where the 0 subscript indicates the present epoch. We use the term Ω_X to show that this equation does not assume anything about the nature of the additional energy component (dark energy), which is discussed below. In fact we could have used Ω_Λ or Ω_{DE} in the current concordance model.

Big bang nucleosynthesis and observations of large scale structure give a good determination of the mass content of the Universe, allowing Ω_m and Ω_{rad} to be fixed. However, observations in the 1980s and 1990s started to show inconsistencies with the cosmological model at the time – that of a matter-dominated, expanding Universe with a present-epoch Hubble constant of $H_0 \simeq 0.7\,\mathrm{kms}^{-1}\mathrm{Mpc}$ and $\Omega_\Lambda = 0$. This was the so-called 'age problem', where the predicted age of the Universe seemed to be smaller than the age of the oldest stars. Angular-diameter distances to the last scattering surface at $z = 1100$ measured from the CMB are in fact 1.7 times smaller than those predicted by an isotropic and homogeneous Universe containing only pressureless matter (see Räsänen, 2009). Since the inflationary scenario, which by then was well established, predicts a flat $\Omega_{\mathrm{total}} = 1$ universe, there was a problem with the cosmological model.

It was realised that one of the three assumptions of the cosmological model had to be wrong. Either the Universe contains exotic matter with a negative pressure, or standard General Relativity is wrong, or the Universe is not homogeneous and isotropic. (The solution could also lie in some combination of the three.) Most of the research in the last decade has followed the first approach, and the term 'concordance model' refers to an FLRW universe, following General Relativistic cosmology, containing dark energy.

In this thesis, we work within an FLRW model. Within this framework, two main proposals were put forward: one was ΛCDM, in which there is a contribution to the energy density from a term similar to the cosmological constant (or the cosmological constant itself), and the other was $\nu+$CDM, where the missing mass came from massive neutrinos ($m_\nu \simeq 7$eV).

The first strong evidence of dark energy[5] came in 1998-9, when observations of the luminosities of type Ia supernovae indicated that the expansion of the Universe is accelerating (Riess et al., 1998; Perlmutter et al., 1999). Concurrently, other observations constrained the neutrino mass to $m_\nu \ll 7$eV, thus discounting the $\nu +$ CDM model and confirming ΛCDM as the concordance model (see Figure 1.1).

Since then, numerous observations have been carried out, including supernovae, the cosmic microwave background, large-scale structure and baryon acoustic oscillations. The values of the present epoch matter and radiation components are well established (see, for example, the WMAP-5 values for the cosmological parameters in Komatsu et al., 2009):

$$\Omega_{m,0} \equiv \frac{8\pi G\rho_{m,0}}{3H_0^2} \sim 0.3 \quad , \quad \Omega_{\rm rad,0} \equiv \frac{8\pi G\rho_{\rm rad,0}}{3H_0^2} \sim 1\times 10^{-4}, \tag{1.122}$$

where H_0 is the present value of the Hubble parameter. The data also indicate that the Universe is currently nearly spatially flat:

$$|\Omega_K| \ll 1. \tag{1.123}$$

This is normally taken to imply that the spatial curvature $K = 0$, since

$$\Omega_{k,0} = 0 \equiv \frac{-K}{a_0^2H_0^2} \sim 0, \tag{1.124}$$

and thus to justify the inflationary paradigm. However, inflation only tells us that $\Omega_K \to 0$, so that the curvature may have had a nonzero value in the past. In the present Universe, however, the distinction is negligible. In any case, Equation 1.121 implies that there has to be a nonzero Λ (a constant term added to the Einstein equation) such that

$$\Omega_{\Lambda,0} \equiv \frac{\Lambda}{3H_0^2} \sim 0.7. \tag{1.125}$$

Inserting these values into the Friedmann equation lead to the dramatic conclusion that

[5]The term 'dark energy' was coined around 1998 by analogy to 'dark matter' (see Turner, 1999).

the expansion of the Universe is accelerating:

$$\ddot{a}_0 = H_0^2 \left(\Omega_\Lambda - \frac{1}{2}\Omega_m - \Omega_{\rm rad} \right) > 0, \tag{1.126}$$

where a_0 is the present value of the scale factor $a(t)$.

At this point we should emphasise that this conclusion only holds if the Universe is homogeneous and isotropic (i.e. a Friedmann-Lemaître model). In such a Universe, the distance to a given redshift z and the time elapsed since that redshift are tightly related via the only free function, $a(t)$. If the Universe is isotropic around us, but not homogeneous (i.e. a non-Copernican Tolman-Bondi-Lemaîetre model), then this relation would be lost and present data might not imply acceleration. A Copernican model where this relation again breaks down is the inhomogeneous Universe, where the acceleration can be produced via nonlinear averaging — the backreaction of inhomogeneities (see, for example, Räsänen 2009 and Wiltshire 2009).

1.13.1 The dark energy equation of state

Since dark energy is a fluid component of the Universe in the Standard Model, it is the equation of state that has the potential to distinguish between dark energy candidates.

The most important distinction that can be made between different dark energy models in the context of this thesis is whether the energy density of this component is constant, filling space homogeneously, or whether it is some form of quintessence field whose energy density can vary in time and space[6]. We therefore consider the redshift evolution of w, so we start by defining w as an arbitrary function of redshift z. There are a number of different parameterisations of $w(z)$, some of which are discussed in Linder (2003, and references therein). Throughout our work, we use the most common parameterisation, proposed by Chevallier & Polarski (2001) and Linder (2003), which is also the one chosen by the Dark Energy Task Force (Albrecht et al., 2006). It characterises the evolution of the equation of state by the derivative of w with respect to the logarithm of the scale factor:

$$w(z) = w_0 - \frac{{\rm d}w}{{\rm d}\ln a}. \tag{1.127}$$

If we define

$$w_a = -\frac{{\rm d}w}{a\,{\rm d}\ln a}, \tag{1.128}$$

then the equation becomes

$$w(a) = w_0 + w_a(1-a), \tag{1.129}$$

which is the most commonly used form. This parameterisation is sometimes termed the Chevallier-Linder-Polarski (or CPL) parameterisation.

At the present epoch, $a = 1$, and therefore $w(a) = w_0$. Revisiting Equation 1.52,

[6]There are, however, other models, such as $f(R)$, Chameleon Models, etc. See Durrer & Maartens 2008a for a review.

the expression can now be written:

$$H^2(a) = H_0^2 \left[\Omega_m a^{-3} + \Omega_{\rm rad} a^{-4} + \Omega_{\rm DE} a^{-3(w_0+w_a)} {\rm e}^{-3w_a(1-a)}\right] . \qquad (1.130)$$

The term Ω_X in Equation 1.121 represents the cosmological constant if $w(a) = -1$. Otherwise it represents dark energy with constant w. If w varies, it represents a dark energy component with a varying equation of state.

It has been shown that this parameterisation is stable and robust over large redshift ranges. A wide range of functional forms of $w(a)$ can be parameterised by the $w_0 - w_a$ combination. However, there are some dark energy models which it cannot reproduce (see Wang & Freese, 2006; Johri & Rath, 2007; Avelino et al., 2006)

The problem with the dark energy paradigm, put simply, is that the parameters are not constrained well enough to rule out certain models. We have fairly good bounds on the dark energy density: $\Omega_{\rm DE} = 0.721 \pm 0.015$. However, the dark energy equation of state is still poorly constrained. Even for a constant w model, corresponding to ΛCDM, we have $w = -0.972^{+0.061}_{-0.060}$ (using WMAP5+BAO+Sne, Dunkley et al. 2009). A time-varying $w(a)$ could mimic a constant w, thereby disguising underlying physics.

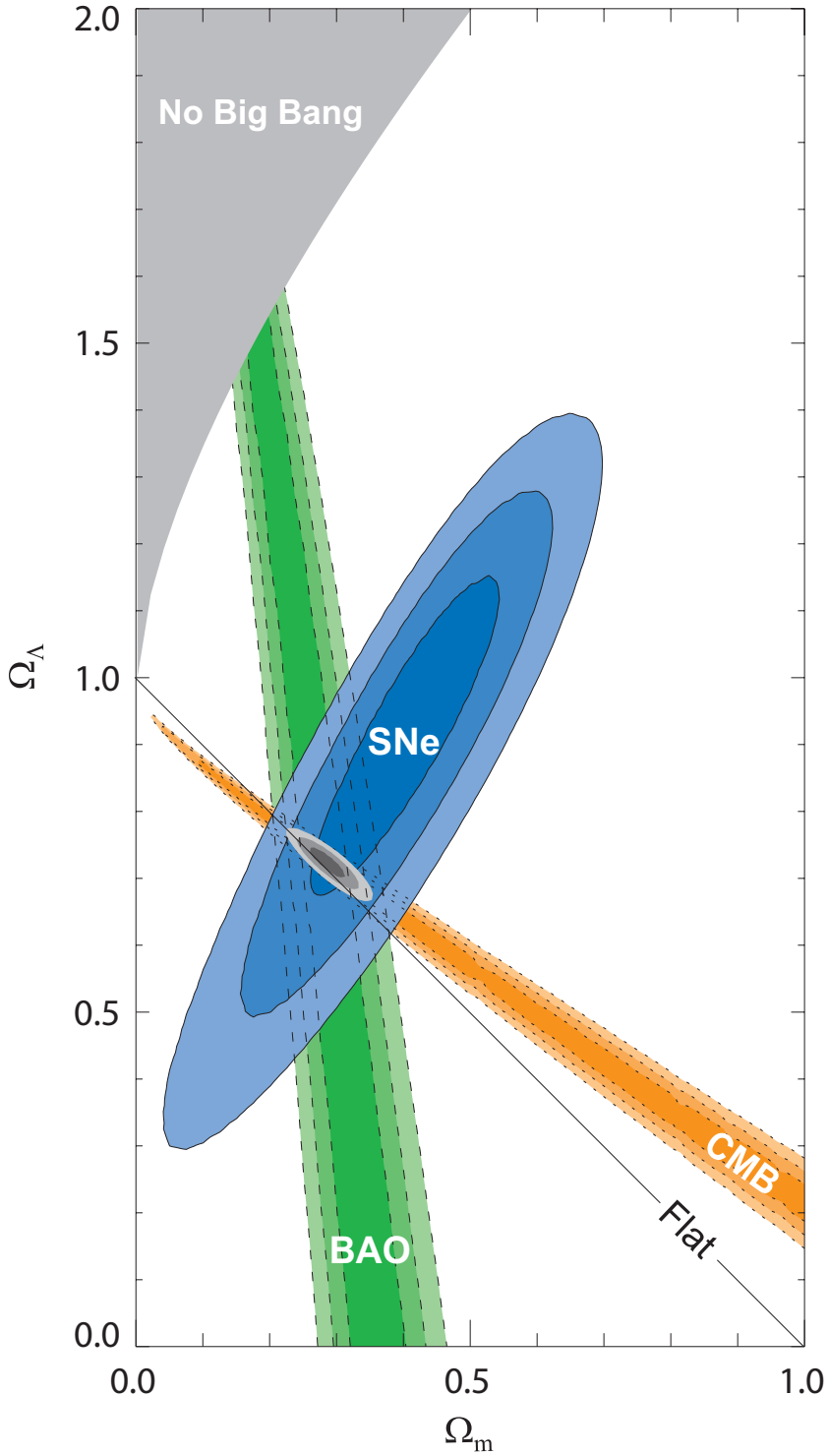

Figure 1.1: The 68.3%, 95.4% and 99.7% confidence regions for Ω_m and Ω_Λ, showing results from CMB, BAO and Union Supernovae experiments, as well as the combined constraints from the different techniques (filled grey contours). Note that these results assume $w = -1$ (i.e. $\Omega_\Lambda = \Omega_{\rm DE}$). The plot shows the degeneracies between the two parameters, as well as the limits imposed by the choice of physical theory (from Kowalski et al. 2008).

Chapter 2

Weak lensing and cosmic shear

This chapter contains an outline of gravitational lensing, with an emphasis upon weak lensing, since it is the principal observational technique considered in this thesis. In particular, we consider cosmic shear.

Although the theory of cosmic shear had been worked out from the 1960s to the early 1990s (see Schneider 2006 for a review), the first detection had to await the development of instruments sensitive enough to make the required obserxvations, and image analysis software to accurately correct for unwanted effects when measuring the shapes of galaxies. Then, in March 2000, four groups independently announced the first discovery of cosmic shear (Bacon et al., 2000; Kaiser, 2000; Van Waerbeke et al., 2000; Wittman et al., 2000). Since then, cosmic shear has established itself as an important technique in observational cosmology. Concurrently, with the dark energy paradigm becoming accepted by the scientific community, it became necessary to find observational techniques to probe this cosmological component. Cosmic shear has a very strong potential in this respect. The precision offered by experimental techniques is now catching up with the requirements of the theoretical formalism, and the next generation of weak lensing surveys (see Albrecht et al., 2006) should offer new insights into the properties of dark energy, at least by yielding stricter bounds on parameters within the cosmological model.

We start with a general introduction to the formalism of weak lensing, explaining the essential quantities and terminology. We then proceed with a description of each of the types of lensing encountered in astrophysical situations. The phenomenon of weak gravitational lensing manifests itself as a distortion and magnification for individual lensed galaxies. In our work, we only use ellipticity measurements, which are a first-order distortion effect caused by cosmic shear.

We then present the essential calculations used in cosmic shear, giving the effective 2D convergence spectrum derived using the Limber equation. Finally, we give a brief outline of the formalism of tomographic cosmic shear.

The aim of this chapter is therefore to present the cosmic shear formalism, and to explain the relationship between gravitational lensing and ellipticity. The measured ellipticity allows us to calculate the lensing power spectrum, which depends directly upon the values of the parameters in our cosmological model. Hence the ability of weak lensing probes to constrain cosmological parameters.

2.1 Gravitational lensing formalism

The phenomenon of deflection of light by a gravity was studied long before general relativity. In Newtonian mechanics, a photon considered as a massive particle will have its path deviated by a gravitating mass. In General Relativity, the effect is twice as large as in Newtonian physics, and the experimental confirmation of the value for light deflection was among the most important steps in the acceptance of GR by the scientific community.

The basic physical process underlying gravitational lensing in GR is the fact that light rays travel along null geodesics. If spacetime is curved by the presence of mass-energy, these light rays will deviate from their Euclidean path. Even before the full development of GR, this phenomenon was first studied by Einstein (1911), who showed that a photon must be affected by a gravitational field, using conservation of energy applied to Newtonian gravitation theory. In GR, a light ray grazing the surface of the sun is deflected by 1.75 arc seconds, whereas Newtonian gravity predicts a value of 0.87 arc seconds. In 1919, Einstein's formula for light deflection was confirmed during the observation of a solar eclipse (Dyson et al., 1920).

Cosmic shear is the extension of the process of light deflection to the cosmological régime. This idea is often attributed to Richard Feynman, in a lecture given at Caltech in 1964 (see Réfrégier, 2003b). From the 1960s to the 1990s, several theorists studied the phenomenon of light deflection in an inhomogeneous universe (e.g Kristian & Sachs, 1966; Gunn, 1967; Schneider & Weiss, 1988; Jaroszynski et al., 1990; Lee & Paczynski, 1990). During the early 1990s, predictions for the statistics measured from weak lensing distortions were then worked out by several groups (e.g. Babul & Lee, 1991; Blandford et al., 1991; Kaiser, 1992; Miralda-Escude, 1991; Villumsen, 1996). In the light of several current and future high-precision weak lensing surveys to constrain cosmological parameters, the theory of the subject was studied in many reviews (among which are Bernardeau et al., 1997; Jain & Seljak, 1997; Kamionkowski et al., 1998; Kaiser, 1998; Hu & Tegmark, 1999; Bartelmann & Schneider, 2001; Réfrégier, 2003b; Van Waerbeke & Mellier, 2003). Here we present the theory of cosmic shear.

In GR, there may exist more than one null geodesic connecting the world-line of a source to the observation event. Bodies more compact, more massive or more distant than the sun can therefore bend spacetime sufficiently strongly so that multiple light rays from one source reach the observer. The observer will then see an image in the direction of each ray, leading to multiple images of the same source. The first multiple-image system was discovered by Walsh et al. (1979).

While a point source leads to deflection of light rays, tidal gravitational fields also cause differential deflection of light bundles, leading to a change in the size and shape of their cross-section. Since the number of photons in the light bundle is conserved, the surface brightness of the source is unchanged. A change in the cross-sectional area of a light bundle therefore leads to a change in the observed flux. Changes in the cross-sectional shape lead to distortions in the image. This deformation is difficult to identify if the intrinsic shape of the source is not known. In the case of single lens systems, it can only be identified if the effect is strong, as in the case of Einstein rings and arcs in galaxy clusters. Nevertheless, it is still possible to infer the tidal field from the distortion in single images.

In standard descriptions of gravitational lensing, there are three assumptions that are made:

1. The gravitational lens potential is small, so that it can be effectively described by a Newtonian potential: $|\Phi| \ll c^2$.
2. The lenses are slowly moving, so that a Special Relativistic treatment is not needed: $v_{\rm lens} \ll c$.
3. Individual lenses are assumed to be thin: $L \ll c/H_0$, where L is the thickness of the lens and c/H_0 is the present-day Hubble radius. Large-scale curvature only becomes important on scales much larger than the lens.

Under these assumptions, lens systems, which in practice consist of lensing galaxies or galaxy clusters, can be treated as lenses embedded in an expanding cosmological background in general relativity (the FRW metric). The path of light rays from the source to the observer can be approximated by three sections: from the source to a region close to the lens as geodesics of the FRW metric, from close to the lens to the observer, again as geodesics on the background FRW metric, and finally a weakly-perturbed, connecting metric close to the lens.

The first condition allows us to use the weak field limit of GR to derive the form of the metric (recall Equation 1.9). Since $\Phi \ll c$ and the time variation of the potential is small, the metric can be written as

$$\mathrm{d}s^2 = -g_{\mu\nu}\,\mathrm{d}x^\mu\,\mathrm{d}x^\nu = (1+2\Phi)\,\mathrm{d}t^2 - (1-2\Phi)\delta_{\alpha\beta}\,\mathrm{d}x^\alpha\,\mathrm{d}x^\beta \tag{2.1}$$

where Φ is the Newtonian potential.

The geodesic equation in GR is given by:

$$a^\mu = u^\mu_{;\nu}u^\nu = \dot{u}^\mu + \Gamma^\mu_{\nu\lambda}u^\lambda u^\nu = 0. \tag{2.2}$$

The weak field limit also assumes that there is no strong time variation in the metric (i.e. $g_{0i} = 0$ where Roman letters are used for the spatial part of the metric), so the geodesic equation in the weak field limit can be written[1]

$$\dot{u}^i = \left[2u^i\dot{\Phi} + \left(1+u^2\right)\delta_{ij} - 2u^iu^j\right)\nabla_j\Phi\right]. \tag{2.3}$$

In the slow motion limit, when $u_i \ll c$, we recover the Newtonian equation of motion:

$$\dot{u}_i = \nabla_i\Phi. \tag{2.4}$$

In the ultra-relativistic limit, where $u_i \sim r_i c$ for the unit vector r_i along the photon's path, we have:

$$\dot{r}_i = 2(\delta^K_{ij} - r_ir_j)\nabla_j\Phi = 2\nabla^\perp_j\Phi, \tag{2.5}$$

[1]The assumption of an FRW metric simplifies the mathematical description of the lensing system. It should be noted that dropping this assumption, for instance in Tolman-Bondi-Lemaìtre models, would modify the lensing equation.

where the gradient operator perpendicular to r is defined as

$$\nabla_j^{\perp} \equiv (\delta_{ij}^K - r_i r_j)\nabla_j. \tag{2.6}$$

In the Newtonian limit, it is the term $g_{00,j}/2$ which dominates, so the deflection results from the time part only, with the curvature of space being neglected. Comparing Equations 2.4 and 2.5, we can see that the coefficient of the potential gradient term differs by a factor of 2. This difference is due to the spatial curvature terms. Ultra-relativistic particles experience an extra 'force' due to this curvature. There is a second difference between slow and ultra-relativistic particles. In the latter case, the force parallel to the particle's trajectory is cancelled out by the spatial curvature terms. The particle only experiences a transverse deflection.

2.1.1 The deflection angle

By analogy to an optical lens system, we can define a refractive index for a gravitational lens:

$$n = 1 = \frac{2}{c^2}\Phi, \tag{2.7}$$

where Φ is the gravitational potential of the lensing mass region. Following through with our analogy, the potential is normalised so that it approaches zero at infinity, and is negative, so that the refractive index is positive. We can define a deflection angle using Fermat's principle and integrating n perpendicular to the light path (see Figure 2.1):

$$\hat{\alpha} = \frac{2}{c^2}\int \vec{\nabla}_{\perp}\Phi \,\mathrm{d}z, \tag{2.8}$$

where the integration is formally carried out along the whole light path with the gradient taken perpendicular to it. The deflection angle is therefore the integral of the change in the path of the particle over time, and it depends on the shape of the potential Φ.

Consider a point mass of mass M_{point}, with a Newtonian potential

$$\Phi(\xi, z) = -\frac{GM_{\mathrm{point}}}{\sqrt{\xi^2 + z^2}}, \tag{2.9}$$

where ξ is the impact parameter and z is the distance along the unperturbed light path. The deflection angle is then

$$\hat{\alpha} = \frac{4GM_{\mathrm{point}}}{c^2\xi}, \tag{2.10}$$

where ξ is the surface mass density, defined as the mass density projected onto a plane perpendicular to the incoming light ray. This is twice the value obtained in Newtonian gravity. If the condition $\xi \gg R_{\mathrm{S}}$ is followed, that is, the deflection angle is much greater than the Schwarzchild radius of the lens, then the deflection angle is small ($\hat{\alpha} \ll 1$).

In astrophysical situation, the lensing mass is of course a three-dimensional object, not a point mass. Moreover, the light rays are smoothly curved. However, if the deflection angle is small, the path of the light rays can be approximated by straight-line segments in

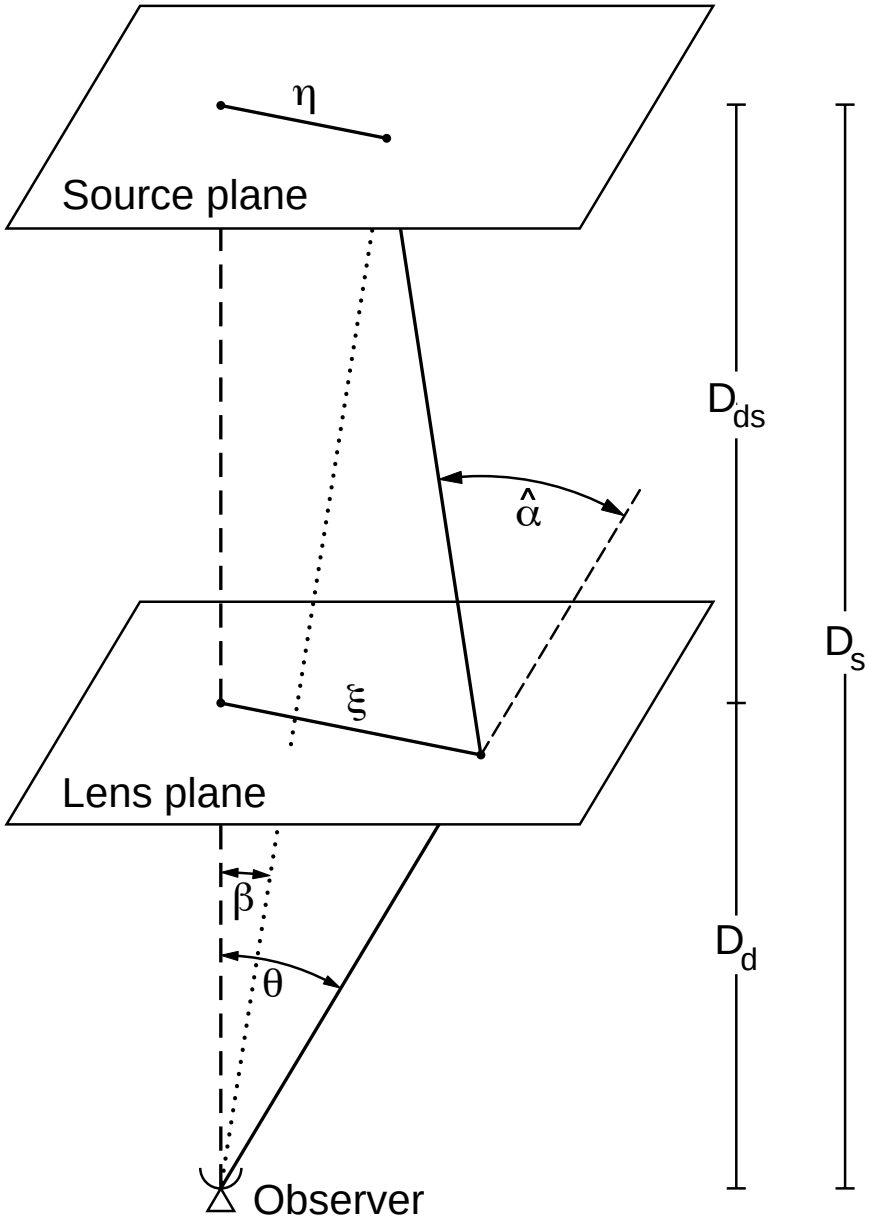

Figure 2.1: Schematic diagram of a gravitational lens system (from Bartelmann & Schneider, 2001). All the distances D are angular diameter distances. The deflection angle is $\hat{\alpha}$.

the neighbourhood of the deflecting mass. This corresponds to the Born approximation in nuclear and atomic physics (see Bartelmann & Schneider 2001 for further details).

2.1.2 The thin lens approximation

The assumption that the lens can be approximated by a plane is known as the thin lens approximation. It assumes that the deflection caused by the lens occurs within a narrow redshift range $\Delta z \pm \xi$. The thin lens approximation is useful because it allows us to to project the mass distribution of the lens onto the lens plane, and therefore to characterise the lens by its surface mass density Σ:

$$\Sigma(\xi) = \int \rho(\boldsymbol{\xi}, z)\, \mathrm{d}z, \tag{2.11}$$

where the impact parameter is generalised to a vector $\boldsymbol{\xi}$ in the lens plane. The deflection angle is then the sum of the deflections from all the mass elements in the plane:

$$\hat{\boldsymbol{\alpha}} = \frac{4G}{c^2} \int \frac{(\boldsymbol{\xi} - \boldsymbol{\xi}')\Sigma(\boldsymbol{\xi})}{|\boldsymbol{\xi} - \boldsymbol{\xi}'|}\, \mathrm{d}^2\boldsymbol{\xi}' \tag{2.12}$$

$$\hat{\alpha} = \frac{4GM_{<\xi}}{c^2\xi}, \tag{2.13}$$

where $M_{<\xi}$ is the mass enclosed within the radius ξ.

2.1.3 The lensing equation

The basic quantities in gravitational lensing formalism can be derived by examining the geometry of a typical observer-lens-source configuration, shown in Figure 2.1. The distances D, given as angular diameter distances in the diagram, are related to the redshifts by $D = D_{\mathrm{ang}}(z)$, such that a mass concentration at redshift z_{d} will be at angular diameter distance D_{d}. The three important distances are: the observer-lens distance D_{d}, the lens-source distance D_{s}, and the observer-source distance D_{ds}. The reduced deflection angle is defined as:

$$\boldsymbol{\alpha} = \frac{D_{\mathrm{ds}}}{D_{\mathrm{d}}}\hat{\boldsymbol{\alpha}} \tag{2.14}$$

The position of the source on the source plane $\boldsymbol{\eta}$ can be described in terms of the deflection angle $\boldsymbol{\alpha}$ and the distances between the different planes:

$$\boldsymbol{\eta} = \frac{D_{\mathrm{s}}}{D_{\mathrm{d}}}\boldsymbol{\xi} - D_{\mathrm{ds}}\boldsymbol{\alpha}(\boldsymbol{\xi}). \tag{2.15}$$

The two essential angles in Figure 2.1 are $\boldsymbol{\beta}$, the true unlensed angular position of the galaxy, and $\boldsymbol{\theta}$, the observed lensed angular position. These are related by the deflection angle in the lensing equation:

$$\boldsymbol{\theta} D_{\mathrm{s}} = \boldsymbol{\beta} D_{\mathrm{s}} + \hat{\boldsymbol{\alpha}} D_{\mathrm{ds}} \tag{2.16}$$

Rearranging, and using Equation 2.14, we obtain:

$$\begin{aligned}\boldsymbol{\beta} &= \boldsymbol{\theta} - \hat{\boldsymbol{\alpha}}\frac{D_{\rm ds}}{D_{\rm d}} \\ \boldsymbol{\beta} &= \boldsymbol{\theta} - \boldsymbol{\alpha}. \end{aligned} \tag{2.17}$$

This is the central equation in gravitational lensing formalism. It relates the observed position of a galaxy $\boldsymbol{\theta}$ to its actual position $\boldsymbol{\beta}$ via the deflection angle $\hat{\boldsymbol{\alpha}}$. It also gives us one feature which distinguishes between strong and weak lensing. The solutions $\boldsymbol{\theta}$ for the lens equation give us the angular positions of the images of a source at $\boldsymbol{\beta}$. If the equation for $\boldsymbol{\theta}$ has more than one solution then multiple images will be formed. A necessary condition for this is that the lens must be a strong lens. A strong lens is one for which the dimensionless mass surface density, defined as

$$\kappa(\boldsymbol{\theta}) = \frac{\Sigma(\boldsymbol{\theta})}{\Sigma_{\rm cr}}, \tag{2.18}$$

is greater than or equal to unity in at least one place: $\kappa(\boldsymbol{\theta}) \geq 1$. The quantity $\Sigma_{\rm cr}$ is the critical surface mass density, defined as:

$$\Sigma_{\rm cr} = \frac{c^2}{4\pi G}\frac{D_{\rm s}}{D_{\rm d}D_{\rm ds}} \tag{2.19}$$

The quantity κ is known as the convergence, and its value distinguishes a strong lens from a weak lens. For weak lensing, $|\kappa| \ll 1$, while for strong lensing, $|\kappa| >\sim 1$. At points where $\Sigma > \Sigma_{\rm cr}$, the convergence $\kappa(\boldsymbol{\theta}) > 1$, and the lens is said to be supercritical.

2.1.4 The effective lensing potential

Light rays travel along geodesics which depend on the background spacetime. To relate the convergence to the gravitational potential of the lens, we start with the effective lensing potential, which is defined as the scaled, projected, Newtonian potential of the lens:

$$\psi(\boldsymbol{\theta}) = \frac{D_{\rm ds}}{D_{\rm d}D_{\rm s}}\frac{2}{c}\int \Phi(\boldsymbol{\xi}, z)\,{\rm d}z. \tag{2.20}$$

Taking the gradient of ψ we obtain

$$\vec{\nabla}_\theta\psi = D_{\rm d}\vec{\nabla}_\xi\psi \tag{2.21}$$

$$\vec{\nabla}_\theta\psi = \frac{D_{\rm ds}}{D_{\rm s}}\frac{2}{c}\int \vec{\nabla}_\perp\boldsymbol{\Phi}\,{\rm d}z. \tag{2.22}$$

By comparing the right-hand side of the above equation to 2.12, we can see that the reduced deflection angle is related to the effective lensing potential by

$$\vec{\nabla}_\theta\psi = \boldsymbol{\alpha}. \tag{2.23}$$

The mass density of a lens is related to its potential by Poisson's equation

$$\vec{\nabla}^2_{\xi}\Phi = 4\pi G\rho(\boldsymbol{\xi}, z). \tag{2.24}$$

Therefore, if we take the Laplacian of the LHS of Equation 2.20 (i.e. ψ), we can relate the effective lensing potential of the lens to its mass distribution:

$$\vec{\nabla}_{\theta}\psi = \frac{2}{c^2}\frac{D_{\rm d}D_{\rm ds}}{D_{\rm s}}\int \nabla^2\vec{\xi}\vec{\Phi}\,{\rm d}z \tag{2.25}$$

$$\vec{\nabla}_{\theta}\psi = \frac{2}{c^2}\frac{D_{\rm d}D_{\rm ds}}{D_{\rm s}}4\pi G\Sigma(\boldsymbol{\theta}) = 2\frac{\Sigma(\boldsymbol{\theta})}{\Sigma_c r}. \tag{2.26}$$

Thus, the effective lensing potential is related to the convergence by:

$$\vec{\nabla}^2_{\theta}\psi = 2\kappa(\boldsymbol{\theta}). \tag{2.27}$$

Referring to Equation 2.12, the reduced deflection angle can be written:

$$\boldsymbol{\alpha} = \frac{1}{\pi}\int \kappa(\boldsymbol{\theta}')\frac{\boldsymbol{\theta}-\boldsymbol{\theta}'}{|\boldsymbol{\theta}-\boldsymbol{\theta}'|^2}\,{\rm d}^2\boldsymbol{\theta}', \tag{2.28}$$

so that using Equation 2.27, the effective lensing potential can be related to the convergence by:

$$\psi(\boldsymbol{\theta}) = \frac{1}{\pi}\int \kappa(\boldsymbol{\theta})\ln(\boldsymbol{\theta}-\boldsymbol{\theta}')\,{\rm d}^2\boldsymbol{\theta}'. \tag{2.29}$$

2.1.5 Convergence, shear and magnification

The surface brightness of a lensed galaxy is conserved. Physically, this is obvious since there is no emission or absorption of photons in the lensing process. Mathematically, it follows by Liouville's theorem: the flux within a given set of geodesics, which is an entire bounded function, is constant. The surface brightness in the source plane is related to the observed surface brightness in the image plane by:

$$I(\boldsymbol{\theta}) = I^{\rm s}[\beta(\boldsymbol{\theta})], \tag{2.30}$$

where I is the surface brightness, and the angles are those shown in Figure 2.1.

If the angular size of the source is much smaller than that of the region in which the properties of the lens change, then the distortion of the image of the source can be described by a linear mapping A_{ij} between the source and the image planes. The matrix A_{ij}, called the distortion matrix, is of central importance in gravitational lensing formalism. This matrix can be expressed in two ways. The first way is to write is as the Jacobian matrix of the lens, defined by:

$$A_{ij} = \frac{\partial\boldsymbol{\beta}_i}{\partial\boldsymbol{\theta}_j} = \frac{\partial}{\partial\boldsymbol{\theta}_j}(\boldsymbol{\theta}_i - \boldsymbol{\alpha}_i). \tag{2.31}$$

The second way is to relate it to the Hessian matrix ψ_{ij} of ψ, using Equation 2.23:

$$A_{ij} = \delta_{ij} - \frac{\partial \boldsymbol{\alpha}_i}{\partial \boldsymbol{\theta}_j} = \delta_{ij} - \frac{\partial^2 \psi(\boldsymbol{\theta})}{\partial \boldsymbol{\theta}_i \partial \boldsymbol{\theta}_j} = \delta_{ij} - \psi_{ij} \equiv M_{ij}^{-1}, \tag{2.32}$$

where M_{ij} is the magnification matrix. Equation 2.23 can now be rearranged and written as:

$$\kappa = \frac{1}{2}(\psi_{11} + \psi_{12}). \tag{2.33}$$

The complex shear is defined by:

$$\gamma = \gamma_1 + i\gamma_2 = |\gamma| \mathrm{e}^{2i\phi} \tag{2.34}$$

where γ is the distortion of the image and ϕ is the orientation of the distortion. The shear is related to ψ by:

$$\gamma_1(\boldsymbol{\theta}) = \frac{1}{2}(\psi_1 1 - \psi_{22} \equiv \gamma(\boldsymbol{\theta}) \cos[2\phi(\boldsymbol{\theta})] \tag{2.35}$$

$$\gamma_2(\boldsymbol{\theta}) = \psi_{21} = \psi_{12} \equiv \gamma(\boldsymbol{\theta}) \sin[2\phi(\boldsymbol{\theta})]. \tag{2.36}$$

The distortion matrix A can be written in terms of the shear and convergence:

$$A = \begin{pmatrix} 1 - \kappa - \gamma_1 & -\gamma_2 \\ -\gamma_2 & 1 - \kappa + \gamma_1 \end{pmatrix} \tag{2.37}$$

$$A = (1 - \kappa) \begin{pmatrix} 1 & 0 \\ 0 & 1 \end{pmatrix} - \gamma \begin{pmatrix} \cos(2\phi) & \sin(2\phi) \\ \sin(2\phi) & -\cos(2\phi) \end{pmatrix}. \tag{2.38}$$

This is sometimes expressed in terms of the reduced shear $g(\boldsymbol{\theta}) = \gamma(\boldsymbol{\theta})/[1-\kappa(\boldsymbol{\theta})]$, so that:

$$A = (1 - \kappa) \begin{pmatrix} 1 - g_1 & -g_2 \\ -g_2 & 1 + g_1 \end{pmatrix} \tag{2.39}$$

Equation 2.38 has an important physical interpretation:

- The convergence κ causes an isotropic focussing of light rays and an isotropic magnification of the source. The shape of the source galaxy is not altered by convergence alone.
- The shear γ introduces an anisotropic mapping from the source to the image plane causing the image to become stretched along some direction ϕ by a magnitude γ.

The weak lensing calculations in this thesis only consider the latter effect, i.e. shear.

It only remains for us to define the magnification. From Equation 2.30, for a point $\boldsymbol{\theta}_0$ in the image plane corresponding to a point in the source plane $\beta_0 = \beta(\boldsymbol{\theta}_0)$, we have:

$$I(\boldsymbol{\theta}) = I^{\mathrm{s}}[\beta_0 + A(\boldsymbol{\theta}_0)(\boldsymbol{\theta} - \boldsymbol{\theta}_0)]. \tag{2.40}$$

Equation 2.37 describes the mapping of a circular source to an elliptic image. The ratio of the semi-major axes of the ellipse to the radius of the circular source is $1 - \kappa \pm \gamma$. The

flux observed from the image and the unlensed source are integrals over the respective surface brightness. The magnification is then the ratio of the image and source flux, and since the surface brightness is conserved, the magnification is also the ratio of the area of the unlensed galaxy to the lensed image. The magnification is given by:

$$\mu(\boldsymbol{\theta}) = \det M = \frac{1}{\det A} = \frac{1}{(1-\kappa)^2 - \gamma^2}. \tag{2.41}$$

The magnification observable is the magnitude of the magnification $|\mu|$.

2.1.6 Mass profiles

In modelling weak lensing, we need to assign a mass density profile to astrophysical objects. There are several models in current use, but we shall only discuss the two most common ones: the singular isothermal sphere, and the Navarro-Frenk-White model. For a review of models, see Keeton (2001), and references therein.

The singular isothermal sphere (SIS) is among the simplest of mass density profiles. It describes a wide range of astrophysical objects, including dark matter halos and virialised galaxies, with sufficient accuracy. The density profile of an SIS is (Schneider, 2006):

$$\rho(r) = \frac{\sigma_\nu^2}{2\pi G r^2}, \tag{2.42}$$

where r is the radius from the centre of the cluster and σ_ν is the one-dimensional velocity dispersion of stars (or galaxies) in the galaxy (or galaxy cluster). The surface mass density is calculated by projecting the density along the line-of-sight:

$$\Sigma(\xi) = \frac{\sigma_\nu^2}{2G\xi}. \tag{2.43}$$

The SIS has the property that the shear induced at a particular position is equal to the convergence at that point, i.e. $|\gamma(\xi)| = \kappa(\xi)$. For an SIS the convergence is

$$\kappa(\theta) = \frac{\theta_E}{2\theta} \quad \text{where} \quad \theta_E = 4\pi \left(\frac{\sigma_\nu}{c}\right)^2 \frac{D_{ds}}{D_s}. \tag{2.44}$$

The scaled deflection angle is constant for an SIS: $|\boldsymbol{\alpha}| = \theta_E$. Similarly, the effective lensing potential is: $\psi = \theta_E|\boldsymbol{\theta}|$. The shear can then be deduced from Equations 2.35:

$$\gamma(\boldsymbol{\theta}) = -\frac{\theta_E}{2|\boldsymbol{\theta}|} \mathrm{e}^{2i\phi}. \tag{2.45}$$

The SIS is a good approximation in many situations, but it breaks down in two ways: firstly, the mass distribution is infinite, and secondly, the density diverges for $\xi = 0$. In order to apply this approximation, therefore, it is often truncated at small and large radii.

Another widely used profile is the NFW profile, developed by Navarro, Frenk, & White (1997), who found that the density profiles of many dark matter haloes in numerical

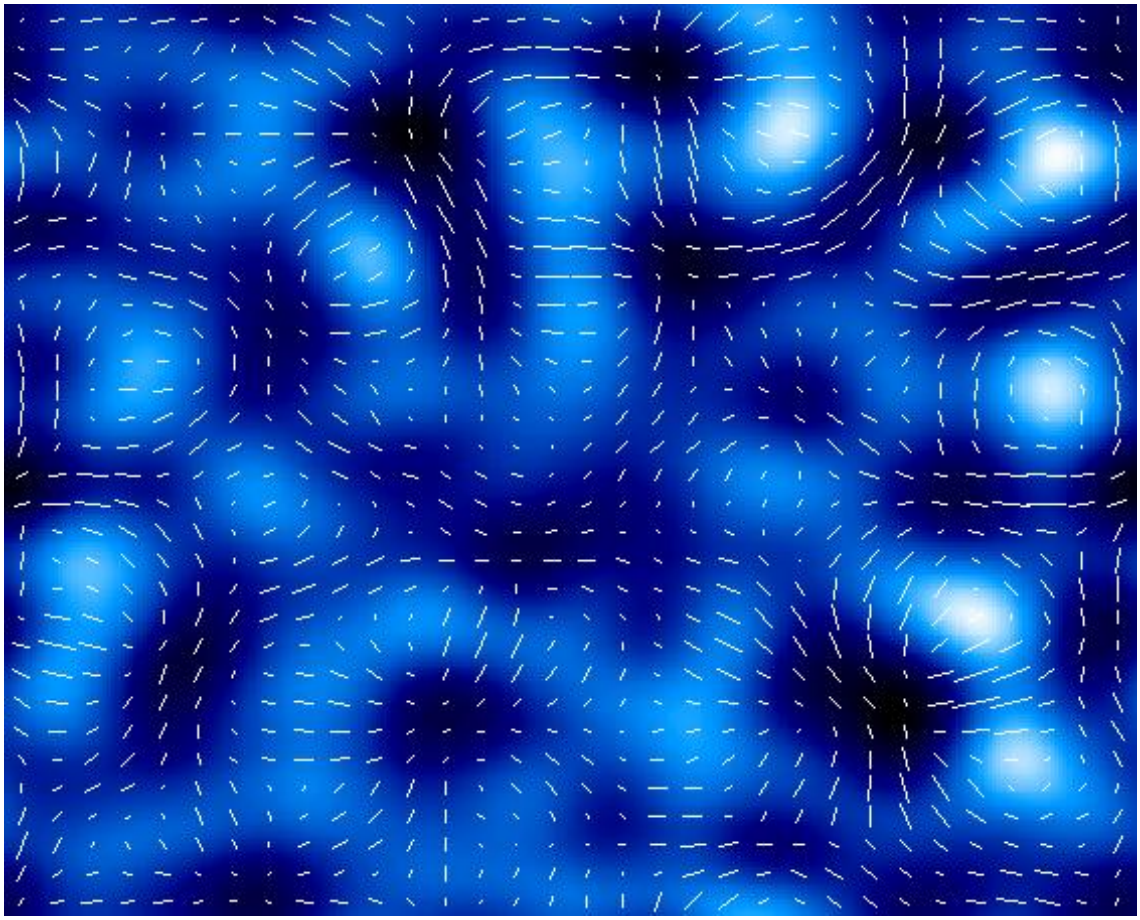

Figure 2.2: Convergence map with the shear overlaid, showing the strong link between the shear and convergence fields. Overdense, high convergence regions (shown in white) tend to be surrounded by a ring shear pattern, while underdense regions (in black) tend to be sourrounded by radial shear patterns (from `www.icosmo.org`).

simulations could be fitted by:

$$\rho(s) = \rho_c^0 \frac{\nu c^2 g(c)}{3s(1+cs)^2}, \tag{2.46}$$

where s is the radius in units of the virial radius $s = r/r_v$, c is the 'concentration parameter', which is related to the density of the halo, and $g(c) = 1/[\ln(1+c) - c/(1+c)]$. Typical values for the concentration parameter range from $c = 5$ for clusters of galaxies to $c = 10$ for large bright objects. The exact value depends on the mass of the object and on the primordial matter power spectrum. The NFW profile diverges from the SIS at small and large radii, while being a good approximation at intermediate radii.

2.2 Types of lensing

Gravitational lensing effects can be broadly divided into three main categories, which will be briefly explained in this section, in order to clarify the discussion of weak lensing in the next section. It should be emphasised that these categories are not sharply divided, and indeed there are many lensing configurations which fall under more than one category.

- Micro lensing occurs when the size of the lensing mass is small, so that the object behaves like a point source. This occurs in the case of single stars or planets. The magnification effect causes a temporary change in the brightness of the object, since microlensing causes a measurable increase in the flux.

- Strong lensing occurs when an image appears within or near a caustic, due to the light path in the lens plane passing within a critical curve. It can produce distorted, magnified and multiple images.

- Weak lensing produces weakly distorted, single images of sources outside of caustics. There is no standard definition of the term 'weak lensing', but observationally we can identify its statistical nature as the key aspect which distinguishes this effect from other forms of gravitational lensing. In other words, weak lensing can only be inferred by observing a (statistically) large number of images. This distinguishes it from strong lensing, where the effect is visible in single systems. Both weak and strong lensing are categorised as macro lensing, since the lensing is caused by extended massive objects, such as galaxies, galaxy clusters, or dark matter halos. The term weak lensing is generally applied to the case where the effect is caused by one lens. In the general case, where lensing may be due to more than one structure, the term 'cosmic lensing' is sometimes used. Cosmic lensing, therefore, is the term used to describe lensing caused by the general matter distribution of the Universe. This effect occurs even when an apparently empty region of the sky is observed. Lensing in this régime is studied using statistical techniques, such as the two-point correlation function of the shape distortions.

2.3 Weak lensing

In this section we shall examine the effects produced by weak lensing, and the formalism of weak lensing. There are two ways in which weak lensing can produce a measurable effect. Firstly, background galaxies will be weakly distorted by foreground structures, which can be either large-scale structure or galaxy clusters (see Villumsen 1996; Wittman et al. 2000). This effect is called weak shear. Secondly, the weak magnification effect can change the observed number density of source background galaxies or change the size of an image of a given surface brightness (see Van Waerbeke 2009 for a recent review of the two effects).

The terms 'weak lensing' and 'cosmic shear' are sometimes employed interchangeably. Strictly speaking, cosmic shear refers to shear by all foreground structures, including large-scale structure not in the line of sight of the lensed object, while weak lensing also includes magnification effects. The two terms are also distinguished by the régime in which observations are made: either around large galaxy cluster, or in the field (away from large densities), in which case the cosmic shear effect will be the dominant one. In this thesis, we will only work with cosmic shear, and the term 'weak lensing' in the context of our calculations should be understood to refer only to this effect, unless otherwise specified.

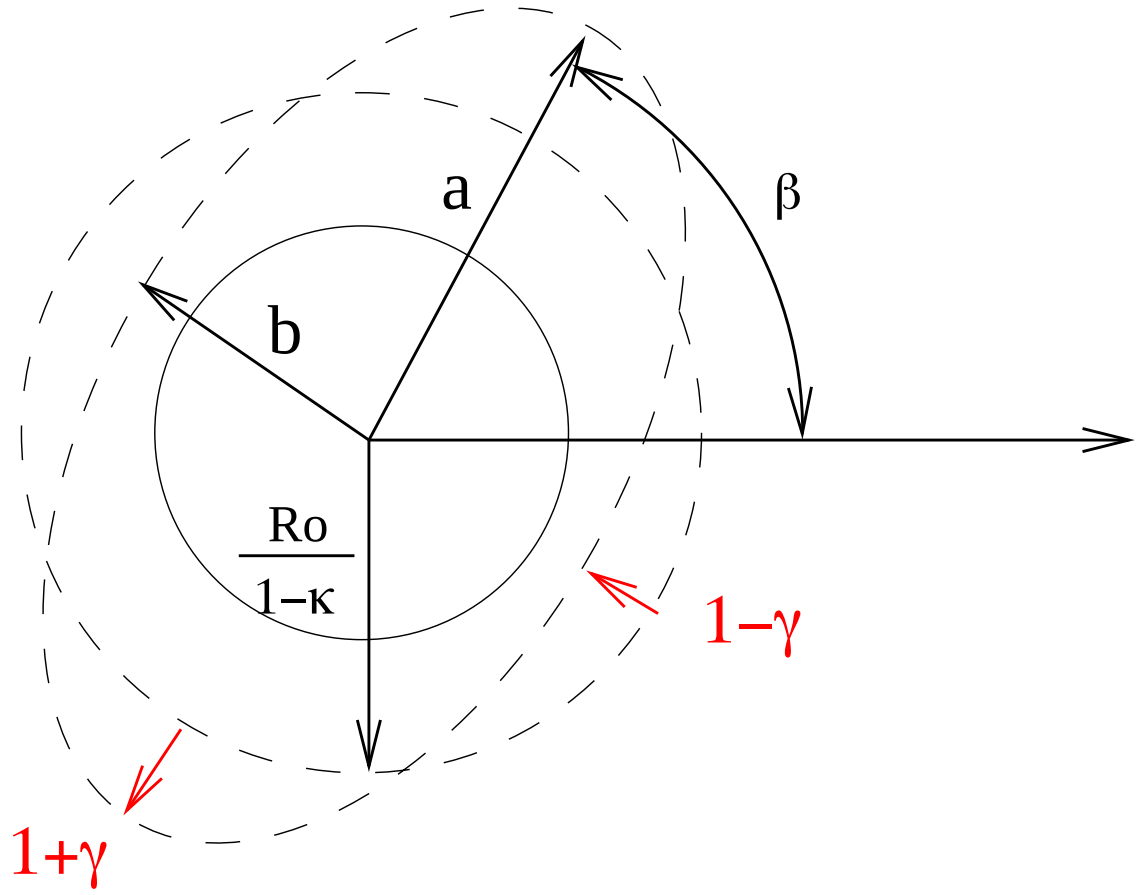

Figure 2.3: Schematic diagram showing lensing effects (shear and magnification) on a galaxy. In the source plane, the galaxy is circular, with radius R_0. The convergence κ stretches its average radius to $R_0/(1-\kappa)$ and the shear γ distorts the galaxy along some angle β. This results in an elliptical image with a and b as the semi-major and semi-minor axes respectively. In other words, convergence increases the average radius of the image, and shear stretches the circle into an ellipse (from Munshi et al. 2008).

2.3.1 Ellipticity

The effect of foreground structure is to distort the image of a background galaxy due to weak shear — a circular galaxy appears elliptical. However, we know that not all galaxies are circular. Therefore, for an elliptical galaxy, weak shear induces an additional ellipticity.

Referring to Figure 2.3, we may define the ellipticity of a galaxy as:

$$\epsilon = \frac{a^2 - b^2}{a^2 + b^2} \tag{2.47}$$

or as

$$\epsilon = \frac{a - b}{a + b}, \tag{2.48}$$

where a and b and the semi-major and semi-minor axes of the ellipse, respectively. We shall retain the first definition (2.47) throughout this chapter.

We need a way of relating the observed ellipticity to the shear. Consider a galaxy with a surface brightness profile $I(\boldsymbol{\theta})$ that is well defined for all angular separations from the centre $\overline{\boldsymbol{\theta}}$ of the image, so that:

$$\overline{\boldsymbol{\theta}} \equiv \frac{\int \mathrm{d}^2\boldsymbol{\theta} w[I(\boldsymbol{\theta})]\boldsymbol{\theta}}{\int \mathrm{d}^2\boldsymbol{\theta} w[I(\boldsymbol{\theta})]} \tag{2.49}$$

where $w[I(\boldsymbol{\theta})]$ is a suitably chosen weight function so that the integrals converge. The tensor of second brightness moments is:

$$Q_{ij} = \frac{\int \mathrm{d}^2\boldsymbol{\theta} w[I(\boldsymbol{\theta})](\theta_i - \overline{\theta_i})(\theta_j - \overline{\theta_j})}{\int \mathrm{d}^2\boldsymbol{\theta} w[I(\boldsymbol{\theta})]} \quad ; \quad i, j \in \{1, 2\}. \tag{2.50}$$

The trace part of the tensor Q_{ij} contains the size information while the traceless part contains ellipticity information. Thus for a circular image $Q_{11} = Q_{22}$ and $Q_{12} = Q_{21} = 0$. From the definition of Q_{ij}, a complex ellipticity, analogous to the complex shear, can be defined:

$$\epsilon = \epsilon_1 + i\epsilon_2 = |\epsilon| \mathrm{e}^{2i\phi} \tag{2.51}$$

where

$$\epsilon = \frac{Q_{11} - Q_{22} + 2iQ_{12}}{Q_{11} + Q_{22}} \tag{2.52}$$

or

$$\epsilon = \frac{Q_{11} - Q_{22} + 2iQ_{12}}{Q_{11} + Q_{22} + 2(Q_{11}Q_{22} - Q_{12}^2)^{1/2}}. \tag{2.53}$$

We shall use the definition in Equation 2.53. For a circular image, $\epsilon_1 = \epsilon_2 = 0$ (see Figure 2.4).

Bartelmann & Schneider (2001) and Schneider (2006) show that the original ellip-

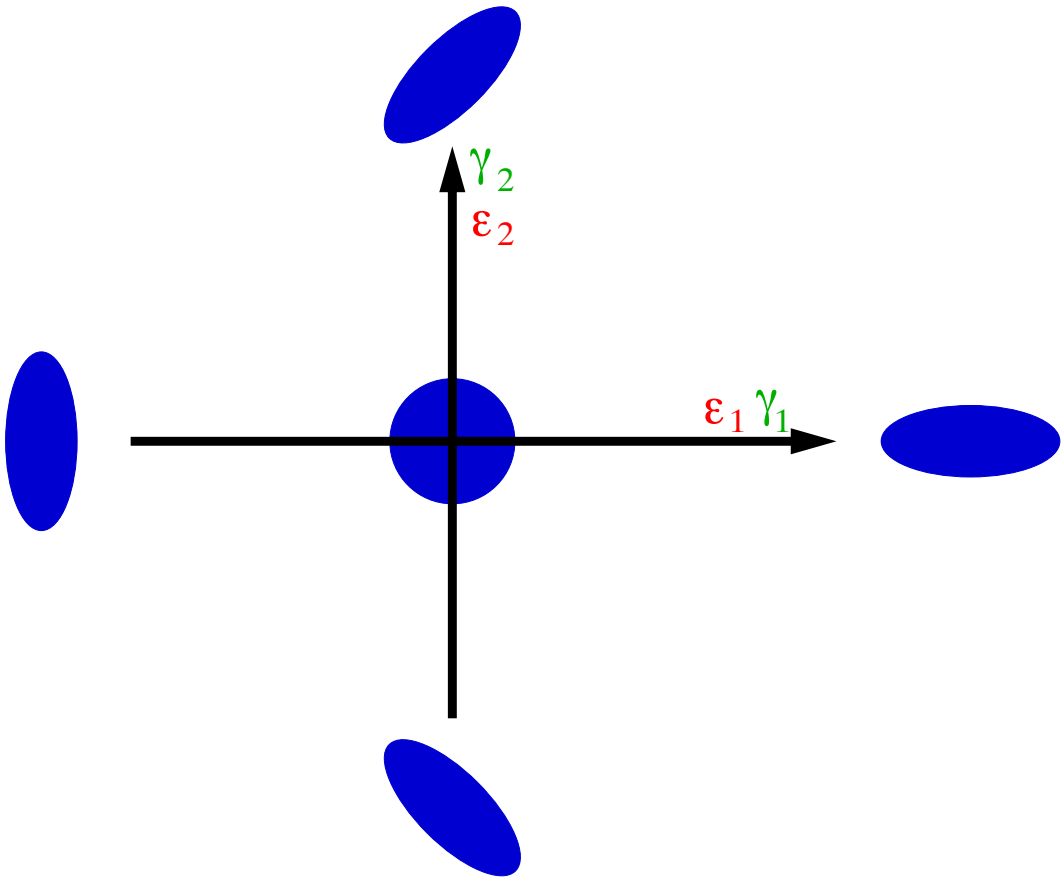

Figure 2.4: Schematic illustration of the geometrical meaning of the shear γ and the ellipticity ϵ. Using a Cartesian axis, a positive shear component γ_1 corresponds to an elongation along the x-axis. A negative component gives a compression along the same axis. A positive (or negative) shear component γ_2 corresponds to an elongation (or compression) along the $x = y$ direction. For a circular object (shown at the centre), both ellipticity components are equal to zero. The ellipticity components ϵ_1 and ϵ_2 correspond to the same compression and elongation as the shear components (from Réfrégier 2003b).

ticity ϵ^S of a source galaxy is transformed under lensing, by Equation 2.53 as:

$$\epsilon^S = \begin{cases} \dfrac{\epsilon - g}{1 - g^*\epsilon} & \text{for} \quad |g| \leq 1 \\ \\ \dfrac{\epsilon - g\epsilon^*}{\epsilon^* - g^*} & \text{for} \quad |g| > 1. \end{cases} \tag{2.54}$$

To write ϵ in terms of ϵ^S, the inverse transformation is obtained by interchanging ϵ with ϵ^* and replacing g by $-g$. In the weak lensing case, $|g| \ll 1$, and the inverse of Equation 2.54 reduces to:

$$\epsilon \approx \epsilon^S + g. \tag{2.55}$$

The above equation applies to individual galaxies, but it cannot be used if the ellipticity of the individual source is unknown. At this point, we use a key property of weak lensing observations — their statistical nature. When a large statistical sample of galaxies is used, the average intrinsic ellipticity should be zero, since there is no preferred orientation of galaxies in the Universe. Mathematically, therefore:

$$\langle \epsilon^S \rangle = 0. \tag{2.56}$$

The average additional ellipticity in the weak lensing régime then becomes:

$$\langle \epsilon \rangle = 0 + \langle g \rangle. \tag{2.57}$$

An estimator for the shear can be deduced by assuming that the galaxy covers a small angular patch in the sky, so that the light from each part of the galaxy experiences approximately the same gravitational field:

$$\gamma \approx g \approx \langle g \rangle = \langle \epsilon \rangle. \tag{2.58}$$

This result holds for a redshift-distributed source population (Bartelmann & Schneider, 2001). Equation 2.58 implies that the variance in the shear is related to the variance in the ellipticity by:

$$\sigma_\gamma^2 = \sigma_\epsilon^2. \tag{2.59}$$

Using the definition of complex ellipticity in Equation 2.52 we would obtain $\langle \epsilon \rangle = 0 + 2\langle g \rangle$, $\gamma \approx \langle \epsilon \rangle$, and $\sigma_\gamma^2 = \sigma_\epsilon^2/4$. In our calculations, we shall retain the definition for the variance in the ellipticity in Equation 2.59.

2.3.2 Higher order weak lensing

So far we have assumed that the distortion matrix is constant across the whole image, producing an ellipticity. However, the matirx A can vary across an image, producing higher order effects and leading to a circular source being distorted not into an ellipse, but into an arc. This effect is termed flexion. Going back to the distortion matrix, we

can write this quantity in a form which allows a clear physical interpretation:

$$A = \begin{pmatrix} 1-\kappa & 0 \\ 0 & 1-\kappa \end{pmatrix} + \begin{pmatrix} -\gamma_1 & -\gamma_2 \\ -\gamma_2 & \gamma_1 \end{pmatrix} + \begin{pmatrix} 0 & \rho \\ -\rho & 0 \end{pmatrix}, \tag{2.60}$$

where κ and γ have the usual meaning of convergence and shear, respectively, and ρ is a rotation, which is not observed in weak lensing, but can be caused by telescope rotation. The image's surface brightness $f_{\rm I}$ at a position θ can be written in terms of the source surface brightness $f_{\rm S}$:

$$f_{\rm i}(\theta_i) = f_{\rm S}(A_{ij}\theta_j). \tag{2.61}$$

If A varies across the image, we can take its mean, and write the corrections to this mean as a Taylor series to second order:

$$f_{\rm i}(\theta_i) = f_{\rm S}\left(A_{ij}\theta_j + \frac{1}{2}D_{ijk}\theta_j\theta_k\right). \tag{2.62}$$

The tensor D in the above equation contains the information about the amount of flexion in the image. It is given by

$$D_{ijk} = \partial_i A_{jk} = \frac{\partial^3\psi}{\partial\theta_i\partial\theta_j\partial\theta_k}. \tag{2.63}$$

This can be written in terms of flexion components:

$$F = \frac{1}{2}\partial\partial\partial^*\psi \quad G = \frac{1}{2}\partial\partial\partial\psi, \tag{2.64}$$

respectively known as the 1-flexion and 3-flexion. The latter has 120° rotational symmetry, while the former has 360° rotational symmetry (i.e. it is a vector). The description of flexion in lensed objects is given by the components of F and G:

$$-2D_{ij1} = \begin{pmatrix} 3F_1 & F_2 \\ F_2 & F_1 \end{pmatrix} + \begin{pmatrix} G_1 & G_2 \\ G_2 & -G_1 \end{pmatrix}$$

$$-2D_{ij2} = \begin{pmatrix} F_2 & F_1 \\ F_1 & 3F_2 \end{pmatrix} + \begin{pmatrix} G_2 & -G_1 \\ -G_1 & -G_2 \end{pmatrix}. \tag{2.65}$$

There exists an additional second-order effect which is termed 'twist and turn'. This appears when the remaining degrees of freedom in D are found (see Bacon & Schäfer,

2009):

$$-2D_{ij1} = \begin{pmatrix} 3F_1 & F_2 \\ F_2 & F_1 \end{pmatrix} + \begin{pmatrix} G_1 & G_2 \\ G_2 & -G_1 \end{pmatrix} + \begin{pmatrix} 0 & -C_1 \\ C_1 & 0 \end{pmatrix} + \begin{pmatrix} 0 & T_1 - T_2 \\ T_1 - T - 2 & -2T_1 - 2T_2 \end{pmatrix}$$

$$-2D_{ij2} = \begin{pmatrix} F_2 & F_1 \\ F_1 & 3F_2 \end{pmatrix} + \begin{pmatrix} G_2 & -G_1 \\ -G_1 & -G_2 \end{pmatrix} + \begin{pmatrix} 0 & -C_1 \\ C_2 & 0 \end{pmatrix} + \begin{pmatrix} -2T_1 + 2T_2 & T_1 + T_2 \\ T_1 + T_2 & 0 \end{pmatrix}. \tag{2.66}$$

The terms C and T are called the 'twist' and 'turn', respectively. These terms have no effects on circularly symmetric objects. In this respect, they are similar to ρ. The interest of these higher-order lensing effects lies in their potential application to future high-precision weak lensing surveys.

2.3.3 Tangential shear

The components of complex shear γ_1 and γ_2 are defined relative to a local Cartesian coordinate frame. Consider a pair of galaxy images with an angular separation ϕ_c (i.e. the polar angle of the separation vector $\boldsymbol{\theta}$) about the centre of the coordinate frame. Then the tangential and cross-component of the shear at this position for this pair of galaxies, respectively aligned perpendicular and parallel to the radius vector, are:

$$\gamma_t = \mathrm{Re}[\gamma \mathrm{e}^{-2i\phi_c}] \quad \text{and} \quad \gamma_\times = \mathrm{Im}[\gamma \mathrm{e}^{-2i\phi_c}], \tag{2.67}$$

where Re and Im denote the real and imaginary parts, respectively. Equivalently,

$$\gamma_t = -[\gamma - 1\cos(2\phi_c) + \gamma_2 \sin(2\phi_c)] \quad \text{and} \quad \gamma_\times = -\gamma_1 \sin(2\phi_c) + \gamma_2 \cos(2\phi_c). \tag{2.68}$$

We can then define the correlation functions $\langle \gamma_t \gamma_t \rangle$, $\langle \gamma_\times \gamma_\times \rangle$ as well as the mixed correlator $\langle \gamma_t \gamma_\times \rangle$. This allows us to write the definition

$$\xi_\pm(\theta) = \langle \gamma_t \gamma_t \rangle(\theta) \pm \langle \gamma_\times \gamma_\times \rangle(\theta), \quad \text{and} \quad \xi_\times(\theta) = \langle \gamma_t \gamma_\times \rangle(\theta). \tag{2.69}$$

Due to parity symmetry, $\xi_\times(\theta)$ is expected to vanish since a parity transformation in the coordinates means that $\gamma_t \to \gamma_t$ but $\gamma_\times \to -\gamma_\times$. The residual cross-component shear $\gamma_\times$ can therefore be used to estimate the noise on the measurement of the tangential shear.

2.3.4 E-modes and B-modes

At the level of 2-point statistics, one expects that (Schneider, 2006):

$$\int_0^\infty \mathrm{d}\theta\, \theta \xi_+(\theta) \mathrm{J}_0(\theta \ell) = \int_0^\infty \mathrm{d}\theta\, \theta \xi_-(\theta) \mathrm{J}_4(\theta \ell), \tag{2.70}$$

where J_0 and J_4 are Bessel integrals, and $\xi_\pm$ are defined in Equation 2.69 . The observed shear field is not guaranteed to satisfy these relations, due to noise, systematics, or other

effects. Small derivations from the above relations are therefore due to non-lensing effects. Shear components which satisfy Equation 2.70 are called E-modes, while those that do not are called B-modes (the names are analogous to those employed for the CMB polarisation field).

There may be two possible causes for B-modes that are not due to systematic effects. Firstly, the Born approximation may not be strictly valid. This, however, is expected to give very small resulting B-modes (see Hilbert et al., 2009). Secondly, there may be clustering of source galaxies. Again, the effect is expected to be very small. However, the current best guess for the origin of B-modes remains intrinsic alignment of galaxy ellipticities (see Kilbinger et al., 2006). It is beyond the scope of this thesis to go into the details of these mechanisms. A detailed discussion of E- and B-modes, together with the relevant formalism and possible causes, is found in Schneider (2006), and references therein, and also in Schneider et al. (2002).

2.3.5 Shear measurement methods

The above discussion shows that the ellipticity observable is related to the shear, and by measuring the former we can calculate the latter. The difficulty of weak lensing probes is to detect the true lensing signal while correcting for instrumental and atmospheric distortions, which can be up to one order of magnitude higher than the gravitational shear distortion. There are a number of complementary techniques to measure the ellipticity of a galaxy induced by cosmic shear. The aim of these methods is to measure the true induced ellipticity by correcting for any non-gravitational source of alignment due to the point-spread function and camera distortions.

The first method to be developed, and also among the most commonly used, is the KSB method (Kaiser, Squires, & Broadhurst, 1995). This allows for the removal of the smearing of a galaxy's image due to an anisotropic point spread function on the instrument. The KSB method has been intensively tested and is at the basis of two other techniques: the 'extended KSB' (Kaiser, 2000) and the 'modified KSB' (Rhodes et al., 2000). Another method, developed more recently, is shapelets (Réfrégier, 2003a; Réfrégier & Bacon, 2003). In the shapelet formalism, the galaxy's image is decomposed into spherical polar harmonics, with the shear signal corresponding to particular 'quantum numbers'. This method, which uses Cartesian coordinates, has been further developed by Massey & Réfrégier (2005), who use polar coordinates. An overview of further methods, with the relevant citations, is given in Réfrégier (2003b), Van Waerbeke & Mellier (2003) and Bridle et al. (2009b).

2.4 Cosmic shear

Weak lensing does not only occur in the presence of galaxy clusters. Even an apparently 'empty' field background should produce some shear on background galaxies, due to the intervening LSS. The term 'cosmic shear' is used to describe shear due to lensing by LSS away from galaxy clusters. The formalism of cosmic shear will therefore be a generalisation of the weak shear formalism for a single lens.

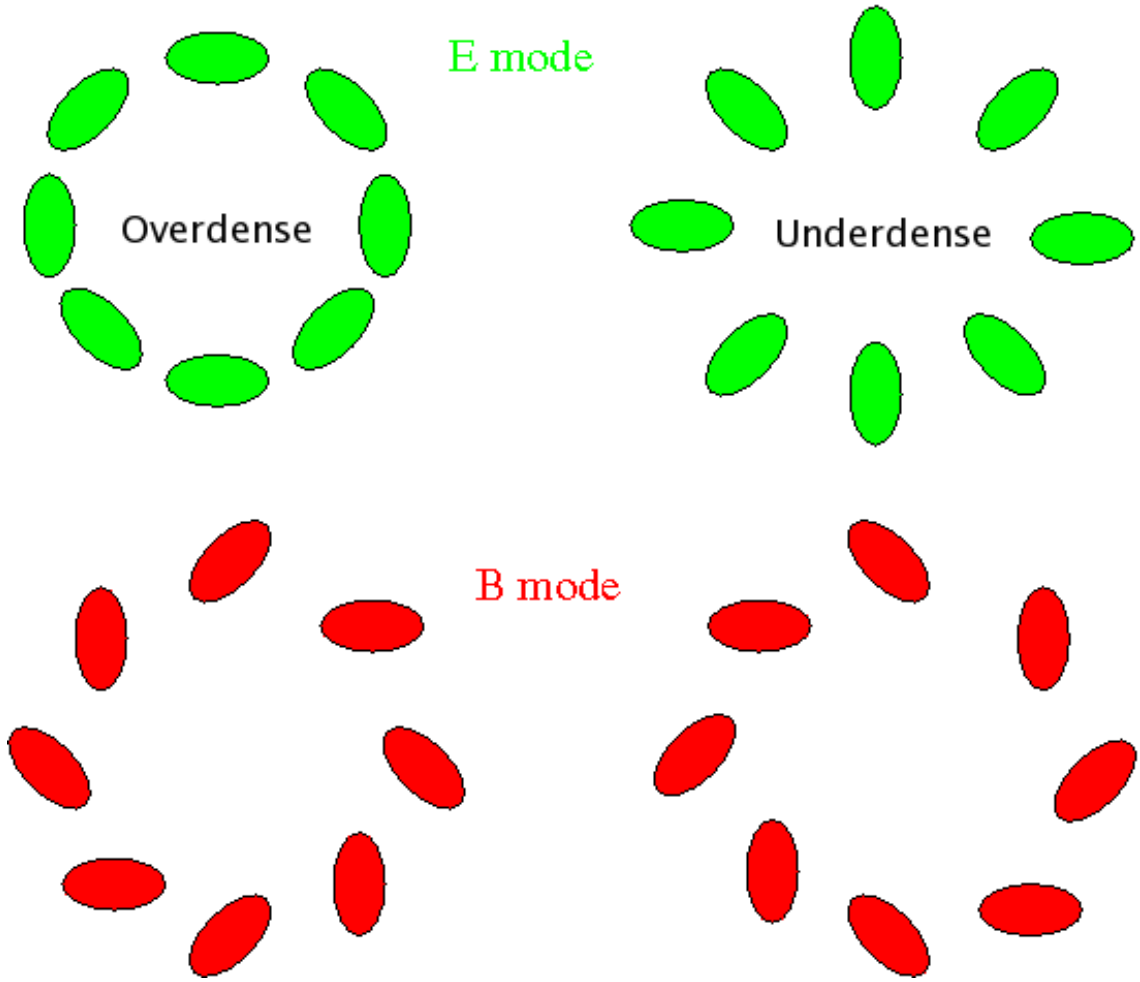

Figure 2.5: Representation of E- and B-modes of the shear. The upper row shows a typical E-mode shear pattern caused by a mass overdensity (left) or underdensity (right), giving the tangential and radial alignment of the shear, respectively. The lower row shows a B-mode pattern, which is obtained from the E-mode pattern by rotating all shears by 45°. B-modes cannot be produced by gravitational lensing (from Van Waerbeke & Mellier 2003).

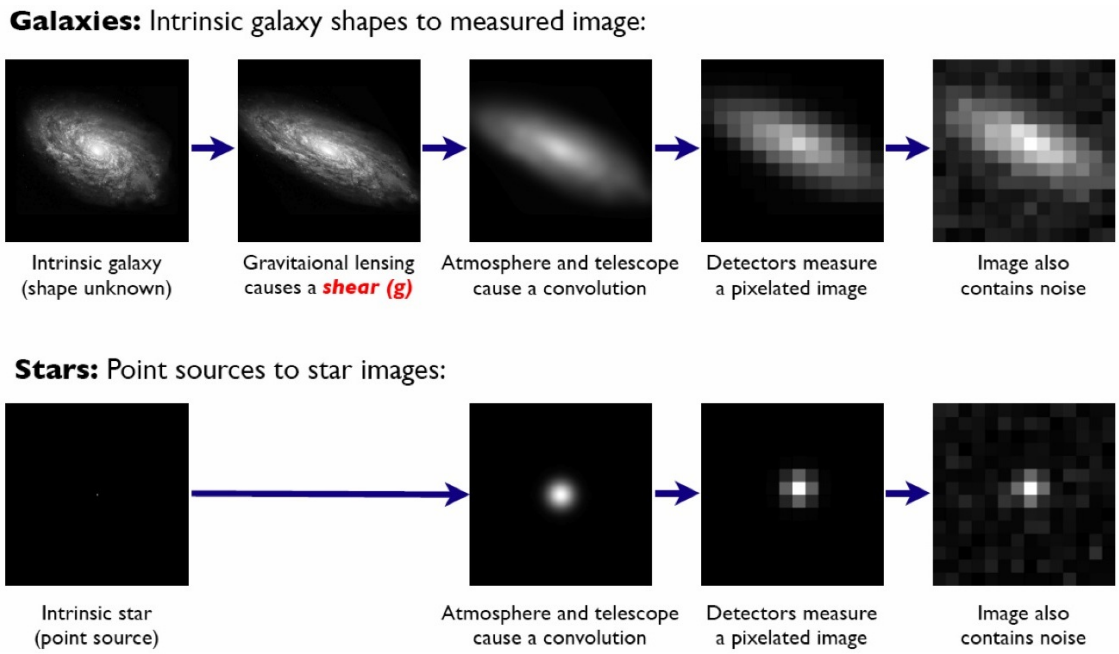

Figure 2.6: The effect of weak lensing as detected on the observed image of a galaxy (top panels) and a point source such as a star (bottom panel). The series of pictures illustrates how the final observed signal is a sum of the lensing signal and noise, after convolution with the point-spread-function (PSF) of the experiment, which causes blurring. In contrast, no shear signal can be observed in the case of individual stars, since they act as a point source. This can be utilised to correct for the effect of the contaminant signals, since star images are subject to the same PSF and noise as galaxy images. Although the different shear measurement techniques vary in their details, they all involve some form of the inverse of this transform i.e. starting from the image on the right-hand side, they work backwards to the left-hand side (figure taken from Bridle et al., 2009b).

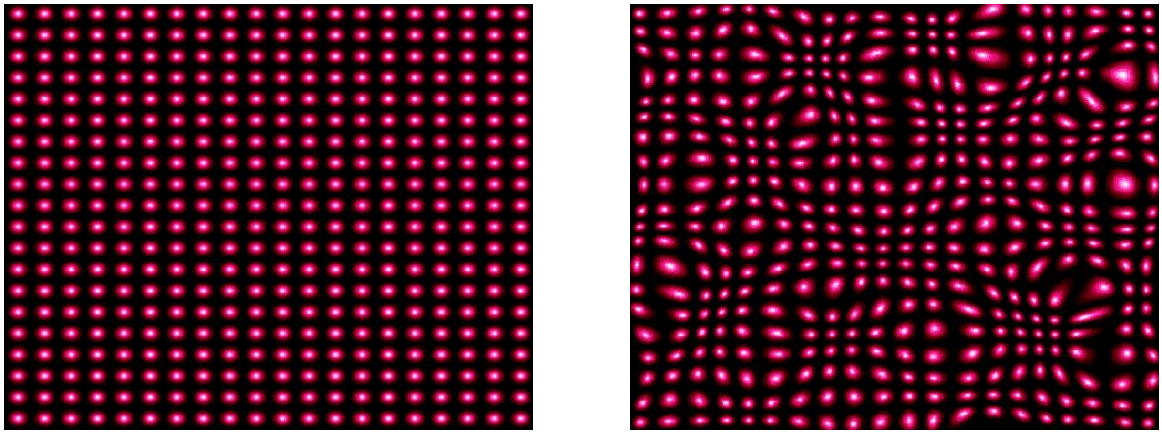

Figure 2.7: The effect of image distortion. On the left we see an unlensed image of a group of galaxies, represented by circular Gaussian mass distributions on a regular grid. On the left we can see the effect of lensing, calculated using a Gaussian random field for the dark matter density. For illustration purposes, the lensing effect has been exaggerated by a factor of 10 (from `www.icosmo.org`).

The treatment is analogous to that of a single lens system. By generalising Equation 2.20, the effective cosmological lensing potential $\phi(r, \boldsymbol{\theta})$ can be related to the 3D comoving gravitational potential of the lens $\Phi(r, \boldsymbol{\theta})$ by (see Bartelmann & Schneider, 2001):

$$\phi(r, \boldsymbol{\theta}) = \frac{2}{c^2} \int_0^r \mathrm{d}r' \left[\frac{S_k(r - r')}{S_k(r) S_k(r')} \right] \Phi(r', \boldsymbol{\theta}), \tag{2.71}$$

where r is the comoving distance and S_k is defined in Equation 1.24. We shall henceforth write any function $r(S_k)$ as r.

The effective lensing potential, defined in Equation 2.23, can be generalised to obtain the cosmic lensing potential:

$$\nabla^2 \phi = 2\kappa. \tag{2.72}$$

The value of κ at a position on the sky $\boldsymbol{\theta}$ for source galaxies at a distance r, known as the convergence field or the effective convergence, can be written as:

$$\kappa(r, \boldsymbol{\theta}) = \frac{1}{c^2} \int_0^r \mathrm{d}r' \left[\frac{(r - r')}{r r'} \right] r'^2 \frac{\partial^2 \Phi(r', \boldsymbol{\theta})}{\partial r'^2}. \tag{2.73}$$

Poisson's equation for the 3D potential is:

$$\begin{aligned} \nabla^2 \Phi(r) &= 4\pi G \rho_m a^2 \delta \\ &= \frac{3}{2} H_0^2 \Omega_m a^{-1} \delta \end{aligned} \tag{2.74}$$

where ρ_m is the cosmological matter density, a is the scale factor, and δ is the relative matter density contrast. Using this, Equation 2.73 can be rewritten:

$$\kappa(r, \boldsymbol{\theta}) = \frac{3}{2} \left(\frac{H_0}{c} \right)^2 \Omega_m \int_0^r \mathrm{d}r' \left[\frac{(r - r')}{r} \right] r'^2 \frac{\delta(r'\boldsymbol{\theta}, r')}{a(r'^2)}, \tag{2.75}$$

where $\delta(r\boldsymbol{\theta}, r)$ is the fractional matter overdensity at comoving distance r and position $\boldsymbol{\theta}$. To apply this to a real cosmological matter distribution, we include a normalised redshift distribution for the source galaxies $P(z)\,\mathrm{d}z = G(r)\,\mathrm{d}r$, and integrate over the redshift distribution. The convergence field can then be generalised to:

$$\kappa(r, \boldsymbol{\theta}) = \frac{3}{2} \left(\frac{H_0}{c} \right)^2 \Omega_m \int_0^r r'\,\mathrm{d}r' \overline{W}(r, r') \frac{\delta(r'\boldsymbol{\theta}, r')}{a(r'^2)} \tag{2.76}$$

where

$$\overline{W}(r, r') = \int_{r'}^r \mathrm{d}\tilde{r} G(\tilde{r}) \left[\frac{\tilde{r} - r'}{\tilde{r}} \right]. \tag{2.77}$$

Equations 2.33 and 2.34 can now be generalised via the transformation $\psi \to \phi$

$$\begin{aligned} \kappa(r, \boldsymbol{\theta}) &= \tfrac{1}{2}(\phi_{11} + \phi_{22}) \\ \gamma_1(r, \boldsymbol{\theta}) &= \tfrac{1}{2}(\phi_{11} - \phi_{22}) \\ \gamma_2(r, \boldsymbol{\theta}) &= \phi_{12} = \phi_{21}. \end{aligned} \tag{2.78}$$

2.4.1 Effective 2D convergence spectrum

When we observe a patch of sky, we can only measure angular correlations between galaxies, so we need a way to infer the real-space correlations and thus construct the matter power spectrum. This is done using the Limber (1953) approximation.

The equations for cosmic shear presented in the previous section can be recast so that the shear is a continuous field in Fourier space. The Fourier transform of $\kappa(\boldsymbol{\theta})$ is:

$$\kappa(\boldsymbol{\theta}) = \int \frac{\mathrm{d}^2\ell}{2\pi}\kappa(\boldsymbol{\ell})\mathrm{e}^{i\ell.\boldsymbol{\theta}}. \tag{2.79}$$

The two-dimensional effective convergence power spectrum $C_\ell^{\kappa\kappa}$ can then be defined through:

$$\langle\kappa(\boldsymbol{\ell})\kappa^*(\boldsymbol{\ell}')\rangle = (2\pi)^2 C_\ell^{\kappa\kappa}\delta_D(\boldsymbol{\ell}-\boldsymbol{\ell}') \tag{2.80}$$

where δ_D is the Dirac delta function.

In general, under the assumptions of statistical isotropy and small angles (which are valid for weak lensing observations) the two-point observables of a set of two-dimensional scalar fields $x_i(\hat{\mathbf{n}})$, where $\mathbf{n}$ represents the direction on the sky, are given by their angular power spectra

$$\langle x_i^*(\mathbf{l})x_j(\mathbf{l}')\rangle = (2\pi)^2\delta(\mathbf{l}-\mathbf{l}')C_\ell^{x_i x_j}\,, \tag{2.81}$$

where $\mathbf{l}$ is the Fourier wavevector or multipole

$$x_i(\hat{\mathbf{n}}) = \int \frac{d^2\ell}{(2\pi)^2}x_i(\mathbf{l})\mathrm{e}^{i\mathbf{l}\cdot\hat{\mathbf{n}}}. \tag{2.82}$$

We relate these two-dimensional angular fields to three-dimensional source fields $s_i(\mathbf{r};z)$ by a weighted projection

$$x_i(\hat{\mathbf{n}}) = \int dz W_i(z)s_i(\mathbf{r}_i = \hat{\mathbf{n}}D_A, z), \tag{2.83}$$

where $D_A(z)$ is the angular diameter distance in comoving coordinates and $W_i(z)$ is some weight function.

The three-dimensional power spectra are then projected onto the two-dimensional lensing correlation function using the relation given by the Limber equation (Limber, 1953; Kaiser, 1992):

$$C_\ell^{S_iS_j} = \int \mathrm{d}z\frac{H}{D_A^2}W_i(z)W_j(z)P^{S_iS_j}(k=\ell/D_A,z), \tag{2.84}$$

where $H(z)\equiv a^{-1}da/dt$ is the Hubble parameter. The three-dimensional source power spectrum is defined by

$$\langle s_i^*(\mathbf{k})s_j(\mathbf{k}')\rangle = (2\pi)^3\delta(\mathbf{k}-\mathbf{k}')P^{s_is_j}(k). \tag{2.85}$$

The Limber approximation is assumed to be accurate for the purpose of our weak lensing survey. However, Simon (2007) has pointed out that the assumptions upon which it

is based break down beyond a certain galaxy separation, so that the equation becomes increasingly inaccurate for larger angular separations.

In our calculations, the two dimensional fields are the 'lens' galaxy number density fluctuations and the electric or ϵ component of the weak lensing shear field measured with 'source' galaxies. One can use different binning strategies for the lens and source galaxies of a given survey: redshift, luminosity, colour, etc.. Weak lensing tomography divides the galaxies into redshift bins.

In Equation 2.84 the source field is the three-dimensional number $n_V(\mathbf{r}, z)$ or rather its fluctuations:

$$s_i(\mathbf{r}, z) = \delta_g = \frac{\delta n_V}{\overline{n}_V}, \tag{2.86}$$

and the weight for the angular fluctuation field $g(\hat{\mathbf{n}})$ is the normalised redshift distribution function

$$W_g(z) = \frac{D_A^2}{H}\frac{\overline{n}_V}{\overline{n}_A}, \tag{2.87}$$

where the normalisation factor

$$\overline{n}_A = \int dz \frac{D_A^2}{H}\overline{n}_V \tag{2.88}$$

is the angular number density in sr^{-1}. The weights are normalised so that $\int W_g(z)dz = 1$.

The ϵ field itself is a projection of the mass density fluctuation

$$s(\boldsymbol{r}; z) = \delta_m = \frac{\delta\rho_m}{\rho_m}, \tag{2.89}$$

and hence is equal to the convergence $\kappa(\boldsymbol{n})$.

In tomographic weak lensing, the only observable being considered is the correlation between and within redshift bins. The Limber equation therefore has the form:

$$C_\ell^{ij} = \int \mathrm{d}z \frac{H}{D_A^2} W_i(z) W_j(z) P(k = \ell/D_A, z), \tag{2.90}$$

where i, j denote redshift bins. The weighting function $W_i(z)$ is defined by the lensing efficiency:

$$W_i(z) = \frac{3}{2}\Omega_m \frac{H_0}{H}\frac{H_0 D_{OL}}{a}\int_z^\infty \mathrm{d}z' \frac{D_{LS}}{D_{OS}} W_i(z'), \tag{2.91}$$

where the angular diameter distance to the lens is D_{OL}, the distance to the source is D_{OS}, and the distance between the source and the lens is D_{LS} (see Hu & Jain 2004 for details). In general, the distribution of source galaxies $W_g(z')$ need not be the same as for the lens galaxies above. Furthermore, the normalised redshift distribution W_g is the direct observable, so that the efficiency W_i for a known W_g may be used to probe cosmology.

Kaiser (1998) showed that by applying Limber's equation in Fourier space, the 2D effective convergence spectrum can be be related to the 3D matter power spectrum P_δ by:

$$C_\ell^{\kappa\kappa} = \frac{9}{4}\left(\frac{H_0}{c}\right)^4 \Omega_m^2 \int_0^{r_H} \mathrm{d}r P_\delta(\ell/r, r)\left[\frac{\overline{W}(r)}{a(r)}\right]^2. \tag{2.92}$$

This important equation is at the heart of this thesis, since it allows us to relate a the convergence, which is measured by weak lensing probes, to cosmological parameters via the matter power spectrum. The expression can be applied to actual weak lensing experiment s, and also to future experiments, for which we need to find the predicted cosmological parameter constraints. Note that it is the *total* matter density Ω_m which enters the equation. This quantity includes baryonic matter, cold dark matter, and hot dark matter (neutrinos). Weak lensing therefore depends on the total matter content, and the only physical process involved is gravitation. Since most of the matter content of the Universe is dark matter, which has not been directly observed, it is immediately evident that the weak lensing provides a sensitive probe of dark matter in particular. The other quantity of interest is matter power spectrum. Weak lensing therefore also probes the evolution of structure. This obviously depends on the various matter densities, but also on the geometry of the Universe, which is also governed by dark energy, and its evolution.

2.5 Systematic effects

Here we review the main sources of systematics in weak lensing measurements, and strategies to overcome systematics. A discussion of systematic effects, and of techniques to reduce these effects, is found in Réfrégier (2003b) and Schneider (2006).

Intrinsic correlations

The essential quantity in weak lensing observations is the cosmic shear signal, obtained by correlating the measured ellipticities of distant galaxies. We have already seen how the statistical nature of weak lensing overcomes the obvious difficulty in determining the true additional ellipticity when galaxies are not circular (Equation 2.56). In fact, the intrinsic ellipticity is typically one order of magnitude larger than the ellipticity induced by gravitational shear. This is overcome by measuring the ellipticity correlations for many pairs of galaxies. Expressing the measured ellipticity ϵ as the sum of the intrinsic ellipticity $\epsilon^{\rm S}$ and gravitational shear γ, in the standard weak shear treatment. The correlation between the ellipticities for two galaxies i and j is then:

$$\langle \epsilon_i \epsilon_j \rangle = \langle \gamma_i \gamma_j \rangle + + \langle \epsilon_i^{\rm S} \epsilon_j^{\rm S} \rangle + \langle \gamma_i \epsilon_j^{\rm S} \rangle + \langle \epsilon_i^{\rm S} \gamma_j \rangle. \tag{2.93}$$

Equation 2.56 is then obtained by assuming that the intrinsic ellipticities of galaxies are randomly distributed, so that they are correlated neither with the intrinsic ellipticities nor with the shears of neighbouring galaxies. All the terms on the right-hand side of the above equations except the first one then reduce to zero, and the correlated ellipticities then give the shear signal.

However, in high-precision cosmic shear measurements, the assumption of random intrinsic ellipticities is no longer accurate, since galaxies can be intrinsically aligned and therefore possess correlated intrinsic ellipticities. There are three main systematic effects that can contaminate the shear signal.

Two physically close galaxies can be aligned by the same dark matter halo surrounding them. This means that the second term on the right-hand side of Equation 2.93 is

non-zero, and the cosmic shear measurement is therefore contaminated. This systematic effect is termed intrinsic ellipticity correlation (or 'II correlations').

If galaxy i is located at a significantly lower redshift than galaxy j (i.e. closer to the observer), then this second RHS term should vanish, because the shear signal of galaxy i is not correlated with the intrinsic shape of a background object (unless we encounter the rather improbable situation of an extended matter structure along the line-of-sight, for instance). However, the third term on the right-hand-side of Equation 2.93 can contribute to the ellipticity correlator. If a matter structure causes the alignment of a nearby galaxy and at the same time contributes to the lensing signal of a background galaxy, then shear-ellipticity correlations are produced. These so-called 'GI correlations', first discussed by Hirata & Seljak (2004) produce a net anti-correlation. This is due to the fact that the shear of the background galaxy is preferentially tangential to the deflecting matter concentration, whereas the foreground galaxy is on average radially aligned with the matter structure.

Both II and GI contamination can contribute as much as 10% to the lensing signal[2]. Indeed, third order statistics might be contaminated by III, GII and GGI terms to a higher level than for two-point statistics (see Semboloni et al., 2008). There exist solutions to intrinsic alignment contaminants. Weak lensing techniques which include redshift information, such as tomography and 3D weak lensing, reduce the problem of II correlations by decoupling the long-distance line-of-sight effects from the the physical proximity of the galaxies (see e.g. King & Schneider, 2003). Using this approach, a nulling technique for shear-intrinsic ellipticity has been proposed by Joachimi & Schneider (2008, 2009). Another solution is to put priors on the intrinsic alignments (Bridle & King, 2007; Kitching et al., 2008c).

Measurement systematics

Any imaging system will produce some blurring of point objects, which is described by the point spread function (PSF). This can cause an additional ellipticity in the image, which can cause serious systematics, especially if the PSF is anisotropic (see Kaiser et al., 1995). Even if the PSF ellipticity is isotropic, there will be some limit to the precision of shear measurements (see Hirata & Seljak, 2003). Another source of instrument systematics is the pixel-to-pixel nonlinearity which can exist in CCD cameras, and which can induce bias in the shear measurements. Since future surveys require shear measurements of the order of 1% with an accuracy better than 0.1%, smaller shear signals will require an even better accuracy.

The challenge of weak lensing observations is to disentangle the distortions caused by weak lensing from those caused by systematics. The lensing signal is only a few percent in amplitude, and systematic effects may produce a larger signal. The various shear measurement methods involve a number of steps designed to reduce systematic effects to a minimum (see Réfrégier, 2003b, and references therein). The first step is image processing, where the final reduced images are produced, and any instrumental distortion caused by the telescope is corrected for. The next step is to derive an estimator

[2]Additionally, II correlations may be responsible for B-modes

for the shear from the shapes of the galaxies in the final reduced images. This involves a correction for PSF effects (see Figure 2.6 for a schematic illustration of these steps).

To this end, various methods have been devised, and there is an ongoing effort to test these methods and establish whether they will achieve the required precision. The need to compare the various methods has given rise to various collaborations, of which will mention two.

The Shear Testing Programme[3], now in its fourth year (2009), is a collaborative project which aims to improve the accuracy and reliability of these various methods. It provides a series of public image simulations, and provides a forum where technical knowledge can be shared. The first- and second-year results are respectively published in Heymans et al. (2006) and Massey et al. (2007). Another collaboration is the GREAT08 PASCAL Challenge [4], based on STEP4, which is aimed at the wider scientific community beyond weak lensing research. The first results are found in Bridle et al. (2009a). The results of GREAT08 show that the shear measurement problem is essentially a statistical problem, not an astrophysical one, and that different methods are successful in different regions of parameter space. They also highlight the steady improvement in measurement methods[5], and show that further optimisation will yield the required accuracy in shear measurement.

Redshift distribution systematics

To convert cosmic shear measurements into the 3D matter power spectrum, the redshift distribution of the background galaxies must be known. An uncertainty in the median galaxy redshift leads to an uncertainty in the amplitude of the matter power spectrum (Hu & Tegmark, 1999). The problem of photometric redshift systematics can be met given a number of galaxies in the spectroscopic calibration sample of $10^4 - 10^5$ (Ma et al., 2006; Amara & Réfrégier, 2007).

Theoretical uncertainties

To obtain cosmological parameter constraints from weak lensing, one must essentially compare the observations to the predictions of some theoretical model. Most of the signal in cosmic shear surveys comes from small scales and therefore from the nonlinear part of the matter power spectrum. The existing nonlinear corrections to the matter power spectrum (Peacock & Dodds, 1996; Ma, 1998) are only accurate to about 10% and disagree with one another to this level in the nonlinear régime (see Huterer, 2001). Newer prescriptions such as those by Smith et al. (2003) offer more accurate predictions particularly for non-ΛCDM cosmological models. The error in the nonlinear part may still be significant if effect of massive neutrinos is included (see for instance Saito et al., 2008). Current semi-analytical models need to be improved to match the degree of statistical accuracy expected for future weak lensing surveys. The solution is to run a suite of N-body ray-tracing simulations (see e.g. White & Vale, 2004; Huterer & Takada, 2005; Hilbert et al., 2009; Sato et al., 2009; Teyssier et al., 2009).

[3] `http://www.physics.ubc.ca/~heymans/step.html`

[4] `http://www.great08challenge.info`

[5] The next phase of the collaboration is GREAT 10 (`www.great10challenge.info`).

Chapter 3

Parameter forecasts

In this chapter we present the theory of Fisher matrix analysis, developed by R.A. Fisher. This technique enables us to quantify the accuracy with which an experiment, past or future, can measure the parameters of a theoretical model. We start with an introduction to the general formalism. This is followed by a presentation of the Cramér-Rao Theorem, which is at the basis of Fisher matrix analysis.

We then present the Fisher matrix technique used in this thesis, where we calculate error forecasts for a future weak lensing experiment. We give the derivation of the Fisher matrix for this experiment, where the probability distribution is assumed to be Gaussian. Finally, we give details of the numerical calculation of the Fisher matrix used in our work.

3.1 Bayesian statistics

The notion of probability is central to the calculation of cosmological parameter constraints. It allows us to model the data with particular cosmological models and to interpret our parameter constraints in a logical manner. In going from general principles to observations, we want to apply deductive reasoning to problems which require inductive reasoning. This is known as the epistemic philosophical stance on probability, describing the property of a system when the causative mechanism is unknown or uncertain.

There are a number of interpretations that can be used when dealing with probability. These fall broadly into the following categories:

- *Propensity:* In this interpretation, probabilities are objective properties of the system. This is the approach taken in the Heisenberg formalism, for instance.
- *Relative Frequency:* This interprets the relative frequency (probability) of an event as arising from the number of times this event would occur relative to an infinite ensemble of 'identical' experiments.
- *Bayesian probability:* This takes probability theory as a logic of inference — probabilities are the likelihood of an event being such, given all available information.

The propensity interpretation is difficult to reconcile with cosmology. It would require the probability of a cosmological parameter to be measured as a certain value to be an intrinsic property of the Universe.

The frequentist interpretation can be used in cosmology, and will yield sensible uncertainties, but the underlying philosophy clashes with the idea of a theoretical cosmological model. In this approach, the uncertainty in the measurement of, say, w would result from the fact that each time an observation is made, the measured value would be slightly, and randomly, different. The spread of measured values after an infinite number of experiments would then yield the inferred uncertainty. This approach creates a problem, since we do not perform experiments on the Universe, we merely observe the outcome of its evolution.

The Bayesian approach is the most logically consistent way of making assertions in cosmology. The central notion is that the laws of probability apply equally to propositions of all kinds. Probabilistic statements are interpreted as assertions about the 'degree of belief' given the data available. In other words, the statement: '$w_0 = -0.95 \pm 0.05$ at 68% confidence' is interpreted as 'It is 68% certain that the value of w_0 falls between -0.9 and -1, given the data available'.

The main criticism of the Bayesian approach is that any assertion depends on a given data set. However, if the data sets and priors are the same, then there will be agreement between different experiments. Among the critics of Bayesian statistics was R.A. Fisher himself, who developed the Fisher matrix formalism used in this thesis. However, Fisher later changed his views, and came to see Bayes's ideas as anticipating his own fiducial inference approach (for a review and a discussion, see Aldrich, 2008, and references therein).

The Fisher matrix formalism uses the Bayesian approach to give us the *probable errors* on parameters measured in an experiment. The approach is widely used in cosmology due to its relative computational simplicity and its sound mathematical basis. It is also useful in optimal experiment design, where the aim is to maximise the information. In the Fisher matrix formalism, this corresponds to minimising the variance of the score. In the following section, we shall introduce the formalism of Fisher matrix analysis.

3.2 The Fisher matrix formalism

The science of cosmology has seen a steady improvement in experimental techniques in the last few decades. An increase in the number of experiments, as well as the amount of data available, has brought to the fore the question of how best to analyse the data.

A weak lensing survey starts with a series of images, made up of a number of pixels. Each pixel represents the raw data, which must be analysed to obtain scientific results. The number of operations typically scales as the number of pixels cubed, which means that brute force calculations become impossible, and alternative solutions must be found the analyse the data to extract scientific information. This is true for current weak lensing experiments, as well as future experiments such as the all-sky weak lensing survey considered in this thesis.

The final aim of weak lensing surveys, as applied to the problem of dark energy or other cosmological sectors, is to constrain cosmological parameters. This is a problem common to many branches of science. Given an experiment, what is the uncertainty in our measurement? How do we optimise our experiment to obtain the best precision in our measurement? These questions were first answered by Fisher (1935). In our case, the problem reduces itself to finding how well we can measure cosmological parameters given a future weak lensing survey.

In this thesis we are concerned with parameter error estimation, not model selection. We do not interpret results to infer the preferred theoretical framework. The notion of a model can be either a completely different paradigm (e.g. General Relativistic gravity or higher-dimensional gravity), or basically the same model, with a different parameter set (e.g. the Standard Model with Λ or dark energy with varying w).

3.2.1 The likelihood function

The central quantity in analysis is the likelihood function. This is defined as the probability that a given experiment would obtain a certain data set given a certain theory. The likelihood function therefore assumes that the model structure is known and that only the parameters within the structure are to be estimated. It is solely dependent on the unknown parameters θ, as everything else is known or assumed. The probability and the associated likelihood differ only in terms of what is known or assumed. In the likelihood function, the model is assumed and the data either come from past experiments (observed data) or from future experiments (assumed observations). In either case, the interest lies in estimating the unknown parameters.

We shall now present the mathematical formalism for the maximum likelihood

method. Throughout this chapter, we shall follow the notation in Tegmark et al. (1997). Suppose we have a data set consisting of n real numbers $x_1, x_2, \ldots, x_n$, denoting, for instance, the number of lensed galaxies in a weak lensing survey. We write these numbers as an n-dimensional vector $\boldsymbol{x}$. The data set $\boldsymbol{x}$ is therefore assumed to be a random variable with some probability distribution $L(\boldsymbol{x}; \boldsymbol{\Theta}, \sigma_\theta)$, which depends on a vector of model parameters

$$\boldsymbol{\Theta} = (\theta_1, \theta_2, ..., \theta_m). \tag{3.1}$$

The variance in each theoretical parameter θ is denoted by the σ_θ^2. In the simplest case where we have only one model parameter θ, with N_m data points, the likelihood function is the product of all the individual likelihood functions:

$$L = \frac{1}{(2\pi\sigma_\theta^2)^{N_m/2}} \exp\left\{ -\frac{\sum_{i=1}^{N_m}(x_i - \theta)^2}{2\sigma_\theta^2} \right\} \tag{3.2}$$

Then the probability of obtaining the data points $\boldsymbol{x}$ given the parameters $\boldsymbol{\Theta}$ is

$$P[\boldsymbol{x}|\boldsymbol{\Theta}] \equiv L(\boldsymbol{x}; \boldsymbol{\Theta}, \sigma_\theta), \tag{3.3}$$

where $P[x|y]$ denotes the probability of x given y. It is important to note that the likelihood function of the parameters is not the same as the probability model of the data, although the two are related. We are interested in the value of the theoretical parameters $\boldsymbol{\Theta}$. Thus we do not wish to calculate $P[\boldsymbol{x}|\boldsymbol{\Theta}, \sigma_\theta]$ but rather $P[\boldsymbol{\Theta}, \sigma_\theta|\boldsymbol{x}]$. The latter can be obtained from the former using an important result which was first applied in probability theory, known as Bayes's Theorem (Bayes & Price, 1763):

$$P[B \cap A] = P[B|A]P[A] = P[A|B]P[B]. \tag{3.4}$$

In our context, this means that

$$P[\boldsymbol{\Theta}, \sigma_\theta|\boldsymbol{x}] = \frac{P[\boldsymbol{x}|\boldsymbol{\Theta}, \sigma_\theta]P[\boldsymbol{\Theta}, \sigma_\theta]}{P[\boldsymbol{x}]}. \tag{3.5}$$

The terms are the following: $P[\boldsymbol{\Theta}, \sigma_\theta|\boldsymbol{x}]$ is the posterior probability for the parameters; $P[\boldsymbol{x}|\boldsymbol{\Theta}, \sigma_\theta]$ is the likelihood, as described above; $P[\boldsymbol{\Theta}, \sigma_\theta]$ is the prior, and expresses our knowledge of the parameters prior to the experiment, which may be the result of previous experiment or of theory (e.g. some parameters, such as the neutrino mass, have to be positive); $P[\boldsymbol{x}]$ is called the evidence. When all the values of the parameters are assumed to be equally likely, then the prior $P[\boldsymbol{\Theta}, \sigma_\theta]$ is assumed to be constant, and is referred to as a flat prior.

Let $\boldsymbol{\Theta}_0$ denote the true parameter values and let $\boldsymbol{\Theta}$ denote our estimate of $\boldsymbol{\Theta}_0$. For $\boldsymbol{\Theta}$ to be a good estimate, it must be unbiased, that is

$$\langle \boldsymbol{\Theta} \rangle = \boldsymbol{\Theta}_0, \tag{3.6}$$

where the angled brackets denote the expectation value. The error bars around $\boldsymbol{\Theta}$ must

also be as small as possible. In other words, the standard deviations must be minimised:

$$\Delta\theta_i \equiv \left(\left\langle\theta_i^2\right\rangle - \langle\theta_i\rangle^2\right)^{1/2}. \tag{3.7}$$

When these two conditions are satisfied, θ_i is known as the 'best unbiased estimator' (BUE). The maximum likelihood estimator (MLE) is defined as the parameter vector $\boldsymbol{\Theta}_{\rm ML}$ which maximises the likelihood function $L(\boldsymbol{x};\boldsymbol{\Theta})$. When $\boldsymbol{x}$ is a given data set, $L(\boldsymbol{x}|\boldsymbol{\Theta})$ is then interpreted as a function of the model parameters $\boldsymbol{\Theta}$. In other words, we are finding the likelihood of obtaining $\boldsymbol{x}$ given $\boldsymbol{\Theta}$. In this case, the term MLE is used rather than BUE.

Parameter estimation consists in finding the place where the likelihood function is a maximum. At this point we shall introduce the following definition involving the likelihood function defined in Equation 3.2:

$$\mathcal{L} = -\ln L. \tag{3.8}$$

If we Taylor expand $\mathcal{L}$ around the ML-estimate $\boldsymbol{\Theta}$, we obtain:

$$\ln L(\boldsymbol{\Theta}|\boldsymbol{x}) \approx \ln L(\boldsymbol{\Theta}_{\rm ML}|\boldsymbol{x}) + \sum_i \Delta\theta_i \frac{\partial}{\partial\theta_i}\ln L(\boldsymbol{\Theta}_{\rm ML}|\boldsymbol{x}) + \sum_{ij}\frac{1}{2}\Delta\theta_i\Delta\theta_j\frac{\partial^2}{\partial\theta_i\partial\theta_j}\ln L(\boldsymbol{\Theta}_{\rm ML}|\boldsymbol{x}) + \mathcal{O}(\frac{\partial^3}{\partial\theta_i\partial\theta_j\partial\theta_k}) + \ldots \tag{3.9}$$

The number of terms in the expansion can be reduced by considering a Gaussian approximation. The first derivatives $\partial\mathcal{L}/\partial\theta_i$ will vanish at this point, since by definition the likelihood function has its maximum here. If we assume that there are no local maxima in parameter space, the behaviour of the likelihood function will be dominated by the quadratic terms. Since $L = \exp[-\mathcal{L}]$, the likelihood function is approximated by a Gaussian near the ML-point. The Gaussian approximation depends on the size of the error bars. If they are small everywhere, L usually drops sharply before third order terms become important, so this Gaussian is a good approximation to L over all the parameter space.

Although the Gaussian form is an approximation, it is general enough to be applied to a wide range of situations in cosmology. Even if the probability distribution is not Gaussian, the error $\Delta\theta_i$ on the theoretical parameters given by the Fisher matrix is still useful, since it is the minimum attainable error (by the Cramér-Rao inequality). In any case, the real error is not expected to be much larger than that given by the Fisher matrix, and the Gaussian assumption greatly simplifies the calculation (see Bunn 1995; Vogeley & Szalay 1996 and Tegmark et al. 1997 for a discussion).

The covariance matrix $\boldsymbol{T}$ is defined as

$$\boldsymbol{T} \equiv \langle\boldsymbol{\Theta}\boldsymbol{\Theta}^\top\rangle - \langle\boldsymbol{\Theta}\rangle\langle\boldsymbol{\Theta}\rangle^\top, \tag{3.10}$$

where the superscript $^\top$ denotes the transpose. The Gaussian approximation allows us to define the covariance as the inverse of the second derivatives at the ML-point (i.e. the

inverse of the Hessian matrix):

$$(\boldsymbol{T}^{-1})_{ij} \equiv \frac{\partial^2 \mathcal{L}}{\partial\theta_i \partial\theta_j}. \tag{3.11}$$

The Fisher information matrix, defined as

$$\boldsymbol{F}_{ij} \equiv \left\langle \frac{\partial^2 \mathcal{L}}{\partial\theta_i \partial\theta_j} \right\rangle, \tag{3.12}$$

is the expectation value of the covariance matrix at the point $\boldsymbol{\Theta} = \boldsymbol{\Theta}_0$. It tells us how fast the likelihood function falls off around the ML-point; that is, it is a measure of the width and shape of the peak. More formally, it is the curvature of log-likelihood surface about its maximum. The Hessian matrix described above tells us whether the estimates of θ_i and θ_j are correlated or not. This is a statement about the estimates of the parameters, not about the parameters themselves. In other words, the parameters may be entirely independent, but if they have a similar effect on the data, then their estimate may be correlated[1].

Error forecasts using the Fisher matrix technique depend on a number of powerful theorems. The three most important ones, which are explained below, are the following (see e.g. Kenney & Keeping 1951; Kendall & Stuart 1979; Jun 1998 for details):

1. For any unbiased estimator,
$$\Delta\theta_i \geq \frac{1}{\sqrt{\boldsymbol{F}_{ii}}}. \tag{3.13}$$

2. If there is a best unbiased estimator $\boldsymbol{\Theta}$, then it is the maximum likelihood estimator or a function thereof.

3. The maximum likelihood estimator estimator is asymptotically the best unbiased estimator.

The first theorem is known as the Cramér-Rao inequality (first formulated by Rao 1945 and Cramér 1946). This inequality places a lower limit on the error bars that can be attained on the estimated parameters, regardless of the design of the experiment. If all the other parameters are known, this gives us the minimum error bar attainable on θ_i (see Heavens 2009 for a proof). The 1σ uncertainty on any one parameter is therefore $1/\sqrt{\boldsymbol{F}}$. This uncertainty is known as the conditional error estimate. It is defined as the lower error limit on a parameter if all other parameters are known (that is, if the error on each is zero). If the other parameters are also estimated from the data, the minimum standard deviation rises to

$$\Delta\theta_i \geq \sqrt{\boldsymbol{F}^{-1}_{ii}}. \tag{3.14}$$

This can be shown by assuming that the joint probability of two parameters is

$$P(\theta_1, \theta_2) \propto \exp\left\{-\frac{1}{2}\theta_i F_{ij} \theta_j\right\}, \tag{3.15}$$

[1]e.g. The value of the baryon mass density Ω_b is entirely independent of the dark energy equation of state w, but the estimates of the two quantities are correlated.

where we assume that the distribution peaks at $\theta_i = 0$ for simplicity. Allowing θ_2 to vary is equivalent to integrating this probability distribution over all possible values of θ_2. This is known as marginalising over θ_2. Then

$$P(\theta_1) = \int \mathrm{d}\theta_2 P(\theta_1, \theta_2) \tag{3.16}$$

$$\propto \exp\left\{-\frac{\theta_1^2}{2}\left(\frac{\boldsymbol{F}_{11}\boldsymbol{F}_{22} - \boldsymbol{F}_{12}\boldsymbol{F}_{21}}{\boldsymbol{F}_{22}}\right)\right\}. \tag{3.17}$$

The term in parentheses is equal to $1/(F^{-1})_{11}$. Thus if the other parameters are also unknown, the 1σ error on θ_i is indeed $\sqrt{\boldsymbol{F}_{ii}^{-1}}$. This quantity is known as the marginal error, and is defined as the error attainable on a parameter given that there are errors on all other parameters within the model.

By using the marginal error all correlations between parameters are taken into account. An estimate of the correlation can be quantified from the Fisher matrix by defining the correlation matrix, or degeneracy matrix, as

$$\boldsymbol{D}_{ij} = \frac{{\boldsymbol{F}_{\boldsymbol{ij}}}^{-1}}{\sqrt{\boldsymbol{F}_{ii}^{-1}\boldsymbol{F}_{jj}^{-1}}} \tag{3.18}$$

If $0 < \boldsymbol{D}_{ij} \leqslant 1$ then the parameters are correlated. When $\boldsymbol{D}_{ij} = 1$ the parameters are totally correlated. If $-1 \leqslant \boldsymbol{D}_{ij} < 0$ then the parameters are anti-correlated. Again, when $\boldsymbol{D}_{ij} = -1$ the parameters are totally anticorrelated.

The second theorem shows that if there exists a best method, then it is the maximum likelihood method.

The third theorem means that in the limit of a very large data set, the maximum likelihood estimate is for all practical purposes the best estimate, that is, the one for which the Cramér-Rao bound becomes an equality.

3.3 Fisher analysis in weak lensing experiments

In thesis we are concerned with the predicted cosmological constraints from future weak lensing experiments. Applying the results in the previous section, we can see that to calculate the expected errors from a weak lensing experiment, we only need three quantities:

1. A set of observables that are assumed to describe the true Universe. In our case, this is the set of lensing convergence power spectra C_ℓ.

2. The uncertainty on the observables δC_ℓ from a given experiment, given by Equation 4.31.

3. A set of cosmological parameters $\boldsymbol{\Theta}$ for which we want to forecast the errors.

The observed convergence power spectra C_ℓ^{obs} are assumed to be close to the true C_ℓs. If we define

$$\chi^2(\theta_i) = \sum_\ell \frac{(C_\ell(\theta_i) - C_\ell^{\mathrm{obs}})^2}{(\delta C_\ell)^2} \tag{3.19}$$

then we expect χ^2 to reach a minimum at the point in parameter space where $\theta_i = \theta_{0i}$, the true values of the parameters. Let us consider a model with just one parameter θ. Expanding χ^2 about its minimum at θ_0, we obtain

$$\chi^2(\theta_i) = \chi(\theta) + \mathcal{F}(\theta - \theta_0)^2. \tag{3.20}$$

The linear term in the above equation vanishes since χ^2 is a minimum at the actual parameter value. The coefficient of the quadratic term $\mathcal{F}$ is

$$\mathcal{F} = \frac{1}{2}\frac{\partial^2\chi^2}{\partial\theta^2}\bigg|_{\theta=\theta_0}. \tag{3.21}$$

This curvature quantity measures how fast χ^2 changes away from its minimum, and it is equivalent to the curvature of the likelihood function only if the errors on C_ℓ have a Gaussian distribution. In general, however, they are not, so $\mathcal{F}$ is not really the curvature $-\partial^2 \ln \mathcal{L}/\partial\theta_i$. In practice, the distribution is close enough to Gaussian to give us accurate error estimates if we make the assumption of Gaussianity. This assumption is used in the Fisher matrix analysis carried out in this thesis. Using the definition of $\chi^2(\theta_i)$, we obtain:

$$\boldsymbol{F} = \sum_\ell \frac{1}{(\delta C_\ell)^2}\left[\left(\frac{\partial C_\ell}{\partial\theta_i}\right) + (C_\ell - C_\ell^{\rm obs})\frac{\partial^2 C_\ell}{\partial\theta_i^2}\right]. \tag{3.22}$$

In the absence of experimental data, we do not have any information about $C_\ell^{\rm obs}$. However, if the true C_ℓ values are close to the observed values, the term $C_\ell - C_\ell^{\rm obs}$ is on average zero, since the difference will sometimes be positive, and sometimes negative, and the differences will cancel out on average. The first term in the above equation will therefore dominate, and therefore

$$\mathcal{F} \to \sum_\ell \frac{1}{\delta C_\ell^2}\frac{\partial C_\ell}{\partial\theta_i}\frac{\partial C_\ell}{\partial\theta_j}. \tag{3.23}$$

The curvature matrix $\mathcal{F}$ as defined above, using the assumption that the C_ℓs have a Gaussian distribution, is equivalent to the Fisher matrix

$$F_{ij} = \sum_\ell \frac{1}{\delta C_\ell^2}\frac{\partial C_\ell}{\partial\theta_i}\frac{\partial C_\ell}{\partial\theta_j}. \tag{3.24}$$

This important expression allows us to calculate the model parameter errors for future experiments, simply by knowing the experimental parameters (to determine δC_ℓ) and the derivatives of C_ℓ around their assumed values.

The 1σ errors around each parameter are then given by[2]

$$\sigma(\theta_i) = \sqrt{\boldsymbol{F}^{-1}_{ii}}. \tag{3.25}$$

This is known as the marginalised error, where there is no prior information on the other parameters (i.e. the other parameters are allowed to vary). The fixed error, or conditional

[2]The error on the parameter θ is sometimes denoted by $\Delta\theta$ instead of σ.

error, when the other parameters are assumed to be known, is

$$\sigma(\theta_i) = \frac{1}{\sqrt{F_{ii}}}. \tag{3.26}$$

This will clearly be smaller than the marginalised error for the same parameter. In an n parameter model, the smaller the number of parameters for which we have no prior information, the smaller the marginalised errors on the unknown parameters. This can be seen from the definition of the marginalised error in Equation 3.25.

3.4 Calculation of the Fisher matrix

The Fisher matrix formalism presented above is used in this thesis to calculate the Fisher matrix by numerical means. For a central cosmological model and using our experiment parameters, we calculate the lensing power spectrum C_ℓ. We then calculate the derivative matrices of C_ℓ using a finite difference approximation:

$$\frac{\partial C_\ell}{\partial \theta} \approx \frac{1}{2\Delta}\left[C_\ell(\theta_{+\Delta}) - C_\ell(\theta_{-\Delta}) - \frac{1}{6}\Big\{C_\ell(\theta_{+2\Delta}) - C_\ell(\theta_{-2\Delta}) - 2C_\ell(\theta_{+\Delta}) + 2C_\ell(\theta_{-\Delta})\Big\}\right], \tag{3.27}$$

where we calculate the lensing power spectrum four times, varying one parameter at a time by an amount $\pm\Delta$ and $\pm 2\Delta$. In the equation above,

$$\begin{aligned} C_\ell(\theta_{+\Delta}) &= C_\ell(\theta + \Delta) \\ C_\ell(\theta_{-\Delta}) &= C_\ell(\theta - \Delta) \\ C_\ell(\theta_{+2\Delta}) &= C_\ell(\theta + 2\Delta) \\ C_\ell(\theta_{-2\Delta}) &= C_\ell(\theta - 2\Delta). \end{aligned} \tag{3.28}$$

In the work presented in Chapter 4 of this thesis, we use a value of $\Delta = 0.006$. Our calculation strategy is designed to minimise the risk of a degenerate or ill-conditioned Fisher matrix, which reflects the inability to constrain all parameters with the same level of precision. We therefore keep all parameter variations at the same order of magnitude (see e.g. Albrecht et al., 2009).

Chapter 4

Constraints on cosmological parameters using an all-sky weak lensing survey

Weak gravitational lensing provides a sensitive probe of cosmological parameters by measuring the mass distribution and the geometry of the low redshift Universe. In this chapter we present the main results of our work on error forecasts using a future weak lensing survey. We study the potential of an all-sky weak lensing tomographic survey to constrain all the cosmological parameters of a generalised dark energy + neutrino + CDM model. In particular, we focus on three sectors of the mode: dark energy, massive neutrinos (hot dark matter), and the primordial power spectrum. Using the Fisher matrix formalism with and without CMB priors, we examine how the constraints vary as the parameter set is enlarged.

We find that weak lensing with CMB priors provides robust constraints of dark energy parameters and can simultaneously provide strong constraints in all three sectors. Implications for the planning of future surveys are then discussed in Chapter 5.

4.1 Weak lensing as a cosmological probe

The aim of the work carried out in this chapter is to study the constraints on cosmological parameters that can be obtained using a future weak lensing survey. As discussed in Chapter 3, we study parameter constraints within a theoretical model using Fisher matrix analysis without inferring anything about the correctness of the model, which would involve a higher-order estimate. In particular, we examine the effect of adding further parameters to the model on parameter constraints. The smaller parameter set may be interpreted as a simpler model, i.e. a special case of the more complex model where the additional parameters are set to zero. The additional parameters, as will be described below, may be an indication of new physics: the deviation of the power spectrum from scale invariance, or a varying dark energy equation of state, both require a particular physical mechanism.

The purpose of this work in relation to future weak lensing surveys is therefore to answer the following question: How well can a future weak lensing survey constrain the parameters of a model more complex than ΛCDM? The question of parameter optimisation for such a survey can then be addressed. Weak lensing is just one of many probes available in observational cosmology, so we also study the constraints that can be obtained in combination with CMB probes. Since weak lensing and the CMB involve physics on significantly different scales, they are complementary techniques which can break the parameter degeneracies within each method.

The ΛCDM concordance model of the Universe is the inflationary model, with the mass-energy content made up of cold dark matter, baryonic matter, massive neutrinos, and dark energy. The existence of the matter components is confirmed both by cosmological observations (baryons and cold dark matter) and by particle physics (baryons and massive neutrinos). This model provides a remarkable fit to independent data sets, with a minimal set of parameters (see for instance the latest WMAP-5 results in Nolta et al., 2009; Komatsu et al., 2009).

In this part of the thesis we consider extensions of the ΛCDM paradigm. Current observational data are consistent with dark energy being a cosmological constant Λ. This is equivalent to a dark energy component with a constant equation of state parameter $w = -1$. Current constraints on w, however, are not strong enough to rule out other dark energy models. Moreover, there are degeneracies between the effects of dark energy, hot dark matter (neutrinos), and the shape of the primordial power spectrum.

Weak lensing, which probes the matter spectrum at low redshifts ($z \sim 1$), without making any assumptions about the nature of the matter content, has the potential to constrain cosmological parameters (see Hoekstra & Jain 2008 for a recent review). In this chapter we shall use the method of tomographic cosmic shear (Hu & Jain, 2004).

Error forecasts for future weak lensing surveys show that this probe can constrain dark energy parameters particularly well (see for instance Réfrégier, 2009). It can also be used to constrain neutrino mass parameters, since neutrinos also have an effect on the matter power spectrum at low redshifts. Expected bounds for neutrino masses have been obtained using weak lensing tomography with the future LSST experiment (Hannestad, Tu, & Wong, 2006) and 3D weak lensing with the future DUNE/EUCLID mission (Kitching, Taylor, & Heavens, 2008c). Constraints on neutrino mass parameters from CFHTLS

weak lensing data have been obtained by Tereno et al. (2009) and Ichiki, Takada, & Takahashi (2009). These parameters have also been constrained using galaxy surveys (Takada et al., 2006), and CMB experiments (Lesgourgues & Pastor, 2006). Forecast have also been made for future redshift surveys (see e.g. Hannestad & Wong, 2007; Abdalla & Rawlings, 2007; Abdalla et al., 2009), combined Planck+Lyman-α forest data (Gratton et al., 2008), using combined particle detector and CMB experiments (Host et al., 2007) and the Integrated Sachs-Wolfe effect (Lesgourgues et al., 2008).

The initial conditions for the matter power spectrum are given by primordial perturbations, which were set up during inflation. The matter power spectrum at the current epoch is the result of the evolution of these perturbations in the matter distribution. Weak lensing can therefore be used to probe the primordial power spectrum, and to constrain primordial spectral index parameters.

Fisher matrix analysis gives us the lower bound on the accuracy with which we can estimate model parameters from a given data set e.g. (Fisher, 1935; Tegmark, Taylor, & Heavens, 1997; Kitching & Amara, 2009). In calculating forecast survey errors, we are implicitly making assumptions about the parameter set (see the discussion of nested models in Heavens, Kitching, & Verde, 2007) . We need to know whether our constraints are robust against variations in the parameterisation of the cosmological model. This is of particular importance when dark energy constraints are considered, because of the degeneracies with other parameters.

In this chapter, we investigate how weak lensing can simultaneously constrain cosmological parameters. In particular, we focus on three groups of parameters: dark energy, massive neutrinos, and the primordial power spectrum. We examine how parameter constraints change when the cosmological parameter set is varied. We calculate the expected constraints when massive neutrino parameters and additional parameters in the primordial power spectrum are added to our parameter set, studying the degeneracy between parameters in different sectors of the cosmological model. Finally, we compare the constraints obtained using weak lensing by itself and in combination with CMB constraints.

Throughout this chapter, we shall work within a Friedmann-Robertson-Walker cosmology. Our model contains baryonic matter, cold dark matter and dark energy, to which we add massive neutrinos. We also consider different parameterisations of the primordial power spectrum which allow for a variation of the primordial spectral index (or 'running') and variation of this running.

In summary, our error forecast calculations essentially consist of three steps:

1. a calculation of the matter power spectrum using analytical fitting formulae,

2. a calculation the resulting lensing power spectrum for an all-sky tomographic weak lensing survey,

3. and finally a calculation of the Fisher matrix for the experiment in question.

Each of these steps will be described in detail below.

To obtain joint lensing+CMB constraints, we repeat the process, using the Planck mission to define our CMB survey parameters. In this case we calculate the CMB power spectrum using a Boltzmann code (CAMB), and we add the respective Fisher matrices to add Planck priors to our weak lensing forecasts.

4.2 Matter power spectrum

The matter power spectrum has already been discussed in Section 1.12.4. In broad terms, this is simply a relation between the potential set up during inflation, and the potential at late epochs:

$$\Phi(k,a) = \Phi_{\rm Prim}(k) \times \{\text{Transfer Function } (k)\} \times \{\text{Growth Function } (a)\}\,. \tag{4.1}$$

The primordial potential is $\Phi_{\rm Prim}$. The transfer function describes the evolution of perturbations during horizon crossing and the matter-radiation transition. The growth factor describes the wavelength-independent growth at late times. The inclusion of massive neutrinos complicates matters by introducing a time dependence in the transfer function. This will be discussed further on, together with the component parts of the above schematic equation.

We use the standard definition of the spectrum in our calculations:

$$P(k,z) = \frac{2\pi^2}{k^3} A_s k^{n_s(k)+3} T^2(k,z) \left(\frac{D(z)}{D(0)}\right)^2, \tag{4.2}$$

where A_s is the normalisation parameter, $T(k,z)$ is the transfer function and $D(z)$ is the growth function (also called the growth factor). The primordial spectral index is denoted by $n_s(k)$. This definition is valid for late epochs, covering the redshift range probed by weak lensing.

4.2.1 The growth function

The growth function is defined as the growing solution of the differential equation

$$\frac{\mathrm{d}^2\delta_m}{\mathrm{d}t^2} + 2H(a)\frac{\mathrm{d}\delta_m}{\mathrm{d}t} = 4\pi G\rho_m(a)\delta_m. \tag{4.3}$$

Defining the growth rate $\delta(a) \propto \delta_m/a$, this equation becomes

$$\frac{\mathrm{d}^2\delta}{\mathrm{d}a^2} + \left(\frac{\mathrm{d}\ln H}{\mathrm{d}a} + \frac{3}{a}\right)\frac{\mathrm{d}\delta}{\mathrm{d}a} - \frac{3\Omega_m H_0^2}{2a^5H^2}\delta = 0. \tag{4.4}$$

We solve this equation with the initial conditions $\delta = 1$ and $\mathrm{d}\delta/\,\mathrm{d}\ln a = 0$. The growth function $D(z)$ is then given by (see Dodelson, 2003, Section 7.5):

$$D(a) = \frac{5\Omega_m}{2}\frac{H(a)}{H_0}\int_0^a \frac{\mathrm{d}a'}{(a'H(a')/H_0)^3}. \tag{4.5}$$

In terms of z, the growth function is (Heath, 1977; Peebles, 1980; Eisenstein & Hu, 1999):

$$D(z) = \frac{5\Omega_m}{2}(1+z_{\rm eq})g(z)\int^z \frac{1+z'}{g(z')^3}\,\mathrm{d}z', \tag{4.6}$$

where

$$g^2(z) = \Omega_m(1+z)^3 + (1-\Omega_m-\Omega_{\rm DE})(1+z)^2 + \Omega_{\rm DE}. \tag{4.7}$$

The redshift of matter-radiation equality $z_{\rm eq}$ is (Eisenstein & Hu, 1999):

$$z_{\rm eq} = 2.50\times10^4\Omega_m h^2(T_{\rm CMB}/2.7)^{-4}, \tag{4.8}$$

where h is given by the Hubble constant parameterisation $H_0 = 100h\,{\rm km\,s^{-1}Mpc^{-1}}$, and $T_{\rm CMB}$ is the CMB temperature in Kelvin.

Note that our parameterisation of the growth function only uses the total mass density Ω_m. However, the neutrinos have an additional, though small, effect on the growth function (Bond et al., 1980; Tegmark, 2005; Lesgourgues & Pastor, 2006; Kiakotou et al., 2008) and the nonlinear power spectrum (Saito et al., 2008; Wong, 2008). Baryonic and neutrino physics affects the nonlinear part of the spectrum, which constitutes a source of theoretical systematics in weak lensing (see Huterer & Takada, 2005; Ishak et al., 2004).

4.2.2 The primordial power spectrum

In our cosmological model, the shape of the primordial power spectrum is of particular interest, since it may mimic some of the small-scale power damping effect of massive neutrinos. In the concordance model, the primordial power spectrum is generally parameterised by a power-law (see e.g. Kosowsky & Turner, 1995; Bridle et al., 2003)

$$\mathcal{P}_\chi(k) = A_s\left(\frac{k}{k_{s0}}\right)^{n_s-1}, \tag{4.9}$$

which corresponds to a scale-invariant, Harrison-Zel'dovich spectrum. There is some arbitrariness in this choice, beyond parameterising the amplitude of the scale-invariant spectrum. In standard slow-roll inflation, the deviation from a scale-invariant spectrum is parameterised by the tilt $n-1 \equiv {\rm d}\ln\mathcal{P}/{\rm d}\ln k$ and its running $n' \equiv {\rm d}n/{\rm d}\ln k$ by Taylor expanding $\ln\mathcal{P}$ around a pivot point $\ln k_0$. Inflation predicts the tilt n_s and the running in terms of the slow-roll parameters, which are functions of its potential and its derivatives. For this reason, it has become customary in the literature to express the primordial power spectrum as a Taylor series truncated at the running, which allows the parameters in this expression to be linked to the slow-roll parameters. However, while this approximation is satisfied by the simplest single-component inflation models, it may generally not be satisfied by multi-component models of inflation. Currently we have a situation where there is no observational reason to disfavour multi-component inflation models, while observations do not rule out a deviation from the scale-invariant spectrum, despite being in agreement with such a spectrum (see the parameter values derived in Dunkley et al., 2009).

What is the effect of our hypothesis on the shape of the primordial power spectrum in our weak lensing Fisher matrix calculation? The assumed functional form of the primordial power spectrum is equivalent to an analysis with a free form primordial power spectrum, where $P(k)$ is estimated in separate k bins but where one imposes a strong correlation between the power in different bins. Shafieloo & Souradeep (2009) show that

this is dominant in selecting the best fit regions, since the assumed form of the primordial power spectrum drives the cosmological parameters to adjust into suitable combinations.

The standard parameterisation of the running of the spectral index adopted in most weak lensing studies is obtained by using a second-order Taylor expansion of $\mathcal{P}_\chi$ in log-log space, defining the running as $\alpha = \mathrm{d}n_s/\mathrm{d}\ln k|_{k_0}$, so that the primordial power spectrum is now scale-dependent, with the scalar spectral index defined by (Spergel et al., 2003; Hannestad et al., 2002)

$$n_s(k) = n_s(k_0) + \frac{1}{2}\frac{\mathrm{d}n_s}{\mathrm{d}\ln k}\bigg|_{k_0} \ln\left(\frac{k}{k_0}\right), \tag{4.10}$$

where k_0 is the pivot scale or pivot point. Although it is motivated by simplicity and standard slow-roll inflation theory, the second-order truncated Taylor expansion is limited and may lead to incorrect parameter estimation (see Abazajian et al., 2005; Leach & Liddle, 2003). Moreover, it assumes that the second and higher derivatives of n_s are negligible, which is not a trivial assumption, especially far away from the pivot scale. This assumption is linked to the standard slow-roll inflation model which assumes that the parameters are both small, and slowly-varying (which is required by observations). This translates to the hierarchy

$$|n-1| \ll |n'| \ll |n''| \ll \ldots. \tag{4.11}$$

The general slow-roll approximation (see Lee et al., 2005; Abazajian et al., 2005, and references therein) drops the assumption of slow variation, and covers the cases of

$$|n-1| \lesssim |n'| \lesssim |n''| \lesssim \ldots, \tag{4.12}$$

which includes 4.11 as a special case.

We wish to investigate how our tomographic weak lensing survey will constrain parameters in a more general primordial power spectrum parameterisation. In order to test this, we allow an extra degree of freedom in the primordial power spectrum by adding a third-order term in the Taylor expansion, which we call β :

$$n_s(k) = n_s(k_0) + \frac{1}{2!}\alpha \ln\left(\frac{k}{k_0}\right) + \frac{1}{3!}\beta \ln\left(\frac{k}{k_0}\right)^2, \tag{4.13}$$

where $\beta = \mathrm{d}^2 n_s/\mathrm{d}\ln k^2|_{k_0}$. We use a fiducial value of $k_0 = 0.05\mathrm{Mpc}^{-1}$ for the primordial power spectrum pivot scale. This value is used in the current CAMB code (Lewis et al., 2000) following some of the early WMAP literature (Spergel et al., 2003, 2007). By definition, it is the point at which the errors on the tilt and its running are decorrelated[1]. Note, however, that this depends on the experiment (in this case, on CMB measurements), and the value may not be the optimum one for a weak lensing experiment. To investigate this, we shall calculate the marginalised error on the primordial power spectrum parameters for different values of k_0 (see Section 4.5.3).

[1]It is analogous to the pivot scale a_n in weak lensing

4.2.3 The transfer function

The transfer function is defined as

$$T(k,z) \equiv \frac{\delta(k,z=0)}{\delta(k,z=\infty)} \frac{\delta(0,z=\infty)}{\delta(0,z=0)}, \tag{4.14}$$

where $\delta(k,z)$ is the density perturbation for wavenumber k and redshift z. We use the Eisenstein & Hu (1999) analytical fitting formula for the time-dependent transfer function to calculate the linear power spectrum, which includes the contribution of baryonic matter, cold dark matter, dark energy and massive neutrinos, with the modification in the transfer function suggested by Kiakotou, Elgarøy, & Lahav (2008). This fitting formula assumes adiabatic scalar initial perturbations, so that we only consider the scalar primordial spectral index (hence the subscript in n_s). We use the Smith et al. (2003) correction to calculate the nonlinear power spectrum. The matter power spectrum is normalised using σ_8, the root mean square amplitude of the density contrast inside an $8\,h^{-1}$Mpc sphere.

In an Einstein-de Sitter model, the growth factor is simply equal to the scale factor. In both open and dark energy cosmologies, however, growth is suppressed at late times. The various cosmological matter components also affect the transfer function. These are reviewed below.

Baryons

Baryons account for about 4% of the total energy density in the Universe, so they only have a small effect on the matter power spectrum. However, they do affect the power spectrum in two ways.

The first effect is the suppression of power on small scales. At early times, before decoupling, baryons were tightly coupled to photons. Baryon overdensities decay when entering the horizon, just like radiation perturbations. After decoupling, the baryons are released from the relatively smooth radiation field and fall into the dark matter gravitational potentials.

The second effect is smaller. The baryon-photon fluid undergoes oscillations before decoupling. This manifests itself as small oscillations in the transfer function centred around $k \simeq 0.1\,h\mathrm{Mpc}^{-1}$, often termed 'baryon wiggles'. They are more noticeable in baryon-only models. Baryon phenomenology in relation to the matter power spectrum is discussed in many papers. See for example, Eisenstein & Hu (1998); Miller (2000), and Rudd et al. (2008). The Eisenstein & Hu (1999) analytical transfer function used in this thesis does not include baryon wiggles.

Dark energy

Dark energy affects the matter power spectrum in three ways.

Firstly, the matter power spectrum turns over at k_{eq}, which is proportional to Ω_m. Therefore, the value of Ω_{DE} in the Standard Model will also affect the position of k_{eq}, so dark energy leads to a turnover in the spectrum at a scale much larger than that predicted by a universe with $\Omega_{\mathrm{DE}} = 0$.

The second effect of dark energy is also indirect. In a flat universe, as the dark energy density goes up, the dark matter density decreases, and this causes the amplitude of the matter power spectrum to increase. The power spectrum for a model with dark energy is therefore normalised higher than for one without.

The third effect of dark energy on density inhomogeneities is direct, and comes about through its effect on the growth factor. The evolution of the Hubble rate depends on the model of dark energy — both on the dark energy density $\Omega_{\rm DE}$ and on its equation of state w — since the Hubble rate evolves as:

$$\frac{H(z)}{H_0} = \left[\frac{\Omega_m}{a^3} + \frac{\Omega_{\rm DE}}{a^{3[1+w]}}\right]^{1/2} \tag{4.15}$$

at late times. The growth factor is therefore affected at late times, which is why weak lensing, which probes the Universe at low redshifts, is sensitive to dark energy.

In addition to this, if dark energy is not a cosmological constant then it also affects the shape of the matter power spectrum on large scales through dark energy perturbations. In our calculations, we neglect dark energy perturbations.

Neutrinos

Neutrinos are known to exist from the Standard Model of particle physics, and the standard Hot Big Bang model predicts the amount of neutrinos in the Universe. The reason why neutrinos affect the matter power spectrum is simply that they are light particles that can move fast (meaning that they are not *cold* dark matter) and can stream out of high-density regions. They therefore cause the suppression of perturbations on scales smaller than the free-streaming scale (for a review, see e.g. Hannestad, 2006; Lesgourgues & Pastor, 2006; Quigg, 2008).

The scale on which perturbations are damped by neutrinos is determined by the comoving distance that a neutrino can travel in one Hubble time at equality. For a neutrino mass $\sim 1\,\mathrm{eV}$, the average velocity, T_ν/m_ν is of order unity at equality. This leads to a suppression of power on all scales smaller than $k_{\rm eq}$. Note that this phenomenon depends on the individual neutrino mass, rather than the total neutrino mass. A lighter neutrino can free-stream out of larger scales, so the suppression begins at lower k for the lighter neutrino species. Heavier neutrinos constitute more of the total neutrino density, and so suppress small-scale power more than lighter neutrino species. This means that to accurately model massive neutrino phenomenology, we need at least two parameters: the neutrino mass fraction Ω_ν, or some expression of this quantity in terms of the total neutrino mass m_ν, and the number of massive neutrino species N_ν. Here we shall use Equation 1.79:

$$\Omega_\nu h^2 = \frac{m_\nu}{94\mathrm{eV}}. \tag{4.16}$$

Neutrinos introduce a scale dependence in the transfer function. In Chapter 1 we have seen how perturbation modes of a certain wavelength λ can grow if they are greater than the Jeans wavelength. Above the Jeans scale, perturbations grow at the same rate independently of the scale. For the baryonic and cold dark matter components, the time and scale dependence of the power spectrum can therefore be separated at low redshifts.

This is not the case with massive neutrinos, which introduce a new length scale given by the size of the comoving Jeans length when the neutrinos become non-relativistic. In terms of the comoving wavenumber $k_{\rm nr}$, this scale is given by:

$$k_{\rm nr} = 0.026 \left(\frac{m_i}{1\,{\rm eV}}\right)^{1/2} \Omega_m^{1/2} h{\rm Mpc}^{-1} \tag{4.17}$$

for three neutrinos of equal mass, each with mass m_i. The growth of Fourier modes with $k > k_{\rm nr}$ is suppressed because of neutrino free-streaming. From the equation above, it is evident that the free-streaming scale varies with the cosmological epoch (since there is an Ω_m-dependence), and therefore the scale and time dependence of the power spectrum cannot be separated. For analytical calculations of the power spectrum, this means that the transfer function depends on both the scale k and on the redshift z.

Neutrino oscillation experiments do not, at present, determine absolute neutrino mass scales, since they only measure the difference in the squares of the masses between neutrino mass eigenstates (see e.g. Quigg, 2008). Cosmological observations, on the other hand, can constrain the neutrino mass fraction, and can distinguish between different mass hierarchies (see Elgarøy & Lahav 2005 for a review of the methods). Indeed, the fact that cosmological constraints could be stronger than constraints from particle accelerators was noticed quite early on (see Primack & Gross 2001 for a review). The 'closure limit' gives us $m_\nu < 90$ eV (first derived by Gerstein & Zel'dovich 1966; Marx & Szalay 1972 and Cowsik & McClelland 1972). Since then, cosmological neutrino bounds have improved significantly, with different methods being used e.g. $m_\nu < 0.9$ eV using SDSS luminous red galaxies (Tegmark et al., 2006) and $m_\nu < 1.3$ eV using WMAP5 CMB observations and a ΛCDM model (Shiraishi et al., 2009). Recent results from weak lensing are found in Tereno et al. (2009) and Ichiki et al. (2009). The latest results from particle physics give us an upper mass bound of 2.0 eV for the electron neutrino from tritium β decay and 2.984 ± 0.008 for the total number of neutrino species from Standard Model fits to LEP data (Particle Data Group, 2008). WMAP5 observations give us $m_\nu < 1.5$ eV using a varying-w dark energy cosmological model, while joint WMAP5+BAO+SNe observations with the same model lower this limit to $m_\nu < 0.66$ eV (Komatsu et al., 2009), i.e. $m \lesssim 0.22$ eV for the single electron neutrino mass.

Observations of neutrino flavour oscillations in atmospheric and solar neutrinos, provide evidence of a difference between the masses of the different species or flavours, as well as for a non-zero mass. For three neutrino mass eigenstates m_1, m_2 and m_3, the squared mass differences are (Particle Data Group, 2008):

$$\begin{aligned} \Delta m^2_{21} &= m_2^2 - m_1^2 = (7.59 \pm 0.20) \times 10^{-5}\,{\rm eV}^2 \\ \Delta m^2_{32} &= |m_3^2 - m_2^2| = (2.43 \pm 0.13) \times 10^{-3}\,{\rm eV}^2, \end{aligned} \tag{4.18}$$

where the ranges indicated are at 90% confidence level. The ambiguity in the sign of Δm^2_{32} allows for two possible mass hierarchies: the normal hierarchy given by the scheme $m_3 \gg m_2 > m_1$, or the inverted hierarchy $m_2 > m_1 \gg m_3$. Given Equation 4.18, constraining the total mass $m_\nu \lesssim 0.1$ eV would automatically exclude an inverted hierarchy. Conversely, a total neutrino mass $m_\nu \sim 2$ eV is only possible with a degenerate neutrino mass scheme. Hence the interest in finding cosmological neutrino mass bounds.

Following Eisenstein & Hu (1999), we assume N_ν, the number of massive (non-relativistic) neutrino species, to be a continuous variable, as opposed to an integer. This is justified since any light particle which does not couple to electrons, photons or ions has the same small-scale power suppression effect as neutrinos, and will therefore contribute to the effective N_ν.

The Eisenstein & Hu transfer function assumes a total of three neutrino species (i.e. $N_{\rm massless} + N_\nu = 3$), with degenerate masses for the most massive eigenstates, i.e. if m_ν is the total neutrino mass, then

$$m_\nu = \sum_{i=0}^{N_\nu} m_i = N_\nu m_i, \tag{4.19}$$

where m_i is the same for all eigenstates. Thus, $N_\nu = 2$ for the normal mass hierarchy (two massive and one very light or massless neutrino), and $N_\nu = 1$ for the inverted mass hierarchy (one massive neutrino), while $N_\nu = 3$ corresponds to the case where all three neutrino species have the same mass (see Quigg, 2008). The temperature of the relativistic neutrinos is assumed to be equal to $(4/11)^{1/3}$ of the photon temperature (Kolb & Turner, 1990).

In comparing parameter constraints in different parameter spaces, we shall use six cosmological models. We start with the simplest model (QCDM) to which we add neutrino and additional primordial power spectrum parameters. Our parameter sets, with the terms used in the text, are shown in Table 4.1. Note that these are nested parameter sets. In other words, the fiducial cosmology is the same throughout, and we only vary the number of parameters for which the Fisher matrix calculation is carried out.

4.3 Fiducial cosmology

In this section we summarise our fiducial cosmological model. We include baryonic matter, cold dark matter and neutrinos, as well as dark energy. We allow for a non-flat geometry by including a dark energy density parameter $\Omega_{\rm DE}$ together with the total matter density Ω_m, such that in general $\Omega_m + \Omega_{\rm DE} \neq 1$. The dynamical dark energy equation of state parameter, $w = p/\rho$, is expressed as function of redshift and is parameterised by a first-order Taylor expansion in the scale factor a (Chevallier & Polarski, 2001; Linder, 2003):

$$w(a) = w_0 + w_a(1 - a), \tag{4.20}$$

where $a = (1 + z)^{-1}$. We parameterise neutrino properties using two parameters: the total neutrino mass m_ν, and the number of massive neutrino species N_ν. The primordial power spectrum is characterised by the scalar spectral index n_s, its running α, and the 'running of the running' β. Since we use the Eisenstein & Hu (1999) transfer function, we only consider adiabatic initial perturbations, and we ignore dark energy perturbations.

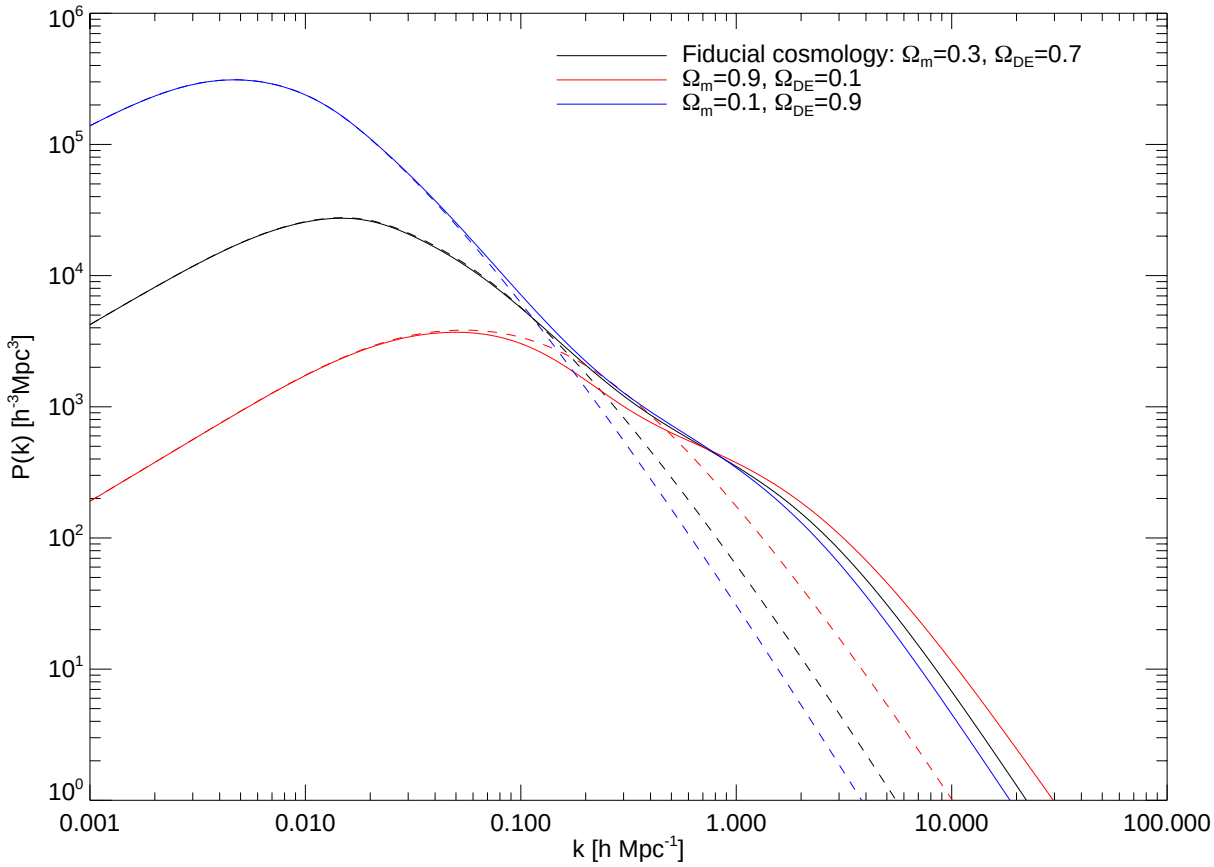

Figure 4.1: The matter power spectrum at $z = 0$ for three cosmological models: fiducial (black) with $\Omega_m = 0.3$, $\Omega_{\rm DE} = 0.7$; $\Omega_m = 0.9$, $\Omega_{\rm DE} = 0.1$ (red); and $\Omega_m = 0.1$, $\Omega_{\rm DE} = 0.9$ (blue). In each case, we show the linear (dotted line) and nonlinear (solid line) power spectra. The power spectra are normalised using σ_8, whose value is kept constant. As the dark energy fraction is increased, the turning point of the power spectrum is shifted to smaller k, while the amplitude increases.

4.3.1 Parameter space

Our most general parameter space consists of:

1. Total matter density – Ω_m (which includes baryonic matter, hot dark matter (i.e. neutrinos and cold dark matter)
2. Baryonic matter density – Ω_b
3. Neutrinos (HDM) – $m_\nu,\ N_\nu$
4. Dark energy parameters – $\Omega_{\rm DE},\ w_0,\ w_a$
5. Hubble parameter – h
6. Primordial power spectrum parameters – $\sigma_8,\ n_s,\ \alpha,\ \beta$ (see Section 4.2)

We shall refer to this fiducial cosmology as 'νQCDM + α + β'[2] We choose fiducial parameter values based on the five-year WMAP results (Dunkley et al., 2009) similar to those used in Kitching et al. (2008c). The values are given in Table 4.1.

In our Fisher matrix formalism, the error forecast on each parameter depends on the sensitivity of the weak lensing observation to changes in the matter power spectrum. In order to probe the effect of the different parameters on the matter power spectrum, we consider the fractional change in the non-linear matter power spectrum $P(k)$, defined as the change in $P(k)$ with respect to the fiducial $P(k)_{\rm fid}$, when one parameter at a time is varied from its fiducial value:

$$\text{Fractional change} = \frac{P(k)_{\rm fid} - P(k)_\Delta}{P(k)_{\rm fid}}, \tag{4.21}$$

where $\Delta = 10\%$ for all parameters in the νQCDM + α + β parameter set The power spectrum is normalised using σ_8. Figure 4.2 shows the fractional change in $P(k)$ at redshift $z = 0$. There are several features of interest in this plot, including the degeneracy between the parameters α, β, m_ν and Ω_b at small scales, as well as the degeneracy between w_0, w_a, $\Omega_{\rm DE}$ and N_ν at large scales. The plot shows that the non-linear matter power spectra for the fiducial model and for the model with non-zero w_a are almost completely degenerate at $z = 0$. This degeneracy is lifted as the redshift increases. This is shown in Figure 4.3, where we calculate the fractional change in $P(k)$ at $z = 1$.

4.4 Tomographic weak lensing

In this section we describe the technique of tomographic weak lensing used in this thesis. In weak lensing surveys, the observable is the convergence power spectrum. In this thesis, we calculate this quantity from the matter power spectrum via the lensing efficiency

[2]We have taken some liberties in using the name 'QCDM' (or Quintessence+CDM), since quintessence implies a specific parameterisation of w. In our cosmological model, we parameterise w by its present epoch value, and its variation.

Parameters	w_0	w_a	$\Omega_{\rm DE}$	Ω_m	Ω_b	h	σ_8	n_s	α	β	m_ν	N_ν
Fiducial values	-0.95	0	0.7	0.3	0.045	0.7	0.8	1	0	0	0.66	3
QCDM	✓	✓	✓	✓	✓	✓	✓	✓	×	×	×	×
QCDM + α	✓	✓	✓	✓	✓	✓	✓	✓	✓	×	×	×
QCDM + α + β	✓	✓	✓	✓	✓	✓	✓	✓	✓	✓	×	×
νQCDM	✓	✓	✓	✓	✓	✓	✓	✓	×	×	✓	✓
νQCDM + α	✓	✓	✓	✓	✓	✓	✓	✓	✓	×	✓	✓
νQCDM + α + β	✓	✓	✓	✓	✓	✓	✓	✓	✓	✓	✓	✓

Table 4.1: Cosmological parameter sets used in our calculations. The central values for each parameter are shown in the row labelled 'Fiducial Values'. For each parameter set, the ticks (✓) and crosses (×) indicate whether a parameter is allowed to vary or not, respectively.

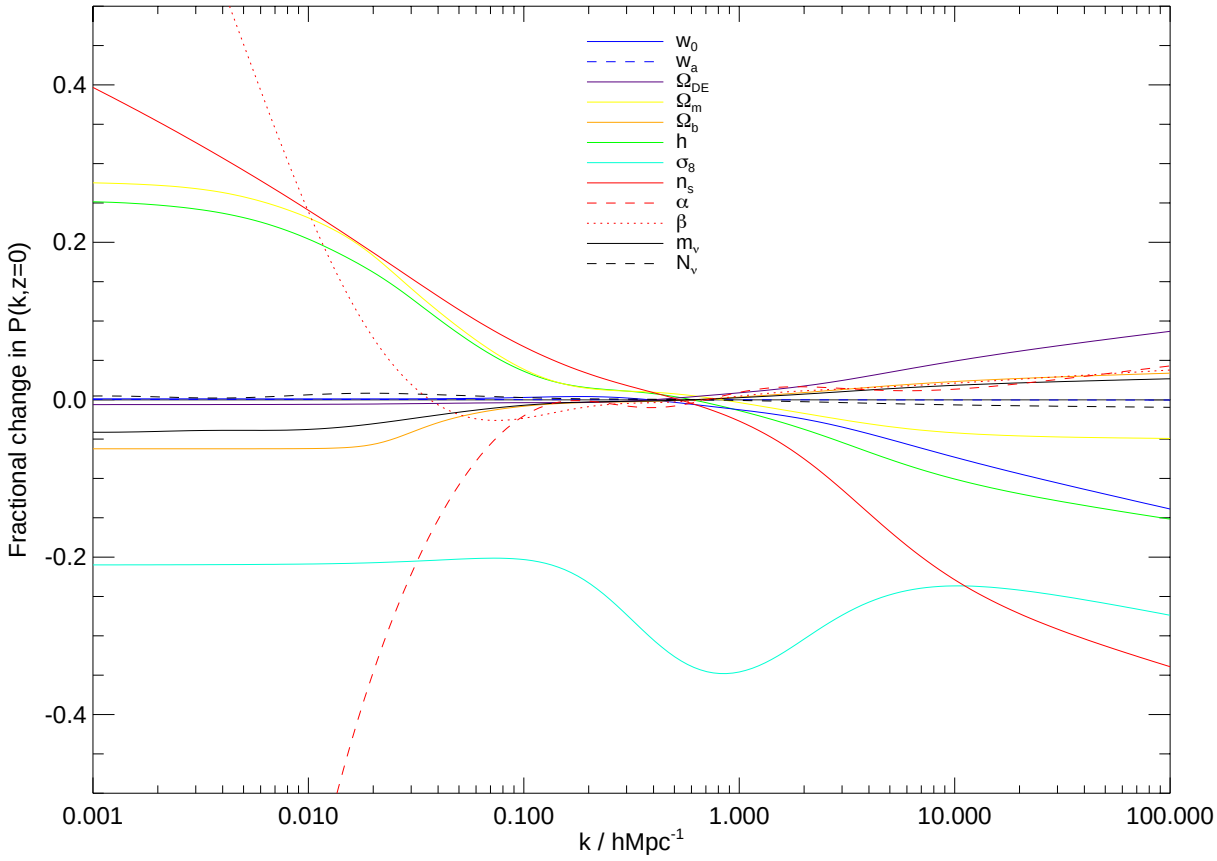

Figure 4.2: The fractional change in the non-linear matter power spectrum $P(k, z)$ at $z = 0$, obtained by varying each parameter in the νQCDM $+ \alpha + \beta$ set by $+10\%$ from its fiducial value.

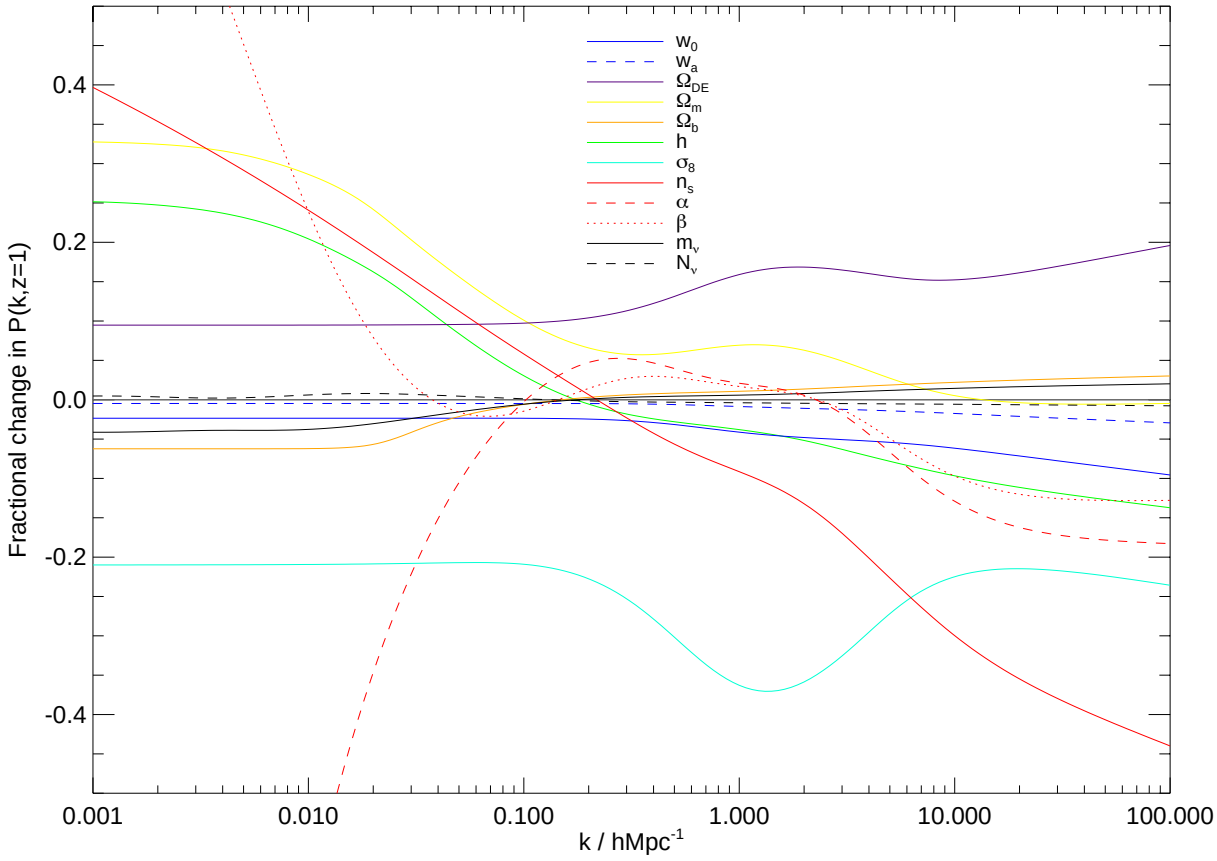

Figure 4.3: The fractional change in the non-linear matter power spectrum $P(k, z)$ at $z = 1$, obtained by varying each parameter in the νQCDM $+ \alpha + \beta$ set by $+10\%$ from its fiducial value.

function. Our convergence power spectrum therefore depends on the survey geometry and on the matter power spectrum.

Different weak lensing techniques extract information from the shear field in different ways. In particular, the lens and source galaxies of a given survey may be divided into N bins according to redshift, luminosity, colour, or any other criteria chosen by the observer. We use the power spectrum tomography formalism by Hu & Jain (2004), with the background lensed galaxies divided into 10 redshift bins. Cosmological models are then constrained by the power spectrum corresponding to the cross-correlations of shears within and between bins. This method allows us to probe the redshift dependence of cosmic shear, and it is especially useful for constraining redshift-dependent cosmological parameters, such as $w(z)$.

The 3D power spectrum is projected onto a 2D lensing correlation function using the Limber (1953) equation, giving us:

$$C_\ell^{ij} = \int \mathrm{d}z \frac{H}{D_A^2} W_i(z) W_j(z) P(k = \ell/D_A, z), \tag{4.22}$$

where i, j denote redshift bins, each index running from 1 to N. The weighting function $W_i(z)$ is defined by the lensing efficiency:

$$W_i(z) = \frac{3}{2}\Omega_m \frac{H_0}{H} \frac{H_0 D_{OL}}{a} \int_z^\infty \mathrm{d}z' \frac{D_{LS}}{D_{OS}} P(z'), \tag{4.23}$$

where the angular diameter distance to the lens is D_{OL}, the distance to the source is D_{OS}, and the distance between the source and the lens is D_{LS} (see Hu & Jain 2004 for details). Our multipole range is $10 < \ell < 5000$.

Since we have no data, the galaxy distribution must be assumed. We use the Smail et al. (1994) probability distribution for magnitude-limited survey, which is a function of redshift z:

$$P(z) = z^a \exp\left[-\left(\frac{z}{z_0}\right)^b\right], \tag{4.24}$$

where a and b are adjustable parameters. We set $a = 2$ and $b = 1.5$. In the above equation, z_0 is determined by the median redshift of the density distribution of the galaxies z_m, which is a parameter depending on the survey geometry (see e.g Amara & Réfrégier, 2007), and we set $z_0 \simeq z_m/\sqrt{2}$. Like the other survey parameters, it is independent of the way in which we calculate the matter power spectrum or the lensing convergence. The other survey parameters are the area of the sky covered by the survey A_s, the observed number density of a galaxies n_g, and the number of redshift bins N. We also choose to include the errors in the measurement of the photometric redshifts and in the observed ellipticity of the galaxies. These are expressed as variances: $\sigma(z)/(1+z)$, and σ_ϵ, respectively (see Bartelmann & Schneider, 2001). The effect of the photometric redshift error is to dilute the shear signal in each redshift by randomly moving galaxies in and out of any particular bin. If it is assumed that the distribution of redshift errors is Gaussian with width $\sigma_z(z_g)$, which depends on the true redshift of the galaxy z_g and has a bias in the mean of the

distribution $z_{\rm bias}$, then

$$P(z|z_g,\sigma_z) = \frac{1}{\sqrt{2\pi}\sigma_z(z_g)}\mathrm{e}^{-(z-z_g+z_{\rm bias})^2/2\sigma_z^2(z_g)}. \tag{4.25}$$

In this thesis we assume that $z_{\rm bias} = 0$ for all experiments (see e.g. Amara & Réfrégier 2007 for a discussion of its effects on a tomographic weak lensing survey).

The expected shear in a redshift bin of width Δz centred on z_i is the average shear given by integrating over all redshifts weighed at each redshift by the expected number density $n(z)$ and the probability of finding a galaxy in the redshift bin in question:

$$\langle\gamma_t, i\rangle = \gamma_{t,\infty}\int_{z_\ell}^{\infty}\mathrm{d}z\frac{S_k[r(z)-r(z_\ell)]}{S_k[r(z)]n(z)}W(z)\int_{z_i-\frac{\Delta z}{2}}^{z_i+\frac{\Delta z}{2}}\mathrm{d}z' P(z-z'|\sigma_z), \tag{4.26}$$

where $W(z)$ is a weighting function. The second z' integral in Equation (4.26) above can be solved for a Gaussian probability distribution so that

$$\langle\gamma_t, i\rangle = \gamma_{t,\infty}\int_{z_\ell}^{\infty}\mathrm{d}z\frac{S_k[r(z)-r(z_\ell)}{S_k[r(z)]n(z)}W(z)P_{\Delta z}[z-z'|\sigma_z(z')], \tag{4.27}$$

where (see e.g. Ma et al., 2006)

$$P_{\Delta z[z|\sigma_z]} = \frac{1}{2}\left[\mathrm{erf}\left(\frac{z+z_{\rm bias}+\Delta z/2}{\sqrt{2\pi}\sigma_z}\right)\right] - \frac{1}{2}\left[\mathrm{erf}\left(\frac{z+z_{\rm bias}-\Delta z/2}{\sqrt{2\pi}\sigma_z}\right)\right] \tag{4.28}$$

is the fraction of the redshift error distribution which lies in a redshift bin of width Δz centred on z and $\mathrm{erf}(x)$ is the error function. The estimated shear is weighted by the number of galaxies scattered from one redshift to another, given by the galaxy redshift distribution $n(z)$. The weighting function is:

$$W(z) = \frac{\tilde{w}(z)}{\int_0^\infty \mathrm{d}z'\tilde{w}(z')n(z')P_{\Delta z}[z-z'|\sigma_z(z)]}, \tag{4.29}$$

where $\tilde{w}(z)$ is some arbitrary weighting function of the shears in the redshift, which will be taken as $\tilde{w}(z) = 1$ in this thesis.

Our survey geometry follows the parameters for a 'wide' all-sky survey covering an area of 20000 square degrees (i.e. the half of the sky that is not obscured by the Milky Way). The survey parameters are shown in Table 4.2. The median redshift of the density distribution of galaxies with redshift z is $z_{\rm median}$ and the observed number density of galaxies is n_g. For discussions of possible future missions with such a survey configuration, see the literature on the DUNE/Euclid mission (e.g. Réfrégier, 2009).

4.4.1 Error forecast

The predictions for cosmological parameter errors presented in this thesis use the Fisher matrix formalism. As described in Chapter 3, the Fisher matrix for the shear power

A_s/sq degree	20 000
$z_{\rm median}$	0.9
$n_g/{\rm arcmin}^2$	35
$\sigma_z(z)/(1+z)$	0.025
σ_ϵ	0.25
$\ell_{\rm max}$	5000
$N_{\rm bins}$	10

Table 4.2: Fiducial parameters for our all-sky weak lensing survey.

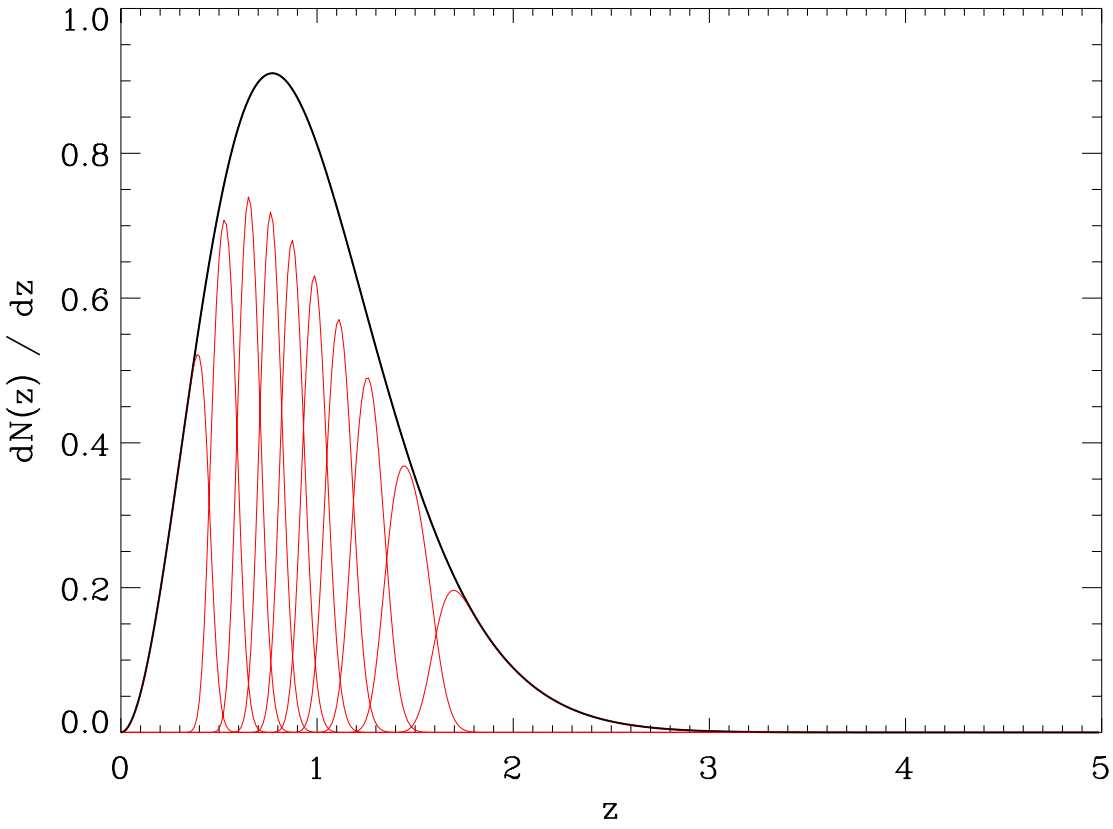

Figure 4.4: The galaxy redshift distribution for a tomographic weak lensing survey with a median redshift of 0.9, with the galaxies divided into 10 redshift bins. The red curves show the galaxy distribution within each bin.

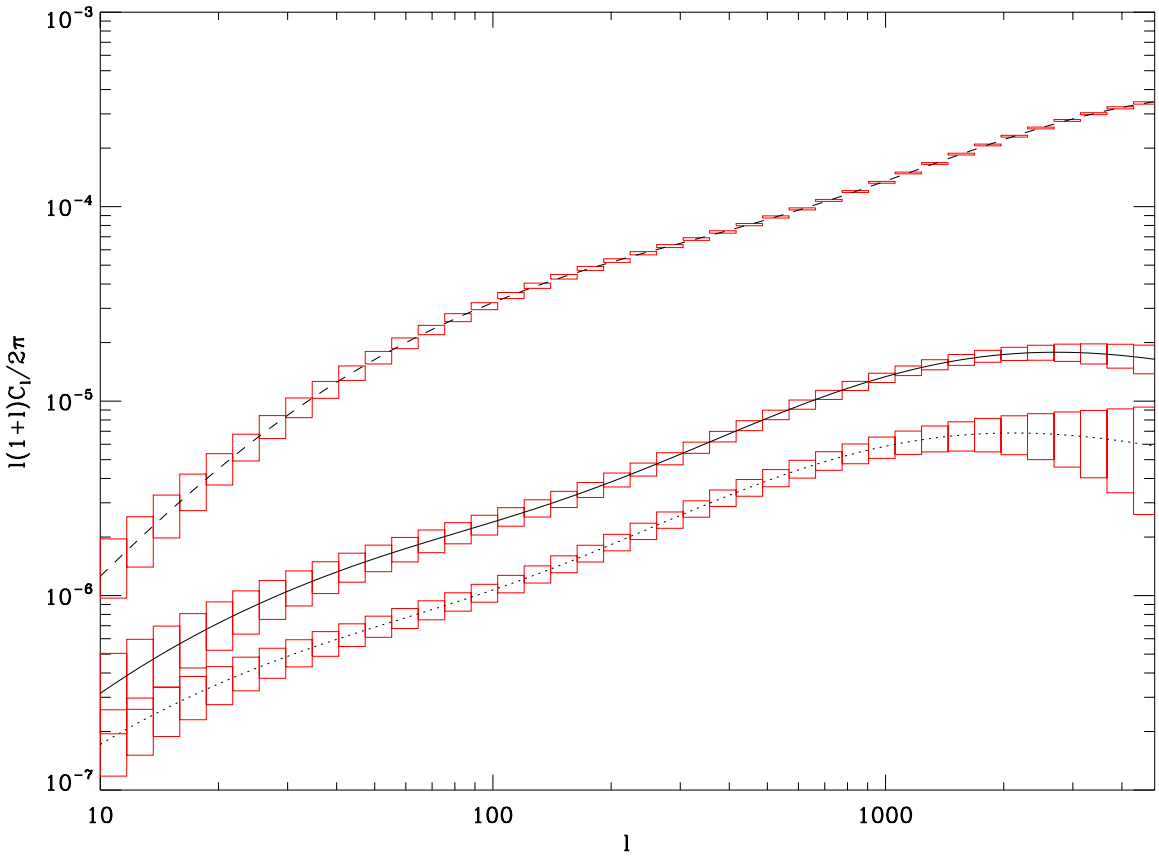

Figure 4.5: The weak lensing power spectrum and associated 1σ error bars for our all-sky tomographic weak lensing survey. The curves represent the auto-correlation within the first (dashed line) and tenth bins (dotted line), with median redshifts of 0.4 and 1.7 respectively, and the cross-correlation between the first and tenth bins (solid line). The error bars are shown in red.

spectrum is given by

$$F_{\alpha\beta} = \sum_{\ell} \left(\frac{1}{\Delta C_\ell}\right)^2 \frac{\partial C_\ell}{\partial p_\alpha} \frac{\partial C_\ell}{\partial p_\beta}, \tag{4.30}$$

where the summation is over modes ℓ which can reliably be measured.

Neglecting non-gaussian corrections, the rms uncertainty in measuring the lensing power spectrum C_ℓ is given by (Kaiser, 1998; Hu & Tegmark, 1999; Huterer, 2001):

$$\Delta C_\ell = \sqrt{\frac{2}{(2\ell+1) f_{\rm sky}}} \left(C_\ell + \frac{\sigma_\gamma^2}{2 n_g}\right). \tag{4.31}$$

In this equation, $f_{\rm sky}$ is the fraction of the sky covered by a survey of area A_s in degrees^2. This is given by

$$f_{\rm sky} = \frac{\mathrm{eff}\, A_s/\mathrm{sr}}{4\pi} \tag{4.32}$$

where eff is the masking efficiency, and A_s is given in steradian by

$$A_s/\mathrm{sr} = \frac{A_s/\mathrm{deg}^2}{(180/\pi)^2}. \tag{4.33}$$

The parameter n_g is the surface density of usable galaxies, and σ_γ^2 is the shear variance per galaxy arising from intrinsic shapes and measurement errors.

Assuming Gaussian likelihood with zero mean gives us the following expression for the Fisher matrix (Hu & Jain, 2004):

$$F_{\alpha\beta} = f_{\rm sky} \sum_{\ell=\ell_{\rm min}}^{\ell_{\rm max}} \frac{(2\ell+1)\Delta\ell}{2} \mathrm{Tr}\left[D_{\ell\alpha} \widetilde{C}_\ell^{-1} D_{\ell\beta} \widetilde{C}_\ell^{-1}\right], \tag{4.34}$$

where the sum is over bands of multipole ℓ of width $\Delta\ell$, Tr is the trace, and $f_{\rm sky}$ is the fraction of sky covered by the survey. The observed power spectra for each pair i, j of redshift bins are written as the sum of the lensing and noise spectra:

$$\widetilde{C}_\ell^{ij} = C_\ell^{ij} + N_\ell^{ij}. \tag{4.35}$$

The derivative matrices are given by

$$[D_\alpha]^{ij} = \frac{\partial C_\ell^{ij}}{\partial p_\alpha}, \tag{4.36}$$

where p_α is the vector of parameters in the theoretical model.

4.4.2 The Figure of Merit

In order to quantify the potential for a survey to constrain dark energy parameters, we use the DETF Figure of Merit (see Linder, 2003; Albrecht et al., 2006). In this parameterisation, we consider the smallest area in parameter space that can be constrained

by a given experiment. The dark energy equation of state can be written as:

$$w(a) = w_i + w_a(a_i - a), \tag{4.37}$$

where $w_i \equiv w(a_i)$ and the expansion is carried out around the scale factor a_i. The square of the the error on $w(a)$ is:

$$\Delta w(a)^2 = \Delta w_i^2 + (a_n - a)^2 \Delta w_a^2 (a_i - a)\mathrm{Cov}(w_i, w_a), \tag{4.38}$$

where $\mathrm{Cov}(w_i, w_a)$ is the covariance between w_i and w_a (equal to the inverse of the corresponding Fisher matrix element). By taking the derivative of this quantity, the scale factor at which the error is minimised can be found. Thus

$$a_{\mathrm{min}} = a_i + \frac{\mathrm{Cov}(w_i, w_a)}{\Delta w_a^2}. \tag{4.39}$$

In the above formalism, the pivot redshift occurs when the covariance between w_n and w_a is zero. In the standard expansion given in Equation 1.129, $a_i = 1$ and the above expression reduces to the equation for the pivot redshift a_n (i.e. $a_{\mathrm{min}} = a_n$). The ellipse for the joint errors in the (w_n, w_a) plane is then the smallest ellipse constrained by a given experiment. Since this ellipse is decorrelated, its area can be closely approximated by:

$$\mathrm{Area} = \Delta w(z_{\mathrm{pivot}}) \Delta w_a. \tag{4.40}$$

The Dark Energy Task Force (Albrecht et al., 2006) has chosen to define the Figure of Merit (FOM) as the inverse of the area enclosed by the 95% confidence limit contour of (w_n, w_a):

$$\mathrm{FOM} = \frac{1}{\Delta w_n \Delta w_a}. \tag{4.41}$$

The FOM quantifies the performance of any given experiment: the larger the FOM, the tighter the constraint on the dark energy equation of state over a large redshift range. Although other definitions of the FOM have been proposed (see e.g. Wang, 2008; Albrecht et al., 2009), the DETF FOM has the advantage of simplicity, and of giving us an optimal pivot redshift which can then be used to set the survey geometry.

4.4.3 Adding Planck priors

Fisher matrix analysis allows us to find the joint constraints from an ensemble of independent experiments by using the sum of the respective Fisher matrices. In general, the joint marginal error ellipses are smaller than or equal to those from the single experiments, since the operations of addition and marginalisation are not commutative. This can be understood physically in terms of adding information from independent experiments. In this chapter, together with lensing-only constraints, we also include joint lensing and CMB constraints. To combine constraints from different probes we add the respective Fisher matrices:

$$\mathbf{F}_{\mathrm{joint}} = \mathbf{F}_{\mathrm{lensing}} + \mathbf{F}_{\mathrm{CMB}}. \tag{4.42}$$

This approach is based on the assumption that the two experiments are decorrelated, which is a valid approximation in our work.

For our CMB priors, we use the Planck mission as our survey (The Planck Collaboration, 2006). The main constraint on cosmology from the CMB comes from the measurement of the angular size of the sound horizon at last scattering. The Planck Fisher matrix is calculated following the method in Rassat et al. (2008), which forecasts errors on cosmological parameter constraints by estimating the error on the measurement of the temperature and E-mode polarisation power spectra. The power spectra are calculated using the publicly available CAMB code (Lewis et al., 2000). We do not use information from B-modes, and only use the 143 GHz channel, assuming other frequencies will be used for the foreground removal. This is conservative compared to other Planck priors in the literature.

The details given in this part are taken from Rassat et al. (2008, Appendix B). The Planck Fisher matrix for the CMB spectrum is given by:

$$F_{ij}^{\rm CMB} = \sum_{\ell} \sum_{X,Y} \frac{\partial C_{X,\ell}}{\partial \theta_i} {\rm Cov}_{\rm XY}^{-1} \frac{\partial C_{Y,\ell}}{\partial \theta_j}, \tag{4.43}$$

where θ_i are the parameters to constrain, $C_{X,\ell}$ is the harmonic power spectrum for the temperature-temperature ($X \equiv TT$), temperature-E-polarisation ($X \equiv TE$) and the E-polarisation-E-polarisation ($X \equiv EE$) power spectrum. The covariance ${\rm Cov}_{\rm XY}^{-1}$ of the errors for the various power spectra is given by the fourth moment of the distribution, which under Gaussian assumptions is entirely given in terms of the $C_{X,\ell}$ with

$$\begin{aligned}
{\rm Cov}_{T,T} &= f_\ell \left(C_{T,\ell} + W_T^{-1} B_\ell^{-2}\right)^2 & (4.44)\\
{\rm Cov}_{E,E} &= f_\ell \left(C_{E,\ell} + W_P^{-1} B_\ell^{-2}\right)^2 & (4.45)\\
{\rm Cov}_{TE,TE} &= f_\ell \Big[C_{TE,\ell}^2 + \left(C_{T,\ell} + W_T^{-1} B_\ell^{-2}\right)\left(C_{E,\ell} + W_P^{-1} B_\ell^{-2}\right)\Big] & (4.46)\\
{\rm Cov}_{T,E} &= f_\ell C_{TE,l}^2 & (4.47)\\
{\rm Cov}_{T,TE} &= f_\ell C_{TE,\ell}\left(C_{T,\ell} + W_T^{-1} B_\ell^{-2}\right) & (4.48)\\
{\rm Cov}_{E,TE} &= f_\ell C_{TE,\ell}\left(C_{E,\ell} + W_P^{-1} B_\ell^{-2}\right) \ , & (4.49)
\end{aligned}$$

where $f_\ell = \frac{\ell}{(2\ell+1) f_{\rm sky}}$ and $W_{T,P} = (\sigma_{T,P}\theta_{\rm fwhm})^{-2}$ is the weight per solid angle for temperature and polarisation, with a 1σ sensitivity per pixel of $\sigma_{T,P}$ with a beam of $\theta_{\rm fwhm}$ extent. The beam window function is given in terms of the full width half maximum (fwhm) beam width by $B_\ell = \exp\left(-\ell(\ell+1)\theta_{\rm fwhm}^2/16\ln 2\right)$ and $f_{\rm sky}$ is the sky fraction. Equation 4.43 usually includes a summation over the Planck frequency channels. This channel has a beam of $\theta_{\rm fwhm} = 7.1'$ and sensitivities of $\sigma_T = 2.2\mu K/K$ and $\sigma_P = 4.2\mu K/K$ (The Planck Collaboration, 2006). To account for Galactic obstruction, we take $f_{\rm sky} = 0.80$. We use $\ell_{\rm min} = 30$ as a minimum ℓ-mode, in order to avoid problems with polarisation foregrounds and subtleties for the modelling of the integrated Sachs-Wolfe effect, which depends on the specific dark energy model (Weller & Lewis, 2003; Caldwell & Doran, 2005).

The full parameter set for the Planck calculation is:
$\{\Omega_m,\ \Omega_{\rm DE},\ h,\ \sigma_8,\ \Omega_b,\ w_0,\ w_a,\ n_s,\ m_\nu,\ N_\nu,\ \alpha,\ \tau\}$. We use the same central values as for our

weak lensing calculations, as described above, with a fiducial value for the reionisation optical depth $\tau = 0.09$, which is subsequently marginalised over. We consider neutrino parameters as $\Omega_\nu h^2$ and N_ν and use a Jacobian to translate this into constraints on m_ν and N_ν.

4.5 Parameter constraints from lensing

Table 4.3 shows the marginalised errors for each parameter in our six cosmological parameter sets. Joint lensing+Planck marginalised errors are shown in Table 4.5. When expected errors for n unknown parameters are calculated using a Fisher matrix, we are implicitly setting the errors on any additional parameters to zero. We should therefore expect QCDM to give us the best parameter constraints. In order to examine the variation in the marginalised errors with respect to the 8-parameter QCDM model, we define the fractional change in the marginalised error Δ for each parameter as

$$\text{Fractional change in error} = \frac{\Delta p_{\text{ext}} - \Delta p_{\text{QCDM}}}{\Delta p_{\text{QCDM}}}, \tag{4.50}$$

where the subscripts $_{\text{ext}}$ and $_{\text{QCDM}}$ denote the 'extended' model and QCDM (our most restricted model) respectively. This quantity is shown in Figure 4.6 for the eight parameters common to all the parameter sets, while Figure 4.15 shows the fractional error change in the joint lensing+Planck constraints.

We have also examined the dependence of the marginalised errors on the fiducial values. The stability of the errors with respect to the central values is an indication of the confidence which we can have in our experiment. In other words, we should expect the precision to be almost constant in the region around the true parameter values. The results for parameters in the dark energy, neutrino and primordial power spectrum sectors for the νQCDM$+\alpha$ parameter set are shown in a series of figures which will be explained further on.

4.5.1 Effect of varying the parameter set

The marginalised errors for the eight parameters in QCDM are shown in the second column of Table 4.3. With QCDM, all the sectors of our model are constrained well, even with our fiducial model containing massive neutrinos. Using our fiducial weak lensing survey with a QCDM parameter set, we obtain $\sim 5\%$ expected precision on w_0. The joint errors on the dark energy parameters w_0 and w_a are shown in Figure 4.16. The FOM in this case is 130.99. With the addition of Planck priors, we find a significant improvement in the error bounds for the Ω_{DE}, Ω_m, Ω_b, h, σ_8, and n_s. The improvement in the error bounds on w_0 and w_a is smaller, with the FOM being increased by a factor of 2.75 (Table 4.5, second column).

With the νQCDM$+\alpha$ parameter set, we obtain the following bounds for the dark energy equation of state parameters, using lensing only:

$$w_0 = -0.95 \pm 0.08 \qquad w_a = 0 \pm 0.33. \tag{4.51}$$

At the pivot redshift z_n, the constraint on $w(z_n)$ improves to

$$w(z_n) = -0.95 \pm 0.05. \tag{4.52}$$

In our calculations, we constrain the total neutrino mass and the number of massive species by measuring their effect on the lensing power spectrum via the matter power spectrum. This is sensitive to the neutrino fraction, related to the total neutrino mass by (Elgarøy & Lahav, 2005)

$$f_\nu \equiv \frac{\Omega_\nu}{\Omega_m} = \frac{1}{94\Omega_m h^2}\left(\frac{m_\nu}{\mathrm{eV}}\right). \tag{4.53}$$

Different massive neutrino species become relativistic at different redshifts. Hence, the matter power spectrum is also sensitive to individual neutrino masses and therefore, in our parameterisation, to the number of the number of massive neutrino species N_ν.

Tereno et al. (2009) find a 3.3 eV upper bound for the total neutrino mass, using CFHTLS–T0003 data, while Ichiki et al. (2009) find an upper bound of 8.1 eV. Using our fiducial νQCDM + α cosmology with neutrino parameter values of $m_\nu = 0.66\,\mathrm{eV}$ and $N_\nu = 3$, our marginalised error forecast for m_ν is 1.20 eV, which gives us a 1σ upper bound of 1.86 eV for the total neutrino mass (see Table 4.3), and an error bound of ± 3.8 for the number of massive neutrino species. With our joint lensing and Planck constraints (Table 4.5), we obtain an error of on the total neutrino mass of $\Delta m_\nu = 0.14$ eV and an error on the number of massive neutrino species of $\Delta N = 0.12$.

4.5.2 Effect of changing the fiducial cosmology

The assumed fiducial cosmology so far has been the one described in Section 4.3, and any derivatives in the Fisher matrix are taken about these fiducial values. Here we consider variations of the fiducial cosmology, and study their effect on the ability of our survey to constrain cosmological parameters (this part of our work has a resonance with Mukherjee et al., 2006; Pahud et al., 2006). In order to test the stability of our error bars as the fiducial values are changed, we define the following quantity:

$$\text{Relative marginalised error} = \frac{\Delta p}{|p|} \tag{4.54}$$

as the marginalised error on a parameter divided by the absolute fiducial value of the parameter. In the case where the denominator is zero (e.g. for w_a), we only consider the numerator. The parameter set used for these calculations is νQCDM + α.

In Figure 4.7 we show the errors for cosmological parameters in the dark energy, neutrino, and primordial power spectrum sectors against the fiducial neutrino mass, using the νQCDM + α parameter set. For the dark energy equation of state parameters w_0 and w_a, we plot the FOM against the fiducial neutrino mass in Figure 4.8. The results show that the errors are stable, even if the fiducial value is varied. This confirms the results by Hannestad et al. (2006), who find that neutrino mass bounds are robust against variations in w and the running spectral index (and also on the relativistic degrees of freedom). We also find that the (w_0, w_a) FOM is stable over a wide range of m_ν values.

We also varied the fiducial value for the primordial spectral index n_s and the dark

Parameter	QCDM	νQCDM	QCDM $+\alpha$	QCDM $+\alpha+\beta$	ν QCDM $+\alpha$	νQCDM $+\alpha+\beta$
w_0	0.05633	0.06443	0.05740	0.06583	0.08099	0.09608
w_a	0.19297	0.23674	0.21567	0.24988	0.32904	0.48144
$\Omega_{\rm DE}$	0.05214	0.05841	0.05287	0.05297	0.05842	0.05856
Ω_m	0.00731	0.00742	0.00731	0.00752	0.00749	0.00756
Ω_b	0.02411	0.02558	0.02544	0.02981	0.03200	0.03201
m_ν/eV		1.10229			1.19614	1.51694
N_ν		3.27380			3.81643	11.12214
h	0.11337	0.23176	0.18660	0.24691	0.41999	0.53253
σ_8	0.01184	0.01230	0.01185	0.01268	0.01307	0.01319
n_s	0.02904	0.03038	0.08662	0.11158	0.11969	0.12003
α			0.04378	0.05661	0.06556	0.07137
β				0.02574		0.08479
FOM	130.99	79.69	114.86	97.59	56.36	38.02

Table 4.3: Predicted marginalised parameter errors for weak lensing alone. We show results using different cosmological parameter sets. The second column shows the results for our most restricted parameter set QCDM. In the third column, we add massive neutrinos. Primordial power spectrum parameters are added in the fourth and fifth columns. In the sixth we add neutrinos and a running of the primordial spectral index. The seventh column shows our most extended model νQCDM$+\alpha+\beta$. We also show the DETF Figure of Merit for each model.

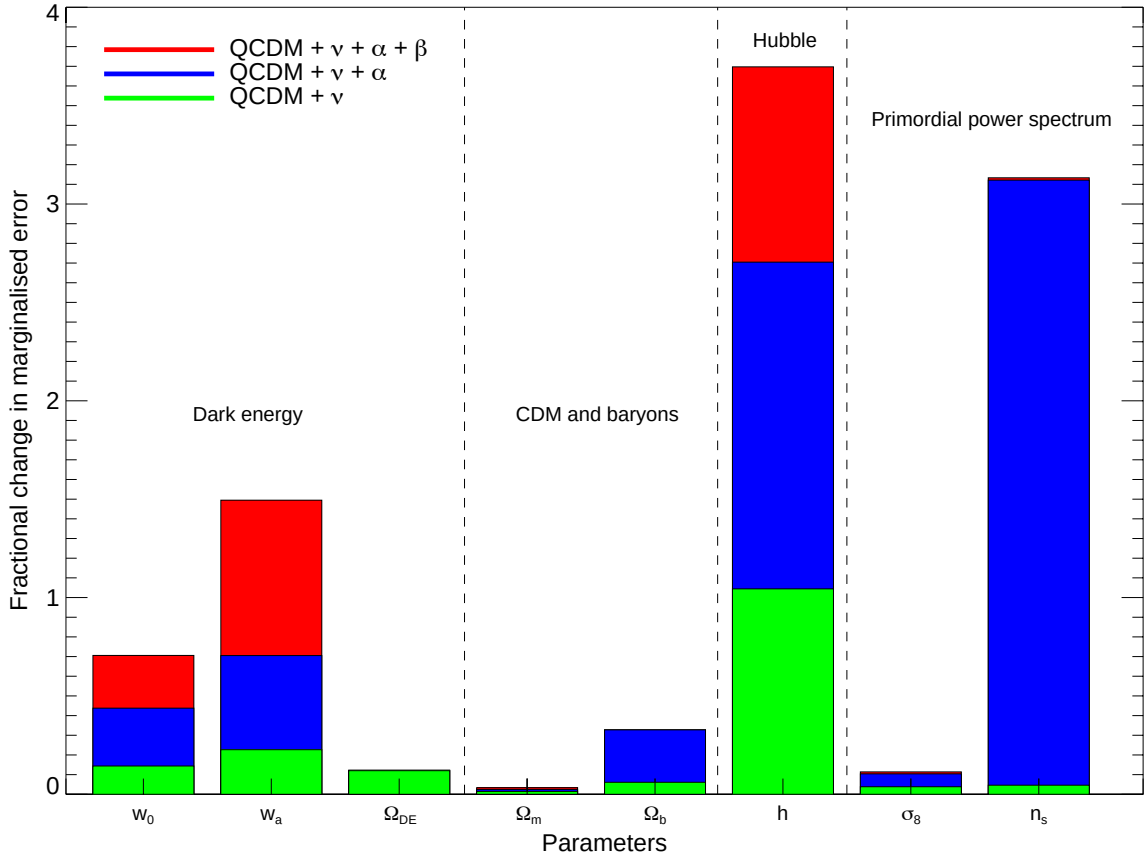

Figure 4.6: Panel 1: The fractional change in the marginalised error for each parameter with respect to the QCDM model, using a lensing Fisher matrix calculation. In this panel, we add neutrino parameters before adding degrees of freedom in the primordial power spectrum. In the second panel (following page) we add primordial power spectrum parameters before adding neutrinos. In each case, the most general parameter space, shown by the red bars, is QCDM $+ \nu + \alpha + \beta$.

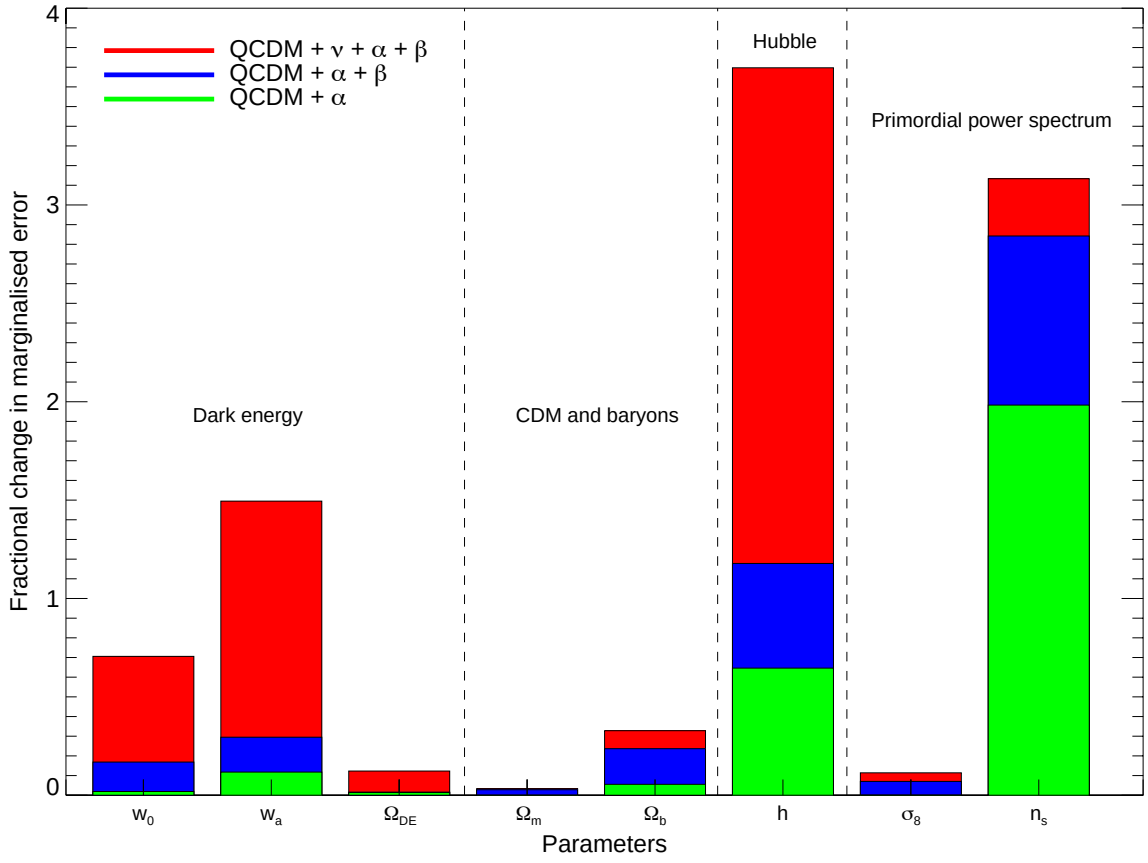

Figure 4.6: Panel 2: The fractional change in the marginalised error for each parameter with respect to the QCDM model, using a lensing Fisher matrix calculation. In this panel we add primordial power spectrum parameters before adding neutrinos.

energy equation of state w_0. The results are shown in Figures 4.9 and 4.11 respectively. We find that the bounds on the neutrino mass and the number of massive neutrino species are stable over a wide range of fiducial values for these parameters (overall, a 20% deviation from the concordance values). We also calculate the FOM resulting from the variation of these fiducial values. We find that the FOM is stable over a wide range of values of n_s (Figure 4.10), while it increases as w_0 is increased from -1 to -0.8 (Figure 4.12). Since the dark energy equation of state is parameterised by $w(a) = w_0 + w_a(a)$, a change in w_0 affects the amplitude of $w(a)$ at all redshifts, and therefore affects the shear as a function of redshift (the lensing efficiency function). Changing the value of w_0 also affects the number distribution of dark matter halos as a function of redshift and mass. In other words, not only does it change the growth factor (and therefore the matter power spectrum), it also changes the lensing power spectrum itself. Figure 4.12 suggests that the sensitivity of weak lensing to the parameters w_o and w_a increases at higher w_0.

We also explored our parameter constraints for two particular dark energy models, which are considered to be just at the limit of what is allowed by current constraints. The first is the SUGRA, or supergravity, model proposed by Weller & Albrecht (2002), which is a form of Quintessence, represented by $w_0 = -0.8$ and $w_a = 0.3$. The second is a phantom model proposed by Caldwell et al. (2003), with $w_0 = -1.2$ and $w_a = -0.3$. To test the effect of changing our dark energy model we carried out our Fisher matrix calculation using the νQCDM + α parameter set and our fiducial lensing survey. The marginalised errors and FOM for these two models are shown in Table 4.4. We find that joint w_0, w_a constraints are considerably weakened in the Phantom model. Constraints on other parameters, however, are weaker in the SUGRA Quintessence model. A negative w_a, as in the Phantom model, represents a dark energy scenario in which the dark energy density was less in the past. The effect of dark energy on the Hubble rate in the past is less in these scenarios, so that it becomes more difficult to constrain dark energy parameters using weak lensing. One must be careful about the falsely optimistic error bounds on cosmological parameters in such scenarios, due to the inability of our analytical transfer function to model dark energy perturbations.

The error on the dark energy density $\Omega_{\rm DE}$ is stable against the addition of massive neutrinos to the parameter set. For the equation of state parameters, we observe a degradation in the marginalised constraints. The FOM is consequently also degraded, as can be seen in Table 4.3. The top panel of Figure 4.6 shows that the parameter most sensitive to the addition of neutrinos is Hubble parameter h, and to a lesser extent, w_0 and w_a. In the latter case, this is due to a degeneracy with neutrinos in the observed effect on the growth function.

Figure 4.16 shows the joint 1σ constraints on the dark energy parameters w_0 and w_a. The addition of massive neutrinos to the QCDM model produces a degradation on these constraints but does not significantly change the orientation of the ellipse. This means that the pivot point a_n remains almost unchanged.

4.5.3 Constraints on the primordial power spectrum

In this section, we discuss the constraints for primordial power spectrum parameters, using different parameterisations of the primordial spectral index. We also examine the

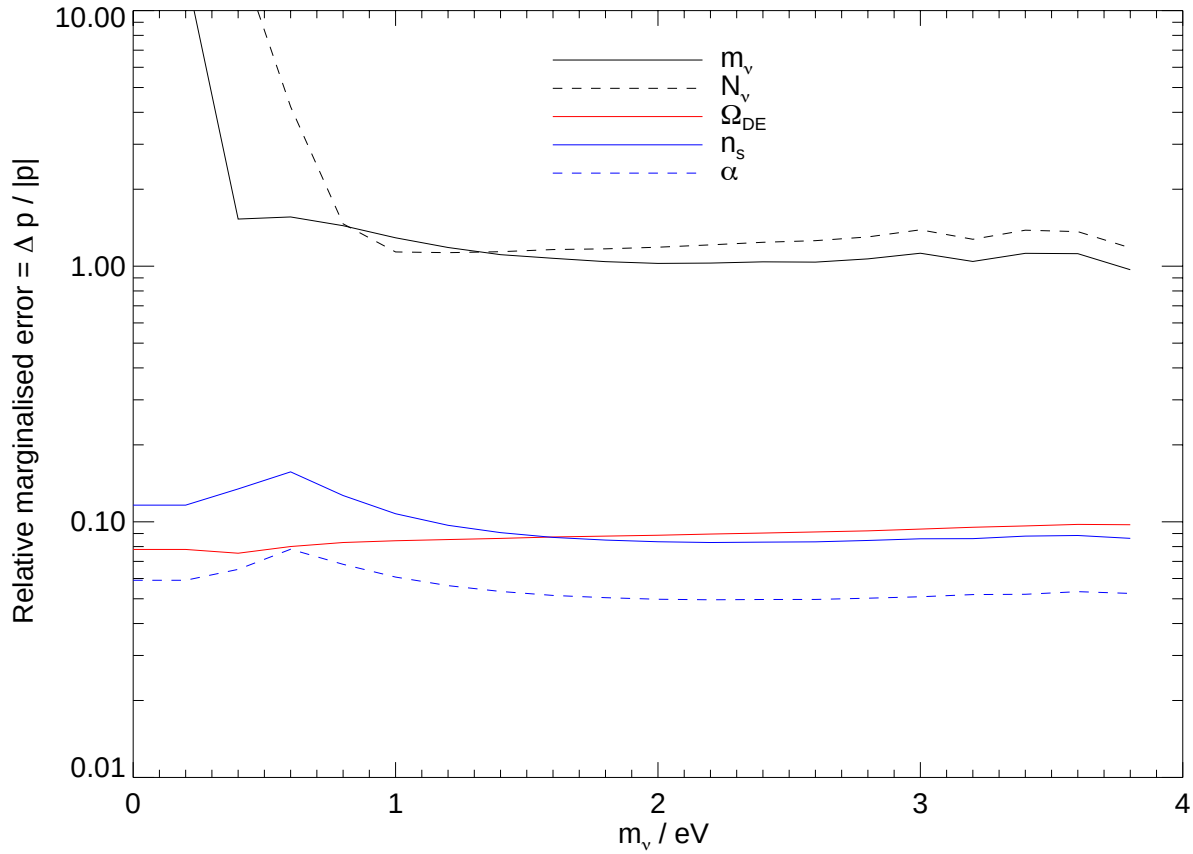

Figure 4.7: Relative marginalised error for parameters in three cosmological sectors, plotted against the fiducial neutrino mass in eV. The relative marginalised error is the marginalised error on the parameter divided by its absolute fiducial value: $\Delta p/|p|$. The plot shows five sets of values on the same axes: In black, the relative marginalised error for the neutrino mass m_ν (solid line), and the number of massive neutrino species N_ν (dashed line); in red (solid), the relative marginalised error for dark energy density $\Omega_{\rm DE}$; in blue, the relative marginalised error for primordial spectral index n_s (solid) and its running α (dashed).

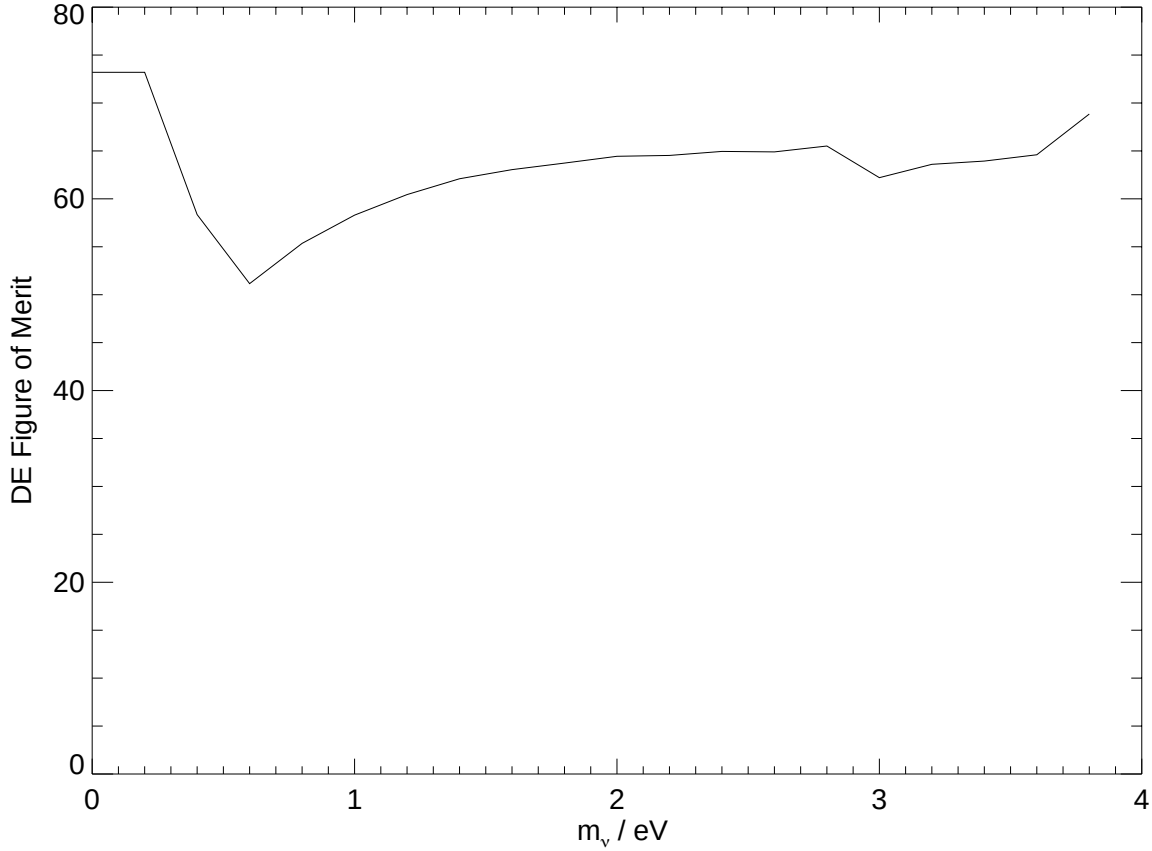

Figure 4.8: The dark energy Figure of Merit plotted against the fiducial value for the total neutrino mass m_ν in eV.

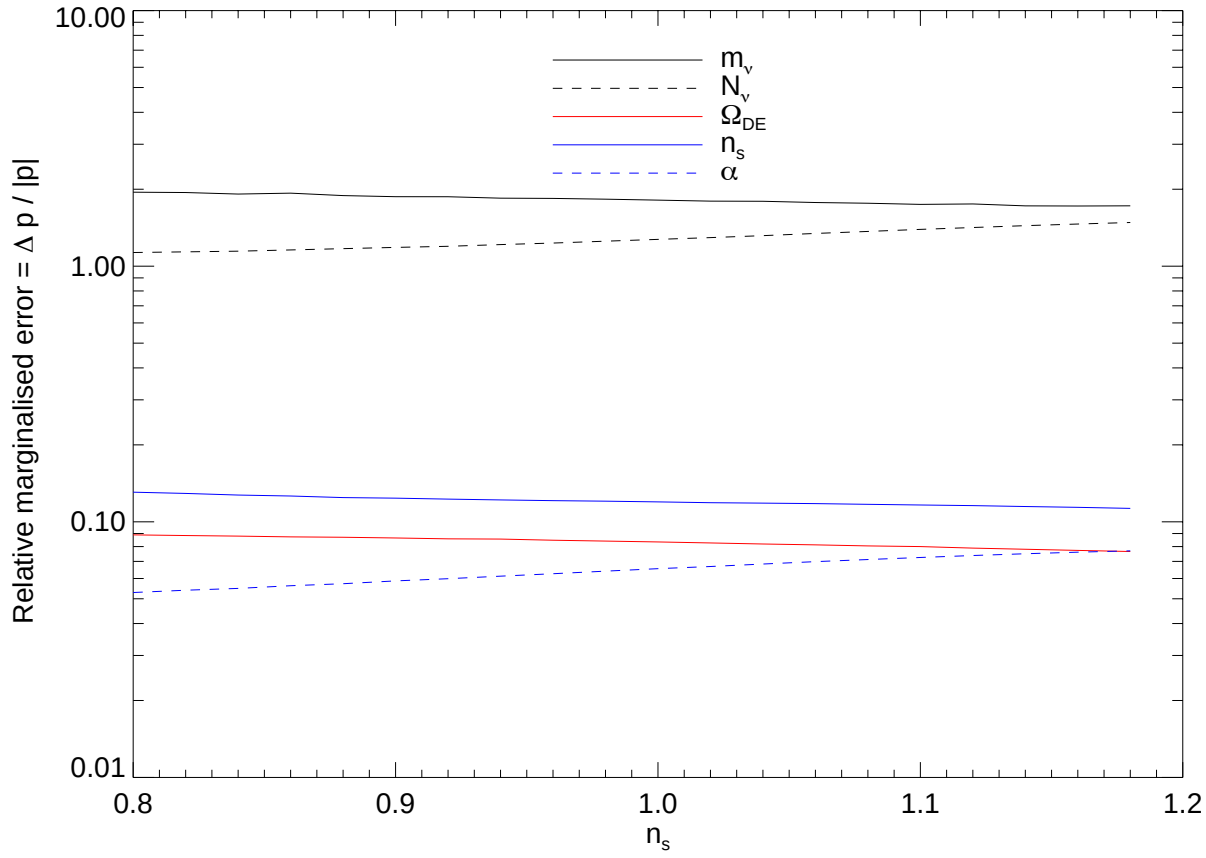

Figure 4.9: Relative marginalised error for parameters in three cosmological sectors, plotted against the fiducial value for the primordial spectral index n_s. The relative marginalised error is the marginalised error on the parameter divided by its absolute fiducial value: $\Delta p/|p|$. The plot shows five sets of values on the same axes: In black, the relative marginalised error for the neutrino mass m_ν (solid line), and the number of massive neutrino species N_ν (dashed line); in red (solid), the relative marginalised error for dark energy density $\Omega_{\rm DE}$; in blue, the relative marginalised error for primordial spectral index n_s (solid) and its running α (dashed).

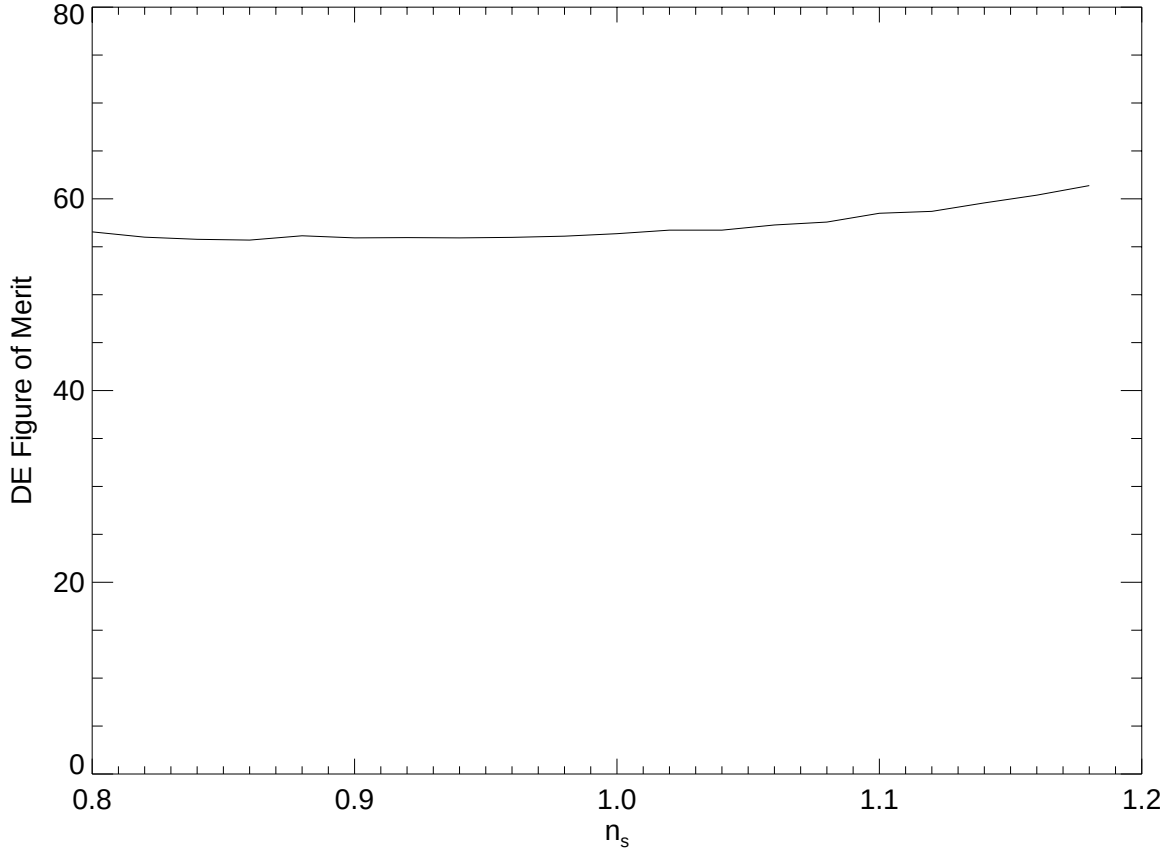

Figure 4.10: The dark energy Figure of Merit plotted against the fiducial value for the primordial spectral index n_s.

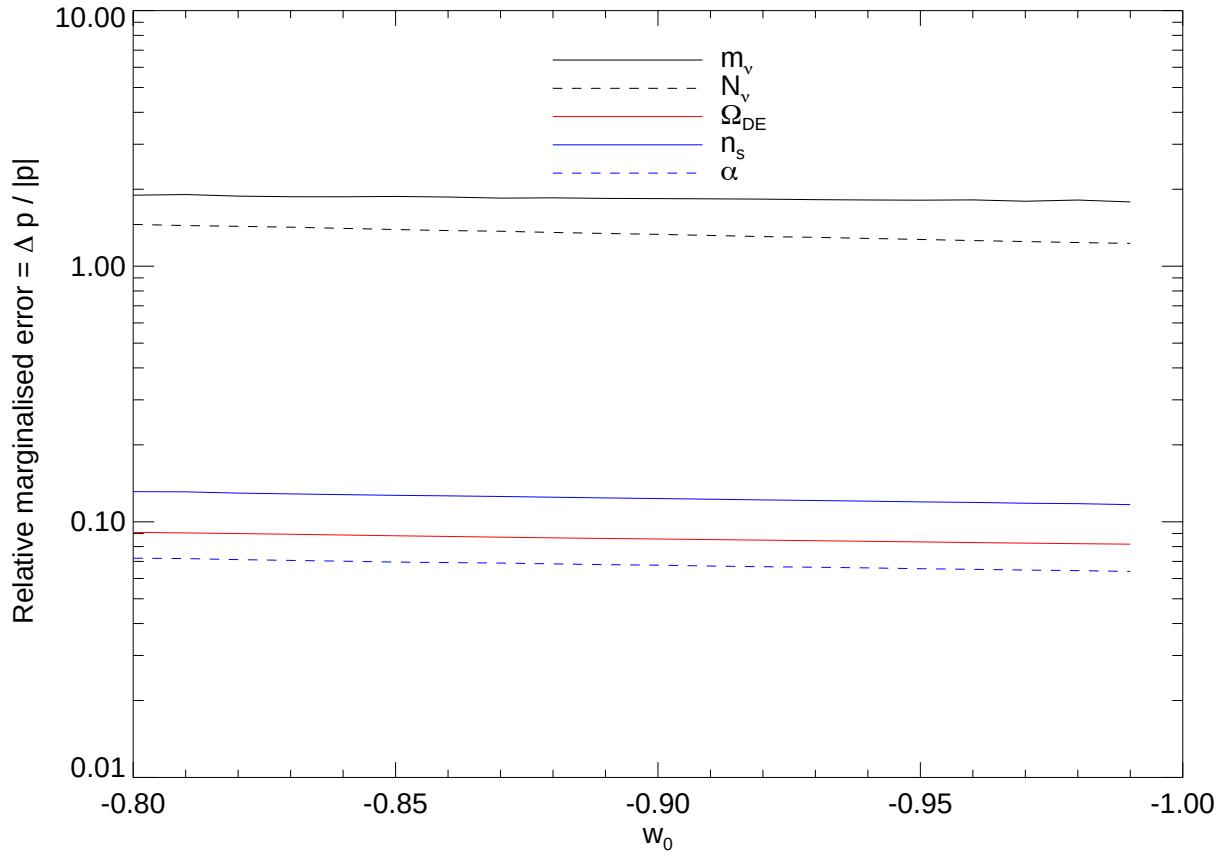

Figure 4.11: Relative marginalised error for parameters in three cosmological sectors, plotted against the fiducial value for the dark energy equation of state parameter w_0. The relative marginalised error is the marginalised error on the parameter divided by its absolute fiducial value: $\Delta p/|p|$. The plot shows five sets of values on the same axes: In black, the relative marginalised error for the neutrino mass m_ν (solid line), and the number of massive neutrino species N_ν (dashed line); in red (solid), the relative marginalised error for dark energy density $\Omega_{\rm DE}$; in blue, the relative marginalised error for primordial spectral index n_s (solid) and its running α (dashed).

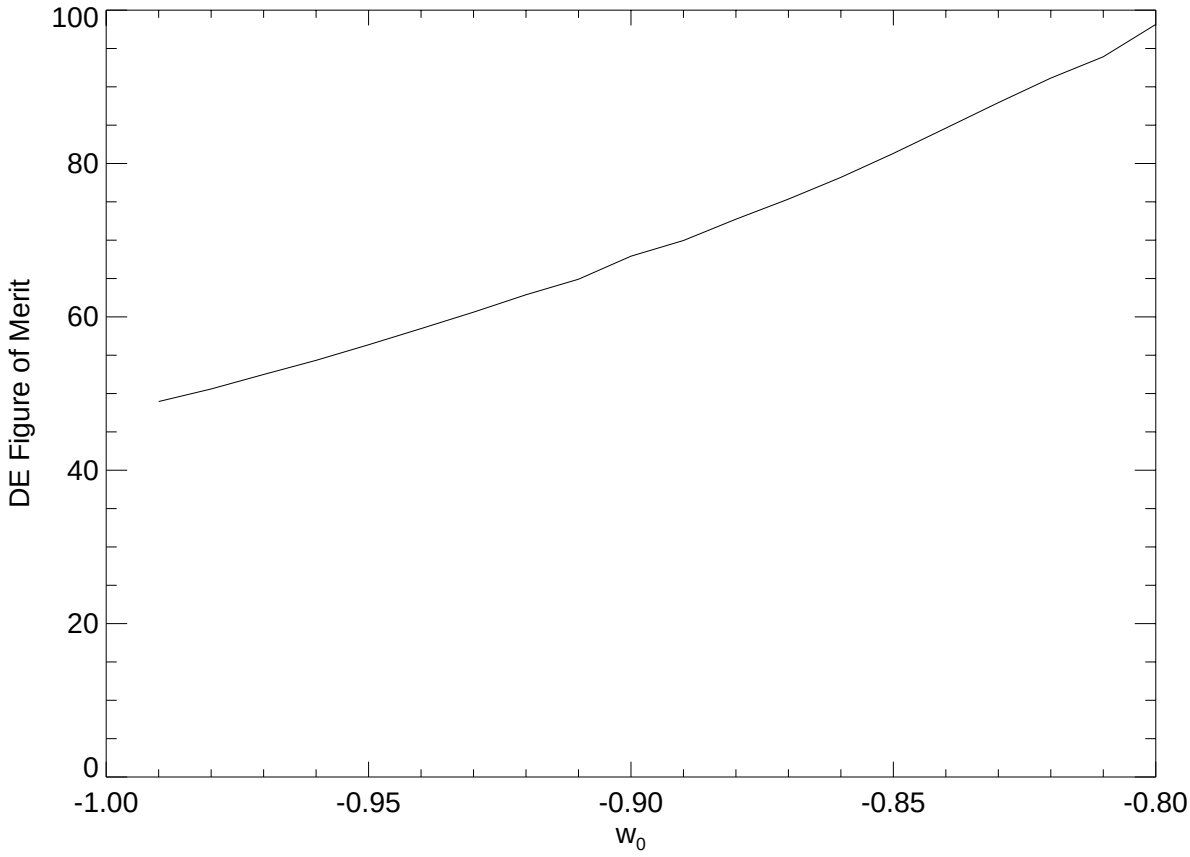

Figure 4.12: The dark energy Figure of Merit plotted against the fiducial value for the dark energy equation of state parameter w_0.

	Phantom	Quintessence
Δw_0	0.11319419	0.060629748
Δw_a	0.56475954	0.22300569
$\Delta\Omega_{\rm DE}$	0.049196426	0.067529670
$\Delta\Omega_m$	0.0082296147	0.0080236744
$\Delta\Omega_b$	0.028589575	0.035248301
Δm_ν/eV	1.1114124	1.3255770
ΔN_ν	2.8106820	4.7902798
Δh	0.38745158	0.45608683
$\Delta\sigma_8$	0.013459380	0.013865601
Δn_s	0.10034771	0.13966256
$\Delta\alpha$	0.055004062	0.076554876
FOM	20.96	121.39

Table 4.4: Predicted marginalised parameter errors for weak lensing alone, for two dark energy models: Phantom ($w_0 = -1.2$, $w_a = -0.3$) and SUGRA Quintessence ($w_0 = -0.8$, $w_a = +0.3$).

variations in our error forecasts for other parameters when we vary our primordial power spectrum parameterisation. Weak lensing forecast constraints on the running spectral index have been studied by Ishak et al. (2004), who also use combined lensing + current CMB constraints. They find that CMB constraints are improved when weak lensing is added, especially for the parameters σ_8, Ω_m, h and $\Omega_{\rm DE}$. Their cosmological model does not include massive neutrinos, however.

The parameterisation of the primordial power spectrum used here assumes a pivot scale k_0 at which the amplitude is defined. We find that the best constraints on n_s in the νQCDM $+ \alpha$ model using our fiducial weak lensing survey are achieved with a pivot scale $k_0 \sim 1\,{\rm Mpc}^{-1}$, which is larger than the value of $0.05\,{\rm Mpc}^{-1}$, adopted in the rest of the thesis. The results are shown in Figure 4.13. This optimum pivot scale is shifted to $\sim 0.3\,{\rm Mpc}^{-1}$ when the parameter β is added, and to $\sim 0.1\,{\rm Mpc}^{-1}$ when α is added. Our results show that a weak lensing survey achieves the maximum sensitivity to n_s and α at higher k with respect to CMB probes. To use the same approach as the dark energy Figure of Merit for the primordial power spectrum sector, we use a simplified form of the DETF FOM, which we shall call the ${\rm FOM}_{\rm prim}$ which is simply the area bounded by the $\Delta n_s \Delta\alpha$ rectangle:

$$ {\rm FOM}_{\rm prim} = \frac{1}{\Delta n_s \Delta\alpha}. \tag{4.55} $$

This definition allows us to define the pivot scale where the product of the marginalised errors on n_s and α as the value of k_0 which gives the maximum ${\rm FOM}_{\rm prim}$. In Figure 4.14 we show the variation of ${\rm FOM}_{\rm prim}$ for different values of k_0.

In Table 4.3 we note that the addition of the parameter α has a small effect on the FOM, while adding a further parameter β produces a larger degradation. The degradation in the Ω_b, Ω_m and σ_8 constraints is negligible against the addition of α, while the parameters h and n_s are most affected, as can be seen in Figure 4.6, Panel 2. The addition of β degrades the constraints on all these parameters, especially n_s.

With weak lensing only, we obtain tighter constraints on α than on n_s with the QCDM $+ \alpha$ and QCDM $+ \alpha + \beta$ parameter sets. This error hierarchy is reversed when Planck priors are added (Tables 4.3 and 4.5, fourth and fifth columns).

Examining Figure 4.16 we observe that the addition of primordial power spectrum parameters produces a small degradation in the joint (w_0, w_a) errors and has little effect on the orientation of the ellipses.

4.5.4 Combined neutrino and primordial power spectrum parameters

We also investigate the effect adding both neutrinos and primordial power spectrum parameters (the models νQCDM $+ \alpha$ and νQCDM $+ \alpha + \beta$). We note that the effect on the FOM is more significant than with neutrinos or α and β alone (Table 4.3). With the full extended model, the effect is especially noticeable on N_ν and β, showing that there are significant degeneracies between the effect of neutrinos on the matter power spectrum and the effect a scale-dependent primordial power spectrum with several degrees of freedom.

Figure 4.6 (red bars) shows that the greatest degradation in constraints with respect to QCDM occurs in the parameters w_a, h, and n_s. There is an additional degeneracy in the

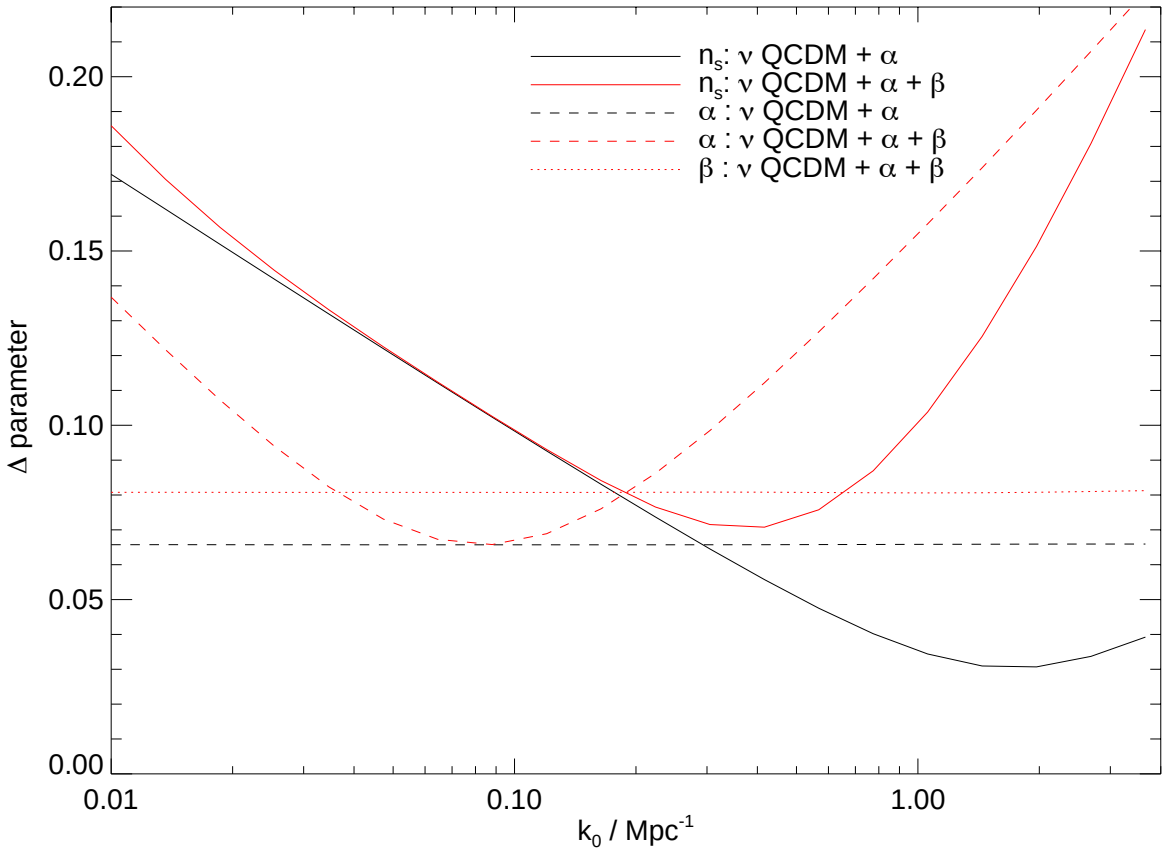

Figure 4.13: The effect of pivot scale on the marginalised errors for primordial power spectrum parameters. The figure shows the marginalised error Δ on primordial power spectrum parameters against pivot scale k_0. The calculation was carried out for two parameter sets: νQCDM + α (shown in black) and νQCDM + α + β (shown in red) using our all-sky fiducial weak lensing survey. We show the marginalised errors for the parameters n_s (solid line), α (dashed line) and β (dotted line).

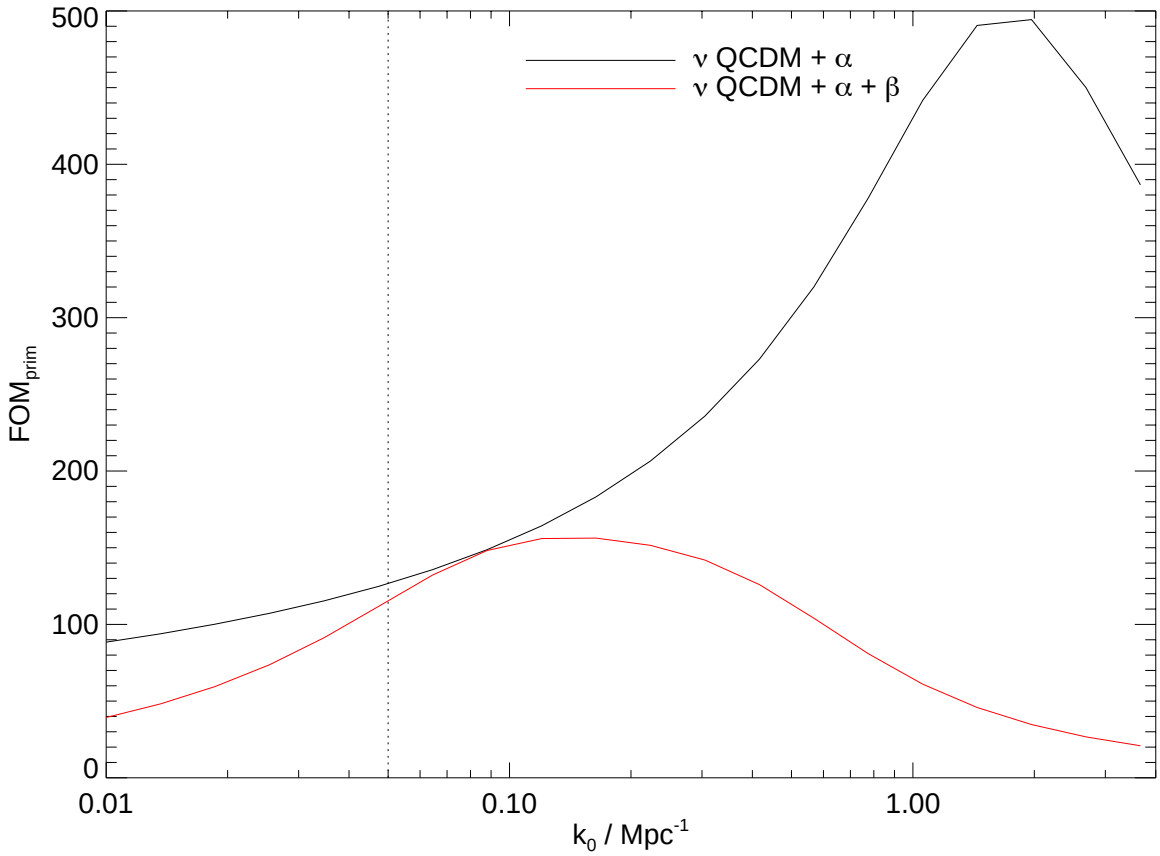

Figure 4.14: The 'Figure of Merit for the primordial power spectrum', as described in the text, for the two parameter sets. The vertical dotted line indicates the value of $k_0 = 0.05\,\mathrm{Mpc}^{-1}$.

matter power spectrum between the small-scale power-suppression effect of massive neutrinos and the form of the primordial power spectrum for certain values of the primordial spectral index.

With weak lensing only, we obtain tighter constraints on α than on n_s, which is in agreement with the results obtained by Kitching et al. (2008b) and Ishak et al. (2004). Although the precision for both parameters is degraded when neutrinos are added, this error hierarchy is preserved, even when CMB constraints are added (see Section 4.6 below).

The dependence of neutrino mass bounds on the fiducial value of the running of the primordial spectral index has been studied by Feng et al. (2006), who use a combination of WMAP3, 2dF galaxy clustering, and SNIa data. They find that these constraints are strengthened in the presence of a nonzero α. In order to study the dependence of weak lensing neutrino mass constraints on this parameter, we calculated the Fisher matrix for the νQCDM $+ \alpha$ parameter set using different fiducial values of the running in the range $-0.05 < \alpha < 0$. We find that our neutrino mass bounds are slightly weakened (from $\Delta m_\nu = 1.196$ eV in the fiducial model to 1.219 eV), but the bounds on the number of massive species are improved (from $\Delta N_\nu = 3.816$ to 3.760).

4.6 Joint lensing and CMB results

The addition of Planck priors has a significant effect on parameter constraints. In the dark energy sector, the main constraints on w_0 and w_a come from the Integrated Sachs-Wolfe effect, although degeneracies between w_0 and w_a remain. The CMB constrains the curvature of the cosmological model very well. Hence it constrains $\Omega_{\rm DE}$. Another parameter which is well-constrained by the CMB is σ_8. This comes about through an indirect effect, since this parameter, as measured by the CMB, is dependent on other parameters, which in turn are well-constrained by this probe. Particularly relevant to this thesis are the constraints placed by the CMB on the primordial power spectrum. Hence, the addition of CMB priors allows us to limit the degeneracy between this sector and other parameters.

When we add Planck priors to our weak lensing forecasts, the FOM is improved by a factor of 6 for the νQCDM $+ \alpha + \beta$ model (Table 4.5), and we obtain better constraints for all parameters, especially Ω_b, $\Omega_{\rm DE}$ (related to the geometry of the Universe), h and n_s. Adding CMB priors also lifts the degeneracy between some parameters, so the extension of the parameter set does not significantly degrade the error bars. This can be seen in Figure 4.15, where Ω_b, h and n_s, which are well-constrained by Planck, are now hardly affected by the addition of extra parameters. It can be seen from Table 4.5 that we obtain better constraints on α than on n_s with the addition of CMB priors, reversing the error hierarchy obtained with lensing only. Moreover, the addition of neutrino parameters does not significantly affect the precision on n_s.

With combined lensing+Planck calculations, we obtain an improvement in the joint (w_0, w_a) constraints (Figure 4.16). The constraints are robust against the addition of neutrino parameters and the primordial power spectrum parameters α and β.

One of the aims of this thesis is to investigate dark energy constraints, so we prefer to consider a possible non-flat model (i.e. $\Omega_m + \Omega_{\rm DE} \neq 1$) since some dark energy models

involve variations of the Friedmann equations in non-flat geometries (e.g. Dvali & Turner, 2003). The assumption of spatial flatness would give us stronger constraints on our parameters. CMB probes place very strong constraints on the curvature of the Universe. The addition of CMB priors therefore allows us to improve the precision on $\Omega_m + \Omega_{\rm DE}$, with a consequent improvement of precision for the other parameters.

Parameter	QCDM	νQCDM	QCDM $+\alpha$	QCDM $+\alpha+\beta$	ν QCDM $+\alpha$	νQCDM $+\alpha+\beta$
w_0	0.04942	0.04984	0.04943	0.05055	0.04987	0.05142
w_a	0.17943	0.18231	0.17946	0.18260	0.18275	0.18482
$\Omega_{\rm DE}$	0.00644	0.00661	0.00721	0.00722	0.00730	0.00730
Ω_m	0.00389	0.00391	0.00391	0.00391	0.00393	0.00393
Ω_b	0.00091	0.00119	0.00101	0.00101	0.00128	0.00128
m_ν/eV		0.14172			0.14172	0.14176
N_ν		0.11694			0.11821	0.11924
h	0.00599	0.01360	0.00625	0.00625	0.01381	0.01382
σ_8	0.00461	0.00491	0.00467	0.00470	0.00492	0.00501
n_s	0.00332	0.00549	0.00356	0.00360	0.00557	0.00563
α			0.00515	0.00519	0.00545	0.00545
β				0.01779		0.01834
FOM	357.12	258.40	357.01	348.70	251.51	240.59

Table 4.5: Predicted marginalised parameter errors for for cosmic shear combined with Planck priors.

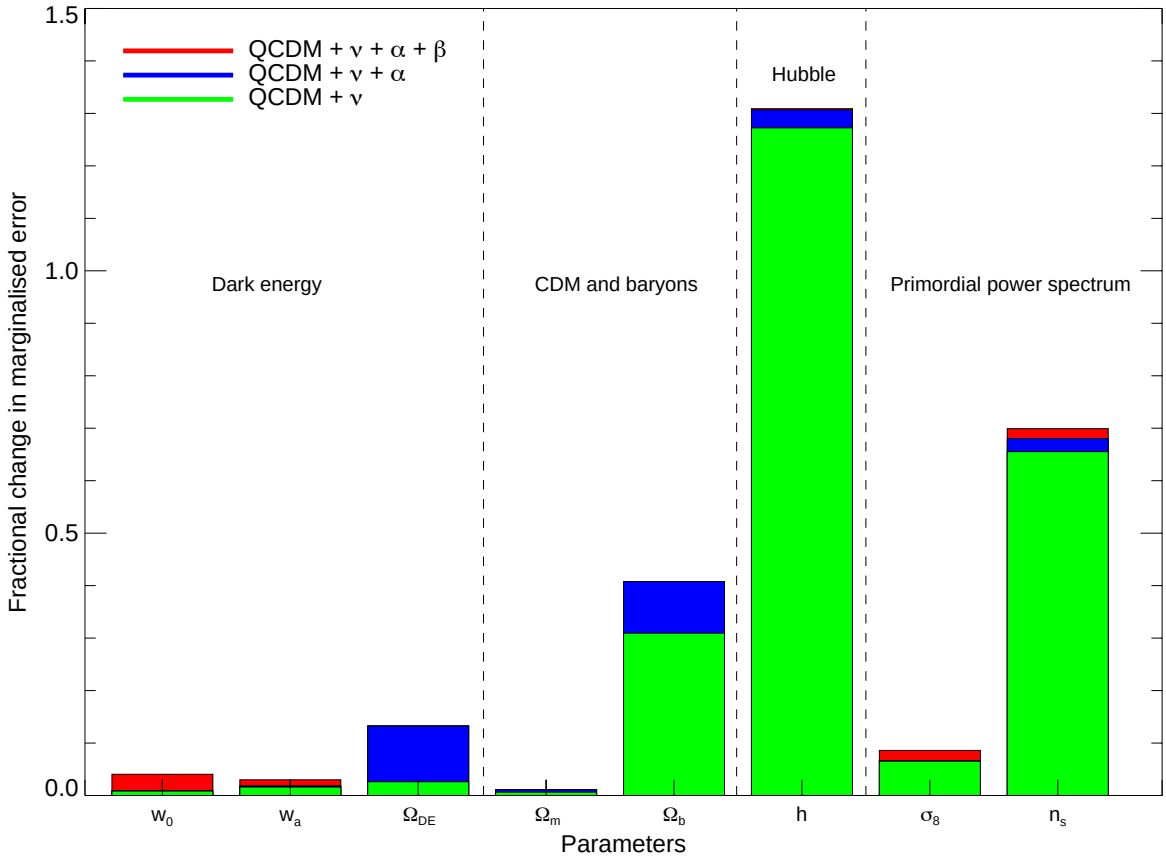

Figure 4.15: Panel 1: Fractional change in marginalised errors with respect to QCDM, using a joint lensing+Planck Fisher matrix. As in Figure 4.6, in the first panel we add neutrino parameters before adding the parameter α, and in the second panel we consider different parameterisations of the primordial power spectrum without adding neutrinos to our parameter space.

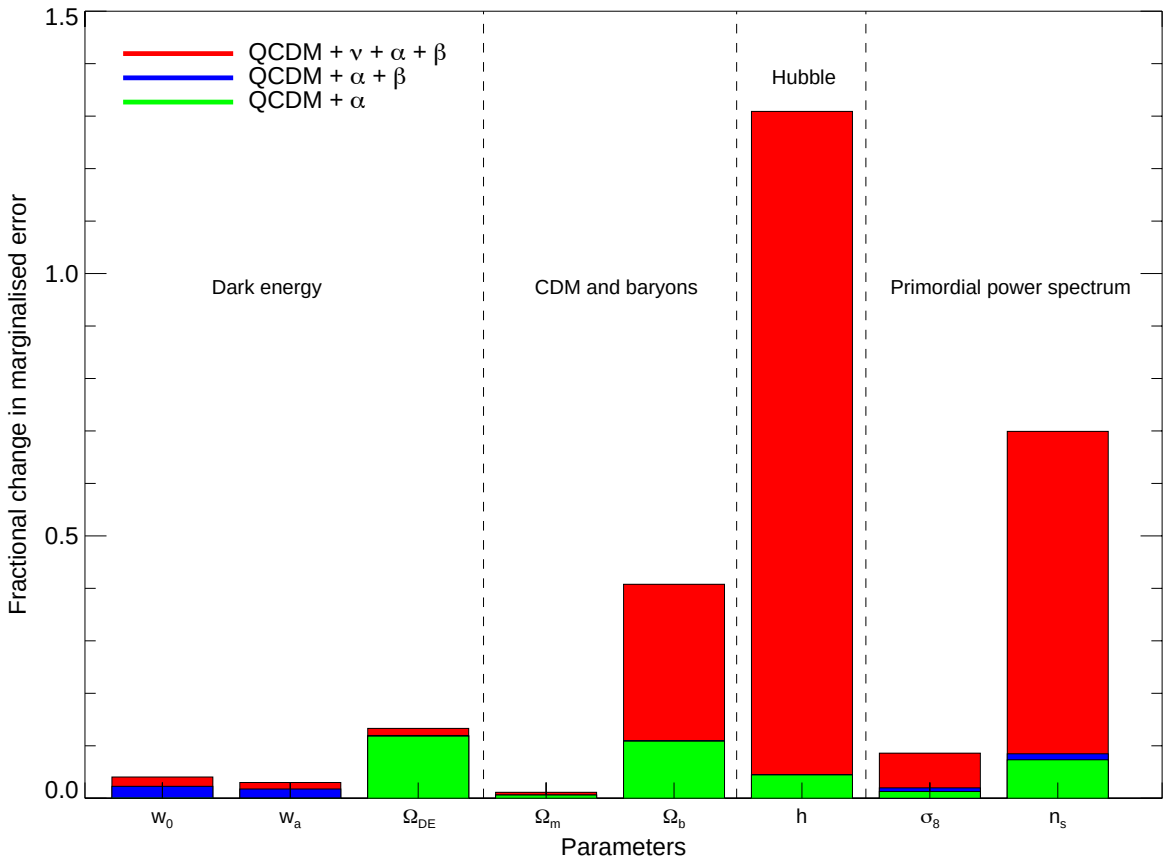

Figure 4.15: Panel 2: Fractional change in marginalised errors with respect to QCDM, using a joint lensing+Planck Fisher matrix. In this panel we consider different parameterisations of the primordial power spectrum.

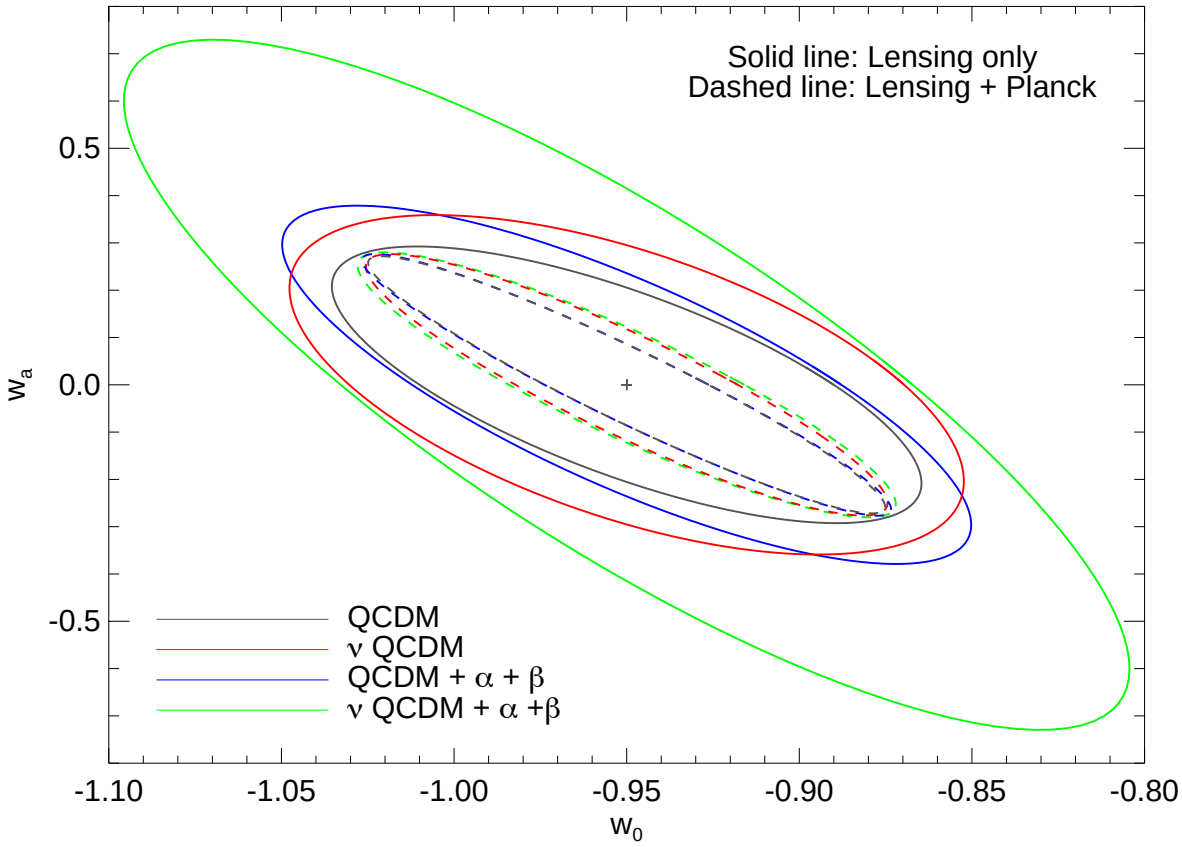

Figure 4.16: Joint 1σ constraints in the (w_0, w_a) plane from our Fisher matrix calculation with four different parameter sets. QCDM ,νQCDM, QCDM$+\alpha+\beta$ and νQCDM$+\alpha+\beta$ are shown in grey, red, blue and green respectively. The solid ellipses show the constraints using lensing only, while the dashed ellipses show the constraints with the addition of Planck priors from our CMB Fisher matrix calculation. The lensing-only error ellipses show that the addition of neutrinos or primordial power spectrum on their own do not significantly affect the precision on the dark energy equation of state parameters, but their simultaneous addition has a significant affect. With the addition of CMB priors, we recover this precision, even with the most extended parameter set.

4.7 Summary

In this chapter we have calculated forecast errors using the Fisher matrix formalism for an all-sky tomographic weak lensing survey, and for weak lensing+Planck. We have used different cosmological parameter sets, studying the effect of the addition of parameters in the model, and of a change in the fiducial cosmology. We have shown that error forecasts for some parameters are stable against changes in the parameter set (Table 4.3), and that degeneracies between the dark energy parameters w_0 and w_a are not significantly affected by the addition of parameters (Figure 4.16). The marginalised errors are shown to be stable against a wide range of fiducial values for three parameters in particular: m_ν, n_s and w_0.

Error forecasts for neutrino parameters have been studied by Kitching et al. (2008a), who use joint 3D weak lensing + Planck forecasts. We find that our joint lensing + CMB constraints are weaker in the neutrino sector, by factor of 4.5 and 1.5 for m_ν and N_ν respectively, a difference which we attribute to the differences in the calculation. Kitching et al. use more optimistic assumptions for the Planck Fisher matrix calculation (Kitching, private communication), a different parameter set for the Planck Fisher matrix (inclusion of the tensor to scalar ratio r), and a different weak lensing method (3D weak lensing). They also use the modified growth function suggested by Kiakotou et al. (2008) and a different parameterisation of the primordial power spectrum in terms of n_s and α (Kitching, private communication).

Our results have a resonance with De Bernardis et al. (2009), in which it is shown that the neutrino mass hierarchy can be constrained using cosmic shear, using a more general parameterisation of the neutrino mass splitting. We find that for the parameters that are common between the two calculations there is an agreement between the predicted errors, despite the slightly different parameter sets and assumptions.

In the neutrino sector, parameter constraints would be improved by a hierarchical parameterisation in which different neutrino species have non-degenerate masses. This would model more accurately the process whereby each massive species becomes non-relativistic at a different redshift. While the different transition redshifts have only a very small effect on the CMB anisotropy power spectrum, the effect is non-negligible in future cosmic shear experiments which measure the matter power spectrum to a sufficient accuracy to discriminate between different mass hierarchies.

In this chapter we have also focussed on the uncertainties in the form of the primordial power spectrum. We have investigated the shift in the optimal pivot scale for primordial power spectrum constraints with the addition of extra parameters (Figure 4.13), showing that it tends to be larger by a factor of 2-20 compared to the commonly used CMB-measurement value . We have shown that parameter constraints are dependent on the parameterisation of the primordial power spectrum. With the addition of CMB priors, we have shown that we can obtain improved constraints in this sector, which reduces the dependency on constraints on the parameter set.

In the dark energy sector, the joint (w_0, w_a) constraints are remarkably robust against the addition of massive neutrinos and of primordial power spectrum parameters to the parameter set, with only a weak degradation in the precision. When the all the parameters are added simultaneously, the degradation in the precision is more sig-

nificant. We find that the addition of CMB priors allows us to recover the precision on these parameters, and on parameters in the other sectors, even when m_ν, N_ν, α and β are added simultaneously.

Using the results in this chapter we conclude that future weak lensing surveys, in combination with CMB priors from future experiments, have the potential to constrain the parameters in all cosmological sectors. We also show that the survey precision is stable against changes in the parameterisation of the cosmological model. This is important in the light of the need to test as wide a range of theories as possible.

We now turn to the question of finding the best survey strategy to maximise our parameter constraints.

Chapter 5

Tomographic weak lensing survey optimisation

In this chapter, we examine how the design of a future all-sky tomographic weak lensing survey can be optimised to measure cosmological parameters. We focus on three sectors: dark energy, neutrinos, and the primordial power spectrum.

We examine how the constraints on these cosmological sectors are affected by three survey design parameters: the survey area A_s, the galaxy count per sq arcmin n_g, and the median redshift z_m. We also study the impact of the multipole range on the survey precision.

5.1 Defining an optimum survey

Our weak lensing survey forecast errors are limited by many factors, which can be grouped into three main areas: the statistical error imposed by the survey geometry, the photometric redshift errors, and the uncertainties in the power spectrum arising from shear measurement systematics and theoretical uncertainties. Future weak lensing missions have set 0.1% as the precision on ellipticity measurements, with percent-level precision on the measurement of w. We need to know how to optimise our survey strategy to achieve the desired precision in our error bounds. In this section, we shall discuss the limitations on this precision, together with the optimisation of the survey geometry.

The optimisation of weak lensing surveys and the minimisation of systematics has been investigated in many papers. Among the more recent ones are Amara & Réfrégier (2007, 2008); Heymans et al. (2006); Massey et al. (2007); Paulin-Henriksson et al. (2008); Amara et al. (2009). These studies have converged towards a common optimum survey design featuring a wide survey with well-controlled and stable point-spread functions, with precise photometric redshift measurements. Such design criteria are covered by upcoming all-sky surveys such as the Large Synoptic Survey Telescope [1] (LSST), the Panoramic Survey Telescope & Rapid Response System (Pan-STARRS)[2], DUNE/Euclid[3], or the Joint Dark Energy Mission[4] (JDEM).

In this chapter we study the optimisation of an all-sky tomographic weak lensing survey whose design parameters are based on the DUNE/Euclid concept. The optimisation of such a survey has been investigated by Amara & Réfrégier (2007), who focus on the dark energy Figure of Merit. They use a ΛCDM fiducial cosmological model with a spatially flat Universe, and the BBKS transfer function (Bardeen et al., 1986) with the Peacock & Dodds (1996) non-linear correction. Their parameter set is therefore $\{\Omega_m, \Omega_b, w_0, w_a, h, \sigma_8, n_s\}$. Here, we investigate whether the results are modified by the addition of massive neutrinos to the cosmological model, and the extension of the parameter set for which we calculate the Fisher matrix. We also examine the optimisation for two other cosmological sectors: neutrinos and the primordial power spectrum. The aim is to investigate whether the same optimum survey design applies for all parameters. In the final part of our calculation we extend the parameter set to include 12 parameters, as described in Chapter 4.

To this end, we study the optimisation using our fiducial cosmological model, as described in Chapter 4, using the Eisenstein & Hu (1999) transfer function and the Smith et al. (2003) non-linear correction described in Section 4.2. For our fiducial survey geometry, we use the parameters for a 'shallow survey', as described in Amara & Réfrégier (2007): $z_m = 0.9$, $n_g = 35$ galaxies per sq arcmin, survey area = 20000 sq degree, together with the weak lensing formalism which we also use in Chapter 4. We consider two cosmological parameter sets: νQCDM + α and νQCDM + α + β, with the following fiducial values: $\Omega_{\rm DE} = 0.7$, $w_0 = -0.95$, $w_a = 0$, $\Omega_m = 0$, $\Omega_b = 0.045$, $m_\nu = 0.66\,\mathrm{eV}$, $N = 3$,

[1] http:www://lsst.org

[2] http://www.pan-starrs.ifa.hawaii.edu

[3] As of 2009, DUNE is included in the Euclid concept. See http://www.dune-mission.net and http://sci.esa.int/science-e/www/area/index.cfm?fareaid=102

[4] http://jdem.gsfc.nasa.gov

$h = 0.7$, $\sigma_8 = 0.8$, $n_s = 1$, $\alpha = 0$, $\beta = 0$.

We calculate the Fisher matrix for the νQCDM + α parameter set varying three survey parameters: the median redshift z_m, the number of galaxies per square arcminute n_g, and the area of the survey in square degrees A_s. We also study the effect of changing the maximum multipole $\ell_{\rm max}$.

5.2 Varying the survey parameters

Any future survey will be limited by a finite observing time. Within a realistic timeframe, considered to be roughly 3 years, either the depth or the survey area will have to be limited. We therefore need to study the trade-off between these two parameters, and the optimum survey strategy which maximises the precision of our measurements. A very wide, shallow survey will yield poor cosmological constraints since the shot noise is large, while a very deep survey will also yield poor constraints because very little area can be covered, and the cosmic variance will be large. The three most important parameters in this study are the area of the survey A_s, the number density of lensed galaxies n_g, and the redshift distribution of the galaxies, which is a function of the median redshift of the survey z_m.

We have carried out a Fisher matrix calculation for our νQCDM+α data set (chosen as the most common generalisation of ΛCDM) for different values of the three survey parameters described above. Our aim is to study the impact of these parameters on the FOM, and on the constraints in three cosmological sectors: dark energy, neutrinos and the primordial power spectrum.

To this end, we show a set of set figures similar to Figures 4.7 to 4.12 in Chapter 4. Figure 5.1 shows the impact of the survey area on the precision on Ω_m, m_ν, N, n_s and α. We also note that the scaling is similar for all these parameters. The FOM also scales linearly with the survey area (Figure 5.2).

In Figure 5.3, we see that the scaling of the precision on DE, neutrino and primordial power spectrum parameters with the galaxy count n_g is stronger than with the survey area, with the precision on Ω_m being slightly more sensitive to n_g than the other parameters. In this case, the FOM shows a linear scaling with n_g (Figure 5.4).

The precision on these cosmological parameters shows the strongest dependence on z_m. This is shown in Figure 5.5 (thin lines). We observe a factor of ~ 10 improvement in the relative error in the range $z_m = 0.2$ to 1.4. Again, the dependence of Ω_m on the survey parameter is slightly stronger than the other cosmological parameters. The FOM also shows a strong dependence on the median redshift (Figure 5.6, thin lines), with the scaling being non-linear.

The FOM shows a nonlinear scaling with z_m, tending towards a constant as z_m approaches 1.5 (Figure 5.6). At higher redshifts, we have two effects: information from lensing becomes weaker, and dark energy no longer dominates. These two effects combine to give us a slight tailing off of the improvement on the FOM beyond $z_m \sim 1$.

The dark energy Figure of Merit is generally taken as the criterion for measuring the quality of a weak lensing survey. However, we have shown in this thesis that weak lensing can constrain other parameters apart from dark energy. The question then is whether the same optimisation strategy applies across all cosmological parameters. The results in this

section show that this is indeed the case, since the scaling of the precision is the same for all parameters. In other words, a survey optimised for weak lensing constraints will also be the optimum survey for other parameters. There are two reasons for this. One is the sensitivity to the survey design of the cosmological parameters themselves. The other is the degeneracy between the dark energy sector and the other parameters. By constraining dark energy more strongly, we also improve parameter constraints in other sectors. Although it may be desirable to achieve the maximum precision by using the optimum values for the individual survey parameters, some trade-offs may be necessary due to the finite observing time. With our tomographic weak lensing survey, we find that the dominant factor in the precision is the survey area.

5.3 The multipole range

In this thesis we calculate the theoretical matter power spectrum $P(k, z)$ using an analytical formula, as described in Chapter 4. This, however, is subject to uncertainties, since baryonic physics will render the model uncertain at small scales. This creates an addition systematic effect in our projections. To circumvent this problem, the maximum k value for the power spectrum calculation is sometimes chosen to be as low as possible, so that it lies within the linear régime of $P(k)$. However, due to the Limber approximation, there is a correspondence between the spatial wavenumber k and the angular wavenumber ℓ (see Hu & Jain, 2004). For our survey, with a median redshift of 0.9, we need $k \sim 100$ to cover an ℓ range up to 5000.

If we limit ourselves to smaller k-range, we cannot use the larger ℓ values. To study how this impacts our parameter precision, we calculate the relative error for different values of $\ell_{\max}$ in Figure 5.7 (thin lines). We consider the range $10^3 < \ell_{\max} < 10^5$, which corresponds to discarding nonlinear modes (lower bound) to including sub-arcmin scales (upper bound). The minimum multipole is kept constant at $\ell_{\min} = 10$. We use a νQCDM + α parameter set with the fiducial values

We observe that the precision is not significantly improved beyond $\ell_{\max} \sim 10^4$. The scaling for the precision on m_ν with $\ell_{\max}$ is stronger than the other parameters below $\ell_{\max} = 10^4$. This suggests that most of the information in this sector comes from modes corresponding to the nonlinear part of the matter power spectrum, but a maximum ℓ mode of 5000 is a good compromise. Beyond this value, the improvement in precision becomes less significant. This also holds for the FOM, as seen in Figure 5.8. Below this value of ℓ, however, $\ell_{\max}$ has a significant impact on the precision, especially on the FOM. This is in agreement with the results of Amara & Réfrégier (2007), who use a cosmological model with no massive neutrinos or running of the spectral index and assume a spatially flat Universe.

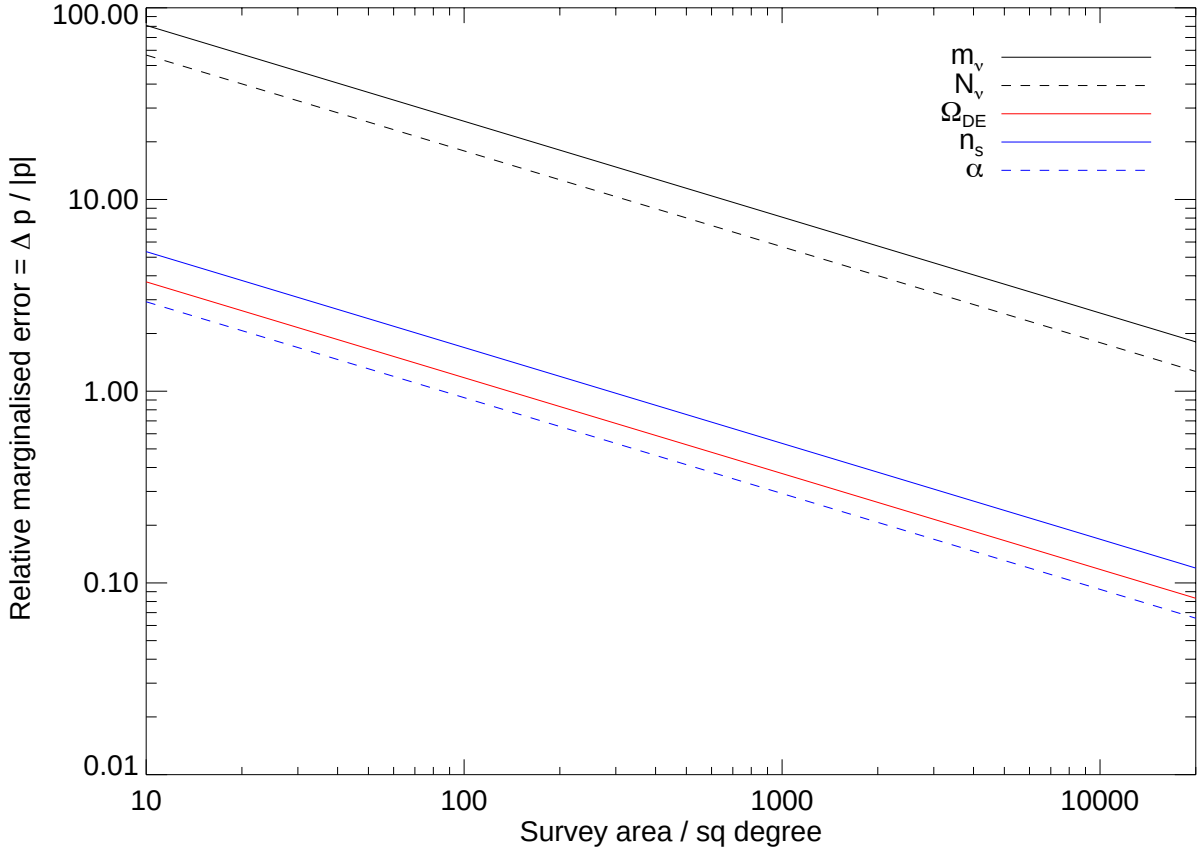

Figure 5.1: Relative marginalised error for parameters in three cosmological sectors against the area of the survey A_s. The relative marginalised error is the marginalised error on the parameter divided by its absolute fiducial value: $\Delta p/|p|$. The plot shows five sets of values on the same axes: In black, the relative marginalised error for the neutrino mass m_ν (solid line), and the number of massive neutrino species N_ν (dashed line); in red (solid), the relative marginalised error for dark energy density $\Omega_{\rm DE}$; in blue, the relative marginalised error for primordial spectral index n_s (solid) and its running α (dashed).

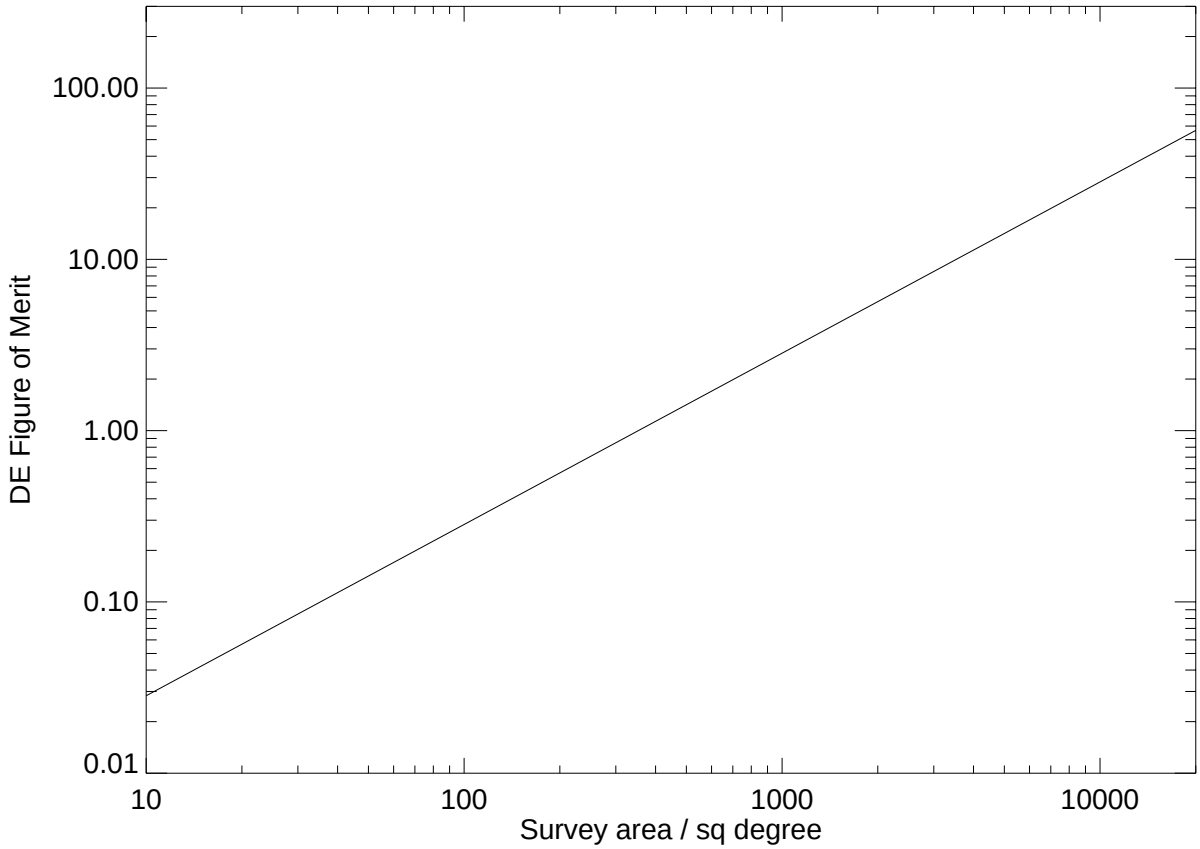

Figure 5.2: The dark energy Figure of Merit against the area of the survey A_s.

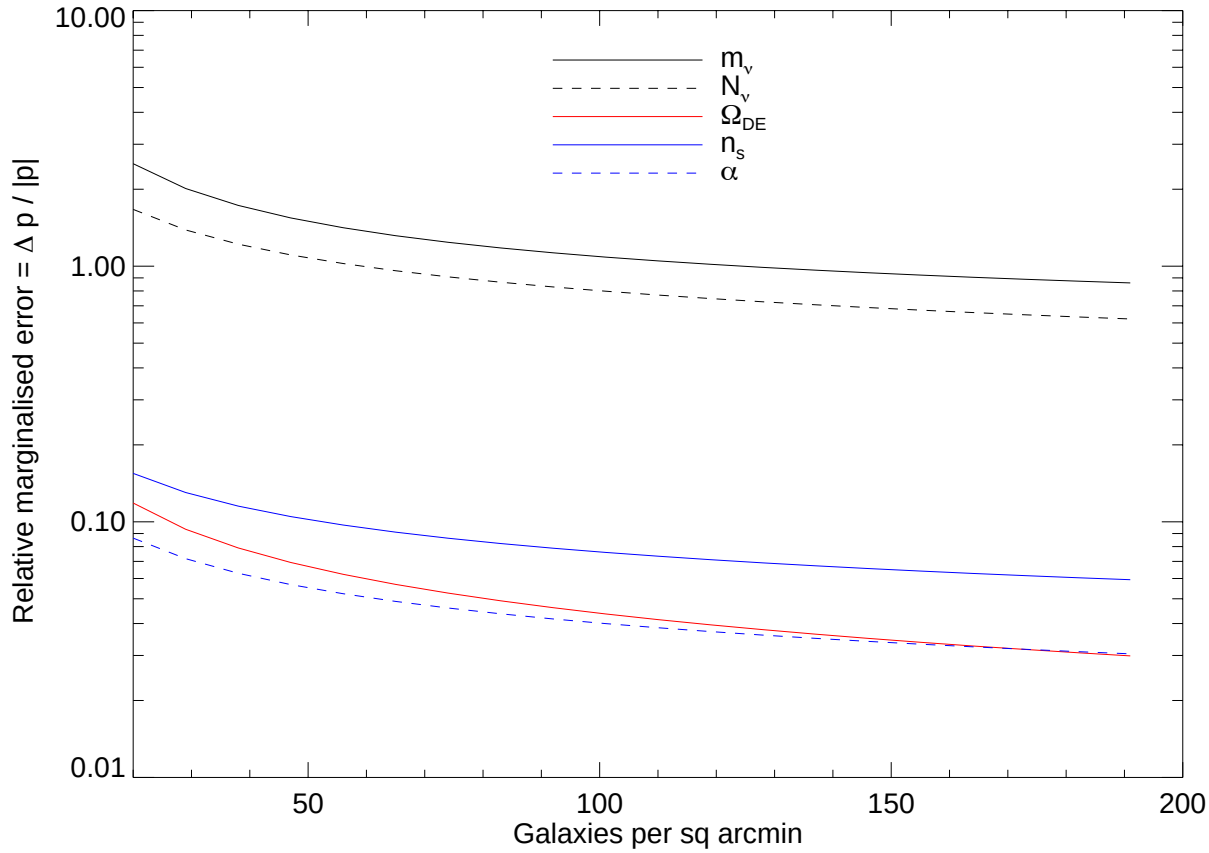

Figure 5.3: Relative marginalised error for parameters in three cosmological sectors against the number of galaxies per square arcminute n_g. The relative marginalised error is the marginalised error on the parameter divided by its absolute fiducial value: $\Delta p/|p|$. The plot shows five sets of values on the same axes: In black, the relative marginalised error for the neutrino mass m_ν (solid line), and the number of massive neutrino species N_ν (dashed line); in red (solid), the relative marginalised error for dark energy density $\Omega_{\rm DE}$; in blue, the relative marginalised error for primordial spectral index n_s (solid) and its running α (dashed).

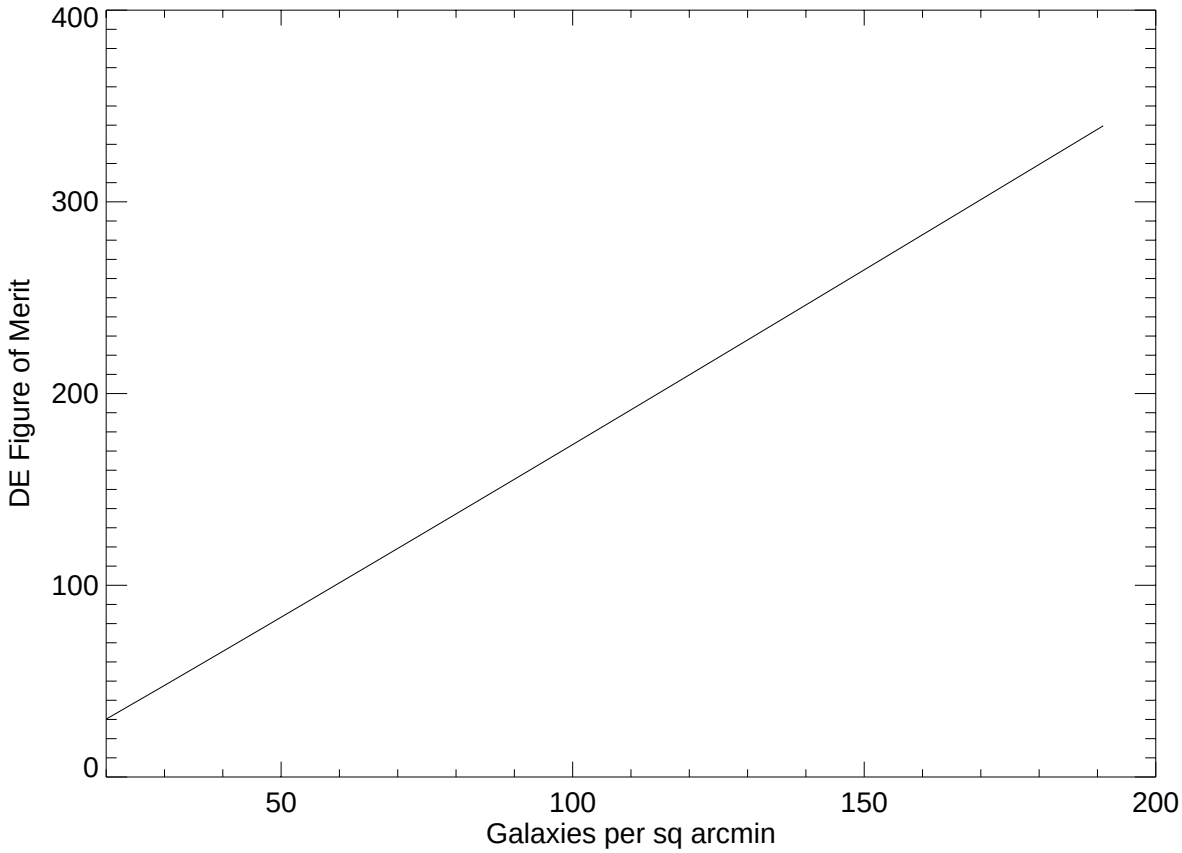

Figure 5.4: The dark energy Figure of Merit against the number of galaxies per square arcminute n_g.

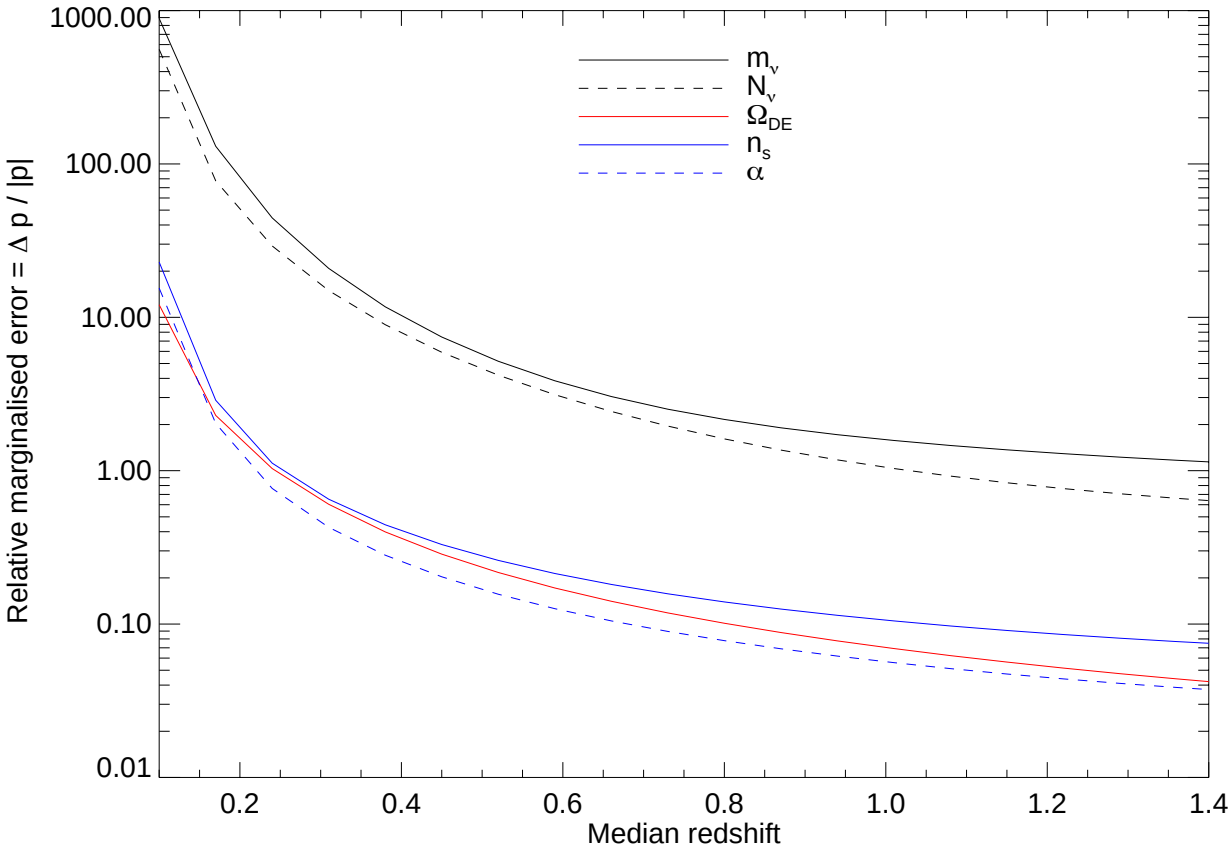

Figure 5.5: Relative marginalised error for parameters in three cosmological sectors against the median redshift of the survey z_m. The relative marginalised error is the marginalised error on the parameter divided by its absolute fiducial value: $\Delta p/|p|$. The plot shows five sets of values on the same axes: In black, the relative marginalised error for the neutrino mass m_ν (solid line), and the number of massive neutrino species N_ν (dashed line); in red (solid), the relative marginalised error for dark energy density $\Omega_{\rm DE}$; in blue, the relative marginalised error for primordial spectral index n_s (solid) and its running α (dashed).

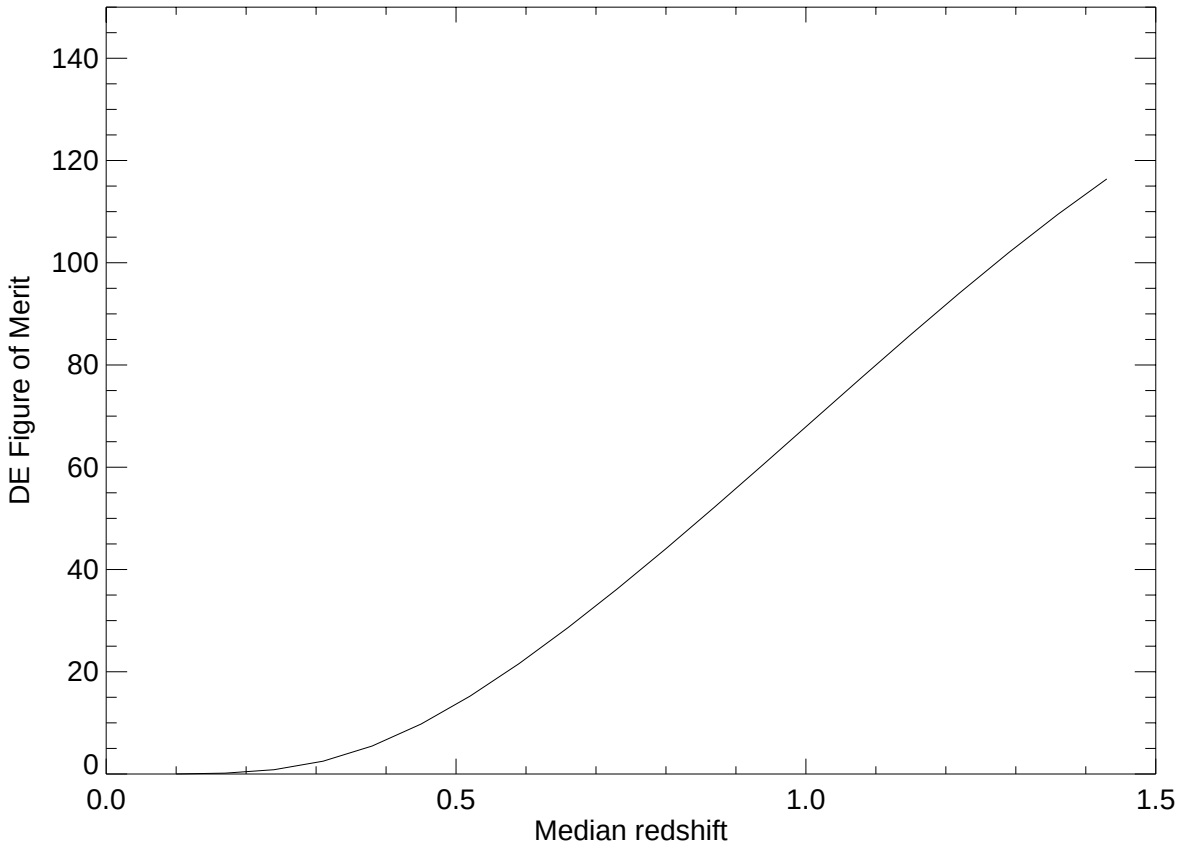

Figure 5.6: The dark energy Figure of Merit against the median redshift of the survey z_m.

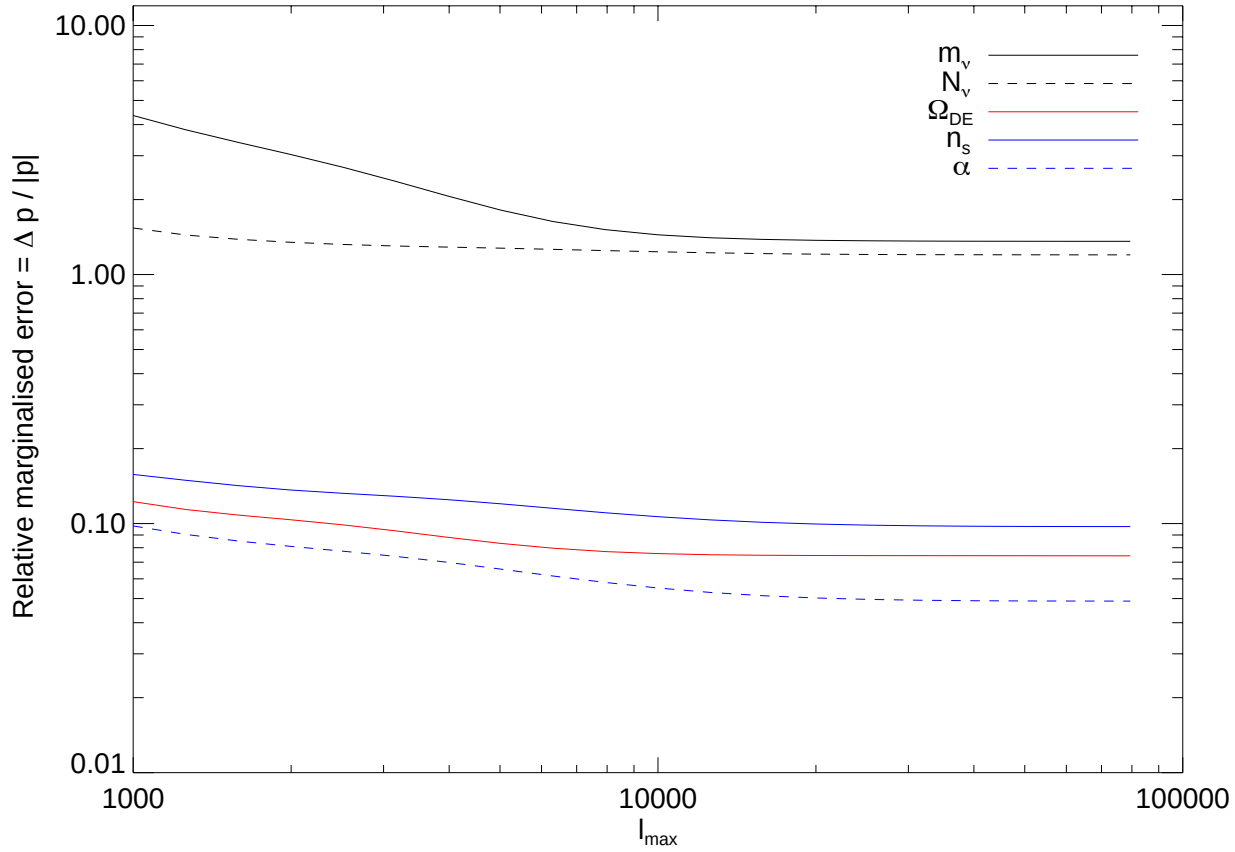

Figure 5.7: Relative marginalised error for parameters in three cosmological sectors against the maximum ℓ value. The relative marginalised error is the marginalised error on the parameter divided by its absolute fiducial value: $\Delta p/|p|$. The plot shows five sets of values on the same axes: In black, the relative marginalised error for the neutrino mass m_ν (solid line), and the number of massive neutrino species N_ν (dashed line); in red (solid), the relative marginalised error for dark energy density $\Omega_{\rm DE}$; in blue, the relative marginalised error for primordial spectral index n_s (solid) and its running α (dashed).

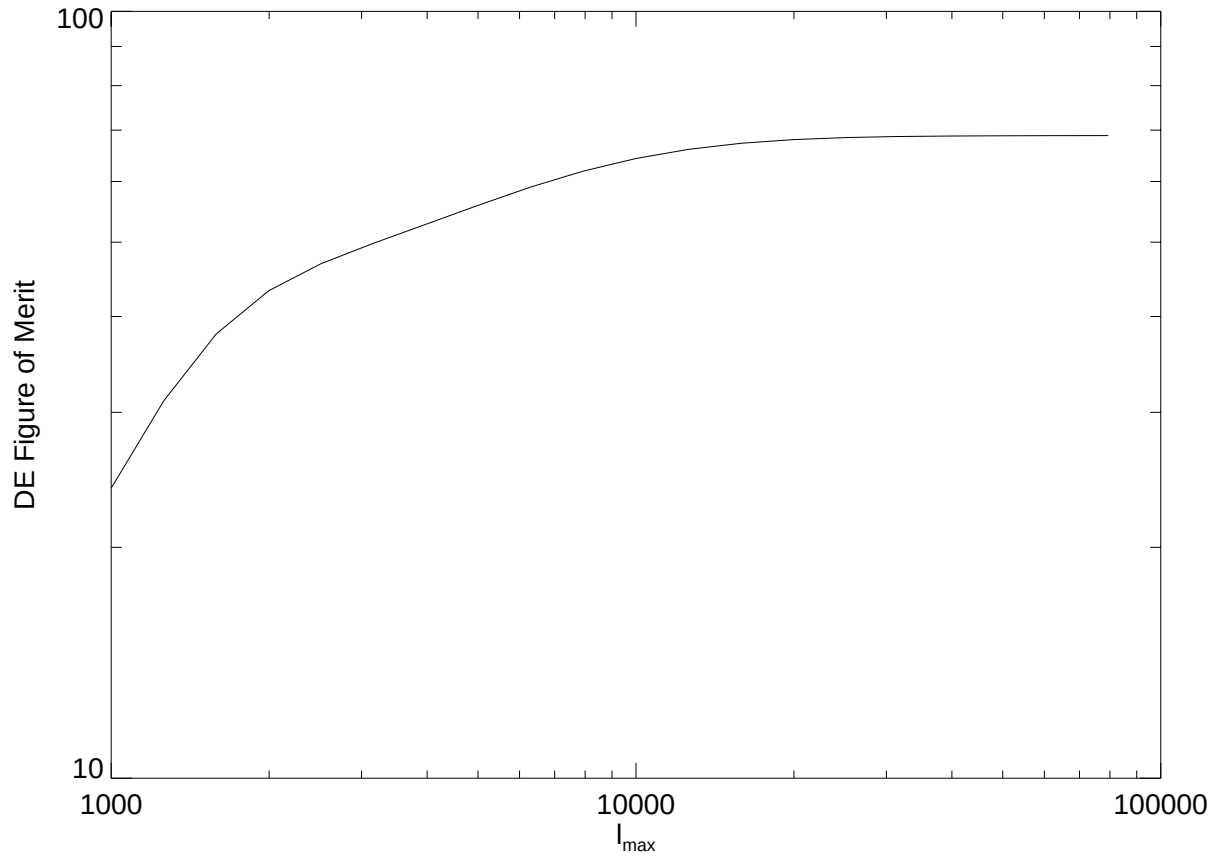

Figure 5.8: The dark energy Figure of Merit against the maximum multipole $\ell_{\rm max}$.

5.4 Optimisation for all parameters in hypothesis space

Optimisation studies for weak lensing surveys are usually carried out with respect to the dark energy equation of state parameters. The results obtained in Chapter 4 of this thesis show that weak lensing has the potential to constrain all sectors of the cosmological model, even with the 12-parameter νQCDM $+ \alpha + \beta$ hypothesis space. It is therefore pertinent to examine the effect of the survey design on all 12 parameters as well as the FOM.

We repeated the calculations carried out in the previous section for the νQCDM$+\alpha+\beta$ parameter set, examining the effect of varying the four survey parameters previously considered. The results are shown in four figures, where we have plotted the relative marginalised error for the 12 parameters of the model, as well as the dark energy Figure of Merit (shown by the thick black line on the plots).

In Figure 5.9 we vary the survey area, while keeping all other parameters constant. The marginalised errors follow the scaling in Figures 5.1 and 5.2, the only difference being the increased amplitude of the errors. Moreover, all 12 parameters show the same scaling relation with the survey area.

In Figure 5.10 we vary the galaxy count per square arcminute. Again, the marginalised errors and FOM follow the scaling for the 11-parameter model shown in Figures 5.3 and 5.4.

In Figure 5.11 we vary the median redshift. We observe a slight difference in the scaling between different cosmological parameters in the model, but the marginalised errors all decrease as the redshift is increased. This follows the scaling relation observed in Figure 5.5.

Finally, we vary the maximum multipole in Figure 5.12. The minimum multipole is kept fixed at $\ell_{\rm min} = 10$, as in the calculations for the νQCDM $+ \alpha$ set. Although all the marginalised errors decrease as $\ell_{\rm max}$ is increased, following the behaviour observed in Figure 5.7, the scaling is different for different parameters, especially in the range $100 < \ell_{\rm max} < 10^4$.

Our results show that the dependence of the parameter precision on the survey design is similar for all 12 cosmological parameters. Moreover, the scaling relation is not significantly affected by adding the parameter β to the hypothesis space, as can be observed by comparing the results obtained in this section with those from the previous sections. In this section, we also confirm the dependence of the FOM on the survey geometry studied by Amara & Réfrégier (2007), who work with a smaller parameter set.

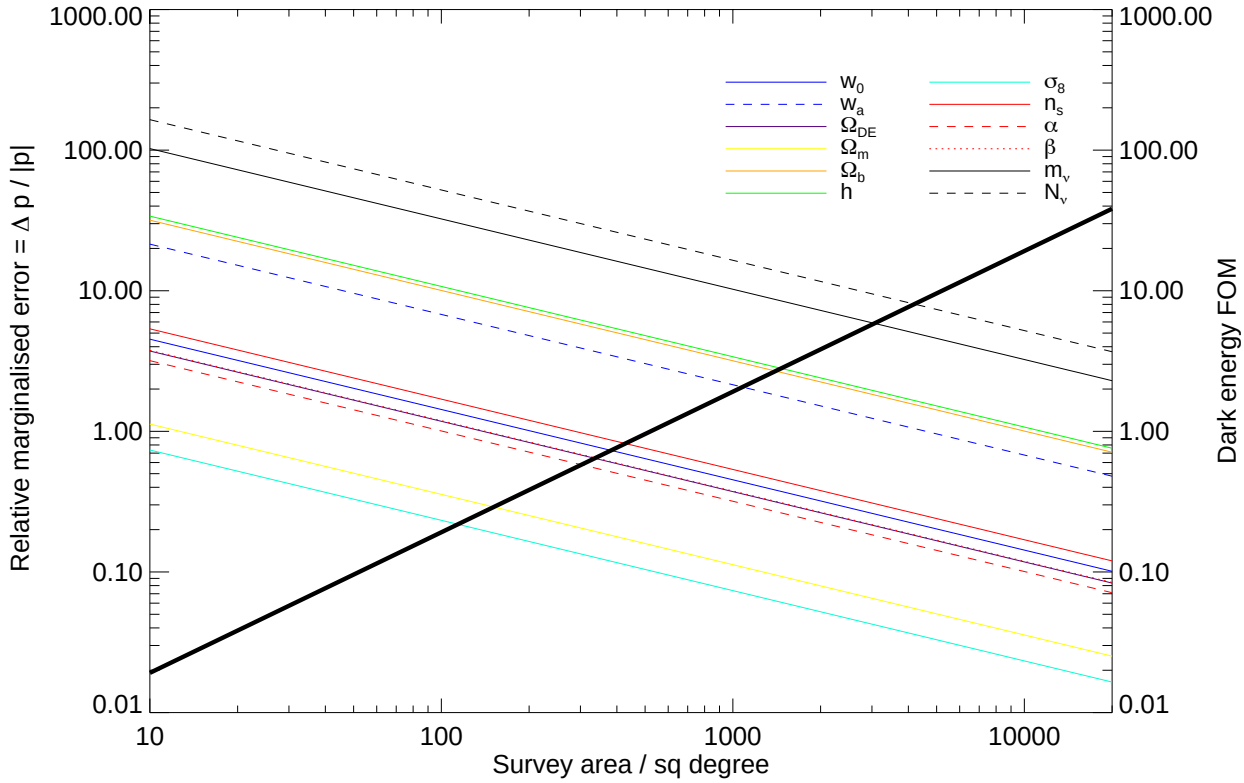

Figure 5.9: Dependence of cosmological parameter precision on the survey area. The plot shows the relative marginalized error, defined as $\Delta p/|p|$ for the twelve parameters in νQCDM $+ \alpha + \beta$. The thick black line shows the (w_0, w_a) Figure of Merit.

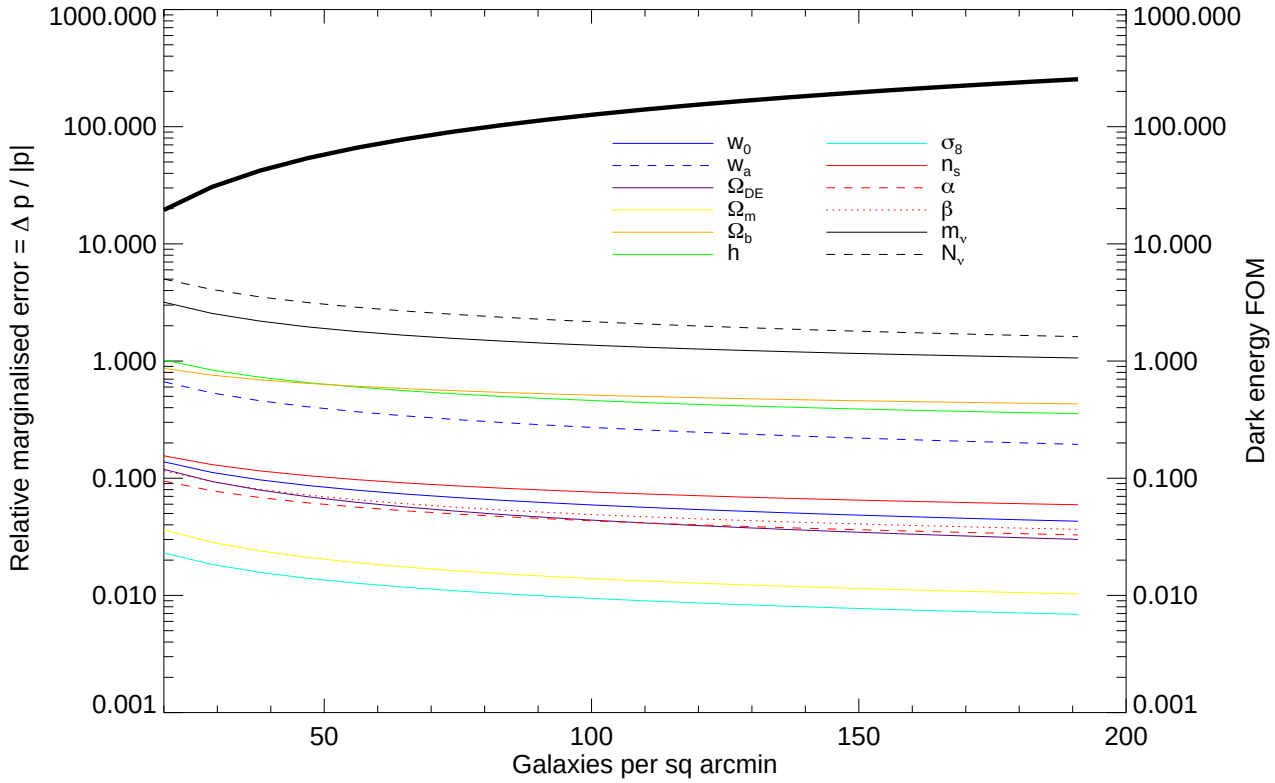

Figure 5.10: Dependence of cosmological parameter precision on the galaxy count. The plot shows the relative marginalized error, defined as $\Delta p/|p|$ for the twelve parameters in νQCDM $+ \alpha + \beta$. The thick black line shows the (w_0, w_a) Figure of Merit.

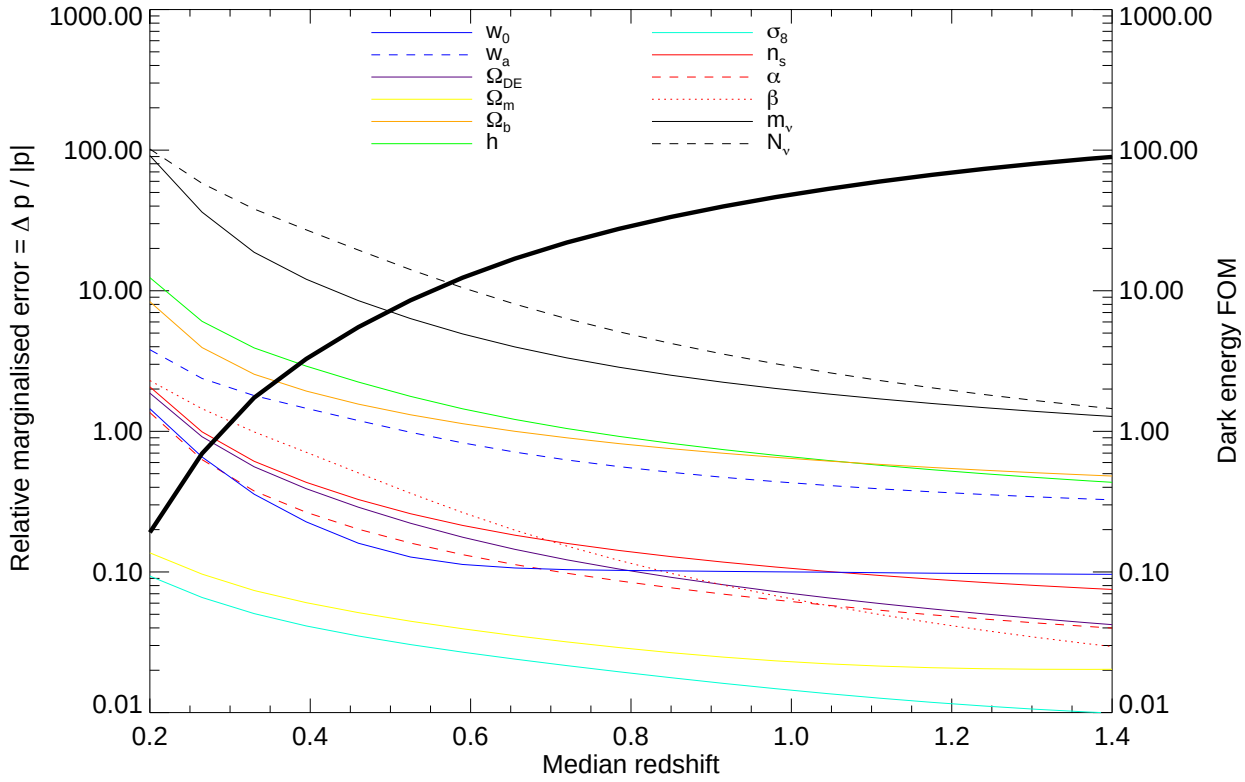

Figure 5.11: Dependence of cosmological parameter precision on the median redshift. The plot shows the relative marginalized error, defined as $\Delta p/|p|$ for the twelve parameters in νQCDM $+ \alpha + \beta$. The thick black line shows the (w_0, w_a) Figure of Merit.

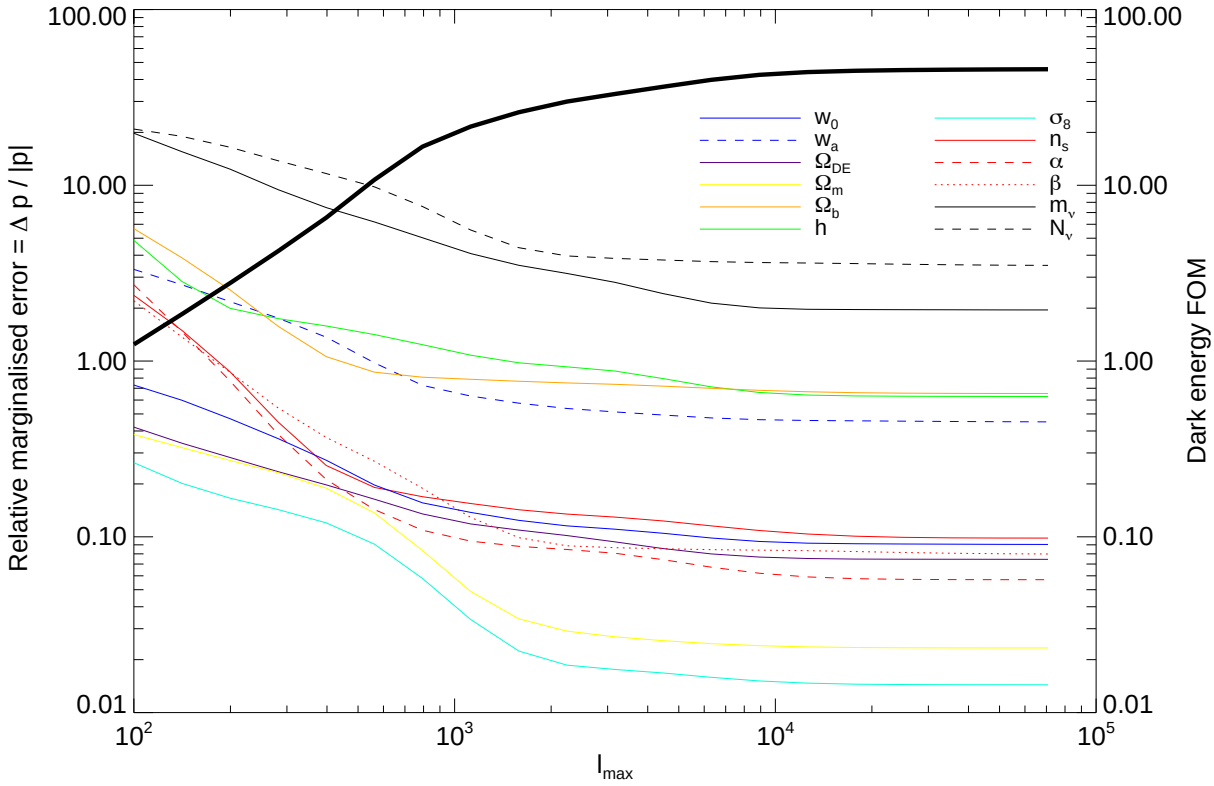

Figure 5.12: Dependence of cosmological parameter precision on the maximum multipole. The plot shows the relative marginalized error, defined as $\Delta p/|p|$ for the twelve parameters in νQCDM $+ \alpha + \beta$. The thick black line shows the (w_0, w_a) Figure of Merit.

5.5 Summary

In this chapter we have studied how the three properties of the survey design A_s, n_g and z_m affect the precision of our survey. We found that future surveys will improve over current measurements mostly by increasing the survey area. The best survey strategy is therefore to aim at increasing the survey area, then the number of galaxies, and finally the survey redshift. We also looked at survey optimisation for other cosmological sectors apart from dark energy, and found that the optimisation is similar for the different parameters.

We have examined the impact of the ℓ-mode cutoff, and found that the greatest improvement in the precision on the joint (w_0, w_a) parameters is obtained in the range $10^3 < \ell_{\rm max} < 10^4$. Beyond $\ell_{\rm max} \sim 10^4$ the gain in the precision is minimal. This confirms the results in Amara & Réfrégier (2007). A similar behaviour is observed for the precision on the other parameters (neutrinos, dark energy density, and the primordial power spectrum), with the precision on the neutrino mass m_ν showing a stronger dependence on the maximum multipole.

Weak lensing surveys seeking to maximise the precision on dark energy parameters and on neutrino mass bounds should therefore aim to cover multipoles at least up to $\ell_{\rm max} = 10^4$.

The calculations in this Chapter were carried out for two parameter sets: νQCDM$+\alpha$, and νQCDM$+\alpha+\beta$. There are two conclusions to be drawn from our results.

Firstly, the dependence of the parameter precision on the survey design is similar in these two parameter sets. The dependence of the FOM on the survey design also follows the results in Amara & Réfrégier (2007), who used a 7-parameter cosmological model with the assumption of flatness[5]. This indicates that the optimisation strategy is independent of the hypothesis space, both for the dark energy equation of state, as well as for the other parameters. In other words, the optimum weak lensing survey design for measuring the dark energy equation of state will also be the optimum survey for measuring other cosmological parameters.

Secondly, we have shown that all the cosmological parameters show a similar dependence on the survey design in both the 11- and 12-parameter hypothesis spaces. A change in the survey design would result in a rescaling of the marginalised errors for the cosmological parameters (shown in Table 4.3), but would not significantly modify the fractional change in the marginalised errors. This indicates that the results obtained in Chapter 4, Figure 4.6 are robust to changes in the survey parameters.

The results obtained in this Chapter show that the optimisation strategy for a weak lensing survey designed to constrain the dark energy equation of state can be applied to the other cosmological parameters, independently of the number of parameters in the cosmological model.

[5]The parameter set in Amara & Réfrégier (2007) is: $\{w_0,\ w_a,\ \Omega_m,\ \Omega_b,\ h,\ \sigma_8,\ n_s\}$.

Chapter 6

Conclusion

This chapter will conclude this thesis by summarising the progress made in understanding different cosmological sectors, especially dark energy, and the main results presented. We start with a review of some of the unanswered questions in cosmology. We then give an overview of future weak lensing experiments, and other methods used to constrain dark energy. This is followed by a summary of the results presented in this thesis. Finally, we review possible future work in connection with our methods.

6.1 Beyond dark energy

This thesis started by summarising the current state of concordance cosmology. This assumes that General Relativity is correct, an assumption which is justified by the tests which GR has undergone. We have reviewed the components making up the Universe, describing how $\sim 95\%$ of the content is unaccounted for. Dark matter, which makes up around 30% of the mass-energy of the Universe is a matter-like component which is cold (sub-relativistic) and weakly interacting, in the current paradigm.

We have also explained how the discrepancy between the observed acceleration of the expansion of the Universe and the predictions of GR leads to the conclusion that there must be a cosmological component with a negative equation of state parameter making up around 70% of the mass-energy content of the Universe: dark energy.

The dark energy paradigm, however, does not fix the nature of this component. There exist many theories which attempt to explain its nature. In particular, one can ask whether the priors of the concordance model — homogeneity and isotropy — are correct.

Outside of the dark energy paradigm, there are ongoing investigations on the effect of the backreaction due to an inhomogeneous Universe (e.g. Räsänen, 2009; Wiltshire, 2009), with different lines of research offering different interpretations of the Buchert equations, where the Friedmann equations are supplemented by an additional backreaction term (Buchert, 2000). A review of the backreaction approach is found in Célérier (2007). Whether one can explain all of the observed expansion history of the Universe as a consequence of the growth of inhomogeneities without invoking some additional fluid component is the subject of ongoing debate (Buchert, 2008). This approach, even if it eventually does not replace the dark energy paradigm, is still valid as a correction to the homogeneity assumption.

Another assumption of the concordance model is that the primordial power spectrum is scale-invariant, or nearly so. Support for this comes from the theory of inflation, which is another cornerstone of concordance cosmology. However, the data can be fitted by assuming a scale-dependence primordial power spectrum, and there have been recent attempts to investigate this (e.g. Blanchard et al., 2003; Sarkar, 2009).

Within the dark energy paradigm, the theories can be divided into two broad categories: Either dark energy is a modification of gravity on large scales, or dark energy is a scalar field (or fields) of some kind.

A cosmological constant Λ is the simplest modification which can be made to gravity, and it is equivalent to dark energy with a constant equation of state. Dark energy can also be attributed to the energy of the vacuum, although the energy predicted by the standard model of particle physics is either 0 (using super-symmetry), or 10^{120} orders of magnitude larger than the observed cosmological value. There are ongoing attempts to solve this 'fine-tuning problem' using string theory (see e.g. Susskind, 2007), causal sets (Sorkin, 2000), or by using anthropic arguments.

The other approach is to attribute dark energy to a scalar field whose potential has evolved in some way that it currently exerts a negative pressure. Such fields, in theories within the framework of GR, are termed Quintessence. Their distinguishing feature is that they allow the equation of state of dark energy to evolve. Alternatives to Quintessence within the same approach include K-essence, Phantom Fields, or the Chaplygin Gas (see

e.g. Durrer & Maartens, 2008b, and references therein).

The other strategy is to depart from GR and modify the laws of gravity and posit dark energy as the manifestation of an effect arising from extra dimensions, or higher-order corrections. Within this category, the most successful theories have been of two types. DGP dark energy (Dvali, Gabadadze, & Porrati, 2000) considers the Universe as a 4D brane within a 5D Minkowskian bulk. The weakness of gravity relative to the other forces is explained by gravity 'leaking' into the higher dimensions as it acts through the bulk, whereas the other forces act within the brane. The other class of theories is $f(R)$ gravity, where the Ricci scalar R in the Lagrangian is replaced by some function $f(R)$. Such theories correspond to scalar-tensor gravity with vanishing Brans-Dicke parameter (see e.g. Amendola et al., 2007).

There exists a wide range of proposals besides these. An exhaustive list is beyond the scope of this thesis. We simply note that most of them give different predictions for the equation of state of dark energy, or for its evolution. To distinguish between these proposals we need to pin down the exact evolution of the equation of state.

6.2 The future of weak lensing

This section will summarise future weak lensing experiments. We shall adopt the classification used in the Dark Energy Task Force (DETF) report (Albrecht et al., 2006), which considers future scenarios for dark energy experiments. The report highlights four stages of development:

- **Stage I:** This represents what is currently known, and includes the primary evidence for the acceleration of the Universe from Type Ia supernovae (Riess et al., 1998; Perlmutter et al., 1999), which remain the strongest direct evidence for acceleration. Current CMB anisotropy probes such as WMAP[1] provide strong evidence for a flat Universe, which leads to the conclusion that around 30% of the Universe is made up of dark and baryonic matter, and 70% is made up of dark energy. The cosmological parameter values from WMAP are in very good agreement with Type Ia supernova results (Dunkley et al., 2009). Baryon acoustic oscillations from the Sloan Digital Sky Survey[2] (SDSS) provide geometric evidence for dark energy, particularly when combined with the CMB.

  In the field of weak lensing, the largest survey to date is the Canada-France-Hawaii Telescope Legacy Survey (CFHTLS)[3] which has provided constraints on both dark energy, and other parameters such as neutrino masses (Tereno et al., 2009; Ichiki et al., 2009). Among the more recent results, Kilbinger et al. (2009) obtain a constraint on the dark energy equation of state of $-1.10 < w < -0.94$ at 68% confidence.

- **Stage II:** These are projects that are currently under way, which, once completed, will provide better constraints on dark energy. Such projects include the CFHT

[1] `map.gsfc.nasa.gov`
[2] `www.sdss.org`
[3] `www.cfht.hawaii.edu/Science/CFHLS`

survey, SDSS, now in its eighth year, and WMAP, now in its fifth year.

- **Stage III:** These are near-term projects which are currently proposed. Most consist of new cameras mounted on existing terrestrial telescopes.

- **Stage IV:** This consists of next-generation all-sky, or near all-sky photometric surveys with median redshifts of $z_m \sim 1$ which are expected to obtain error bounds on w_0 of around 5% or less. Such surveys include DUNE/Euclid (introduced in Chapter 4), the Large Synoptic Survey Telescope[4] (LSST), the Joint Dark Energy Mission[5] (JDEM), the Supernovae Acceleration Probe[6] (SNAP), the James Webb Space Telescope[7] (JWST), and the Square Kilometre Array[8] (SKA). The time frame for such projects is around 2015-2020.

6.3 Tomographic weak lensing as a cosmological probe

In Chapter 4 we have used forecast parameter constraints using weak lensing tomography with an all-sky survey. This thesis has focussed on three groups of parameters: neutrinos, the primordial power spectrum, and dark energy. Here we give a brief summary of the results of our work, discussing these three cosmological sectors in this order.

The first sector is neutrinos. The existence of neutrinos is now confirmed by various results from particle physics. According to the Standard Model of particle physics, there exist three neutrino flavours. Neutrino oscillations, which require the neutrino to have a nonzero mass, were discovered by Fukuda et al. (1998). The implications of the discovery of neutrino mass for cosmology are significant. In particular, the results from particle physics experiments can be used to set priors on cosmological neutrino bounds. Weak lensing is a powerful probe of cosmological neutrino mass, since it is a direct measure of the matter distribution which results from structure formation, which is affected by neutrino properties. This thesis confirms the results in other weak lensing studies: Weak lensing tomography, in combination with other probes, can constrain the total neutrino mass m_ν and the number of massive neutrino species N_ν, giving us a constraint on the individual mass of the most massive species. In the modelling of neutrino behaviour in cosmology, the strategy should be to seek a more accurate parameterisation of their mass hierarchy, and of their contribution to the matter power spectrum.

The second sector that we focussed on was the primordial power spectrum. This is probed in weak lensing through its effect as the initial condition for the evolution of the matter power spectrum, and therefore weak lensing is less effective at constraining the parameters in this sector than high-redshift probes such as the CMB. Nonetheless, we have shown that weak lensing can constrain the scalar spectral index n_s and its running α. In combination with CMB priors, it can constrain both parameters to sub-percentage level. We have introduced a third-order truncated Taylor series expression for the primordial

[4] www.lsst.org
[5] http://jdem.gsfc.nasa.gov
[6] www.snap.lbl.gov
[7] www.jwst.nasa.gov
[8] www.skatelescope.org

power spectrum:

$$n_s(k) = n_s(k_0) + \frac{1}{2!}\alpha \ln\left(\frac{k}{k_0}\right) + \frac{1}{3!}\beta \ln\left(\frac{k}{k_0}\right)^2, \tag{6.1}$$

showing that the more relaxed hypothesis on the form of the primordial power spectrum results in a weak degradation of our parameter constraints in all sectors. By adding CMB priors, we have shown that the precision is almost completely recovered in the dark energy sector, and also in other cosmological sectors. Our work highlights the complementarity of cosmological probes. We have also studied another assumption in the primordial power spectrum sector: the position of the pivot scale k_0. We find that the optimum pivot scale k_0 for our all-sky weak lensing survey is different from the optimum value for CMB anisotropy probes, and that it depends on the chosen parameterisation of the primordial power spectrum.

The third sector of interest is dark energy. Perhaps the biggest unresolved question in current cosmology are the following: What is dark energy? Why has it begun to affect the expansion rate now? The question of the nature of dark energy can be subdivided into two questions: Is dark energy a cosmological constant? If a cosmological constant is ruled out, then what is dark energy? The first question is addressed in the formalism used in this thesis, where we parameterise the dark energy equation of state $w = p_{\rm DE}/\rho_{\rm DE}c^2$ by $w(a) = w_0 + w_a(1-a)$. As an example, if we have a result of $w(z) = -0.8 \pm 0.006$ where a is any pivot redshift, then this would represent a 3σ deviation from a cosmological constant model.

In this thesis we have studied the parameter constraints that can be obtained on dark energy parameters, and we have shown that constraints on $w(z)$ depend on the fiducial value of this redshift-dependent parameter. Using a dynamical dark energy + CDM + neutrino fiducial model, with a running of the spectral index, combining weak lensing tomography and CMB priors, we have shown that the precision in all cosmological sectors depends only weakly on the number of parameters we are trying to constrain simultaneously. By adding CMB priors, a significant improvement can be made on our forecasts, and stability of the error bounds against the addition of parameters is increased.

This thesis concludes that tomographic weak lensing in combination with CMB anisotropy probes has the potential to constrain dark energy parameters to percent level, and to simultaneously constrain the total neutrino mass and initial condition parameters.

6.4 Survey optimisation

In Chapter 5 we study the optimisation of an all-sky tomographic weak lensing survey. Our analysis is similar to that of Amara & Réfrégier (2007) who use the dark energy Figure of Merit as the measure of the precision of the survey, but we also examine the constraints in other cosmological sectors, namely neutrinos and the primordial spectral index, and extend the calculation to our 12-parameter νQCDM + α + β set. We find that the dependence of the parameter precision on the survey geometry is very similar for all parameters. This means that one can optimise a weak lensing survey of this type to maximise the precision on the (w_0, w_a) parameter combination, and using the same

configuration, also obtain the best precision in the other sectors.

We find that the dominant survey parameter is the survey area. Given a finite observation time, the best strategy is therefore to have as wide a survey as possible. We also examine the dependence of the survey precision on the maximum multipole. Our results show that parameter precision is significantly improved in the region $\ell_{\rm max} < 10^4$, but the gain in precision is negligible for $\ell_{\rm max} > 10^4$. This confirms the findings of Amara & Réfrégier (2007), who use a smaller cosmological parameter set.

Given the agreement between our results are those in Amara & Réfrégier (2007), this thesis concludes that the weak lensing optimisation strategy is largely independent of the parameters we seek to constrain.

6.5 Further work

In this section we give a overview of the possible refinements of the methods used in this thesis. Such effects become important as the measurement precision is improved, and will certainly be required for Stage IV experiments.

6.5.1 Combining experiments

This thesis has used the techniques of weak lensing and cosmic microwave background anisotropies to constrain cosmological parameters using the Fisher matrix framework. We find that constraints are always improved when different probes are combined. This is not just due to the addition of extra information in the Fisher matrix calculation. Different experiments probe physics at different scales. This is especially true of weak lensing and the CMB. The DETF report (Albrecht et al., 2006) finds that a combination of techniques from one or more Stage III projects gives a factor of 3 improvement over Stage II in the DETF Figure of Merit. A combination of Stage IV techniques in turn produces a factor of 10 gain over Stage II.

In our thesis we simply added lensing and CMB Fisher matrices to obtain joint constraints. However, this addition does not take into the covariances between probes. CMB photons are lensed by large-scale structure along the line-of-sight. Even though the effect is small since the the source redshift of CMB photons is much greater than the source redshift of a background galaxy, it must be taken into account for a robust combination of methods. Indeed the correlation between large-scale structure and the CMB provides another cosmological probe via the integrated Sachs-Wolfe effect (see e.g. Giannantonio et al., 2008). In a similar way, there is a correlation between lensing and BAOs, since they are both measures of the matter power spectrum.

6.5.2 Systematic effects

This thesis has taken the approach of including only two statistical errors: the uncertaintly in the photometric redshift error σ_0, the uncertainty in the ellipticity measurement σ_ϵ, and the finite number density of galaxies. We have set these errors to a certain value in the survey parameters, and then calculated our error forecasts. Systematic effects (e.g. bias in photometric redshifts, intrinsic alignment of galaxies, PSF effects, etc.) have been

ignored. A more robust formalism would include such parameters as elements in the Fisher matrix and then fully marginalise over them. This approach is taken by Amara & Réfrégier (2007), who include photometric redshift errors in their Fisher matrix in their optimisation study, and by others (see e.g. Ma et al., 2006; Abdalla et al., 2008; Zhan et al., 2009).

6.5.3 Beyond the Fisher matrix

The error forecasts in this thesis are based on the Fisher matrix formalism. This primary advantage of the Fisher matrix is that it allows parameter errors to be estimated quickly and accurately. For every parameter considered, we only need to calculate the covariance of two points in parameter space. The disadvantage is that it is based on the assumption of Gaussian likelihoods. At the other extreme are formalisms that calculate the likelihood at every point in parameter space. These are computationally very expensive, but are guaranteed to reproduce the exact constraint. One compromise is the Markov Chain Monte-Carlo approach (see e.g. Verde et al., 2003), which is widely used in the determination of cosmological parameters from data, and in parameter prediction to predict the correct shapes of likelihood surfaces.

6.5.4 Further diagnostics of dark energy

In this thesis we have assumed a slight generalisation of ΛCDM where the equation of state of dark energy is allowed to vary. The dynamical dark energy parameterisation adopted is that of Chevallier & Polarski (2001) and Linder (2003), where the variation is a function of redshift or scale factor: $w(a) = w_0 + w_a(1 + a)$. We probe the nature of dark energy using weak lensing via its effect on the growth of structure and on the geometry of the Universe. To distinguish between a constant-w model (equivalent to ΛCDM) and deviations from this model, we therefore need to constrain w_0 and w_a. There exist other diagnostics of dark energy, among them $Om(z)$ and the q-probe, proposed by Sahni et al. (2008), which can distinguish dynamical DE from a cosmological constant without reference to the value of the matter density. It would be instructive to compare constraints on $Om(z)$ from weak lensing with those obtained using other probes.

6.6 Summary

This thesis acts as an indicator of the results that can be obtained using future weak lensing surveys. We have started this chapter by discussing the current range of dark energy theories. It may be possible to explain dark energy using a combination of some of these theories. It may also be possible, as in multiverse theories, that there is no particular theory for dark energy, and that the dark energy behaviour observed in our Universe just one out of many. We shall end this thesis by emphasising the important role of weak lensing in particular, and observational cosmology in general. To quote Ellis (2009), "Overall: theory must be subject to experimental and/or observational test; this is the central feature of science."

Bibliography

[1] Abazajian, K., Kadota, K., Stewart, E.D., Parametrizing the power spectrum: beyond the truncated Taylor expansion, *Journal of Cosmology and Astro-Particle Physics*, 2005, vol. 8, pp. 8–+, arXiv:astro-ph/0507224

[2] Abdalla, F.B., Amara, A., Capak, P., Cypriano, E.S., Lahav, O., Rhodes, J., Photometric redshifts for weak lensing tomography from space: the role of optical and near infrared photometry, *MNRAS*, 2008, vol. 387, pp. 969–986, 0705.1437

[3] Abdalla, F.B., Blake, C., Rawlings, S., Forecasts for Dark Energy Measurements with Future HI Surveys, *ArXiv e-prints*, 2009, 0905.4311

[4] Abdalla, F.B., Rawlings, S., Determining neutrino properties using future galaxy redshift surveys, *MNRAS*, 2007, vol. 381, pp. 1313–1328, arXiv:astro-ph/0702314

[5] Albrecht, A., Amendola, L., Bernstein, G., Clowe, D., Eisenstein, D., Guzzo, L., Hirata, C., Huterer, D., Kirshner, R., Kolb, E., Nichol, R., Findings of the Joint Dark Energy Mission Figure of Merit Science Working Group, *ArXiv e-prints*, 2009, 0901.0721

[6] Albrecht, A., Bernstein, G., Cahn, R., Freedman, W.L., Hewitt, J., Hu, W., Huth, J., Kamionkowski, M., Kolb, E.W., Knox, L., Mather, J.C., Staggs, S., Suntzeff, N.B., Report of the Dark Energy Task Force, *https://www.darkenergysurvey.org*, 2006, astro-ph/0609591

[7] Aldrich, J., R.A. Fisher on Bayes and Bayes' Theorem, *Bayesian Analysis*, 2008, vol. 3, no. 1

[8] Amara, A., Réfrégier, A., Optimal surveys for weak-lensing tomography, *MNRAS*, 2007, vol. 381, pp. 1018–1026, arXiv:astro-ph/0610127

[9] Amara, A., Réfrégier, A., Systematic bias in cosmic shear: extending the Fisher matrix, *MNRAS*, 2008, vol. 391, pp. 228–236, 0710.5171

[10] Amara, A., Refregier, A., Paulin-Henriksson, S., Cosmic Shear Systematics: Software-Hardware Balance, *ArXiv e-prints*, 2009, 0905.3176

[11] Amendola, L., Polarski, D., Tsujikawa, S., Are f(R) Dark Energy Models Cosmologically Viable?, *Physical Review Letters*, 2007, vol. 98, no. 13, pp. 131 302–+, arXiv:astro-ph/0603703

[12] Anderson, J.L., *Principles of Relativity Physics*, New York: Academic Press, 1967

[13] Avelino, P.P., Martins, C.J.A.P., Nunes, N.J., Olive, K.A., Reconstructing the dark energy equation of state with varying couplings, *Phys. Rev. D*, 2006, vol. 74, no. 8, pp. 083 508–+, arXiv:astro-ph/0605690

[14] Babul, A., Lee, M.H., Gravitational lensing by smooth inhomogeneities in the universe, *MNRAS*, 1991, vol. 250, pp. 407–413

[15] Bacon, D.J., Réfrégier, A.R., Ellis, R.S., Detection of weak gravitational lensing by large-scale structure, *MNRAS*, 2000, vol. 318, pp. 625–640, arXiv:astro-ph/0003008

[16] Bacon, D.J., Schäfer, B.M., Twist and turn: weak lensing image distortions to second order, *MNRAS*, 2009, vol. 396, pp. 2167–2175, 0807.3663

[17] Bardeen, J.M., Gauge-invariant cosmological perturbations, *Phys. Rev. D*, 1980, vol. 22, pp. 1882–1905

[18] Bardeen, J.M., Bond, J.R., Kaiser, N., Szalay, A.S., The statistics of peaks of Gaussian random fields, *ApJ*, 1986, vol. 304, pp. 15–61

[19] Bartelmann, M., Schneider, P., Weak gravitational lensing, *Phys. Rep.*, 2001, vol. 340, pp. 291–472, arXiv:astro-ph/9912508

[20] Bayes, T., Price, R., An Essay towards solving a Problem in the Doctrine of Chance. By the late Rev. Mr. Bayes, communicated by Mr. Price, in a letter to John Canton, M. A. and F. R. S., *Philosophical Transactions of the Royal Society of London*, 1763, vol. 53, pp. 370–418

[21] Bernardeau, F., van Waerbeke, L., Mellier, Y., Weak lensing statistics as a probe of Ω and power spectrum., *A&A*, 1997, vol. 322, pp. 1–18, arXiv:astro-ph/9609122

[22] Birkhoff, G.D., Matter, electricity and gravitation in flat spacetime, *Proc. Nat. Acad. Sci. U.S.*, 1943, vol. 29, pp. 231–239

[23] Blanchard, A., Douspis, M., Rowan-Robinson, M., Sarkar, S., An alternative to the cosmological "concordance model", *A&A*, 2003, vol. 412, pp. 35–44, arXiv:astro-ph/0304237

[24] Blandford, R.D., Saust, A.B., Brainerd, T.G., Villumsen, J.V., The distortion of distant galaxy images by large-scale structure, *MNRAS*, 1991, vol. 251, pp. 600–627

[25] Bond, J.R., Efstathiou, G., Silk, J., Massive neutrinos and the large-scale structure of the universe, *Physical Review Letters*, 1980, vol. 45, pp. 1980–1984

[26] Brans, C., Dicke, R.H., Mach's principle and a relativistic theory of gravitation, *Phys. Rev.*, 1961, vol. 124, pp. 925–935

[27] Bridle, S., Balan, S.T., Bethge, M., Gentile, M., Harmeling, S., Heymans, C., Hirsch, M., Hosseini, R., Jarvis, M., Kirk, D., Kitching, T., Kuijken, K., Lewis, A., Paulin-Henriksson, S., Scholkopf, B., Velander, M., Voigt, L., Witherick, D., Amara, A., Bernstein, G., Courbin, F., Gill, M., Heavens, A., Mandelbaum, R., Massey, R., Moghaddam, B., Rassat, A., Refregier, A., Rhodes, J., Schrabback, T., Shawe-Taylor, J., Shmakova, M., van Waerbeke, L., Wittman, D., Results of the GREAT08 Challenge: An image analysis competition for cosmological lensing, *ArXiv e-prints*, 2009a, 0908.0945

[28] Bridle, S., King, L., Dark energy constraints from cosmic shear power spectra: impact of intrinsic alignments on photometric redshift requirements, *New Journal of Physics*, 2007, vol. 9, pp. 444–+, 0705.0166

[29] Bridle, S., Shawe-Taylor, J., Amara, A., Applegate, D., Balan, S.T., Berge, J., Bernstein, G., Dahle, H., Erben, T., Gill, M., Heavens, A., Heymans, C., High, F.W., Hoekstra, H., Jarvis, M., Kirk, D., Kitching, T., Kneib, J.P., Kuijken, K., Lagatutta, D., Mandelbaum, R., Massey, R., Mellier, Y., Moghaddam, B., Moudden, Y., Nakajima, R., Paulin-Henriksson, S., Pires, S., Rassat, A., Refregier, A., Rhodes, J., Schrabback, T., Semboloni, E., Shmakova, M., van Waerbeke, L., Witherick, D., Voigt, L., Wittman, D., Handbook for the GREAT08 Challenge: An image analysis competition for cosmological lensing, *Annals of Applied Statistics*, 2009b, vol. 3, no. 1, pp. 6–37

[30] Bridle, S.L., Lewis, A.M., Weller, J., Efstathiou, G., Reconstructing the primordial power spectrum, *MNRAS*, 2003, vol. 342, pp. L72–L78, arXiv:astro-ph/0302306

[31] Buchert, T., On Average Properties of Inhomogeneous Fluids in General Relativity: Dust Cosmologies, *General Relativity and Gravitation*, 2000, vol. 32, pp. 105–126, arXiv:gr-qc/9906015

[32] Buchert, T., Dark Energy from structure: a status report, *General Relativity and Gravitation*, 2008, vol. 40, pp. 467–527, 0707.2153

[33] Bunn, E.F., *Statistical Analysis of Cosmic Microwave Background Anisotropy*, Ph.D. thesis, AA (UNIVERSITY OF CALIFORNIA, BERKELEY.), 1995

[34] Bunn, E.F., White, M., The 4 Year COBE Normalization and Large-Scale Structure, *ApJ*, 1997, vol. 480, pp. 6–+, arXiv:astro-ph/9607060

[35] Caldwell, R.R., Doran, M., Dark-energy evolution across the cosmological-constant boundary, *Phys. Rev. D*, 2005, vol. 72, no. 4, pp. 043 527–+, arXiv:astro-ph/0501104

[36] Caldwell, R.R., Kamionkowski, M., Weinberg, N.N., Phantom Energy: Dark Energy with $w < -1$ Causes a Cosmic Doomsday, *Physical Review Letters*, 2003, vol. 91, no. 7, pp. 071 301–+, arXiv:astro-ph/0302506

[37] Célérier, M.N., The Accelerated Expansion of the Universe Challenged by an Effect of the Inhomogeneities. A Review, *ArXiv Astrophysics e-prints*, 2007, arXiv:astro-ph/0702416

[38] Chevallier, M., Polarski, D., Accelerating Universes with Scaling Dark Matter, *International Journal of Modern Physics D*, 2001, vol. 10, pp. 213–223, arXiv:gr-qc/0009008

[39] Clifford, W.K., Habilitationsvorlesung (English translation), *Nature*, 1873, vol. 8, p. 14

[40] Cowsik, R., McClelland, J., An Upper Limit on the Neutrino Rest Mass, *Physical Review Letters*, 1972, vol. 29, pp. 669–670

[41] Cramér, H., *Mathematical Methods of Statistics*, Princeton, NJ: Princeton Univ. Press., 1946

[42] Damour, T., Nordtvedt, K., General relativity as a cosmological attractor of tensor-scalar theories, *Phys. Rev. Lett.*, 1993a, vol. 70, pp. 2217–2219

[43] Damour, T., Nordtvedt, K., Tensor-scalar cosmological models and their relaxation toward general relativity, *Phys. Rev. D*, 1993b, vol. 48, pp. 3436–3450

[44] De Bernardis, F., Kitching, T.D., Heavens, A., Melchiorri, A., Determining the Neutrino Mass Hierarchy with Cosmology, *ArXiv e-prints*, 2009, 0907.1917

[45] Deser, S., Self-interaction and gauge invariance, *Rel. & Grav.*, 1970, vol. I, pp. 9–18

[46] Dicke, R.H., Mach's principle and invariance under transformation of units, *Phys. Rev.*, 1962, vol. 125, pp. 2163–2167

[47] Dodelson, S., *Modern Cosmology*, New York: Academic Press, 2003

[48] Dunkley, J., Komatsu, E., Nolta, M.R., Spergel, D.N., Larson, D., Hinshaw, G., Page, L., Bennett, C.L., Gold, B., Jarosik, N., Weiland, J.L., Halpern, M., Hill, R.S., Kogut, A., Limon, M., Meyer, S.S., Tucker, G.S., Wollack, E., Wright, E.L., Five-Year Wilkinson Microwave Anisotropy Probe Observations: Likelihoods and Parameters from the WMAP Data, *ApJS*, 2009, vol. 180, pp. 306–329, 0803.0586

[49] Durrer, R., Maartens, R., Dark energy and dark gravity: theory overview, *General Relativity and Gravitation*, 2008a, vol. 40, pp. 301–328, 0711.0077

[50] Durrer, R., Maartens, R., Dark Energy and Modified Gravity, *ArXiv e-prints*, 2008b, 0811.4132

[51] Dvali, G., Gabadadze, G., Porrati, M., 4D gravity on a brane in 5D Minkowski space, *Physics Letters B*, 2000, vol. 485, pp. 208–214, arXiv:hep-th/0005016

[52] Dvali, G., Turner, M.S., Dark Energy as a Modification of the Friedmann Equation, *ArXiv Astrophysics e-prints*, 2003, arXiv:astro-ph/0301510

[53] Dyson, F.W., Eddington, A.S., Davidson, C., A Determination of the Deflection of Light by the Sun's Gravitational Field, from Observations Made at the Total Eclipse of May 29, 1919, *Royal Society of London Philosophical Transactions Series A*, 1920, vol. 220, pp. 291–333

[54] Einstein, A., Zur Elektrodynamik bewegter Körper, *Ann. Phys. (Germany)*, 1905, vol. 17, pp. 891–921

[55] Einstein, A., Über den Einfluss der Schwerkraft auf die Ausbreitung des Lichtes, *Ann. Phys. (Germany)*, 1911, vol. 35, pp. 898–908

[56] Einstein, A., Die Feldgleichungen der Gravitation, *Preuss. Akad. Wiss. Berlin, Sitzber.*, 1915a, pp. 844–847

[57] Einstein, A., Zur Allgemeinen Relativitätstheorie, *Preuss. Akad. Wiss. Berlin, Sitzber.*, 1915b, pp. 799–801

[58] Einstein, A., Kosmologische Betrachtungen zur allgemeinen Relativitätstheorie, *Sitzungsberichte der Königlich Preußischen Akademie der Wissenschaften (Berlin), Seite 142-152.*, 1917, pp. 142–152

[59] Einstein, A., Fokker, A.D., The north current gravitation theory from the viewpoint of absolute differential calculus, *Ann. Phys. (Germany)*, 1914, vol. 44, p. 321

[60] Eisenstein, D.J., Hu, W., Baryonic Features in the Matter Transfer Function, *ApJ*, 1998, vol. 496, pp. 605–+, `arXiv:astro-ph/9709112`

[61] Eisenstein, D.J., Hu, W., Power Spectra for Cold Dark Matter and Its Variants, *ApJ*, 1999, vol. 511, pp. 5–15, `arXiv:astro-ph/9710252`

[62] Elgarøy, Ø., Lahav, O., Neutrino masses from cosmological probes, *New Journal of Physics*, 2005, vol. 7, pp. 61–+, `arXiv:hep-ph/0412075`

[63] Ellis, G.F.R., Dark matter and dark energy proposals: maintaining cosmology as a true science?, in *EAS Publications Series*, vol. 36 of *EAS Publications Series*, 2009 pp. 325–336

[64] Euler, L., Réfléxions sur quelques loix générales de la nature qui s'observent dans les effets des forces quelconques, *Acad. R. Sci. Berlin*, 1750, vol. 4, pp. 189–218

[65] Feng, B., Xia, J.Q., Yokoyama, J., Zhang, X., Zhao, G.B., Weighing neutrinos in the presence of a running primordial spectral index, *Journal of Cosmology and Astro-Particle Physics*, 2006, vol. 12, pp. 11–+, `arXiv:astro-ph/0605742`

[66] Feynman, R.P., *Feynman Lectures on Gravitation*, UK: Penguin, 1995

[67] Fierz, M., Pauli, W., Relativistic wave equations for particles of arbitrary spin in an electromagnetic field, *Proc. R. Soc. London*, 1939, vol. A, no. 173, pp. 211–232

[68] Fisher, R.A., The logic of inductive inference, *J. Roy. Stat. Soc*, 1935, vol. 98, pp. 39–54

[69] Franklin, A., Principle of inertia in the middle ages, *Am. J. Phys.*, 1976, vol. 44, pp. 529–543

[70] Freese, K., Review of Observational Evidence for Dark Matter in the Universe and in upcoming searches for Dark Stars, in *Dark Energy and Dark Matter: Observations, Experiments and Theories*, vol. 36 of *EAS Publications Series*, 2009 pp. 113–126

[71] Friedmann, A., Über die Krümmung des Raumes, *Zeitschrift für Physik*, 1922, vol. 10, no. 1, pp. 377–386

[72] Friedmann, A., Über die Möglichkeit einer Welt mit konstanter negativer Krümmung des Raumes, *Zeitschrift für Physik*, 1924, vol. 21, no. 1, pp. 326–332

[73] Fukuda, Y., Hayakawa, T., Ichihara, E., The Super-Kamiokande Collaboration, Measurements of the Solar Neutrino Flux from Super-Kamiokande's First 300 Days, *Physical Review Letters*, 1998, vol. 81, pp. 1158–1162, arXiv:hep-ex/9805021

[74] Gerstein, G., Zel'dovich, Y.B., Rest mass of the muonic neutrino and cosmology, Журнал Експериментальной и Теоретической Физики, Письма в Редакта *(JETP Letters)*, 1966, vol. 4, no. 174

[75] Giannantonio, T., Scranton, R., Crittenden, R.G., Nichol, R.C., Boughn, S.P., Myers, A.D., Richards, G.T., Combined analysis of the integrated Sachs-Wolfe effect and cosmological implications, *Phys. Rev. D*, 2008, vol. 77, no. 12, pp. 123 520–+, 0801.4380

[76] Gratton, S., Lewis, A., Efstathiou, G., Prospects for constraining neutrino mass using Planck and Lyman-α forest data, *Phys. Rev. D*, 2008, vol. 77, no. 8, pp. 083 507–+, 0705.3100

[77] Gunn, J.E., On the Propagation of Light in Inhomogeneous Cosmologies. I. Mean Effects, *ApJ*, 1967, vol. 150, pp. 737–+

[78] Gupta, S.N., Gravitation and electromagnetism, *Phys. Rev.*, 1954, vol. 96, pp. 1683–1685

[79] Gupta, S.N., Einstein's and other theories of gravitation, *Rev. Mod. Phys.*, 1957, vol. 29, pp. 337–350

[80] Gupta, S.N., Quantum theory of gravitation, in *Recent Developments in General Relativity*, New York: Pergamon, 1962

[81] Guth, A.H., ed., *The inflationary universe. The quest for a new theory of cosmic origins*, Reading, MA: Addison-Wesley, 1997

[82] Hamilton, A.J.S., Kumar, P., Lu, E., Matthews, A., Reconstructing the primordial spectrum of fluctuations of the universe from the observed nonlinear clustering of galaxies, *ApJ*, 1991, vol. 374, pp. L1–L4

[83] Hamilton, W.R., On a general method in dynamics, *Phil. Trans. R. Soc. Lond.*, 1834, vol. II, pp. 247–308

[84] Hamilton, W.R., Second essay on a general method in dynamics, *Phil. Trans. R. Soc. Lond.*, 1835, vol. I, pp. 95–144

[85] Hannestad, S., Primordial Neutrinos, *Annual Review of Nuclear and Particle Science*, 2006, vol. 56, pp. 137–161, arXiv:hep-ph/0602058

[86] Hannestad, S., Hansen, S.H., Villante, F.L., Hamilton, A.J.S., Constraints on inflation from cosmic microwave background and Lyman-/α forest, *Astroparticle Physics*, 2002, vol. 17, pp. 375–382, arXiv:astro-ph/0103047

[87] Hannestad, S., Tu, H., Wong, Y.Y., Measuring neutrino masses and dark energy with weak lensing tomography, *Journal of Cosmology and Astro-Particle Physics*, 2006, vol. 6, pp. 25–+, arXiv:astro-ph/0603019

[88] Hannestad, S., Wong, Y.Y.Y., Neutrino mass from future high redshift galaxy surveys: sensitivity and detection threshold, *Journal of Cosmology and Astro-Particle Physics*, 2007, vol. 7, pp. 4–+, arXiv:astro-ph/0703031

[89] Harrison, E.R., Fluctuations at the Threshold of Classical Cosmology, *Phys. Rev. D*, 1970, vol. 1, pp. 2726–2730

[90] Heath, D.J., The growth of density perturbations in zero pressure Friedmann-Lemaitre universes, *MNRAS*, 1977, vol. 179, pp. 351–358

[91] Heavens, A., Statistical techniques in cosmology, *ArXiv e-prints*, 2009, 0906.0664

[92] Heavens, A.F., Kitching, T.D., Verde, L., On model selection forecasting, dark energy and modified gravity, *MNRAS*, 2007, vol. 380, pp. 1029–1035, arXiv:astro-ph/0703191

[93] Heymans, C., Van Waerbeke, L., Bacon, D., Berge, J., Bernstein, G., Bertin, E., Bridle, S., Brown, M.L., Clowe, D., Dahle, H., Erben, T., Gray, M., Hetterscheidt, M., Hoekstra, H., Hudelot, P., Jarvis, M., Kuijken, K., Margoniner, V., Massey, R., Mellier, Y., Nakajima, R., Refregier, A., Rhodes, J., Schrabback, T., Wittman, D., The Shear Testing Programme - I. Weak lensing analysis of simulated ground-based observations, *MNRAS*, 2006, vol. 368, pp. 1323–1339, arXiv:astro-ph/0506112

[94] Hilbert, S., Hartlap, J., White, S.D.M., Schneider, P., Ray-tracing through the Millennium Simulation: Born corrections and lens-lens coupling in cosmic shear and galaxy-galaxy lensing, *A&A*, 2009, vol. 499, pp. 31–43, 0809.5035

[95] Hirata, C., Seljak, U., Shear calibration biases in weak-lensing surveys, *MNRAS*, 2003, vol. 343, pp. 459–480, arXiv:astro-ph/0301054

[96] Hirata, C.M., Seljak, U., Intrinsic alignment-lensing interference as a contaminant of cosmic shear, *Phys. Rev. D*, 2004, vol. 70, no. 6, pp. 063 526–+, arXiv:astro-ph/0406275

[97] Hoekstra, H., Jain, B., Weak Gravitational Lensing and Its Cosmological Applications, *Annual Review of Nuclear and Particle Science*, 2008, vol. 58, pp. 99–123, 0805.0139

[98] Host, O., Lahav, O., Abdalla, F.B., Eitel, K., Forecasting neutrino masses from combining KATRIN and the CMB observations: Frequentist and Bayesian analyses, *Phys. Rev. D*, 2007, vol. 76, no. 11, pp. 113 005–+, 0709.1317

[99] Hu, W., Jain, B., Joint galaxy-lensing observables and the dark energy, *Phys. Rev. D*, 2004, vol. 70, no. 4, pp. 043 009–+, arXiv:astro-ph/0312395

[100] Hu, W., Tegmark, M., Weak Lensing: Prospects for Measuring Cosmological Parameters, *ApJ*, 1999, vol. 514, pp. L65–L68, arXiv:astro-ph/9811168

[101] Hubble, E., A Relation between Distance and Radial Velocity among Extra-Galactic Nebulae, *Proceedings of the National Academy of Science*, 1929, vol. 15, pp. 168–173

[102] Huterer, D., *Weak lensing and dark energy*, Ph.D. thesis, AA (The University of Chicago), 2001

[103] Huterer, D., Takada, M., Calibrating the nonlinear matter power spectrum: Requirements for future weak lensing surveys, *Astroparticle Physics*, 2005, vol. 23, pp. 369–376, arXiv:astro-ph/0412142

[104] Ichiki, K., Takada, M., Takahashi, T., Constraints on neutrino masses from weak lensing, *Phys. Rev. D*, 2009, vol. 79, no. 2, pp. 023 520–+, 0810.4921

[105] Ishak, M., Hirata, C.M., McDonald, P., Seljak, U., Weak lensing and CMB: Parameter forecasts including a running spectral index, *Phys. Rev. D*, 2004, vol. 69, no. 8, pp. 083 514–+, arXiv:astro-ph/0308446

[106] Jain, B., Mo, H.J., White, S.D.M., The evolution of correlation functions and power spectra in gravitational clustering, *MNRAS*, 1995, vol. 276, pp. L25–L29, arXiv:astro-ph/9501047

[107] Jain, B., Seljak, U., Cosmological Model Predictions for Weak Lensing: Linear and Nonlinear Regimes, *ApJ*, 1997, vol. 484, pp. 560–+, arXiv:astro-ph/9611077

[108] Jaroszynski, M., Park, C., Paczynski, B., Gott, J.R.I., Weak gravitational lensing due to large-scale structure of the universe, *ApJ*, 1990, vol. 365, pp. 22–26

[109] Joachimi, B., Schneider, P., The removal of shear-ellipticity correlations from the cosmic shear signal via nulling techniques, *A&A*, 2008, vol. 488, pp. 829–843, 0804.2292

[110] Joachimi, B., Schneider, P., The removal of shear-ellipticity correlations from the cosmic shear signal: Influence of photometric redshift errors on the nulling technique, *ArXiv e-prints*, 2009, 0905.0393

[111] Johri, V.B., Rath, P.K., Parametrization of the Dark Energy Equation of State, *International Journal of Modern Physics D*, 2007, vol. 16, pp. 1581–1591, arXiv:astro-ph/0510017

[112] Jordan, P., Zum gegenwärtigen Stand der Diracschen kosmologischen Hypothesen, *Z. Phys.*, 1959, vol. 157, pp. 112–121

[113] Jun, S., *Mathematical Statistics*, New York: Springer, 1998

[114] Kaiser, N., Weak gravitational lensing of distant galaxies, *ApJ*, 1992, vol. 388, pp. 272–286

[115] Kaiser, N., Weak Lensing and Cosmology, *ApJ*, 1998, vol. 498, pp. 26–+, arXiv:astro-ph/9610120

[116] Kaiser, N., A New Shear Estimator for Weak-Lensing Observations, *ApJ*, 2000, vol. 537, pp. 555–577, arXiv:astro-ph/9904003

[117] Kaiser, N., Squires, G., Broadhurst, T., A Method for Weak Lensing Observations, *ApJ*, 1995, vol. 449, pp. 460–+, arXiv:astro-ph/9411005

[118] Kamionkowski, M., Babul, A., Réfrégier, A., Theory and statistics of weak lensing from large-scale mass inhomogeneities, *MNRAS*, 1998, vol. 301, pp. 1064–1072, arXiv:astro-ph/9712030

[119] Keeton, C.R., A Catalog of Mass Models for Gravitational Lensing, *ArXiv Astrophysics e-prints*, 2001, arXiv:astro-ph/0102341

[120] Kendall, M.G., Stuart, A., *The advanced theory of statistics*, vol. 2, London: Griffin, 4th edn., 1979

[121] Kenney, J.F., Keeping, E.S., *Mathematics of Statistics, Pt. 2*, Princeton, NJ: Van Nostrand, 2nd edn., 1951

[122] Kiakotou, A., Elgarøy, Ø., Lahav, O., Neutrino mass, dark energy, and the linear growth factor, *Phys. Rev. D*, 2008, vol. 77, no. 6, pp. 063 005–+, arXiv:0709.0253

[123] Kilbinger, M., Benabed, K., Guy, J., Astier, P., Tereno, I., Fu, L., Wraith, D., Coupon, J., Mellier, Y., Balland, C., Bouchet, F.R., Hamana, T., Hardin, D., McCracken, H.J., Pain, R., Regnault, N., Schultheis, M., Yahagi, H., Dark-energy constraints and correlations with systematics from CFHTLS weak lensing, SNLS supernovae Ia and WMAP5, *A&A*, 2009, vol. 497, pp. 677–688, 0810.5129

[124] Kilbinger, M., Schneider, P., Eifler, T., E- and B-mode mixing from incomplete knowledge of the shear correlation, *A&A*, 2006, vol. 457, pp. 15–19, arXiv:astro-ph/0604520

[125] King, L.J., Schneider, P., Separating cosmic shear from intrinsic galaxy alignments: Correlation function tomography, *A&A*, 2003, vol. 398, pp. 23–30, arXiv:astro-ph/0209474

[126] Kitching, T.D., Amara, A., Fisher Matrix Decomposition for Dark Energy Prediction, *ArXiv e-prints*, 2009, 0905.3383

[127] Kitching, T.D., Amara, A., Abdalla, F.B., Réfrégier, A., Cosmological Systematics Beyond Nuisance Parameters : Form Filling Functions, *ArXiv e-prints*, 2008a, 0812.1966

[128] Kitching, T.D., Heavens, A.F., Verde, L., Serra, P., Melchiorri, A., Finding evidence for massive neutrinos using 3D weak lensing, *Phys. Rev. D*, 2008b, vol. 77, no. 10, pp. 103 008–+, arXiv:0801.4565

[129] Kitching, T.D., Taylor, A.N., Heavens, A.F., Systematic effects on dark energy from 3D weak shear, *MNRAS*, 2008c, vol. 389, pp. 173–190, arXiv:0801.3270

[130] Kolb, E.W., Turner, M.S., The early universe., *Frontiers in Physics*, 1990, vol. 69

[131] Komatsu, E., Dunkley, J., Nolta, M.R., Bennett, C.L., Gold, B., Hinshaw, G., Jarosik, N., Larson, D., Limon, M., Page, L., Spergel, D.N., Halpern, M., Hill, R.S., Kogut, A., Meyer, S.S., Tucker, G.S., Weiland, J.L., Wollack, E., Wright, E.L., Five-Year Wilkinson Microwave Anisotropy Probe Observations: Cosmological Interpretation, *ApJS*, 2009, vol. 180, pp. 330–376, 0803.0547

[132] Kosowsky, A., Turner, M.S., CBR anisotropy and the running of the scalar spectral index, *Phys. Rev. D*, 1995, vol. 52, pp. 1739–+, arXiv:astro-ph/9504071

[133] Kowalski, M., Rubin, D., Aldering, G., Agostinho, R.J., Amadon, A., Amanullah, R., Balland, C., Barbary, K., Blanc, G., Challis, P.J., Conley, A., Connolly, N.V., Covarrubias, R., Dawson, K.S., Deustua, S.E., Ellis, R., Fabbro, S., Fadeyev, V., Fan, X., Farris, B., Folatelli, G., Frye, B.L., Garavini, G., Gates, E.L., Germany, L., Goldhaber, G., Goldman, B., Goobar, A., Groom, D.E., Haissinski, J., Hardin, D., Hook, I., Kent, S., Kim, A.G., Knop, R.A., Lidman, C., Linder, E.V., Mendez, J., Meyers, J., Miller, G.J., Moniez, M., Mourão, A.M., Newberg, H., Nobili, S., Nugent, P.E., Pain, R., Perdereau, O., Perlmutter, S., Phillips, M.M., Prasad, V., Quimby, R., Regnault, N., Rich, J., Rubenstein, E.P., Ruiz-Lapuente, P., Santos, F.D., Schaefer, B.E., Schommer, R.A., Smith, R.C., Soderberg, A.M., Spadafora, A.L., Strolger, L.G., Strovink, M., Suntzeff, N.B., Suzuki, N., Thomas, R.C., Walton, N.A., Wang, L., Wood-Vasey, W.M., Yun, J.L., Improved Cosmological Constraints from New, Old, and Combined Supernova Data Sets, *ApJ*, 2008, vol. 686, pp. 749–778, 0804.4142

[134] Kraichnan, R.H., Special-relativistic derivation of generally covariant gravitation theory, *Phys. Rev.*, 1955, vol. 55, pp. 1118–1122

[135] Kretschmann, E., Über den physikalischen Sinn der Relativitätspostulate, A. Einsteins neue und seine ursprungliche Relativitätstheorie, *Ann. Phys. (Germany)*, 1917, vol. 53, pp. 575–614

[136] Kristian, J., Sachs, R.K., Observations in Cosmology, *ApJ*, 1966, vol. 143, pp. 379–+

[137] Kustaanheimo, P., Route dependence of the gravitational redshift, *Phys. Lett.*, 1966, vol. 23, pp. 75–77

[138] Lagrange, L., *Méchanique analytique*, Paris: Chez La Veuve Desaint, 1788

[139] Leach, S.M., Liddle, A.R., Constraining slow-roll inflation with WMAP and 2dF, *Phys. Rev. D*, 2003, vol. 68, no. 12, pp. 123 508–+, arXiv:astro-ph/0306305

[140] Lee, H.C., Sasaki, M., Stewart, E.D., Tanaka, T., Yokoyama, S., A new δN formalism for multi-component inflation, *Journal of Cosmology and Astro-Particle Physics*, 2005, vol. 10, pp. 4–+, arXiv:astro-ph/0506262

[141] Lee, M.H., Paczynski, B., Gravitational lensing by a smoothly variable three-dimensional mass distribution, *ApJ*, 1990, vol. 357, pp. 32–37

[142] Lemaître, G., Un univers homogène de masse constante et de rayon croissant rendant compte de la vitesse radiale des nébuleuses extra-galactiques, *Annales des la Société Scientifique de Bruxelles*, 1927, vol. A, no. 47, pp. 49–56

[143] Lesgourgues, J., Pastor, S., Massive neutrinos and cosmology, *Phys. Rep.*, 2006, vol. 429, pp. 307–379, arXiv:astro-ph/0603494

[144] Lesgourgues, J., Valkenburg, W., Gaztañaga, E., Constraining neutrino masses with the integrated-Sachs-Wolfe-galaxy correlation function, *Phys. Rev. D*, 2008, vol. 77, no. 6, pp. 063 505–+, 0710.5525

[145] Lewis, A., Challinor, A., Lasenby, A., Efficient Computation of Cosmic Microwave Background Anisotropies in Closed Friedmann-Robertson-Walker Models, *ApJ*, 2000, vol. 538, pp. 473–476, arXiv:astro-ph/9911177

[146] Liddle, A.R., Lyth, D.H., COBE, gravitational waves, inflation and extended inflation., *Physics Letters B*, 1992, vol. 291, pp. 391–398, arXiv:astro-ph/9208007

[147] Liddle, A.R., Lyth, D.H., The cold dark matter density perturbation, *Phys. Rep.*, 1993, vol. 231, pp. 1–2, arXiv:astro-ph/9303019

[148] Liddle, A.R., Lyth, D.H., *Cosmological Inflation and Large-Scale Structure*, Cambridge University Press: Cambridge, 2000

[149] Lidsey, J.E., Liddle, A.R., Kolb, E.W., Copeland, E.J., Barreiro, T., Abney, M., Reconstructing the inflaton potential-an overview, *Reviews of Modern Physics*, 1997, vol. 69, pp. 373–410, arXiv:astro-ph/9508078

[150] Lifshitz, E.M., On the gravitational stability of the expanding universe, *J. Phys. (USSR)*, 1946, vol. 46, no. 116

[151] Limber, D.N., The Analysis of Counts of the Extragalactic Nebulae in Terms of a Fluctuating Density Field., *ApJ*, 1953, vol. 117, pp. 134–+

[152] Linde, A., *Inflation and Quantum Cosmology*, New York: Academic Press, 1989

[153] Linder, E.V., Exploring the Expansion History of the Universe, *Physical Review Letters*, 2003, vol. 90, no. 9, pp. 091 301–+, arXiv:astro-ph/0208512

[154] Linder, E.V., Jenkins, A., Cosmic structure growth and dark energy, *MNRAS*, 2003, vol. 346, pp. 573–583, arXiv:astro-ph/0305286

[155] Ma, C.P., Analytical Approximation to the Nonlinear Power Spectrum of Gravitational Clustering, *ApJ*, 1998, vol. 508, pp. L5–L8, arXiv:astro-ph/9809267

[156] Ma, Z., Hu, W., Huterer, D., Effects of Photometric Redshift Uncertainties on Weak-Lensing Tomography, *ApJ*, 2006, vol. 636, pp. 21–29, arXiv:astro-ph/0506614

[157] Marx, G., Szalay, A.S., Cosmological limit on the neutretto rest mass, in *Proc. Neutrino 72*, Technoinform, Hungary, vol. 1, 1972 p. 123

[158] Massey, R., Heymans, C., Bergé, J., Bernstein, G., Bridle, S., Clowe, D., Dahle, H., Ellis, R., Erben, T., Hetterscheidt, M., High, F.W., Hirata, C., Hoekstra, H., Hudelot, P., Jarvis, M., Johnston, D., Kuijken, K., Margoniner, V., Mandelbaum, R., Mellier, Y., Nakajima, R., Paulin-Henriksson, S., Peeples, M., Roat, C., Refregier, A., Rhodes, J., Schrabback, T., Schirmer, M., Seljak, U., Semboloni, E., van Waerbeke, L., The Shear Testing Programme 2: Factors affecting high-precision weak-lensing analyses, *MNRAS*, 2007, vol. 376, pp. 13–38, arXiv:astro-ph/0608643

[159] Massey, R., Réfrégier, A., Polar shapelets, *MNRAS*, 2005, vol. 363, pp. 197–210, arXiv:astro-ph/0408445

[160] de Maupertuis, P.L.M., Recherche des loix du mouvement, *Acad. R. Sci. Berlin*, 1746

[161] Miller, C.J., New Evidence for Baryonic Features in the Power Spectrum, in *Bulletin of the American Astronomical Society*, vol. 32 of *Bulletin of the American Astronomical Society*, 2000 pp. 1584–+

[162] Miralda-Escude, J., The correlation function of galaxy ellipticities produced by gravitational lensing, *ApJ*, 1991, vol. 380, pp. 1–8

[163] Misner, C.W., Thorne, K.S., Wheeler, J.A., *Gravitation*, San Francisco, California: Freeman, 1973

[164] Mukherjee, P., Parkinson, D., Corasaniti, P.S., Liddle, A.R., Kunz, M., Model selection as a science driver for dark energy surveys, *MNRAS*, 2006, vol. 369, pp. 1725–1734, arXiv:astro-ph/0512484

[165] Munshi, D., Valageas, P., van Waerbeke, L., Heavens, A., Cosmology with weak lensing surveys, *Phys. Rep.*, 2008, vol. 462, pp. 67–121, arXiv:astro-ph/0612667

[166] Navarro, J.F., Frenk, C.S., White, S.D.M., A Universal Density Profile from Hierarchical Clustering, *ApJ*, 1997, vol. 490, pp. 493–+, arXiv:astro-ph/9611107

[167] Newton, I., *Philosophiae naturalis principia mathematica*, London: Streater, 1st edn., 1687

[168] Ni, W.T., Theoretical frameworks for testing relativistic gravity, IV: A compendium of metric theories of gravity and their post-Newtonian limits, *Astrophysics J.*, 1972, vol. 176, pp. 769–796

[169] Nolta, M.R., Dunkley, J., Hill, R.S., Hinshaw, G., Komatsu, E., Larson, D., Page, L., Spergel, D.N., Bennett, C.L., Gold, B., Jarosik, N., Odegard, N., Weiland, J.L., Wollack, E., Halpern, M., Kogut, A., Limon, M., Meyer, S.S., Tucker, G.S., Wright, E.L., Five-Year Wilkinson Microwave Anisotropy Probe Observations: Angular Power Spectra, *ApJS*, 2009, vol. 180, pp. 296–305, 0803.0593

[170] Nordstrøm, G., Zur Theorie der Gravitation vom Standpunkt des Relativitäsprinzip, *Ann. Phys. (Germany)*, 1913, vol. 42, pp. 533–554

[171] Norton, J.D., General covariance, gauge theories and the Kretschmann objection, in *Symmetries in Physics: Philosophical Reflections*, edited by K. A. Brading, E. Castellani, Cambridge: Cambridge University Press, 2003

[172] Pahud, C., Liddle, A.R., Mukherjee, P., Parkinson, D., Model selection forecasts for the spectral index from the Planck satellite, *Phys. Rev. D*, 2006, vol. 73, no. 12, pp. 123 524–+, arXiv:astro-ph/0605004

[173] Particle Data Group, Review of Particle Physics, *Physics Letters B*, 2008, vol. 667, pp. 1–6

[174] Paulin-Henriksson, S., Amara, A., Voigt, L., Refregier, A., Bridle, S.L., Point spread function calibration requirements for dark energy from cosmic shear, *A&A*, 2008, vol. 484, pp. 67–77, 0711.4886

[175] Peacock, J.A., *Cosmological Physics*, Cambridge: Cambridge University Press, 1999

[176] Peacock, J.A., Dodds, S.J., Non-linear evolution of cosmological power spectra, *MNRAS*, 1996, vol. 280, pp. L19–L26, arXiv:astro-ph/9603031

[177] Peacock, J.A., Smith, R.E., Halo occupation numbers and galaxy bias, *MNRAS*, 2000, vol. 318, pp. 1144–1156, arXiv:astro-ph/0005010

[178] Peebles, P.J., Ratra, B., The cosmological constant and dark energy, *Reviews of Modern Physics*, 2003, vol. 75, pp. 559–606, arXiv:astro-ph/0207347

[179] Peebles, P.J.E., *The large-scale structure of the universe*, Princeton, NJ: Princeton Series in Physics, 1980

[180] Peebles, P.J.E., Yu, J.T., Primeval Adiabatic Perturbation in an Expanding Universe, *ApJ*, 1970, vol. 162, pp. 815–+

[181] Penzias, A.A., Wilson, R.W., A Measurement of Excess Antenna Temperature at 4080 Mc/s., *ApJ*, 1965, vol. 142, pp. 419–421

[182] Perlmutter, S., Aldering, G., Goldhaber, G., Knop, R.A., Nugent, P., Castro, P.G., Deustua, S., Fabbro, S., Goobar, A., Groom, D.E., Hook, I.M., Kim, A.G., Kim, M.Y., Lee, J.C., Nunes, N.J., Pain, R., Pennypacker, C.R., Quimby, R., Lidman, C., Ellis, R.S., Irwin, M., McMahon, R.G., Ruiz-Lapuente, P., Walton, N., Schaefer, B., Boyle, B.J., Filippenko, A.V., Matheson, T., Fruchter, A.S., Panagia, N., Newberg, H.J.M., Couch, W.J., The Supernova Cosmology Project, Measurements of Omega and Lambda from 42 High-Redshift Supernovae, *ApJ*, 1999, vol. 517, pp. 565–586, arXiv:astro-ph/9812133

[183] Primack, J.R., Gross, M.A.K., Hot dark matter in cosmology, in *Current aspects of neutrino physics*, edited by D. O. Caldwell, Berlin, Heidelberg: Springer, pp. 287–308, 2001

[184] Psaltis, D., Constraining Brans-Dicke Gravity with Millisecond Pulsars in Ultracompact Binaries, *ArXiv Astrophysics e-prints*, 2005, arXiv:astro-ph/0501234

[185] Quigg, C., Cosmic Neutrinos, *ArXiv e-prints*, 2008, vol. 802, 0802.0013

[186] Rao, C., Information and the accuracy attainable in the estimation of statistical parameters, *Bulletin of the Calcutta Mathematical Society*, 1945, vol. 37, pp. 81–89

[187] Räsänen, S., Structure formation as an alternative to dark energy and modified gravity, in *Dark Energy and Dark Matter: Observations, Experiments and Theories*, vol. 36 of *EAS Publications Series*, 2009 pp. 63–74

[188] Rassat, A., Amara, A., Amendola, L., Castander, F.J., Kitching, T., Kunz, M., Réfrégier, A., Wang, Y., Weller, J., Deconstructing Baryon Acoustic Oscillations: A Comparison of Methods, *ArXiv e-prints*, 2008, 0810.0003

[189] Réfrégier, A., Shapelets - I. A method for image analysis, *MNRAS*, 2003a, vol. 338, pp. 35–47, arXiv:astro-ph/0105178

[190] Réfrégier, A., Weak Gravitational Lensing by Large-Scale Structure, *ARA&A*, 2003b, vol. 41, pp. 645–668, arXiv:astro-ph/0307212

[191] Réfrégier, A., The Dark UNiverse Explorer (DUNE): proposal to ESA's cosmic vision, *Experimental Astronomy*, 2009, vol. 23, pp. 17–37, 0802.2522

[192] Réfrégier, A., Bacon, D., Shapelets - II. A method for weak lensing measurements, *MNRAS*, 2003, vol. 338, pp. 48–56, arXiv:astro-ph/0105179

[193] Rhodes, J., Réfrégier, A., Groth, E.J., Weak Lensing Measurements: A Revisited Method and Application toHubble Space Telescope Images, *ApJ*, 2000, vol. 536, pp. 79–100, arXiv:astro-ph/9905090

[194] Riess, A.G., Filippenko, A.V., Challis, P., Clocchiatti, A., Diercks, A., Garnavich, P.M., Gilliland, R.L., Hogan, C.J., Jha, S., Kirshner, R.P., Leibundgut, B., Phillips, M.M., Reiss, D., Schmidt, B.P., Schommer, R.A., Smith,

R.C., Spyromilio, J., Stubbs, C., Suntzeff, N.B., Tonry, J., Observational Evidence from Supernovae for an Accelerating Universe and a Cosmological Constant, *AJ*, 1998, vol. 116, pp. 1009–1038, arXiv:astro-ph/9805201

[195] Robertson, H.P., Kinematics and world structure, *Astrophysical Journal*, 1935, vol. 82, pp. 248–301

[196] Robertson, H.P., Kinematics and world structure, *Astrophysical Journal*, 1936a, vol. 83, pp. 187–201

[197] Robertson, H.P., Kinematics and world structure, *Astrophysical Journal*, 1936b, vol. 83, pp. 257–271

[198] Rudd, D.H., Zentner, A.R., Kravtsov, A.V., Effects of Baryons and Dissipation on the Matter Power Spectrum, *ApJ*, 2008, vol. 672, pp. 19–32, arXiv:astro-ph/0703741

[199] Sahni, V., Shafieloo, A., Starobinsky, A.A., Two new diagnostics of dark energy, *Phys. Rev. D*, 2008, vol. 78, no. 10, pp. 103 502–+, 0807.3548

[200] Saito, S., Takada, M., Taruya, A., Impact of Massive Neutrinos on the Nonlinear Matter Power Spectrum, *Physical Review Letters*, 2008, vol. 100, no. 19, pp. 191 301–+, 0801.0607

[201] Salati, P., The bestiary of dark matter species, in *Dark Energy and Dark Matter: Observations, Experiments and Theories*, vol. 36 of *EAS Publications Series*, 2009 pp. 175–186

[202] Sarkar, S., Does cosmological structure formation require dark energy?, in *EAS Publications Series*, vol. 36 of *EAS Publications Series*, 2009 pp. 3–9

[203] Sato, M., Hamana, T., Takahashi, R., Takada, M., Yoshida, N., Matsubara, T., Sugiyama, N., Simulations of Wide-Field Weak Lensing Surveys. I. Basic Statistics and Non-Gaussian Effects, *ApJ*, 2009, vol. 701, pp. 945–954, 0906.2237

[204] Schild, A., Time, *Texas Quarterly*, 1960, vol. 3, no. 3, pp. 42–62

[205] Schild, A., Gravitational theories of the Whitehead type and the principle of equivalence, in *Evidence for Gravitational Theories*, edited by C. Møller, New York: Academic Press, 1962

[206] Schild, A., Lectures on General Relativity Theory, in *Relativity Theory and Astrophysics: I, Relativity and Cosmology: II, Galactic Structure: III, Stellar Structure*, edited by J. Ehlers, Providence, Rhode Island: American Mathematical Society, 1967

[207] Schneider, P., Weak Gravitational Lensing, in *Gravitational Lensing: Strong, Weak and Micro, Saas-Fee Advanced Courses, Volume 33. ISBN 978-3-540-30309-1. Springer-Verlag Berlin Heidelberg, 2006, p. 269*, edited by P. Schneider, C. S. Kochanek, J. Wambsganss, Berlin, Heidelberg: Springer, pp. 269–+, 2006

[208] Schneider, P., van Waerbeke, L., Kilbinger, M., Mellier, Y., Analysis of two-point statistics of cosmic shear. I. Estimators and covariances, *A&A*, 2002, vol. 396, pp. 1–19, arXiv:astro-ph/0206182

[209] Schneider, P., Weiss, A., Light propagation in inhomogeneous universes, *ApJ*, 1988, vol. 327, pp. 526–543

[210] Seljak, U., Analytic model for galaxy and dark matter clustering, *MNRAS*, 2000, vol. 318, pp. 203–213, arXiv:astro-ph/0001493

[211] Semboloni, E., Heymans, C., van Waerbeke, L., Schneider, P., Sources of contamination to weak lensing three-point statistics: constraints from N-body simulations, *MNRAS*, 2008, vol. 388, pp. 991–1000, 0802.3978

[212] Shafieloo, A., Souradeep, T., Assumptions of the primordial spectrum and cosmological parameter estimation, *ArXiv e-prints*, 2009, 0901.0716

[213] Shiraishi, M., Ichikawa, K., Ichiki, K., Sugiyama, N., Yamaguchi, M., Constraints on neutrino masses from WMAP5 and BBN in the lepton asymmetric universe, *Journal of Cosmology and Astro-Particle Physics*, 2009, vol. 7, pp. 5–+, 0904.4396

[214] Silk, J., Fundamental tests of galaxy formation theory, in *Astrophysical Cosmology Proceedings*, edited by H. A. Brueck, G. V. Coyne, M. S. Longair, 1982 pp. 427–470

[215] Simon, P., How accurate is Limber's equation?, *A&A*, 2007, vol. 473, pp. 711–714, arXiv:astro-ph/0609165

[216] Slipher, V.M., Nebulae, *Proceedings of the American Philosophical Society*, 1917, vol. 56, pp. 403–409

[217] Smail, I., Ellis, R.S., Fitchett, M.J., Gravitational Lensing of Distant Field Galaxies by Rich Clusters - Part One - Faint Galaxy Redshift Distributions, *MNRAS*, 1994, vol. 270, pp. 245–+, arXiv:astro-ph/9402048

[218] Smith, R.E., Peacock, J.A., Jenkins, A., White, S.D.M., Frenk, C.S., Pearce, F.R., Thomas, P.A., Efstathiou, G., Couchman, H.M.P., Stable clustering, the halo model and non-linear cosmological power spectra, *MNRAS*, 2003, vol. 341, pp. 1311–1332, arXiv:astro-ph/0207664

[219] Sorabji, R., *Matter, Space and Motion: Theories in antiquity and their sequel*, London: Duckworth, 1988

[220] Sorkin, R.D., Indications of causal set cosmology, *ArXiv General Relativity and Quantum Cosmology e-prints*, 2000, arXiv:gr-qc/0003043

[221] Spergel, D.N., Bean, R., Doré, O., Nolta, M.R., Bennett, C.L., Dunkley, J., Hinshaw, G., Jarosik, N., Komatsu, E., Page, L., Peiris, H.V., Verde, L., Halpern, M., Hill, R.S., Kogut, A., Limon, M., Meyer, S.S., Odegard, N.,

Tucker, G.S., Weiland, J.L., Wollack, E., Wright, E.L., Three-Year Wilkinson Microwave Anisotropy Probe (WMAP) Observations: Implications for Cosmology, *ApJS*, 2007, vol. 170, pp. 377–408, arXiv:astro-ph/0603449

[222] Spergel, D.N., Verde, L., Peiris, H.V., Komatsu, E., Nolta, M.R., Bennett, C.L., Halpern, M., Hinshaw, G., Jarosik, N., Kogut, A., Limon, M., Meyer, S.S., Page, L., Tucker, G.S., Weiland, J.L., Wollack, E., Wright, E.L., First-Year Wilkinson Microwave Anisotropy Probe (WMAP) Observations: Determination of Cosmological Parameters, *ApJS*, 2003, vol. 148, pp. 175–194, arXiv:astro-ph/0302209

[223] Susskind, L., The anthropic landscape of string theory, in *Universe or Multiverse?*, edited by B. Carr, Cambridge University Press, pp. 247–+, 2007

[224] Takada, M., Komatsu, E., Futamase, T., Cosmology with high-redshift galaxy survey: Neutrino mass and inflation, *PRD*, 2006, vol. 73, no. 8, pp. 083 520–+, arXiv:astro-ph/0512374

[225] Tegmark, M., Cosmological Neutrino Bounds for Non-Cosmologists, *Physica Scripta Volume T*, 2005, vol. 121, pp. 153–155, arXiv:hep-ph/0503257

[226] Tegmark, M., Eisenstein, D.J., Strauss, M.A., Weinberg, D.H., Blanton, M.R., Frieman, J.A., Fukugita, M., Gunn, J.E., Hamilton, A.J.S., Knapp, G.R., Nichol, R.C., Ostriker, J.P., Padmanabhan, N., Percival, W.J., Schlegel, D.J., Schneider, D.P., Scoccimarro, R., Seljak, U., Seo, H.J., Swanson, M., Szalay, A.S., Vogeley, M.S., Yoo, J., Zehavi, I., Abazajian, K., Anderson, S.F., Annis, J., Bahcall, N.A., Bassett, B., Berlind, A., Brinkmann, J., Budavari, T., Castander, F., Connolly, A., Csabai, I., Doi, M., Finkbeiner, D.P., Gillespie, B., Glazebrook, K., Hennessy, G.S., Hogg, D.W., Ivezić, Ž., Jain, B., Johnston, D., Kent, S., Lamb, D.Q., Lee, B.C., Lin, H., Loveday, J., Lupton, R.H., Munn, J.A., Pan, K., Park, C., Peoples, J., Pier, J.R., Pope, A., Richmond, M., Rockosi, C., Scranton, R., Sheth, R.K., Stebbins, A., Stoughton, C., Szapudi, I., Tucker, D.L., vanden Berk, D.E., Yanny, B., York, D.G., Cosmological constraints from the SDSS luminous red galaxies, *Phys. Rev. D*, 2006, vol. 74, no. 12, pp. 123 507–+, arXiv:astro-ph/0608632

[227] Tegmark, M., Taylor, A.N., Heavens, A.F., Karhunen-Loeve Eigenvalue Problems in Cosmology: How Should We Tackle Large Data Sets?, *ApJ*, 1997, vol. 480, pp. 22–+, arXiv:astro-ph/9603021

[228] Tereno, I., Schimd, C., Uzan, J.P., Kilbinger, M., Vincent, F.H., Fu, L., CFHTLS weak-lensing constraints on the neutrino masses, *A&A*, 2009, vol. 500, pp. 657–665, 0810.0555

[229] Teyssier, R., Pires, S., Prunet, S., Aubert, D., Pichon, C., Amara, A., Benabed, K., Colombi, S., Refregier, A., Starck, J., Full-sky weak-lensing simulation with 70 billion particles, *A&A*, 2009, vol. 497, pp. 335–341, 0807.3651

[230] The Planck Collaboration, The Scientific Programme of Planck, *ArXiv Astrophysics e-prints*, 2006, arXiv:astro-ph/0604069

[231] Thirring, W.E., An alternative approach to the theory of gravitation, *Ann. Phys. (U.S.A.)*, 1961, vol. 16, pp. 96–117

[232] Thorne, K.S., Ni, W.T., Will, C.M., Theoretical frameworks for testing relativistic gravity: A review, in *Proceedings on the Conference on Experimental Tests of Gravitational Theories, November 11-13, 1970, California Institute of Technology*, edited by R. W. Davies, J.P.L. Technical Memorandum, 33-499, 1971 pp. 10–31

[233] Turner, M.S., Dark Matter and Dark Energy in the Universe, in *The Third Stromlo Symposium: The Galactic Halo*, edited by B. K. Gibson, R. S. Axelrod, M. E. Putman, vol. 165 of *Astronomical Society of the Pacific Conference Series*, 1999 pp. 431–+

[234] Van Waerbeke, L., Shear and Magnification: Cosmic Complementarity, *ArXiv e-prints*, 2009, 0906.1583

[235] Van Waerbeke, L., Mellier, Y., Gravitational Lensing by Large Scale Structures: A Review, *ArXiv Astrophysics e-prints*, 2003, arXiv:astro-ph/0305089

[236] Van Waerbeke, L., Mellier, Y., Erben, T., Cuillandre, J.C., Bernardeau, F., Maoli, R., Bertin, E., Mc Cracken, H.J., Le Fèvre, O., Fort, B., Dantel-Fort, M., Jain, B., Schneider, P., Detection of correlated galaxy ellipticities from CFHT data: first evidence for gravitational lensing by large-scale structures, *A&A*, 2000, vol. 358, pp. 30–44, arXiv:astro-ph/0002500

[237] Verde, L., Peiris, H.V., Spergel, D.N., Nolta, M.R., Bennett, C.L., Halpern, M., Hinshaw, G., Jarosik, N., Kogut, A., Limon, M., Meyer, S.S., Page, L., Tucker, G.S., Wollack, E., Wright, E.L., First-Year Wilkinson Microwave Anisotropy Probe (WMAP) Observations: Parameter Estimation Methodology, *ApJS*, 2003, vol. 148, pp. 195–211, arXiv:astro-ph/0302218

[238] Villumsen, J.V., Weak lensing by large-scale structure in open, flat and closed universes, *MNRAS*, 1996, vol. 281, pp. 369–383, arXiv:astro-ph/9503011

[239] Vogeley, M.S., Szalay, A.S., Eigenmode Analysis of Galaxy Redshift Surveys. I. Theory and Methods, *ApJ*, 1996, vol. 465, pp. 34–+, arXiv:astro-ph/9601185

[240] Walker, A.G., On Milne's theory of world-structure, *Proceedings of the London Mathematical Society 2*, 1937, vol. 42, pp. 90–127

[241] Walsh, D., Carswell, R.F., Weymann, R.J., 0957 + 561 A, B - Twin quasistellar objects or gravitational lens, *Nature*, 1979, vol. 279, pp. 381–384

[242] Wang, Y., Figure of merit for dark energy constraints from current observational data, *Phys. Rev. D*, 2008, vol. 77, no. 12, pp. 123 525–+, 0803.4295

[243] Wang, Y., Freese, K., Probing dark energy using its density instead of its equation of state, *Physics Letters B*, 2006, vol. 632, pp. 449–452, arXiv:astro-ph/0402208

[244] Weber, H., *B. Riemann: Gesammelte Mathematische Werke*, Dover: New York, 2nd edn., 1953, paperback reprint

[245] Weinberg, S., Photons and gravitons in perturbation theory: Derivation of Maxwell's and Einstein's equations, *Phys. Rev. B*, 1965, vol. 138, pp. 988–1002

[246] Weller, J., Albrecht, A., Future supernovae observations as a probe of dark energy, *Phys. Rev. D*, 2002, vol. 65, no. 10, pp. 103 512–+, arXiv:astro-ph/0106079

[247] Weller, J., Lewis, A.M., Large-scale cosmic microwave background anisotropies and dark energy, *MNRAS*, 2003, vol. 346, pp. 987–993, arXiv:astro-ph/0307104

[248] White, M., Vale, C., Simulations of weak gravitational lensing, *Astroparticle Physics*, 2004, vol. 22, pp. 19–27, arXiv:astro-ph/0312133

[249] Whitehead, A.N., *The Principle of Relativity*, Cambridge University Press: Cambridge, 1922

[250] Will, C.M., Relativistic gravity in the solar system, II: Anisotropy in the Newtonian gravitational constant, *Astrophysics J.*, 1971, vol. 169, pp. 141–156

[251] Will, C.M., *Theory and Experiment in Gravitational Physics*, Cambridge University Press: Cambridge, 2nd edn., 1993

[252] Will, C.M., The Confrontation between General Relativity and Experiment, *Living Rev. Relativity*, 2001, vol. 4, no. 4, available online: http://www.livingreviews.org/lrr-2001-4

[253] Wiltshire, D.L., Gravitational energy as dark energy: Towards concordance cosmology without Lambda, in *Dark Energy and Dark Matter: Observations, Experiments and Theories*, vol. 36 of *EAS Publications Series*, 2009 pp. 91–98

[254] Wittman, D.M., Tyson, J.A., Kirkman, D., Dell'Antonio, I., Bernstein, G., Detection of weak gravitational lensing distortions of distant galaxies by cosmic dark matter at large scales, *Nature*, 2000, vol. 405, pp. 143–148, arXiv:astro-ph/0003014

[255] Wong, Y.Y.Y., Higher order corrections to the large scale matter power spectrum in the presence of massive neutrinos, *Journal of Cosmology and Astro-Particle Physics*, 2008, vol. 10, pp. 35–+, 0809.0693

[256] Zel'dovich, Y.B., A hypothesis, unifying the structure and the entropy of the Universe, *MNRAS*, 1972, vol. 160, pp. 1P–+

[257] Zhan, H., Albrecht, A., Cooray, A., Habib, S., Heavens, A., Heitmann, K., Jain, B., Jee, M.J., Knox, L., Mandelbaum, R., Newman, J., Schmidt, S., Scranton, R., Strauss, M., Tyson, T., Verde, L., Wittman, D., Wood-Vasey, M., Exploring Dark Energy with Next-Generation Photometric Redshift Surveys, *Astronomy*, 2009, vol. 2010, pp. 332–+, 0902.2599